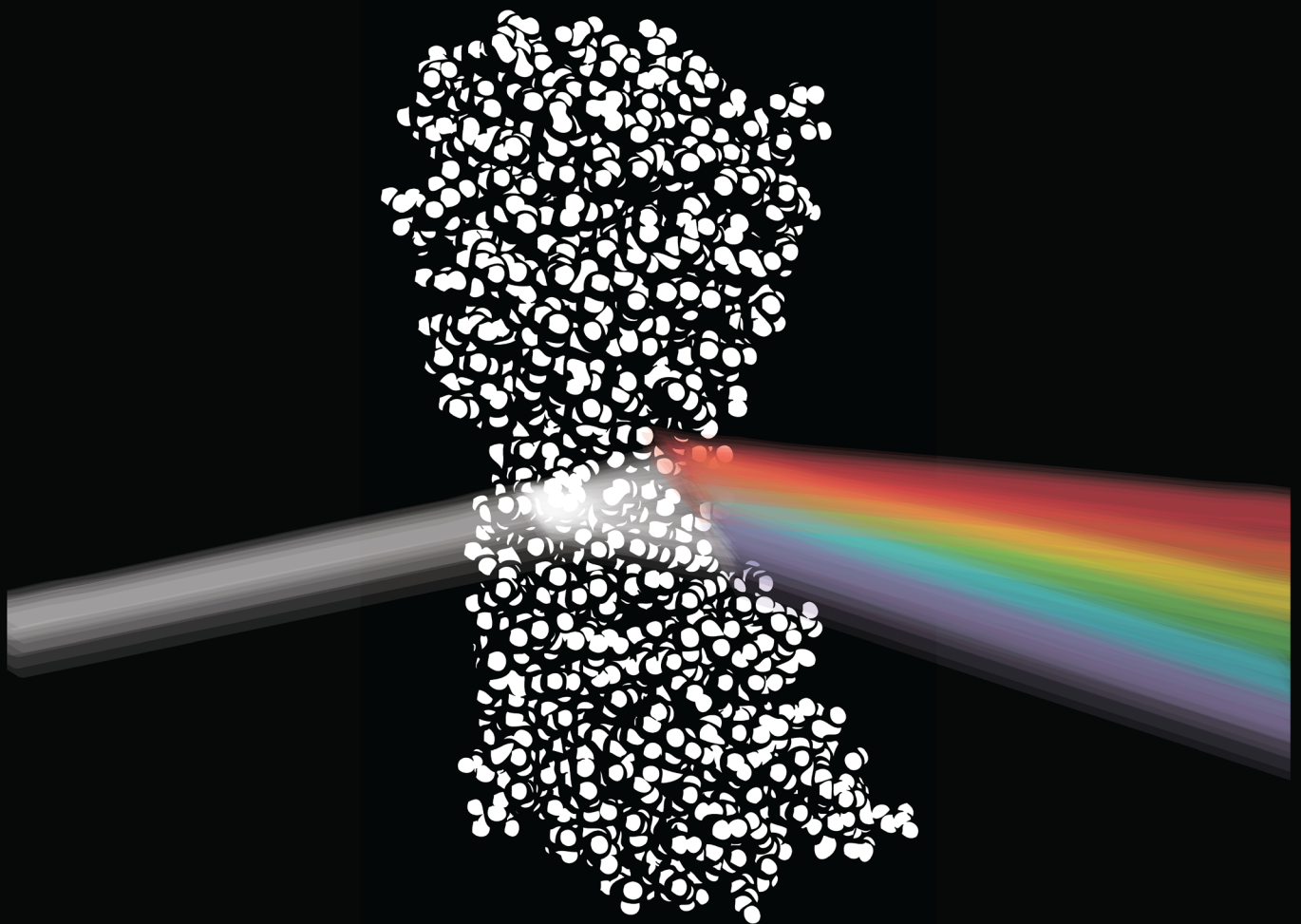


Structure-Function Analysis of the Central Defence Regulator PAD4 in Arabidopsis



PhD Dissertation
Joram A. Dongus

Structure-Function Analysis of the
Central Defence Regulator PAD4
in Arabidopsis

Inaugural-Dissertation

zur

Erlangung des Doktorgrades
der Mathematisch-Naturwissenschaftlichen Fakultät
der Universität zu Köln

vorgelegt von

Joram Andreas Dongus

aus Zeist, die Niederlande

Köln, 2020

Die vorliegende Arbeit wurde am Max Planck Institut für Pflanzenzüchtungsforschung in Köln in der Abteilung für Pflanze-Mikroben Interaktionen (Direktor: Prof. Dr. Paul Schulze-Lefert), Arbeitsgruppe Prof. Dr. Jane Parker durchgeführt.

The work described in this thesis was conducted under the supervision of Prof. Dr. Jane Parker at the Max Planck Institute for Plant Breeding Research (Department of Plant-microbe interactions, Director: Prof. Dr. P. Schulze-Lefert)



MAX-PLANCK-GESELLSCHAFT



Max Planck Institute for
Plant Breeding Research

Berichterstatter: Prof. Dr. Jane E. Parker

Prof. Dr. Alga Zuccaro

Prüfungsvorsitzender: Prof. Dr. Gunther Doehlemann

Tag der Disputation: 30. Juni 2020

Summary

In natural and agricultural environments, pathogens and pests reduce plant growth and fitness. To safeguard global food security in light of climate change, breeders need to generate resistant crop varieties that can withstand invasion of pathogens and pests on a warming planet. For targeted resistance breeding, fundamental knowledge on the plant immune system is essential. However, how these resistance pathways are regulated remains unclear. This thesis aims to expand the knowledge on a central regulator in plant resistance.

Plants evolved a sophisticated two-layered immune system to defend themselves against biotic stressors. The first layer of immune responses is sufficient for plants to defend themselves against the majority of non-host adapted pathogens and pests. However, host-adapted species can colonise the plant by releasing virulence-enhancing effector molecules into the plant cell and repress the plant's first immune responses. The second immune layer uses intracellular receptors that can recognise these hostile effectors, leading to the activation of a strong immune response in local and distal tissues. In the model species *Arabidopsis thaliana*, EDS1 and PAD4 proteins together integrate such signals, thereby functioning as an immune signalling hub against various pathogens. PAD4 also limits aphid colonisation by enhancing aphid resistance responses, completely independent of EDS1. EDS1 and PAD4 are present in nearly all seed plants, suggesting a conserved function of these proteins in plant immunity and aphid resistance. EDS1 and PAD4 need to associate with each other to activate resistance pathways and immunity genes. The N-terminal protein domains are required for the EDS1-PAD4 interaction and their C-terminal domains form a cavity. Recent insights in the EDS1 protein structure revealed that several amino acids on the EDS1 side of the cavity are necessary for immune signalling. However, it remains unknown if the PAD4 cavity is required for immune signalling too.

To gain functional insights in PAD4 structure-function, I first investigated the properties of the PAD4 N-terminal domain, without its C-terminal domain, and thus without the cavity. This revealed that the PAD4 N-terminal domain is sufficient for resistance to aphids. In contrast, the PAD4 N-terminal domain was insufficient to function with EDS1 in pathogen immunity, supporting the hypothesis that the EDS1-PAD4 C-terminal domains function together in immune signalling. Subsequently, I made single amino acid changes in the PAD4 cavity. This revealed that two independent amino acid changes disable EDS1-PAD4 immune signalling, but did not affect PAD4 aphid resistance. This result highlights that PAD4 immune activities are distinct from PAD4 aphid resistance. Moreover, these findings indicate that EDS1 and PAD4 form a cavity that is essential for immune activation. Although EDS1-PAD4 cavity function remains unknown, it likely forms a signalling surface that functions as a protein-interaction platform, inducing downstream signalling and immune gene activation.

Zusammenfassung

In natürlichen und landwirtschaftlichen Umgebungen verringern Krankheitserreger und Schädlinge das Pflanzenwachstum und die Fitness. Um die globale Ernährungssicherheit angesichts des Klimawandels zu gewährleisten, müssen die Züchter resistente Pflanzensorten erzeugen, die dem Eindringen von Krankheitserregern und Schädlingen auf einen sich erwärmenden Planeten standhalten. Für eine gezielte Resistenzzüchtung sind grundlegende Kenntnisse über das pflanzliche Immunsystem unerlässlich. Grundlegendes Wissen darüber, wie diese Resistenzwege reguliert werden fehlt jedoch noch. Diese Doktorarbeit zielt darauf ab, das Wissen über einen zentralen Regulator der Pflanzenresistenz zu erweitern.

Pflanzen entwickelten ein ausgeklügeltes zweischichtiges Immunsystem, um sich gegen diese biotischen Stressfaktoren zu verteidigen. Die erste Schicht des Immunsystems reicht aus die Pflanze gegen die Mehrzahl der nicht an den Wirt angepassten Krankheitserreger und Schädlinge verteidigen zu können. Wirtsangepasste Spezies können die Pflanze jedoch besiedeln, indem sie virulenzverstärkende Effektormoleküle in die Pflanzenzelle freisetzen und die ersten Immunantworten der Pflanze unterdrücken. Die zweite Immunschicht verwendet intrazelluläre Rezeptoren, die diese feindlichen Effektoren erkennen können, was zur Aktivierung einer starken Immunantwort in lokalen und distalen Geweben führt. In der Modellpflanze *Arabidopsis thaliana* integrieren die EDS1- und PAD4-Proteine zusammen solche Signale und fungieren so als Immunsignal-Zentrum gegen verschiedene Krankheitserreger. Völlig unabhängig von EDS1 begrenzt PAD4 auch die Kolonisierung von Blattläusen, indem es die Resistenzreaktionen gegen Blattläuse verstärkt. EDS1 und PAD4 sind in fast allen Samenpflanzen anwesend, was auf eine konservierte Funktion dieser Proteine bei der Pflanzenimmunität und Blattlausresistenz hinweist. EDS1 und PAD4 müssen sich miteinander verbinden, um Resistenzwege und Immunitätsgene zu aktivieren. Die N-terminalen Proteindomänen werden für die EDS1-PAD4-Wechselwirkung benötigt und ihre C-terminalen Domänen bilden eine Höhle. Jüngste Erkenntnisse in der EDS1-Proteinstruktur haben gezeigt, dass mehrere Aminosäuren auf der EDS1-Seite der Höhle für die Immunsignalisierung erforderlich sind. Es bleibt jedoch unbekannt, ob die PAD4-Höhle auch für die Immunsignalisierung erforderlich ist.

Um funktionelle Einblicke in die PAD4-Strukturfunktion zu erhalten, untersuchte ich zunächst die Eigenschaften der PAD4-N-terminalen Domäne ohne ihre C-terminale Domäne und damit ohne Höhle. Dies zeigte, dass die N-terminale Domäne von PAD4 für die Resistenz gegen Blattläuse ausreichend ist. Im Gegensatz dazu war die N-terminale Domäne von PAD4

nicht ausreichend, um mit EDS1 bei der Pathogenimmunität zu funktionieren: dies stützt die Hypothese dass die C-terminalen Domänen von EDS1-PAD4 bei der Immunsignalisierung zusammenwirken. Anschließend nahm ich einzelne Aminosäureveränderungen in die PAD4-Höhle vor. Dies zeigte, dass zwei unabhängige Aminosäureveränderungen das EDS1-PAD4-Immunsignal inaktivieren, die PAD4-Blattlausresistenz jedoch nicht beeinflussen. Dieses Ergebnis unterstreicht, dass sich die PAD4-Immunkomplexaktivitäten von der PAD4-Blattlausresistenz unterscheiden. Darüber hinaus weisen diese Ergebnisse darauf hin, dass EDS1 und PAD4 eine Höhle bilden, die für die Immunaktivierung essenziell ist. Obwohl nicht bekannt ist was der EDS1-PAD4-Hohlraum tatsächlich tut, bildet er wahrscheinlich eine Signaloberfläche, die als Protein-Interaktionsplattform fungiert und die nachgeschaltete Signalübertragung und die Aktivierung von Immunzellen induziert.

Table of Contents

Summary	IV
Zusammenfassung.....	V
Table of Contents	VII
Acknowledgements	X
Abbreviations	XII
Introduction.....	1
NLR triggered immunity.....	2
EDS1-family function in plant immunity	4
EDS1-family protein structure-function in immunity	7
SA-signalling in immunity.....	9
PAD4 responses to Green Peach Aphid	10
Thesis Aims.....	11
Chapter 1: Arabidopsis PAD4 lipase-like domain is sufficient for resistance to green peach aphid....	12
PAD4 ^{LLD} does not interact with EDS1	12
EDS1 ^{LLD} does not interact with PAD4	14
SAG101 ^{LLD} does not interact with EDS1	15
PAD4 ^{LLD} is a stable protein and localizes to the nucleus and cytoplasm.....	17
Expression of PAD4 ^{LLD} confers GPA resistance	19
Arabidopsis ETI and basal immunity require full-length PAD4	20
Chapter 2: Arabidopsis PAD4 EP domain cavity plays an essential role in immunity	24
Selection of PAD4 EP domain cavity variants	25
Screening PAD4 EP domain cavity T1 mutants for <i>susceptibility to Hpa</i> EMWA1.....	27
All PAD4 variants interact with EDS1 <i>in planta</i> , except PAD4 ^{I286A}	28
PAD4 ^{R314A} and PAD4 ^{K380A} are stable and nucleocytoplasmic proteins in Arabidopsis.....	30
Basal immunity and TNL-ETI require PAD4 ^{R314} and PAD4 ^{K380}	34
PAD4 ^{R314A} and PAD4 ^{K380A} susceptibility is independent of <i>Pst</i> DC3000-produced coronatine.....	38
PAD4 ^{R314} and PAD4 ^{K380} are not required for resistance to GPA	39
Chapter 3: Identification of active PAD4 protein complexes during <i>Pst avrRps4</i> infection.....	44
Experimental outline and rationale	44

GO-Term analysis	45
Differential interactors of PAD4 ^{WT} and PAD4 ^{K380A} at 4 and 6 hpi	47
MES10 T-DNA mutants are resistant to <i>Hpa</i> EMWA1	53
TPR1 and SGT1b do not interact with PAD4 in <i>N. benthamiana</i>	55
Chapter 4: Cytoplasmic-enriched PAD4 causes autoimmunity in Arabidopsis	59
Nuclear- and cytoplasmic-enriched PAD4 lines are resistant to <i>Hpa</i> EMWA1	59
Cytoplasm-enriched PAD4 induces autoimmunity in Arabidopsis	60
NESgPAD4 autoimmunity depends on <i>EDS1</i> but not <i>ICS1</i> -generated SA	63
NESgPAD4 autoimmunity does not depend on PAD4 ^{S118}	66
Discussion	69
PAD4 is unlikely to function as a hydrolase.....	69
PAD4 S-D-H triad-independent GPA activities	72
<i>PAD4</i> cis-regulation in plant resistance	73
PAD4 ^{R314A} and PAD4 ^{K380A} susceptibility is not dependent on <i>Pst</i> -produced coronatine	74
EDS1-family heterodimerisation is essential for immunity	75
TIR-NADase activity and the EDS1-family EP domain cavity.....	77
Perspectives on CC-NLR structure-function and signalling via EDS1-PAD4	80
Immune signalling components downstream of NLRs and EDS1-PAD4	81
Interaction between EDS1-family proteins and phytohormone processing enzymes	82
NESgPAD4 phenocopies EDS1-NLS	83
SGT1b in NESgPAD4 autoimmunity	84
ICS1-produced SA in NESgPAD4 autoimmunity.....	85
Concluding remarks and outlook	86
Materials and Methods	89
Materials	89
Plant Materials.....	89
Pathogen/Pest Strains	90
Bacterial Strains	90
Antibiotics.....	91

Antibodies.....	91
Chemicals.....	92
Enzymes.....	92
Oligonucleotides.....	93
Vectors.....	101
Media.....	103
Buffers and Solutions.....	104
Methods.....	105
Plant methods.....	105
Bacterial methods.....	107
Biochemical methods.....	109
Molecular biological methods.....	113
<i>In silico</i> analyses.....	118
References.....	120
Erklärung.....	136

Acknowledgements

Foremost, I want to thank my supervisor and promotor, Prof. Dr. Jane E. Parker. Jane, thank you for your guidance, wisdom and our scientific discussions. I am very grateful to have had you guide me through my PhD!

I would like to thank the members of my thesis committee, Prof. Dr. Alga Zuccaro and Prof. Dr. Gunther Doehlemann for taking the time and effort for critically evaluating my thesis. Thanks to Prof. Dr. Karsten Niefind for his continued scientific support throughout my thesis as a collaborator, Thesis Advisory Committee (TAC) member and as a “Beisitzer” during my defence.

I also want to give special thanks to Dr. Franziska Turck for kick-starting my scientific career, as a member in my TAC and as the founder of our musical escapades in the TATA bar, a.k.a. Band Camp! Many thanks also to Prof. Dr. Jyoti Shah, Monika Patel and Lani Archer for testing GPA responses in my PAD4 mutant variants. I am very grateful for Dr. Martijn van Zanten, Dr. Marcel Proveniers, and Ing. Evelien Stouten, you suggested me to consider doing a PhD back in 2013, thank you for giving me the confidence to dream big!

Dear JP Groupies! Deepak, your scientific input, our discussions, and yes your wisdom too, have made me a better scientist. Jaqueline, you are one of the kindest and most helpful persons I have ever met, thank you for all of your insights over the years! Also big thanks to the NRG1 team, Dmitry and Xinhua, our Plant Cell paper has become a beautiful story! Xiexie Jingde and Xinhua for having me as your student in Chinese language, culture and cuisine! Patrick, thank you for your wise words as a PhD rep., during my interview, and for the amazing concerts we have been to over the years! Thanks to Friedrike, Charles, Anthony, Joel, Oliver, Federica, Yunli, Haitao and Clementine, it was a blast! Last but not least, thanks to the students who put their faith in me as a supervisor. Laura Herold, Lucas Dijkgraaf and Eva Penner, I hope you learned at least half as much from me, as I learned from you, I am very grateful for your help and for making me a better coach.

Thanks to my colleagues from the lab-kitchen, greenhouse, technical department and administration for hidden, but essential support. Special thanks to our MPIPZ PhD coordinator Dr. Stephan Wagner for your support, taking part in my TAC meetings, organising pizza’s during PhD. representative meetings, and building the foundation for this thesis!

A PhD does not revolve around science alone and I would therefore like to thank many people who made this experience extra special. I am very grateful for Dr. Wolfgang Schuchert for helping me organise the “Scientists Garden,” I hope it will continue for many years to come.

Thanks Pádraic for teaching me the fine-art of Oca breeding and for your endless flow of quirky “fun facts”! A shout out to the “PAs”: Leona, Alessandro, Beta (+Gerald), Ivo, Kees, Lennert, Lucas, Nora, Alan, Andrea, Marco, Charles, Chloé and Adrian R.; PhD retreats, TATA bars, hikes around Cologne and trips to Wageningen and Solda are cherished memories. Speaking of TATA bars, thanks Ale and Leo for organising this with me for the last 2 years! And thanks to everyone else who has made these TATA bar events happen! Very special thanks to Marco, Franziska, Sergio, Ale, Victor and Fred for Band Camp. Making music together, stepping out of the living room and onto the stage, playing our favourite songs, live in front of an audience, I will truly cherish these memories forever!

Heel veel dank pap, mam, Robert, Adrian en Max voor jullie afleiding, en mentale en logistieke ondersteuning tijdens deze hele tocht. Vielen lieben Dank Oma Linde und Thomas für eure Unterstützung während meine Doktorarbeit! Bedankt Opa Bob en de hele Roebeling clan voor alle nodige afleiding en inspiratie om dat te doen wat je leuk vindt en waar je voldoening uit haalt!

Allerliefste Annabel, de meeste dank gaat naar jou, zonder jou ondersteuning had ik dit niet kunnen doen. Op naar ons volgende avontuur!

Abbreviations

Amino acids

Amino acid	3-letter abbreviation	1-letter abbreviation
Alanine	Ala	A
Arginine	Arg	R
Asparagine	Asn	N
Aspartic acid	Asp	D
Cysteine	Cys	C
Glutamic acid	Glu	E
Glutamine	Gln	Q
Glycine	Gly	G
Histidine	His	H
Isoleucine	Ile	I
Leucine	Leu	L
Lysine	Lys	K
Methionine	Met	M
Phenylalanine	Phe	F
Proline	Pro	P
Serine	Ser	S
Threonine	Thr	T
Tryptophan	Trp	W
Tyrosine	Tyr	Y
Valine	Val	V

Further abbreviations

°C	degree Celsius
aa	amino acid
ACD2	ACCELERATED CELL DEATH 2
ACN	acetonitrile
ADF3	ACTIN-DEPOLYMERIZING FACTOR 3
ADR1	ACCELERATED DISEASE RESISTANCE 1
ALD1	AGD2-LIKE DEFENSE RESPONSE PROTEIN 1
AOC2	ALLENE OXIDASE CYCLASE 2
Arabidopsis	<i>Arabidopsis thaliana</i>
ASPG1	ASPARTIC PROTEASE IN GUARD CELL 1
<i>At</i>	<i>Arabidopsis thaliana</i>
avr	avirulence
BBD1	BIFUNCTIONAL NUCLEASE IN BASAL DEFENSE RESPONSE 1
bp	base pair
CAM1-7	CALMODULIN 1-7

CBP60g	CALMODULIN BINDING PROTEIN 60-LIKEg
CC	coiled-coil
cDNA	complementary DNA
<i>chs1/2/3</i>	<i>chilling sensitive 1/2/3</i>
^c LUC	C-terminal LUC
CNL	CC-NLR
COI1	CORONATINE INSENSITIVE 1
Col-0	Colombia-0
Cor	coronatine
CPK3/CDPK6	CALCIUM DEPENDENT PROTEIN KINASE 3
CPL1	C-TERMINAL DOMAIN PHOSPHATASE-LIKE 1
C-terminal	carboxy-terminal
CUL1/3	CULLIN1/3
d	day(s)
DAMP	damage-associated molecular pattern
ddH ₂ O	distilled, deionized water
DM2h	DANGEROUS MIX 2h
DMSO	dimethylsulfoxide
DNA	deoxyribonucleic acid
DNase	deoxyribonuclease
dNTP	deoxynucleosidetriphosphate
dpi	day(s) post infection
ds	downstream
EDS1	ENHANCED DISEASE SUSCEPTIBILITY1
EDTA	ethylenediaminetetraacetic acid
ELF5A-2	EUKARYOTIC TRANSLATION INITIATION FACTOR 5A-2
EM	electron microscopy
EP domain	EDS1-PAD4 domain
EPS1	ENHANCED PSEUDOMONAS SUSCEPTIBILITY
ERF1	ETHYLENE RESPONSE FACTOR 1
ETI	effector-triggered immunity
FDR	false discovery rate

FMO1	FLAVIN MONOOXYGENASE1
fw	forward
FWHM	Full Width at Half Maximum
g	gravity
GBF1	G-BOX BINDING FACTOR1
gDNA	genomic DNA
GFP	green fluorescent protein
GID1	GA INSENSITIVE DWARF1
GIP1	GBF-INTERACTING PROTEIN 1
GO	gene ontology
GPA	green peach aphid
h	hour(s)
HA	hemagglutinin
HAMP	herbivore-associated molecular pattern
HCD	High-energy collisional dissociation
HDA19	HISTONE DEACETYLASE 19
HELL	HeLo-like
HeLo	Fungal domain; PFAM database: PF14479
HF	High Fidelity
<i>Hpa</i>	<i>Hyaloperonospora arabidopsidis</i>
hpi	hour(s) post infection
HRP	horseradish peroxidase
HSD	honestly significant difference
iBAQ	intensity Based Absolute Quantification
ICS1	ISOCHORISMATE SYNTHASE 1
IMPA4	IMPORTIN ALPHA ISOFORM-4
IP	immunoprecipitation
JA	jasmonic acid
JAZ1/4	JASMONATE ZIM DOMAIN 1/4
KAI2	KARRIKIN INSENSITIVE 2
kb	kilo base(s)
kDa	kilo Dalton

KETCH1	KARYOPHERIN ENABLING THE TRANSPORT OF THE CYTOPLASMIC HYL1
l	litre
<i>Ler</i>	Landsberg <i>erecta</i>
LFQ	label-free quantification
LLD	lipase-like domain
LOX1/5	LIPOXYGENASE 1/5
LRR	leucine-rich repeat
LUC	luciferase
M	molar (mol / l)
MAMP	microbe-associated molecular pattern
MES10	METHYL ESTERASE 10
mg	milligram
min	minute(s)
MLKL	mixed-lineage kinase-domain-like pseudo-kinase
mM	milli molar
MOS6	MODIFIER OF SNC1 6
MPIPZ	Max Planck Institute for Plant Breeding Research
MPL1	MYZUS PERSICAE-INDUCED LIPASE1
mRNA	messenger RNA
NAD ⁺	nicotinamide adenine dinucleotide
<i>Nb</i>	<i>Nicotiana benthamiana</i> ; (wild-) Tobacco
NDR1	NON RACE-SPECIFIC DISEASE RESISTANCE 1
nes	mutated nuclear export signal
NES	nuclear export signal
ng	nano gram
NHP	N-hydroxypipicolinic acid
nLC-MS/MS	nano-scale liquid chromatographic tandem mass spectrometry
NLR	nucleotide-binding leucine-rich repeat
nls	mutated nuclear localisation signal
NLS	nuclear localisation signal
^N LUC	N-terminal LUC
nM	nano molar

NPR1	NON-EXPRESSOR OF PR GENES 1
NRC4	NLR REQUIRED FOR CELL DEATH 4
NRG1	N REQUIREMENT GENE 1
N-terminal	amino-terminal
OD	optical density
<i>Os</i>	<i>Oryza sativa</i> ; rice
(p)35S	35S promoter from Cauliflower Mosaic Virus
PAD4	PHYTOALEXIN DEFICIENT4
PAGE	polyacrylamide gel electrophoresis
PBS3	AVRPPHB SUSCEPTIBLE 3
PCR	polymerase chain reaction
PEG	Polyethylene glycol
pH	negative decimal logarithm of the H ⁺ concentration
PR1	PATHOGENESIS RELATED1
PRR	pattern recognition receptor
<i>Pst</i>	<i>Pseudomonas syringae</i> pv. <i>tomato</i> DC3000
PTI	pattern-triggered immunity
pv.	pathovar
qRT-PCR	quantitative real-time PCR
RNA	ribonucleic acid
ROS	reactive oxygen species
rpm	rotations per minute
RPM1	RESISTANCE TO PSEUDOMONAS SYRINGAE PV. MACULICOLA 1
RPP4/7	RESISTANCE TO PERONOSPORA 4/7
RPS4	RESISTANCE TO PSEUDOMONAS SYRINGAE 4
RPW8	RESISTANCE TO POWDERY MILDEW 8
RRS1-S	RESISTANCE TO RALSTONIA SOLANACEARUM1-SUSCEPTIBLE
RT	room temperature
rv	reverse
SA	salicylic acid
SABP2	SA-BINDING PROTEIN 2

SAG101/13/21/27	SENESCENCE-ASSOCIATED GENE 101/13/21/27
SAR	systemic acquired resistance
SAUL1	SENESCENCE-ASSOCIATED E3 UBIQUITIN LIGASE 1
SCF	SKP-CULLIN-F-box
SDM	site directed mutagenesis
SDS	sodium dodecyl sulphate
SFGH	S-FORMYLGLUTATHIONE HYDROLASE
SGT1b	Suppressor of G2 allele of SKP1
SH	StrepII-3xHA
<i>sid2</i>	<i>salicylic acid induction deficient 2</i> , mutant allele of ICS1
<i>Sl</i>	<i>Solanum lycopersicum</i> ; Tomato
SRFR1	SUPPRESSORS OF RPS4-RLD
StrepII	streptavidin
SUMO	small ubiquitin-like modifier
SZF2	SALT-INDUCIBLE ZINF FINGER 2
T3SS	type III secretion system
TAIR	the Arabidopsis information resource
TBS	Tris buffered saline
T-DNA	transfer DNA
TF	transcription factor
TIR	Toll/ interleukin-1 receptor
TNL	TIR-NLR
TPL	TOPLESS
TPR1/2/3/4	TPL RELATED 1/2/3/4
TPS11	TREHALOSE PHOSPHATE SYNTHASE 11
V	Volt(s)
<i>Va</i>	<i>Vitis aestivalis</i> ; Grapevine
v/v	volume/volume
w/v	weight/volume
Ws-0/-2	Wassilewskija-0/-2
WT	wild-type, here: <i>Arabidopsis thaliana</i> , Col-0
XPO1A	EXPORTIN 1A

Y2H	yeast-two-hybrid
YFP	yellow fluorescent protein
ZAR1	HOPZ-ACTIVATED RESISTANCE 1
μ	micro

Introduction

Pathogenic microbes and pests, such as aphids and nematodes, reduce plant growth and fitness in nature and in agriculture (Dangl *et al.*, 2013). On the other hand, plants depend on a plethora of beneficial microbes and animals for nutrient uptake, pollination or seed dispersal (Dudareva *et al.*, 2006; Hacquard *et al.*, 2017). This dilemma led to the evolution of a sophisticated immune system that supports mutualistic interactions, while defending the plant from parasitic interactions. Studying these interactions is becoming increasingly important to safeguard crop yield on our warming planet. Climate change will not only affect crop yield by exacerbating droughts and floods, it will also alter the distribution of pathogens and pests globally (Mbow *et al.*, 2019). Understanding the plant immune system will assist plant breeders in selecting new crop varieties that will be resistant to the pathogens and pests of the future.

Plants have evolved a two-layered immune system to detect pathogen presence (Boutrot & Zipfel, 2017; Dangl & Jones, 2006; Dodds & Rathjen, 2010). Pattern-triggered immunity (PTI) constitutes the first layer of the immune system and detects pathogens and pests in the extracellular space (Boutrot & Zipfel, 2017). Plasma membrane localised pattern-recognition receptors (PRRs) activate PTI upon recognition of microbe-/ damage-/ herbivore-associated molecular patterns (MAMPs/DAMPs/HAMPs) (Boutrot & Zipfel, 2017; Hogenhout & Bos, 2011). On the other hand, pests and (hemi-) biotrophic pathogens repress plant immune responses by delivering virulence factors, called effectors, into the plant cell (Dangl & Jones, 2006; Hogenhout & Bos, 2011). Intracellular nucleotide-binding leucine-rich repeat (NLR) receptors recognise these effectors and induce effector-trigger immunity (ETI) leading to local and systemic immune responses (Dangl & Jones, 2006; Fu & Dong, 2013; Hartmann & Zeier, 2019). PTI and ETI activate similar immune pathways, however, in ETI the duration and intensity of the immune response is enhanced (Cui *et al.*, 2017). Recent evidence suggests that positive feedback between PTI and ETI pathways are essential for robust local ETI responses (Ngou *et al.*, 2020; Yuan *et al.*, 2020).

NLRs induce ETI upon recognition of specific pathogen-produced effectors (Jones *et al.*, 2016). ETI is characterised by rapid transcriptional mobilisation of resistance pathways and, often, localized host cell death, thereby limiting pathogen infection (Bhandari *et al.*, 2019; Cui *et al.*, 2015). NLR-mediated immune responses are also effective against probing insects and nematodes (Hogenhout & Bos, 2011; Milligan *et al.*, 1998; Rossi *et al.*, 1998; Villada *et al.*, 2009; Wroblewski *et al.*, 2007). In the plant model species *Arabidopsis thaliana* (*At*;

Arabidopsis), basal immunity functions in parallel to ETI, and elicits a weak immune response, which slows down virulent pathogen growth and disease progression (Cui *et al.*, 2015; Cui *et al.*, 2017; Dangl & Jones, 2006). Although the precise activation mechanism for post-infection basal immunity remains elusive, it requires several ETI signalling components (Century *et al.*, 1995; Feys *et al.*, 2001; Glazebrook *et al.*, 1997; Parker *et al.*, 1996). Basal immunity is proposed to be the culmination of weak NLR-triggered ETI combined with residual PTI (Cui *et al.*, 2017; Dangl & Jones, 2006; Gantner *et al.*, 2019).

NLR triggered immunity

NLRs evolved independently in plants and animals through convergent evolution (Jones *et al.*, 2016). Arabidopsis encodes for ~150 highly diversified NLRs, while some plant genomes encode >1000 NLRs (Baggs *et al.*, 2017; Jacob *et al.*, 2013). NLRs are characterized by a variable N-terminal domain, a central nucleotide-binding (NB) domain and C-terminal leucine rich-repeat (LLR) domain (Jones *et al.*, 2016). Upon NLR activation, the NB domain releases ADP and binds ATP, thereby switching the NLR from a closed ADP-bound “off” state, to an open ATP-bound “on” state (Cui *et al.*, 2015; Hu *et al.*, 2013; Wang *et al.*, 2019a&b).

In plants, NLRs are sub-divided into three classes based on their variable N-terminal domain, *i.e.* Toll/Interleukin-1 Receptor/Resistance (TIR) domain NLRs (TNLs), Coiled-Coil (CC) domain NLRs (CNLs), and RESISTANCE TO POWDERY MILDEW 8 (RPW8)-type CC (CC_R) domain NLRs (RNLs) (Cesari, 2017; Jubic *et al.*, 2019; Xiao *et al.*, 2001). These CC_R domains show similarity to mixed-lineage kinase-domain-like pseudo-kinase (MLKL) and HeLo/HELL domains from mammals and fungi, where these domains promote host cell death (Jubic *et al.*, 2019; Petrie *et al.*, 2018). Besides the above-described domains, NLRs can also contain domains from unrelated protein families. Such integrated domains (ID) often function as effector sensors and can be located between the CC and NB domain, or NB and LRR domain, or at the N- or C-terminus (Cesari, 2017).

NLRs recognise effectors using distinct molecular mechanisms (Cesari, 2017; Jones *et al.*, 2016). NLRs can directly recognise effectors, however, indirect recognition is more common, which is best described by the guard and decoy models (Cesari, 2017; Jones *et al.*, 2016). In these models, a protein represses an NLR, which upon cleavage or post-translation modification relieves repression of the NLR, resulting in immune activation (Cesari, 2017; Jones *et al.*, 2016). NLRs localise to various subcellular compartments *in planta* (Cui *et al.*, 2015). For example, the Arabidopsis CNL RESISTANCE TO PSEUDOMONAS SYRINGAE PV. MACULICOLA 1 (*AtRPM1*) localises to the plasma membrane, flax (*Linum usitatissimum*)

TNL L6 and M localise to the Golgi and vacuolar membranes, respectively, while the Tobacco (Wild-tobacco; *Nicotiana benthamiana*; Nb) TNL N is nucleocytoplasmic (Cui *et al.*, 2015).

Certain NLRs function as pairs, where one NLR functions as the effector sensor and the other as the signalling executor (Cesari, 2017; Jones *et al.*, 2016). A well-studied receptor pair in Arabidopsis that I have used extensively in this thesis is the TNL-receptor pair RRS1-S/RPS4 (RESISTANCE TO RALSTONIA SOLANACEARUM1-S/RESISTANCE TO PSEUDOMONAS SYRINGAE4) (Birker *et al.*, 2009; Heidrich *et al.*, 2011; Narusaka *et al.*, 2009; Saucet *et al.*, 2015). RRS1-S and RPS4 form homo- and heterodimers and recognise the effector avrRps4 from *Pseudomonas syringae* pv. *Pisi* (Williams, *et al.*, 2014). RRS1-S functions as the sensor NLR, recognising avrRps4 directly with its C-terminal integrated WRKY transcription factor (TF) domain (Ma *et al.*, 2018; Sarris *et al.*, 2015). RRS1-S localises to the cytoplasm and nucleus, and associates to the DNA *in planta* (Deslandes *et al.*, 2003; Le Roux *et al.*, 2015). On the other hand, RPS4 functions as the executor and localises to the endomembrane, however, RPS4 is required to accumulate in the nucleus for immune signalling, suggesting RRS1-S/RPS4 activate immunity in the nucleus (Sohn *et al.*, 2014; Heidrich *et al.*, 2013; Wirthmueller *et al.*, 2007).

Besides sensor and executor NLRs, plants also encode helper NLRs that integrate signals from multiple sensor NLRs (Jubic *et al.*, 2019). The RNL families N REQUIREMENT GENE 1 (NRG1) and ACCELERATED DISEASE RESISTANCE 1 (ADR1) integrate immune signalling and function as helper NLRs (Bonardi *et al.*, 2011; Castel *et al.*, 2019; Dong *et al.*, 2016; Lapin *et al.*, 2019; Peart *et al.*, 2005; Qi *et al.*, 2018; Wu *et al.*, 2019). In Arabidopsis, NRG1 functions in TNL-ETI and cell death, while ADR1 functions in TNL-ETI, CNL-ETI and basal immunity (Castel *et al.*, 2019; Dong *et al.*, 2016; Lapin *et al.*, 2019; Wu *et al.*, 2019). Furthermore, ADR1 boosts the production of the defence-signalling hormone Salicylic Acid (SA) (Bonardi *et al.*, 2011; Roberts *et al.*, 2013; Dong *et al.*, 2016). In contrast to the highly diversified sensor and executor NLRs, NRG1 and ADR1 are conserved, respectively, in eudicots, and seed plants (angiosperms & gymnosperms), suggesting a conserved function as signal integrators in the plant immune system (Baggs *et al.*, 2017&2019; Jubic *et al.*, 2019; Lapin *et al.*, 2019; Wu *et al.*, 2019).

Similar to animal NLRs, recent insights have shown that plant CNLs and RNLs form oligomers upon activation (Hu *et al.*, 2013; Jubic *et al.*, 2019; Li *et al.*, 2020; Wang *et al.*, 2019a&b). For example, the RNL HR4 forms a 900 kDa oligomer with the CNL RESISTANCE TO PERONOSPORA 7 (RPP7) in Arabidopsis (Li *et al.*, 2020). Furthermore, cryo-electron

microscopy (EM) revealed the (in-) active states of the Arabidopsis CNL ZAR1 (HOPZ-ACTIVATED RESISTANCE 1) (Wang *et al.*, 2019a&b). When ZAR1 switches to the active ATP-bound state, ZAR1 and its interacting partners form a circular pentameric structure, or resistosome (Wang *et al.*, 2019a&b). The ZAR1 N-terminal α 1-helices form a funnel-shaped structure or pore that associates to the plasma membrane. The membrane association and pore formation of the α 1-helices is essential for ZAR1 cell death and resistance function (Wang *et al.*, 2019a&b). The function of this pore remains elusive, however, it has been proposed to function as a Ca^{2+} channel, allowing this second messenger to activate downstream components (Jubic *et al.*, 2019).

TNLs form homo- and heterodimers with their TIR domains to function in immunity signalling (Bernoux *et al.*, 2011; Cui *et al.*, 2015; Williams *et al.*, 2015). However, recent evidence revealed a more sophisticated function of TIR domains. TIR domains from prokaryotes, animals and plants show NAD^+ enzymatic (NADase) activity, which is required for TNL immune function *in planta* (Horsefield *et al.*, 2019; Jubic *et al.*, 2019; Wan *et al.*, 2019). For example, the TIR domain of the executor NLR *AtRPS4* shows NADase activity, while its partner, the sensor TNL RRS1-S, is catalytically inactive and relies on RPS4 for signalling (Horsefield *et al.*, 2019; Jubic *et al.*, 2019; Narusaka *et al.*, 2009; Wan *et al.*, 2019; Williams *et al.*, 2015). Notably, mammalian TIR signalling converges on the pore-forming protein MLKL (Jubic *et al.* 2019; Pajuelo *et al.*, 2018). Similarly, plant TNL signalling converges on the helper NLR families NRG1 and ADR1, which contain a CC_R domain resembling mammalian MLKL (Bonardi *et al.*, 2011; Castel *et al.*, 2019; Dong *et al.*, 2016; Lapin *et al.*, 2019; Jubic *et al.* 2019; Peart *et al.*, 2005; Qi *et al.*, 2018; Wu *et al.*, 2019). NRG1 and ADR1 are postulated to function similar to mammalian MLKL, where plant TNL NADase activity induces NRG1 and ADR1 to form a pore, resulting in immune activation (Jubic *et al.*, 2019). However, mechanistic insights in TNL-ETI signalling mechanisms remain elusive.

EDS1-family function in plant immunity

The EDS1-family is a small family of sequence-related immune regulators in plants, and comprises EDS1 (ENHANCED DISEASE SUSCEPTIBILITY1), PAD4 (PHYTOALEXIN DEFICIENT4) and SAG101 (SENESCENCE-ASSOCIATED GENE101) (Bernacki *et al.*, 2019; Feys *et al.*, 2005; Glazebrook *et al.*, 1997; Ke *et al.*, 2014; Parker *et al.*, 1996; Wagner *et al.*, 2013; Wiermer *et al.*, 2005; Lapin *et al.*, 2019). EDS1 forms stable and mutually exclusive heterodimers with PAD4 and SAG101 (Feys *et al.*, 2001&2005; Lapin *et al.*, 2019; Rietz *et al.*, 2011; Wagner *et al.*, 2013). Arabidopsis EDS1 heterodimers function as a signalling hub,

integrating signals from all tested TNLs, and certain CNLs (Cui *et al.*, 2017; Feys *et al.*, 2005; Rietz *et al.*, 2011; Venugopal *et al.*, 2009; Wagner *et al.*, 2013). Notably, EDS1-family proteins and the helper NLR families ADR1 & NRG1 depend on each other to induce basal immunity and ETI (Figure I.1) (Lapin *et al.*, 2019; Wu *et al.*, 2019).

In *Arabidopsis*, nucleocytoplasmic-localised EDS1-PAD4 heterodimers function together with ADR1 in basal immunity, TNL-ETI and certain CNL-ETI pathways (Figure I.1) (Bonardi *et al.*, 2011; Cui *et al.*, 2017; Lapin *et al.*, 2019; Roberts *et al.*, 2013; Wang *et al.*, 2011; Wiermer *et al.*, 2005; Wu *et al.*, 2019). These immune responses include transcriptional mobilisation of resistance pathways, and production of anti-microbial molecules and the defence hormone salicylic acid (SA) (Bartsch *et al.*, 2006; Bonardi *et al.*, 2011; Cui *et al.*, 2017; Feys *et al.*, 2005;

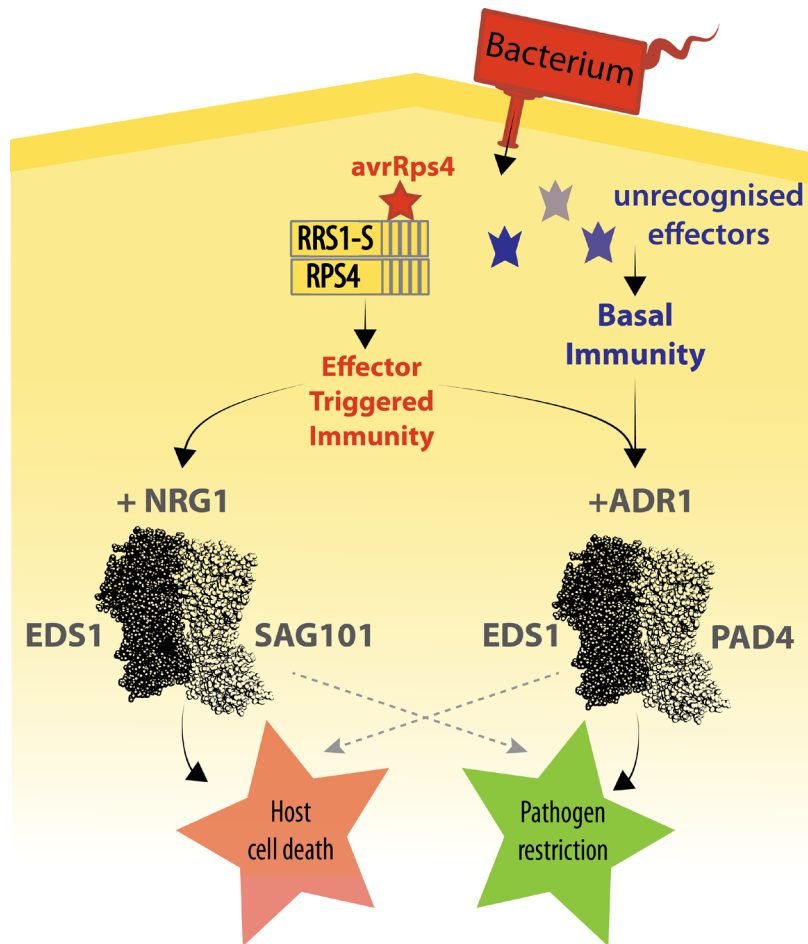


Figure I.1. EDS1-family signalling model in *Arabidopsis* RRS1-S/RPS4 ETI.

Bacterial-produced effectors are secreted into the plant cell. Unrecognised effectors activate basal immunity through an unknown mechanism. The TNL-pair RRS1-S/RPS4 recognises the effector AvrRps4, and induces ETI. Basal immunity and ETI activation depends on the EDS1-PAD4-ADR1 branch leading (mainly) to pathogen restriction (resistance). In ETI, the EDS1-SAG101-NRG1 branch induce (mainly) host cell death. The exact function of NRG1, ADR1 and TNL NADase activity in TNL-ETI remains elusive. This model is based on a model proposed in Lapin *et al.* (2019).

Jirage *et al.*, 1999; Rietz *et al.*, 2011; Wang *et al.*, 2008; Wang *et al.*, 2011; Wiermer *et al.*, 2005; Zhou *et al.*, 1998). On the other hand, EDS1-SAG101 heterodimers function together with NRG1 in TNL-ETI and cell death (Figure I.1) (Feys *et al.*, 2005; Rietz *et al.*, 2011; Lapin *et al.*, 2019; Qi *et al.*, 2018; Wu *et al.*, 2019). Notably, PAD4 does not contribute to local immune responses in Tobacco, instead, these responses depend on the EDS1-SAG101-NRG1 pathway (Gantner *et al.*, 2019; Lapin *et al.*, 2019). In Arabidopsis, *sag101* and *nrg1* mutants do not show enhanced susceptibility phenotypes, unlike *pad4* and *adr1* mutants, indicating SAG101 and NRG1 function redundantly to PAD4 and ADR1 in limiting pathogen growth (Feys *et al.*, 2005; Lapin *et al.*, 2019; Wagner *et al.*, 2013; Wu *et al.*, 2019). This indicates that PAD4 is EDS1's main signalling partner in Arabidopsis pathogen resistance (Figure I.1).

In Arabidopsis immunity, EDS1-PAD4 transcriptional reprogramming requires a nuclear EDS1 pool (Bartsch *et al.*, 2006; Bhattacharjee *et al.*, 2011; Cui *et al.*, 2018; Garcia *et al.*, 2010; Heidrich *et al.*, 2011). Moreover, nuclear-enriched EDS1 displays autoimmunity, suggesting an EDS1-PAD4 nuclear function (Stuttman *et al.*, 2016). However, it remains unclear if nucleocytoplasmic PAD4 is required to reside in the nucleus for immune function. Genetic and molecular studies revealed that activated NLR receptors stimulate EDS1-PAD4 basal immunity activity to transcriptionally boost SA and other immune pathways (Bartsch *et al.*, 2006; Bhandari *et al.*, 2019; Wang *et al.*, 2011; Zhou *et al.*, 1998). Notably, recent evidence indicates that PTI and ETI pathways are both required for pathogen resistance (Ngou *et al.*, 2020; Yuan *et al.*, 2020). Although cross-talk between PTI and EDS1-PAD4 is not well understood, PAD4 stimulates early PTI transcriptional changes, without stimulating MAP kinase signalling, suggesting a role for EDS1-PAD4 in PTI-ETI cross-talk (Cui *et al.*, 2017; Mine *et al.*, 2017a; Tsuda *et al.*, 2009; Wang *et al.*, 2009&2011).

Besides activating immune pathways that confer resistance to (hemi-) biotrophic pathogens, EDS1-PAD4 repress the jasmonic acid (JA) hormone pathway (Cui *et al.*, 2017&2018). Upon recognition of JA by its receptor CORONATINE INSENSITIVE 1 (COI1), JASMONATE ZIM DOMAIN (JAZ) proteins are ubiquitinated and degraded via the 26s proteasome, leading to the depression of the TFs MYC2/3/4 (Katsir *et al.*, 2008; Pieterse *et al.*, 2012; Wasternack & Song, 2017). These MYC TFs induce gene transcription changes that stimulate resistance to necrotrophic pathogens and antagonise EDS1-PAD4 and SA immune pathways. (Bhandari *et al.*, 2019; Cui *et al.*, 2017&2018; Glazebrook *et al.*, 2005; Pieterse *et al.*, 2012). The hemi-biotrophic pathogen *Pseudomonas syringae* pv. *tomato* strain DC3000 takes advantage of this antagonistic effect on EDS1-PAD4 by producing the virulence factor

coronatine, a mimic of bioactive JA-Isoleucine (Bhandari *et al.*, 2019; Brooks *et al.*, 2005; Cui *et al.*, 2018; Zheng *et al.*, 2012). The effect of coronatine on EDS1-PAD4 depends on the transcription factors *MYC2/3/4* that are regulated by JA- and abscisic acid- (ABA) signalling (Bhandari *et al.*, 2019; Cui *et al.*, 2018; Mine *et al.* 2017b; Pieterse *et al.*, 2012).

Beyond limiting pathogen growth locally, EDS1 and PAD4 are required for the activation of systemic acquired resistance (SAR), a signalling pathway that activates immunity genes in distal tissues (Fu & Dong, 2013; Hartmann & Zeier, 2019; Rietz *et al.*, 2011). In TNL-ETI, the enzymes *AGD2-LIKE DEFENSE RESPONSE PROTEIN 1 (ALD1)* and *FLAVIN MONOOXYGENASE1 (FMO1)* are induced in an EDS1, PAD4 and SAG101 dependent manner (Bartsch *et al.*, 2006; Bhandari *et al.*, 2019; Dongus *et al.*, 2020). ALD1 and FMO1 catalyse essential steps in the production of N-hydroxypipicolinic acid (NHP), which together with SA induce SAR in distal tissues (Hartmann & Zeier, 2019). Given the role of the EDS1-family in boosting SA levels and the production of NHP for systemic signalling, it becomes clear that EDS1-family immune signalling reaches farther than intracellular and paracrine signalling (Bartsch *et al.*, 2006; Bhandari *et al.*, 2019; Dongus *et al.*, 2020).

NLR receptors pre-date *ADR1*, *NRG1*, *TNLs*, and the *EDS1*-family, indicating that these signalling components are not required *per se* for a functional plant immune system (Baggs *et al.*, 2017&2019; Jacob *et al.*, 2013; Lapin *et al.*, 2019). However, *EDS1*, *PAD4* and *ADR1* always co-occur in angiosperm and gymnosperm species, while *SAG101*, *NRG1* and *TNLs* always co-occur in eudicots (Lapin *et al.*, 2019; Baggs *et al.*, 2019). This suggests that the *EDS1*-*PAD4*-*ADR1* and *EDS1*-*SAG101*-*NRG1*-*TNL* are conserved immune pathways in seed plants.

EDS1-family protein structure-function in immunity

EDS1, *PAD4* and *SAG101* are characterised by an N-terminal lipase-like domain (LLD) and a C-terminal *EDS1*-*PAD4* (EP) domain. The LLD shows an α/β hydrolase topology resembling eukaryotic class-3 lipase enzymes (Rauwerdink & Kazlauskas, 2015; Wagner *et al.*, 2013; Wang *et al.*, 2018). The EP domain is a unique domain on a structural and sequence level, and consists of α -helical bundles (PFAM database: PF18117; Wagner *et al.*, 2013). The *EDS1* and *PAD4*, but not *SAG101*, LLDs contain a canonical Ser-Asp-His (S-D-H) catalytic triad that is characteristic for α/β hydrolases (Wagner *et al.*, 2013; Rauwerdink & Kazlauskas, 2015). This Serine is part of the GXSXG motif found in lipases, which is conserved throughout *EDS1* and *PAD4* proteins across angiosperm and gymnosperm lineages (Wagner *et al.*, 2013). Strikingly, *Arabidopsis* *EDS1* and *PAD4* S-D-H triad residues are dispensable for *EDS1* and *PAD4*

function in immunity, indicative of a non-catalytic mechanism in pathogen resistance. Genetic and structural analyses support the hypothesis that the Arabidopsis EDS1-family proteins are pseudo-enzymes (Louis *et al.*, 2012a; Voss, *et al.*, 2019; Wagner *et al.*, 2013).

EDS1-family proteins form two types of stable and mutually exclusive heterodimers: EDS1-PAD4 and EDS1-SAG101 (Feys *et al.*, 2005; Lapin *et al.*, 2019; Rietz *et al.*, 2011; Wagner *et al.*, 2013). Arabidopsis EDS1-SAG101 crystal structure-analysis showed that the juxtaposed LLDs are major drivers of heterodimerisation, likely promoting association of the aligned EP domains to form the EDS1-SAG101 EP domain cavity (Bhandari *et al.*, 2019; Wagner *et al.*, 2013). The EDS1-SAG101 crystal structure functioned as a template to generate a structure model of the Arabidopsis EDS1-PAD4 heterodimer and showed a similar structure as EDS1-SAG101 (Figure I.2; Wagner *et al.* 2013). Notably, within EDS1, PAD4 and SAG101, EP

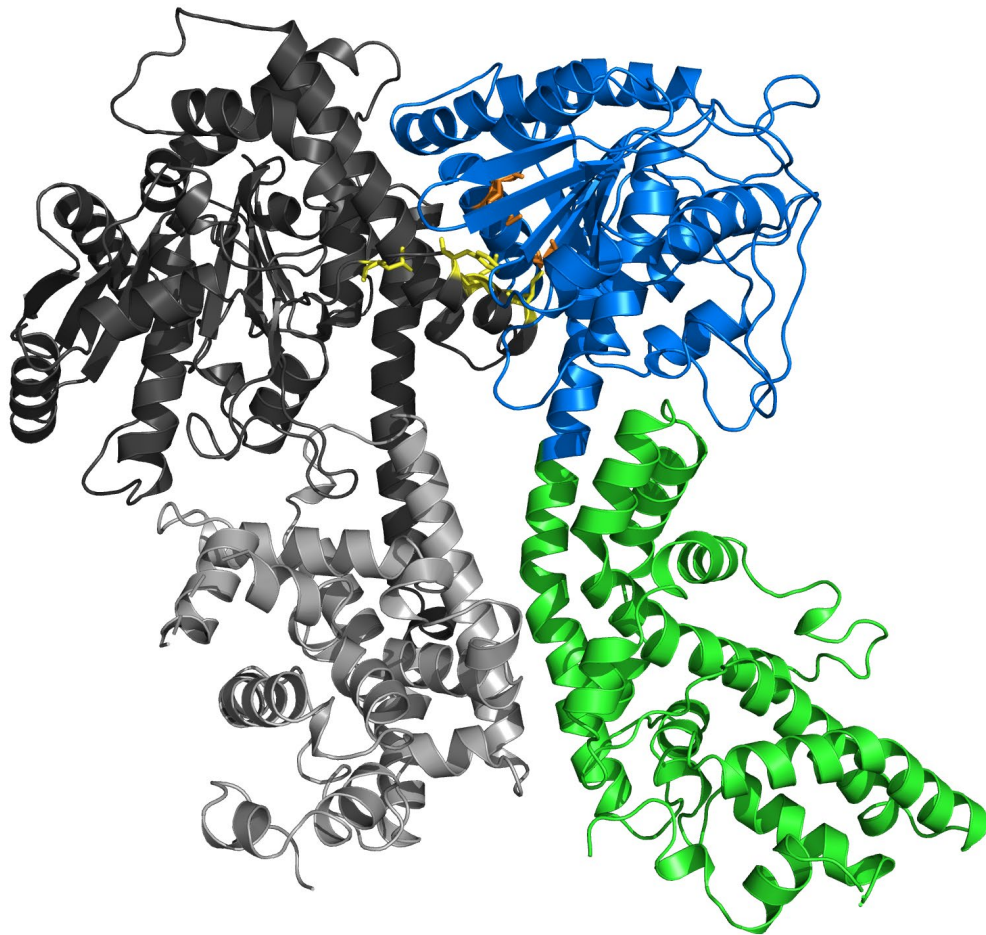


Figure I.2. EDS1-PAD4 structure model.

Arabidopsis EDS1-PAD4 heterodimer model (based on *AtEDS1-AtSAG101* crystal structure; Wagner *et al.*, 2013). EDS1^{LLD} (black), EDS1 EP domain (grey), PAD4^{LLD} (blue) and PAD4 EP domain (green) are represented in cartoon format. EDS1-PAD4-interacting motifs EDS1^{LLIF} and PAD4^{MLF} are coloured as yellow and orange sticks, respectively. Upon heterodimerisation EDS1-PAD4 EP domains form a cavity called the EP domain cavity.

domain cavity residues are highly conserved, suggesting a conserved function in immune signalling. Mutation of the EDS1^{LLIF}-motif and the juxtaposed PAD4^{MLF}-motif abolishes EDS1-PAD4/-SAG101 and EDS1-PAD4 heterodimerisation, respectively (Figure I.2; Rietz *et al.*, 2011; Wagner *et al.*, 2013). Consequently, EDS1^{LLIF} mutants fail to function in basal immunity and ETI (Wagner *et al.*, 2013), highlighting the importance of EDS1-PAD4/-SAG101 heterodimer formation in immunity.

EDS1^{LLD} alone forms heterodimers and is stable, however does not confer pathogen resistance in Arabidopsis, indicating that the EDS1 EP domain is crucial for immune signalling activity (Wagner *et al.*, 2013). Further structure-based analysis identified a surface lining the EDS1 EP domain cavity to be required for basal immunity and ETI in Arabidopsis (Bhandari *et al.*, 2019; Lapin *et al.*, 2019). Moreover, rapid transcriptional reprogramming of host cells in Arabidopsis TNL-ETI depends on this signalling surface (Bhandari *et al.*, 2019). Since EDS1-PAD4 heterodimerise and the EDS1 EP domain cavity functions in immunity, this suggests that the juxtaposed PAD4 EP domain also functions in immunity. However, insights in PAD4 structure-function remain limited (Bhandari *et al.*, 2019; Louis *et al.*, 2012a; Makandar *et al.*, 2015; Neubauer *et al.*, 2020).

SA-signalling in immunity

In Arabidopsis, the phytohormone SA functions in parallel to EDS1-PAD4 in resistance to biotrophic pathogens (Feys *et al.*, 2001; Glazebrook, 2005; Wiermer *et al.*, 2005; Zhou *et al.*, 1998). SA-biosynthesis genes are rapidly upregulated upon pathogen infection, which partially depends on EDS1-PAD4, leading to a rapid accumulation of SA (Bhandari *et al.*, 2019; Cui *et al.*, 2017; Mine *et al.*, 2017a; Wildermuth *et al.*, 2001). Pathogen-induced SA biosynthesis starts in the chloroplast, where ISOCHORISMATE SYNTHASE 1 (ICS1) converts chorismate to isochorismate (IC) (Wildermuth *et al.*, 2001). EDS5 (unrelated to EDS1) transports IC to the cytosol where AVRPPHB SUSCEPTIBLE 3 (PBS3) converts IC to IC-9-Glutamate (Ding & Ding, 2020; Rekhter *et al.*, 2019; Torrens-Spence *et al.*, 2019; Wildermuth *et al.*, 2001). Subsequently, ENHANCED PSEUDOMONAS SUSCEPTIBILITY (EPS1) converts IC-9-Glu to SA, a step that can also occur spontaneously (Torrens-Spence *et al.*, 2019).

The SA receptor NON-EXPRESSOR OF PR GENES 1 (NPR1) senses SA accumulation in Arabidopsis (Ding & Ding, 2020). When SA levels are low, NPR1 is degraded via the 26S proteasome, while the related SA receptors NPR3/4 function antagonistically to NPR1 by repressing SA-responsive genes (Ding & Ding, 2020). When SA levels are high, SA binds NPR3/4 and inhibits NPR3/4-mediated gene repression. Furthermore, SA binding to NPR1

leads to NPR1 stabilisation and relocation to the nucleus. In the nucleus, NPR1 interacts with TGACG-binding factor (TGA) and WRKY-motif TFs to stimulate expression of SA-responsive genes (Ding & Ding, 2020). Typical SA-responsive genes are *PATHOGENESIS RELATED1 (PRI)*, *ICS1* and *PBS3*, which in this thesis functioned as SA-marker genes (Bhandari *et al.*, 2019; Ding & Ding, 2020; Wildermuth *et al.*, 2001; Zhou *et al.*, 1998).

PAD4 responses to Green Peach Aphid

Besides pathogen immunity functions, Arabidopsis PAD4 mediates resistance to the green peach aphid (GPA, *Myzus persicae* Sülzer) (Pegadaraju *et al.*, 2005&2007; Louis & Shah, 2015). GPA population growth is higher on Arabidopsis *pad4* compared to wild-type (WT; Col-0 accession), *eds1*, *sag101* and *eds1/sag101* mutant plants, indicating PAD4 functions independently of EDS1 and SAG101 in GPA resistance (Pegadaraju *et al.*, 2007). GPA population growth on *pad4* is similar to mutants of other components in GPA resistance: *ACTIN-DEPOLYMERIZING FACTOR 3 (ADF3)* and *TREHALOSE PHOSPHATE SYNTHASE11 (TPS11)* (Mondal *et al.*, 2018; Singh *et al.*, 2011). Upon GPA infestation, *PAD4* transcripts are upregulated within 3 hpi and in particular at the leaf penetration site (Couldridge *et al.*, 2007; Louis *et al.*, 2012b; Pegadaraju *et al.*, 2005&2007). GPA-induced *PAD4* expression depends on *ADF3*, *TPS11* and trehalose accumulation (Hodge *et al.*, 2013; Mondal *et al.*, 2018; Singh *et al.*, 2011). Furthermore, the rice-endophytic bacterium *Bacillus velezensis* YC7010 boosts *AtPAD4* expression upon GPA infestation, leading to enhanced GPA resistance in Arabidopsis (Rashid *et al.*, 2017). This indicates the importance of *PAD4* upregulation upon GPA infestation, and the role of the plant-microbiota in plant defence (Hacquard *et al.*, 2017). Notably, *PAD4*-mediated defences against GPA do not depend on SA or camalexin production (Moran & Thompson, 2001; Pegadaraju *et al.*, 2005). In contrast to basal immunity and ETI, GPA resistance depends on the S-D-H triad residues PAD4^{S118} and PAD4^{D178}, but not PAD4^{H229} (Dongus *et al.*, 2020; Louis *et al.*, 2012a; Wagner *et al.*, 2013). These different requirements indicate that PAD4-functions in resistance to GPA are distinct from its immune function in the EDS1-PAD4 heterodimer.

Besides GPA resistance, *AtPAD4* induces leaf senescence upon GPA infestation and is required for GPA anti-xenosis (aphid-deterrence). Similar to GPA resistance, these processes do not require EDS1 and SAG101 (Louis *et al.*, 2012b; Pegadaraju, 2005; Pegadaraju *et al.*, 2007). Upon GPA infestation, PAD4 stimulates leaf senescence through the expression of a specific set of senescence-associated genes: *SAG13/21/27* (unrelated to SAG101) and through degradation of chlorophyll (Pegadaraju *et al.*, 2005&2007). In GPA anti-xenosis, GPA feeding-

preference is determined by a choice-assay. This shows that GPA prefer to settle on *pad4* mutants when compared to wild-type plants, suggesting PAD4 stimulates to production of a GPA repellent (Pegadaraju *et al.*, 2005&2007). However, the molecular mechanisms underlying PAD4-dependent GPA defences remain elusive (Louis & Shah, 2015).

Thesis Aims

Host-adapted pathogens utilise effectors to inhibit plant immunity signalling, however, plants evolved intracellular NLR receptors that can recognise these effectors. All tested TNLs, and certain CNLs, converge on the Arabidopsis EDS1-family, which functions as a signalling hub and activates local and systemic defence responses (Cui *et al.*, 2017; Feys *et al.*, 2005; Rietz *et al.*, 2011; Venugopal *et al.*, 2009; Wagner *et al.*, 2013). Although EDS1 can interact with certain TNLs and some effectors, it remains unclear how TNLs activate EDS1-PAD4, whether it be through direct binding or indirectly through TNL NADase activity (Bhattacharjee *et al.*, 2011; Heidrich *et al.*, 2011; Horsefield *et al.*, 2019; Kim *et al.*, 2012; Wan *et al.*, 2019). Similarly, the molecular mechanisms underlying EDS1-PAD4 transcriptional reprogramming and other downstream processes are not well understood (Bhattacharjee *et al.*, 2011; Bhandari *et al.*, 2019; Cui *et al.*, 2017&2018; Kim *et al.*, 2009; Kwon *et al.* 2009; Lapin *et al.*, 2019).

Structure-guided analyses revealed that EDS1-PAD4 heterodimerisation and the EDS1 EP domain cavity are essential for Arabidopsis immune signalling (Bhandari *et al.*, 2019; Lapin *et al.*, 2019; Rietz *et al.*, 2011; Wagner *et al.*, 2013). However, it remains unclear what the role of PAD4 in the EDS1-PAD4 heterodimer is. Independently of EDS1, PAD4 limits GPA infestation with its LLD located S-D-H triad (Pegadaraju *et al.*, 2005; Louis *et al.*, 2012a). In this thesis, I investigated the molecular function of *AtPAD4* in these resistance pathways. I investigated the properties of the PAD4^{LLD}, without its EP domain, in resistance to GPA and pathogen immunity (Chapter 1; parts of this chapter were published in Dongus *et al.* (2020)). Subsequently, I used structure-guided mutagenesis to investigate the role of the PAD4 EP domain cavity in these resistance pathways (Chapter 2). I performed immunoprecipitation coupled to mass spectrometry on PAD4 in pathogen challenged Arabidopsis plants to identify PAD4 signalling-complexes in TNL-ETI (Chapter 3). Lastly, I aimed to determine the contribution of nuclear and cytoplasmic located PAD4 to pathogen immunity (Chapter 4), and I investigated which genetic and PAD4 structural components are required for a PAD4 induced autoimmune phenotype.

Chapter 1: Arabidopsis PAD4 lipase-like domain is sufficient for resistance to green peach aphid

Arabidopsis PAD4 controls defences against (hemi-) biotrophic pathogens and Green Peach Aphids (GPA) (Cui *et al.*, 2017; Glazebrook *et al.*, 1997; Feys *et al.*, 2005; Pegadaraju *et al.*, 2005). PAD4 consists of two domains, the lipase-like domain (LLD) and the EP domain, however to what extent these domains contribute to these defence responses remains elusive. To gain a deeper insight in the molecular function of PAD4, I investigate here the properties of the PAD4^{LLD} in resistance to GPA and pathogen immunity. Parts of this chapter have been published in Dongus *et al.* (2020).

PAD4^{LLD} does not interact with EDS1

To test PAD4^{LLD} properties, I generated a PAD4^{LLD} protein (Figure 1.1A; blue; residues 1-299) by introducing a stop codon at PAD4^{S300}. First, I set out to determine whether PAD4^{LLD} is still able to interact with EDS1. EDS1-PAD4 heterodimer formation is driven chiefly by specific motifs in the EDS1 and PAD4 lipase-like domains. In EDS1 this is the hydrophobic loop forming EDS1^{LLIF} motif (α -helix H; Figure 1.1A&B; orange), and the juxtaposed PAD4^{MLF} motif (Figure 1.1A&B; yellow; Feys *et al.*, 2001; Wagner *et al.*, 2013). To determine whether this truncated protein is stable and able to interact with EDS1, I transiently overexpressed GFP-tagged PAD4^{LLD} in *N. benthamiana* leaves. PAD4^{LLD} accumulated to similar levels as PAD4^{WT} (Figure 1.1D), however PAD4^{LLD} was unable to co-immunoprecipitate (co-IP) FLAG-tagged EDS1, whereas full-length GFP-PAD4 did (Figure 1.1D). This interaction was also tested using the split-luciferase (LUC) system in *N. benthamiana* (Gehl *et al.*, 2011), where N-terminal LUC (^NLUC) tagged PAD4^{LLD} also failed to interact with C-terminal LUC (^CLUC) tagged EDS1 (Figure 1.1D). This indicates that the interaction between PAD4 and EDS1 depends on the PAD4 EP domain.

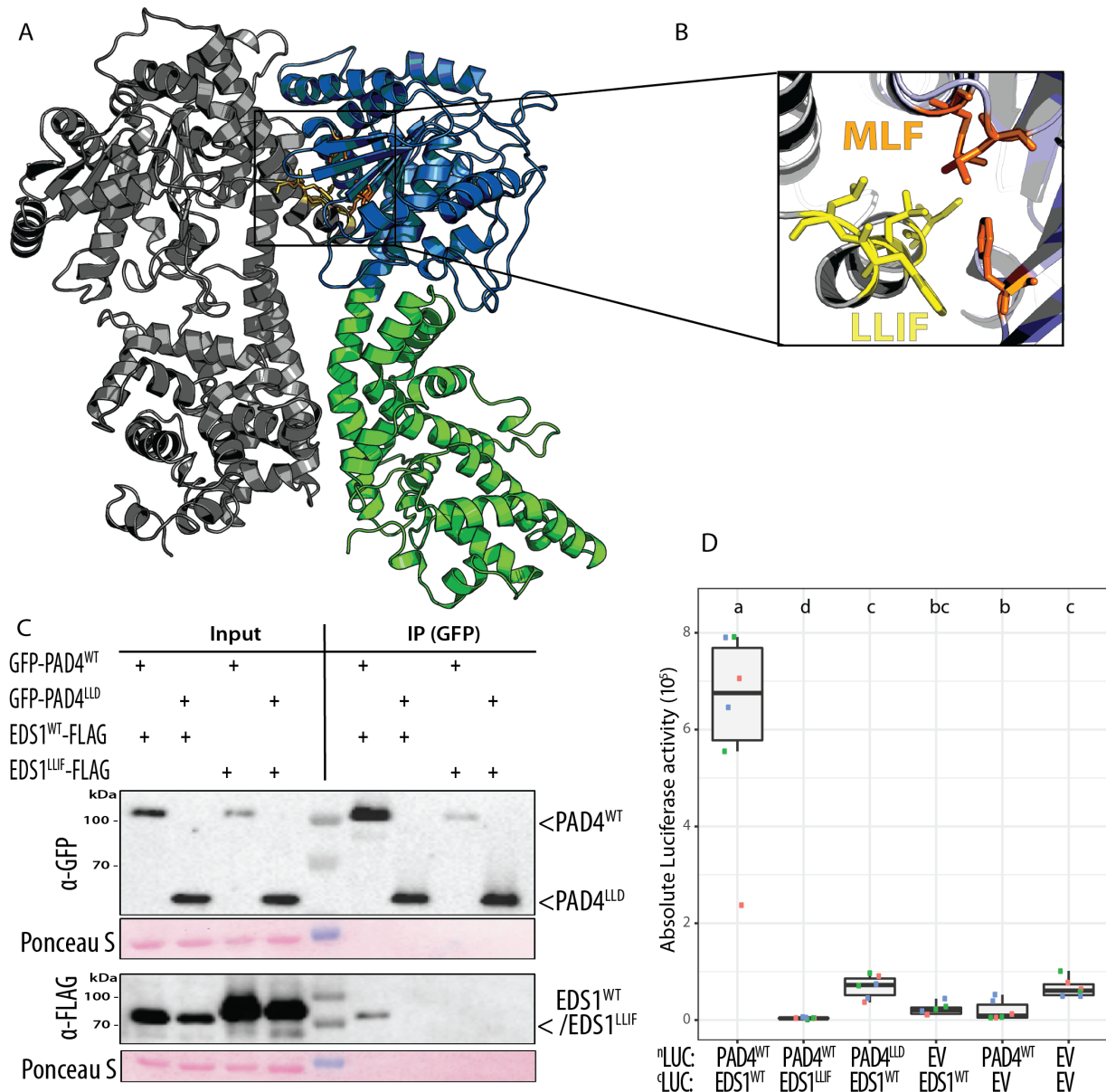


Figure 1.1. PAD4^{LLD} does not interact with EDS1.

A. *Arabidopsis* EDS1-PAD4 heterodimer model (based on *At*EDS1-*At*SAG101 crystal structure; Wagner *et al.*, 2013). EDS1 (grey), PAD4^{LLD} (blue) and PAD4 EP domain (green) are represented in cartoon format. **B.** EDS1-PAD4-interacting motifs EDS1^{LLIF} and PAD4^{MLF} are colored as yellow and orange sticks, respectively. **C.** Co-immunoprecipitation (GFP-trap) of GFP-PAD4^{WT}/PAD4^{LLD} with EDS1^{WT}/EDS1^{LLIF}-3xFLAG transiently co-expressed in *N. benthamiana* leaves (using 35S:*GFP-PAD4*^{WT}/*PAD4*^{LLD} and 35S:*EDS1*^{WT}/*EDS1*^{LLIF}-3xFLAG constructs, respectively). Left: all proteins are expressed in the input. Right: in the IP fraction only EDS1^{WT} co-immunoprecipitates with PAD4^{WT} (positive control). A representative image from three independent experiments is shown. **D.** Absolute luciferase activity from transiently co-expressed ⁿLUC or ^cLUC constructs (35S promoter) in *N. benthamiana*. Data are pooled from three independent experiments with two biological replicates per experiment (n = 6). Colors indicate samples from one independent experiment. Letters indicate statistical significance as determined by one-way ANOVA with multiple testing correction using Tukey-HSD; p < 0.01. C, D generated with Lucas Dijkgraaf.

EDS1^{LLD} does not interact with PAD4

The EDS1-PAD4 interaction depends on the PAD4 EP domain (Figure 1.1). Since the EDS1 and PAD4 EP domains are juxtaposed, the only domain that the PAD4 EP domain could interact with is the EDS1 EP domain. This suggests that PAD4 EP domain interacts with the EDS1 EP domain. However, this is in conflict with Yeast-2-Hybrid (Y2H) data published in Wagner *et al.*, 2013, where EDS1^{LLD} (Residues 1-384; Wagner *et al.*, 2013) is sufficient to interact with PAD4. Thus, my observation that the PAD4^{LLD} is insufficient to interact with EDS1 *in planta* was unexpected. To determine whether the observations in Y2H are representative for the situation *in planta*, I assessed EDS1^{LLD} binding to PAD4 in *N. benthamiana* by co-IP and split-LUC. EDS1^{LLD} did not associate to PAD4 *in planta* (Figure 1.3), indicating that EDS1 and PAD4 require their EP domain for heterodimerisation.

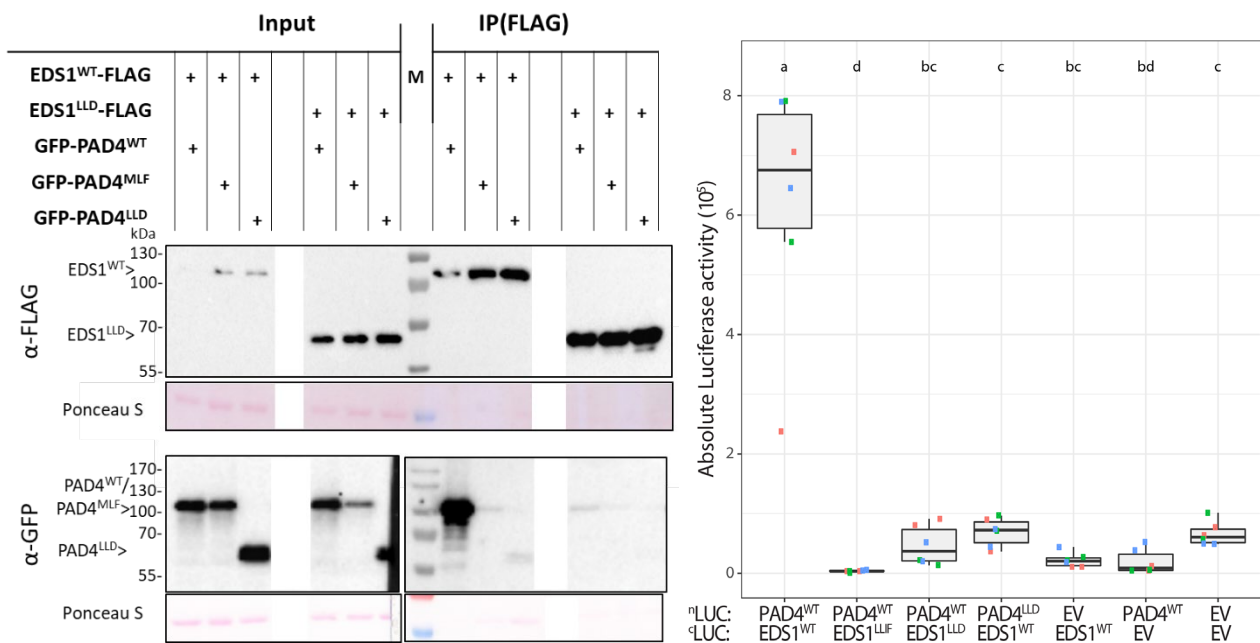


Figure 1.2. EDS1^{LLD} does not interact with PAD4.

Left panel: Transiently expressed PAD4^{LLD} co-expressed with EDS1 and EDS1^{LLD} in *N. benthamiana* leaf tissue. FLAG-bead (Sigma) co-IP performed on tissue harvested 3 days post-infiltration. Wild-type PAD4 is used as a positive control and PAD4^{MLF} as a negative control. A representative image from three independent experiments is shown. Blanked out parts in blots are from a co-IP sample not related to PAD4^{LLD} and EDS1^{LLD}. Right panel: Absolute luciferase (LUC) activity from transiently co-expressed ⁿLUC or ^cLUC constructs (35S promoter) in *N. benthamiana*. Data are pooled from three independent experiments with two biological replicates per experiment (n = 6). Colors indicate samples from one independent experiment. Letters indicate statistical significance as determined by one-way ANOVA with multiple testing correction using Tukey-HSD; *p* < 0.01. Right panel generated by Lucas Dijkgraaf.

SAG101^{LLD} does not interact with EDS1

The results discussed above suggest that the EDS1-PAD4 interaction *in planta* requires a specific surface within PAD4 EP domain to interact with the EDS1 EP domain. This interface would function in addition to the EDS1^{LLIF} and PAD4^{MLF} motifs (Rietz *et al.*, 2011; Wagner *et al.*, 2013). To determine which region of the PAD4 EP domain interacts with EDS1, I designed PAD4 truncations with increasingly larger parts of the PAD4 EP domain added to the PAD4^{LLD}, *i.e.* PAD4¹⁻³³¹, PAD4¹⁻⁴⁰⁸ and PAD4¹⁻⁴⁷⁰ (Figure 1.3, left panel). Stop codons were introduced in the transition zone of two α -helices to maintain proper protein folding. In addition, to investigate if PAD4 its paralog, SAG101, behaves similar to PAD4 in EDS1 heterodimerisation, I also generated SAG101 truncations, *i.e.* SAG101^{LLD} (residues 1-303), SAG101¹⁻³¹⁹, SAG101¹⁻³⁹⁸, SAG101¹⁻⁴⁶³ (Figure 1.3, right panel). I designed these SAG101 truncations in such a way that they resembled the PAD4 truncations as much as possible. For this, I made use of protein alignments and their protein structure models.

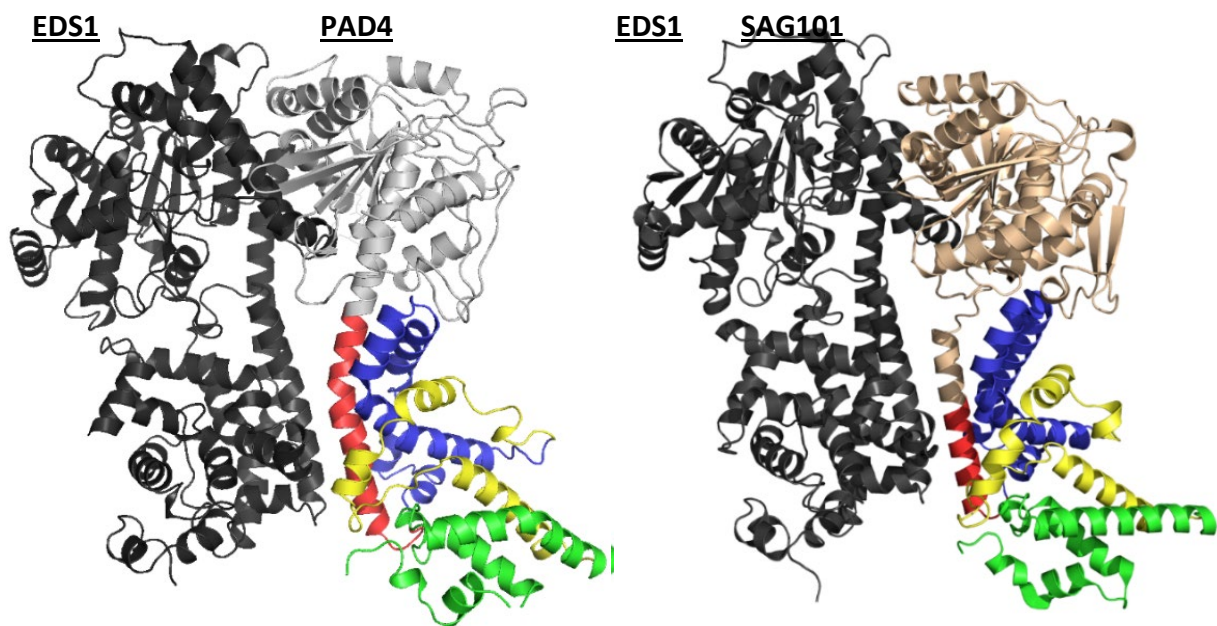


Figure 1.3. Structure models of PAD4 and SAG101 truncations in a complex with EDS1. Arabidopsis EDS1-PAD4 structure model in left panel (Wagner *et al.*, 2013) Arabidopsis EDS1-SAG101 crystal structure in right panel (Wagner *et al.*, 2013). PAD4^{LLD} is shown in grey, SAG101^{LLD} is shown in crème. Different truncations were made by sequentially adding an EP domain region highlighted in red, blue, yellow and green to PAD4^{LLD} and SAG101^{LLD}. Region added to obtain PAD4¹⁻³³¹/SAG101¹⁻³¹⁹ is shown in red. Region added to obtain PAD4¹⁻⁴⁰⁸/SAG101¹⁻³⁹⁸ is shown in blue. Region added to obtain PAD4¹⁻⁴⁷⁰/SAG101¹⁻⁴⁶³ is shown in yellow. Remaining region belonging to full length PAD4 (1-541) and full-length SAG101(1-537) is shown in green. EDS1-PAD4 structure model and EDS1-SAG101 structure were adapted from Wagner *et al.*, 2013.

PAD4 and SAG101 truncations were co-expressed with EDS1 in *N. benthamiana*, and protein accumulation and EDS1 binding was assessed by co-IP (Figure 1.4). The two shortest truncations; PAD4^{LLD} & SAG101^{LLD} and PAD4¹⁻³³¹ & SAG101¹⁻³¹⁹ (Figure 1.3; grey and red) accumulated to similar levels as the full-length protein (Figure 1.3). The two longest PAD4 and SAG101 truncations (Figure 1.3, PAD4¹⁻⁴⁰⁸ & SAG101¹⁻³⁹⁸: blue; PAD4¹⁻⁴⁷⁰ & SAG101¹⁻⁴⁶³: yellow) accumulate very weakly, where PAD4¹⁻⁴⁷⁰ accumulates more than PAD4¹⁻⁴⁰⁸ (Figure 1.4). This suggests that the EP domain residues are destabilizing the proteins and require the LLD and the last six α -helices to stabilize the proteins (Figure 1.3; yellow and green). Notably, none of the PAD4 and SAG101 truncations interacted with EDS1 (Figure 1.4). Furthermore, split-LUC confirmed that SAG101^{LLD} does not interact with EDS1, which also revealed that EDS1^{LLD} also does not interact with SAG101 (Figure 1.5).

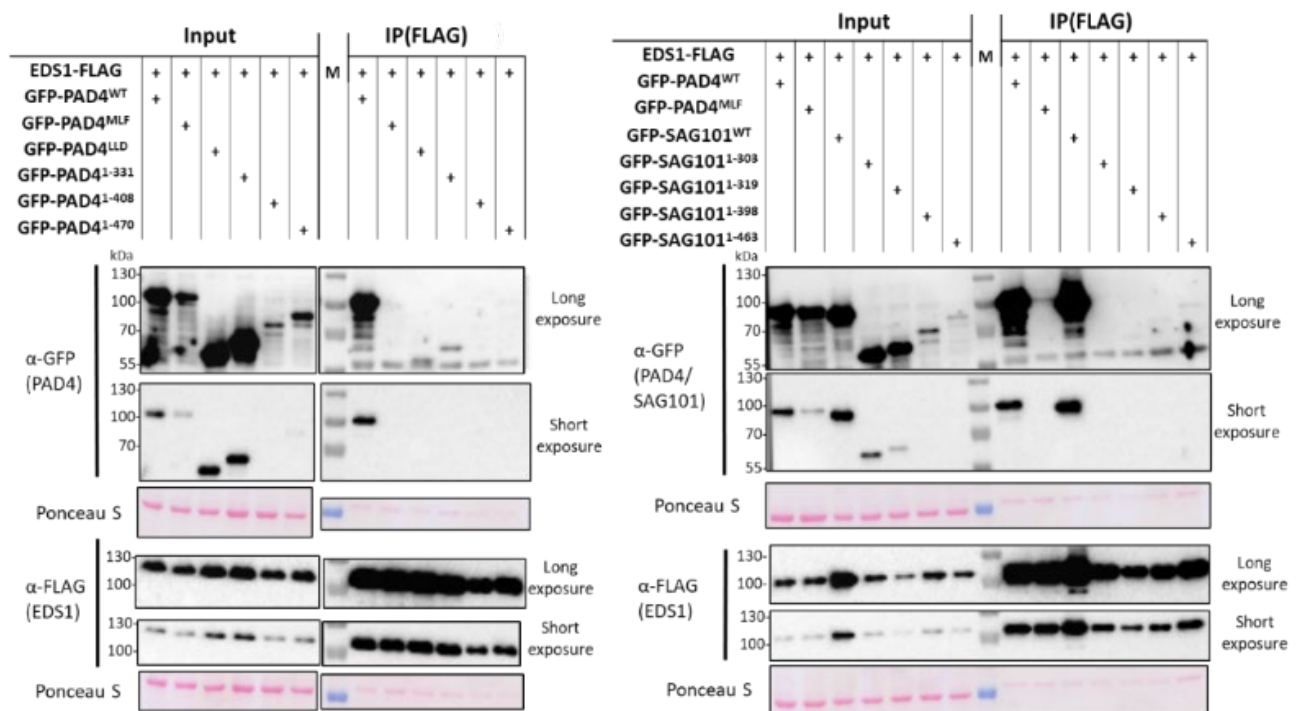


Figure 1.4. PAD4 and SAG101 truncations do not interact with EDS1.

PAD4 (left panel) and SAG101 (right panel) truncations expressed under the 35S promoter co-expressed with 35S::gEDS1-3xFLAG in *N. benthamiana* leaf tissue. FLAG-bead (Sigma) co-IP performed on tissue harvested 3 days post-infiltration. Wild-type PAD4 is used as a positive control and PAD4^{MLF} as a negative control for EDS1 interaction. Similar results were obtained in three other independent biological replicates.

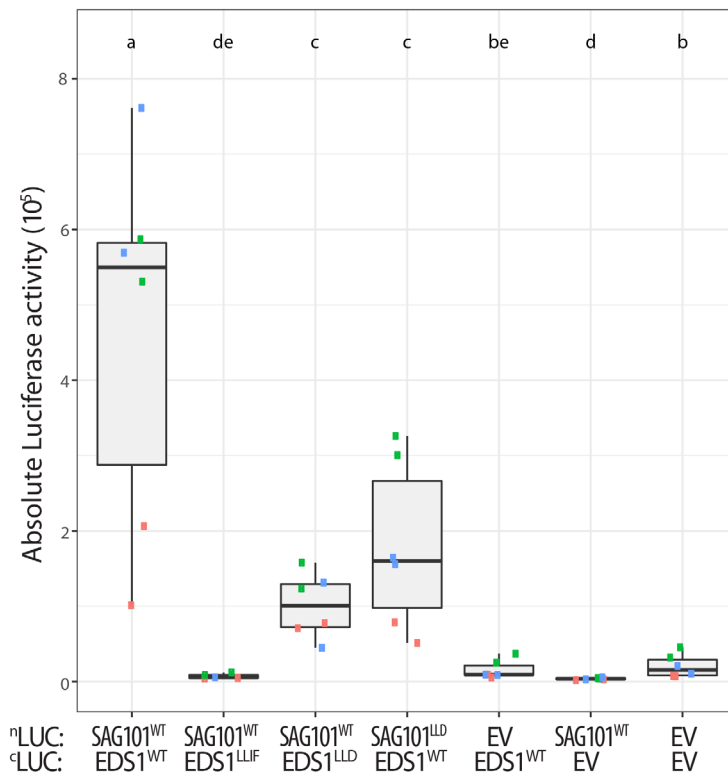


Figure 1.5. EDS1 and SAG101 require their EP domain to interact with one another.

Absolute luciferase (LUC) activity from transiently co-expressed ^NLUC or ^CLUC constructs (35S promoter) in *N. benthamiana*. Data are pooled from three independent experiments with two biological replicates per experiment (n = 6). Colors indicate samples from one independent experiment. Letters indicate statistical significance as determined by one-way ANOVA with multiple testing correction using Tukey-HSD; *p* < 0.01. Data generated by Lucas Dijkgraaf.

In conclusion, these experiments were unable to identify a region in PAD4 and SAG101 EP domains required for EDS1 binding. I hypothesize that the longer truncations do contain an EDS1 binding surface, however, the PAD4 and SAG101 truncations were too unstable to gain insight in EDS1-PAD4 and EDS1-SAG101 heterodimerisation. Furthermore, these results indicate that the interactions between the EDS1-family members are more sophisticated than the current model proposes, where EDS1^{LLIF} and PAD4^{MLF} are the only drivers of heterodimer formation in *Arabidopsis* (Wagner *et al.*, 2013). Taken together, these results indicate that all three members of the EDS1-family require their EP domain for interaction with their partner(s).

PAD4^{LLD} is a stable protein and localizes to the nucleus and cytoplasm

To study the functions of the PAD4^{LLD}, I introduced WT *PAD4* (*pPAD4:StrepII-YFP-cPAD4^{WT}*) or PAD4^{LLD} (*pPAD4:StrepII-YFP-cPAD4^{LLD}*) constructs into *Arabidopsis* (*pad4-1/sag101-3* mutant; Col-0). Two independent stable transgenic PAD4^{LLD} lines exhibited nucleocytoplasmic localisation similar to PAD4^{WT} at 24 h post infection (hpi) with *Pseudomonas syringae* pv. *tomato* (*Pst*) strain DC3000 expressing the effector *avrRps4* (*Pst avrRps4*) (Figure 1.6). *Pst avrRps4* delivers the effector *avrRps4*, which triggers ETI in Col-0 induced by the receptor pair RRS1-S/RPS4 (Birker *et al.*, 2009; Heidrich *et al.*, 2011; Narusaka *et al.*, 2009; Saucet *et al.*, 2015).

PAD4^{LLD} subcellular distribution is in line with previously described nucleocytoplasmic localisations of EDS1^{LLD} and PAD4^{LLD}/SAG101^{EP domain} chimeras *in planta* (Lapin *et al.*, 2019; Wagner *et al.*, 2013). PAD4^{LLD} was also detected in leaf samples treated with *Pst avrRps4* at 24 hpi using immune-detection (western blot), although at much lower levels compared to PAD4^{WT} lines (Figure 1.7A). This is in contrast to my observation in *N. benthamiana* transient assays, where PAD4^{LLD} and PAD4^{WT} accumulation was similar (Figure 1.1D). The reduction in PAD4^{LLD} protein relative to PAD4^{WT} in mock- and *Pst avrRps4*-treated *Arabidopsis* leaves can be partially attributed to lower accumulation of *PAD4* transcripts in *PAD4*^{LLD} lines compared to PAD4^{WT} lines (Figure 1.7B). In summary, PAD4^{LLD} is sufficient to maintain a WT-like nucleocytoplasmic localisation, but loss of the EP domain substantially reduces PAD4 steady-state levels in *Arabidopsis* and PAD4-EDS1 interaction.

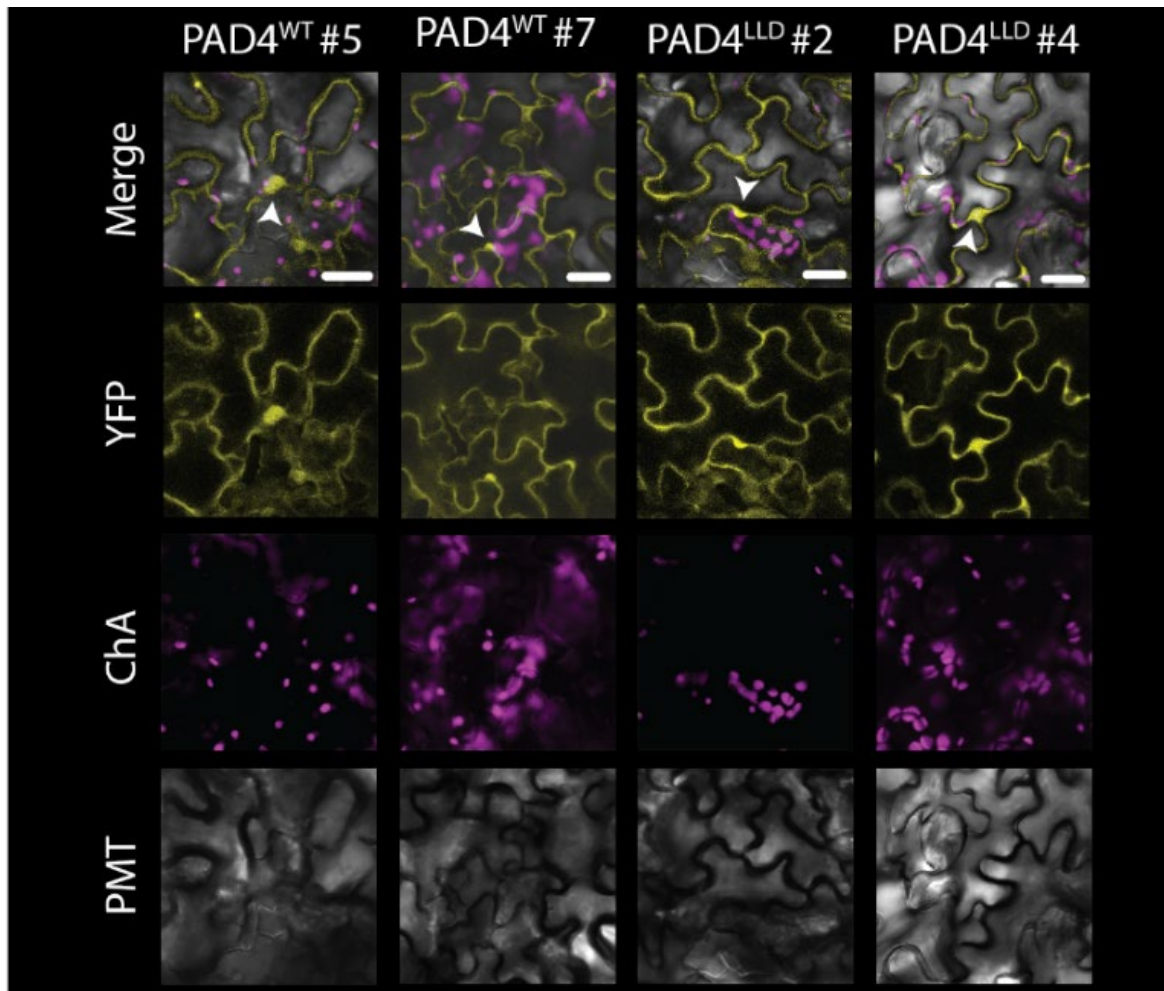
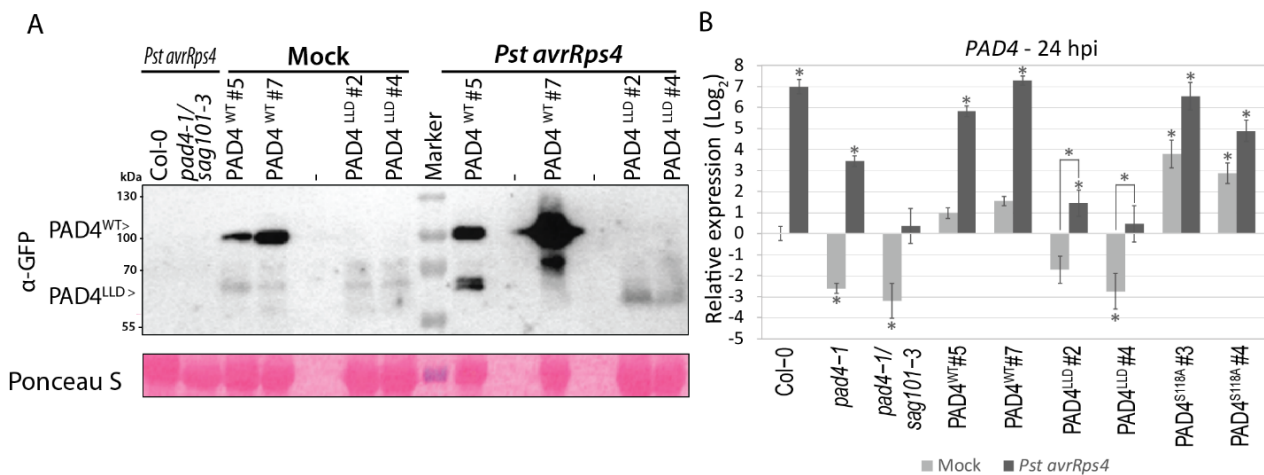


Figure 1.6. PAD4 localisation at 24 hpi with *Pst avrRps4*.

Nucleocytoplasmic localisation of YFP-PAD4^{WT} and YFP-PAD4^{LLD} in *Arabidopsis* transgenic lines (24 hpi, *Pst avrRps4*). I enhanced the confocal microscope sensitivity to determine PAD4 localisation. White arrowhead = nuclei; white bar = 20 μ m. Similar results were obtained in two independent replicates in two biological replicates (n=4). ChA: chlorophyll A (auto-fluorescence); PMT: photon multiplier tube (bright field).

Expression of PAD4^{LLD} confers GPA resistance

In GPA resistance, PAD4 acts independently of EDS1 and was previously shown to be dependent on the PAD4^{LLD} located S¹¹⁸ and D¹⁷⁸, but not H²²⁹. These amino acids are predicted α/β -hydrolase catalytic triad residues (Figure 1.8B&C) (Louis *et al.*, 2012a; Pegadaraju 2007). Since PAD4^{LLD} accumulates in Arabidopsis, we tested whether the PAD4^{LLD} alone is sufficient to restrict aphid population growth. Consistent with previously published data, *pad4-1*, *pad4-1/sag101-3* and PAD4^{S118A} lines (in *pad4-1/eds1-2/EDS1^{SDH}*; Wagner *et al.*, 2013) showed a significant increase in aphid population size compared to Col-0 in a no-choice bioassay (Figure 1.8A) (Louis *et al.*, 2012a; Pegadaraju *et al.*, 2007). The PAD4^{LLD} lines harboured a GPA population at 11 dpi similar to PAD4^{WT} and Col-0, even though these lines expressed low levels of PAD4^{LLD} (Figure 1.7A). Thus, indicating PAD4^{LLD} is sufficient in resistance to GPA infestation. Furthermore, low steady state accumulation of PAD4^{LLD} protein (Figure 1.7A) is sufficient to counter GPA infestation in Arabidopsis. This implies that PAD4^{LLD} has an *in planta* activity. Based on these observations I conclude that PAD4^{LLD} is a stable protein entity able to confer resistance to GPA.



Arabidopsis ETI and basal immunity require full-length PAD4

PAD4^{LLD} lines were as resistant as Col-0 against GPA. To test whether PAD4^{LLD} also functions in EDS1-dependent immunity, I tested basal immunity and TNL-triggered pathogen immunity. Firstly, I measured TNL-ETI using the filamentous biotrophic pathogen *Hyaloperonospora arabidopsidis* (*Hpa*) isolate EMWA1, which is recognized in Col-0 by the TNL *RPP4* (*RESISTANCE TO PERONOSPORA PARASITICA4*) (Van der Biezen *et al.*, 2002; Asai *et al.*, 2018). Col-0, PAD4^{WT} and PAD4^{S118A} lines were resistant to *Hpa* EMWA1, as measured by conidiospore production and based on macroscopic disease and microscopic *Hpa* colonisation phenotypes (Figure 1.9A-C). By contrast, PAD4^{LLD} transgenic lines were fully susceptible, showing conidiospore production and macroscopic and microscopic disease phenotypes resembling *pad4-1/sag101-3* mutants (Figure 1.9A-C).

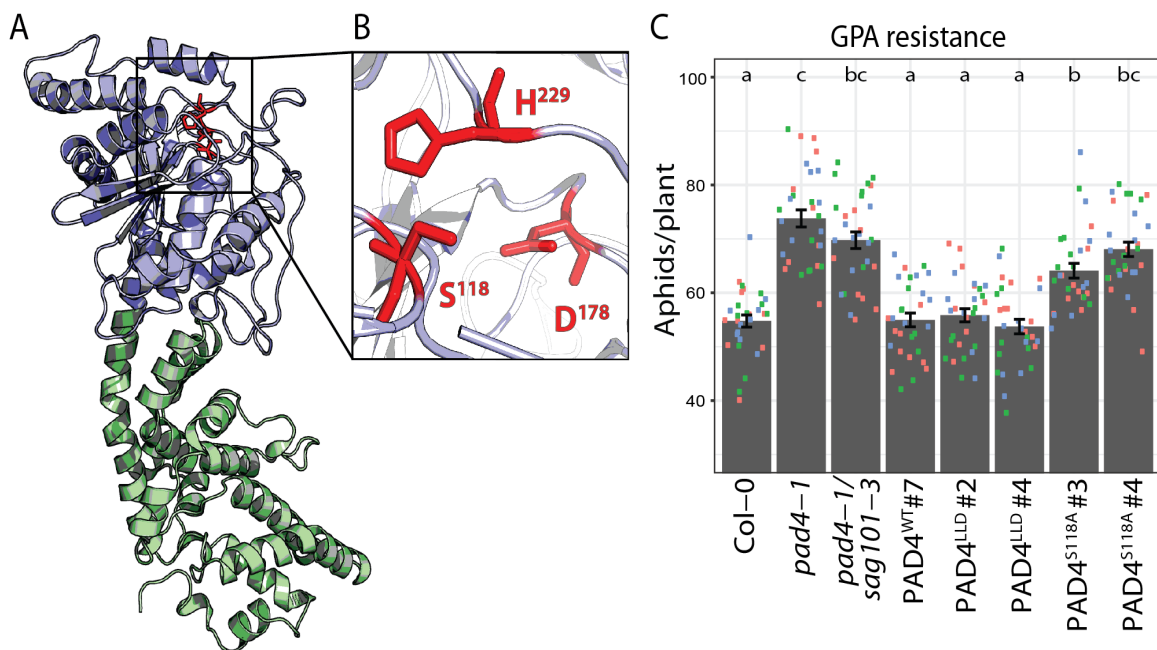


Figure 1.8. PAD4^{LLD} is sufficient for GPA resistance.

A. AtPAD4 monomer model (based on *AtEDS1-AtSAG101* crystal structure; Wagner *et al.*, 2013). PAD4^{LLD} (blue) and PAD4 EP domain (green) are represented in cartoon format. **B.** PAD4 S-D-H triad residues (red). **C.** Numbers of green peach aphids (GPA) per plant at 11 days post-infestation in a no-choice assay. Data are pooled from three independent experiments each with ten biological replicates per experiment ($n = 30$). Squares of the same color represent ten biological replicates in an independent experiment. Bars represent the mean of three experimental replicates \pm SE. Differences between genotypes were determined using ANOVA (Tukey-HSD, $p < 0.01$), letters indicate significance class. GPA data generated by Monika Patel, Lani Archer and Jyoti Shah (University of North Texas).

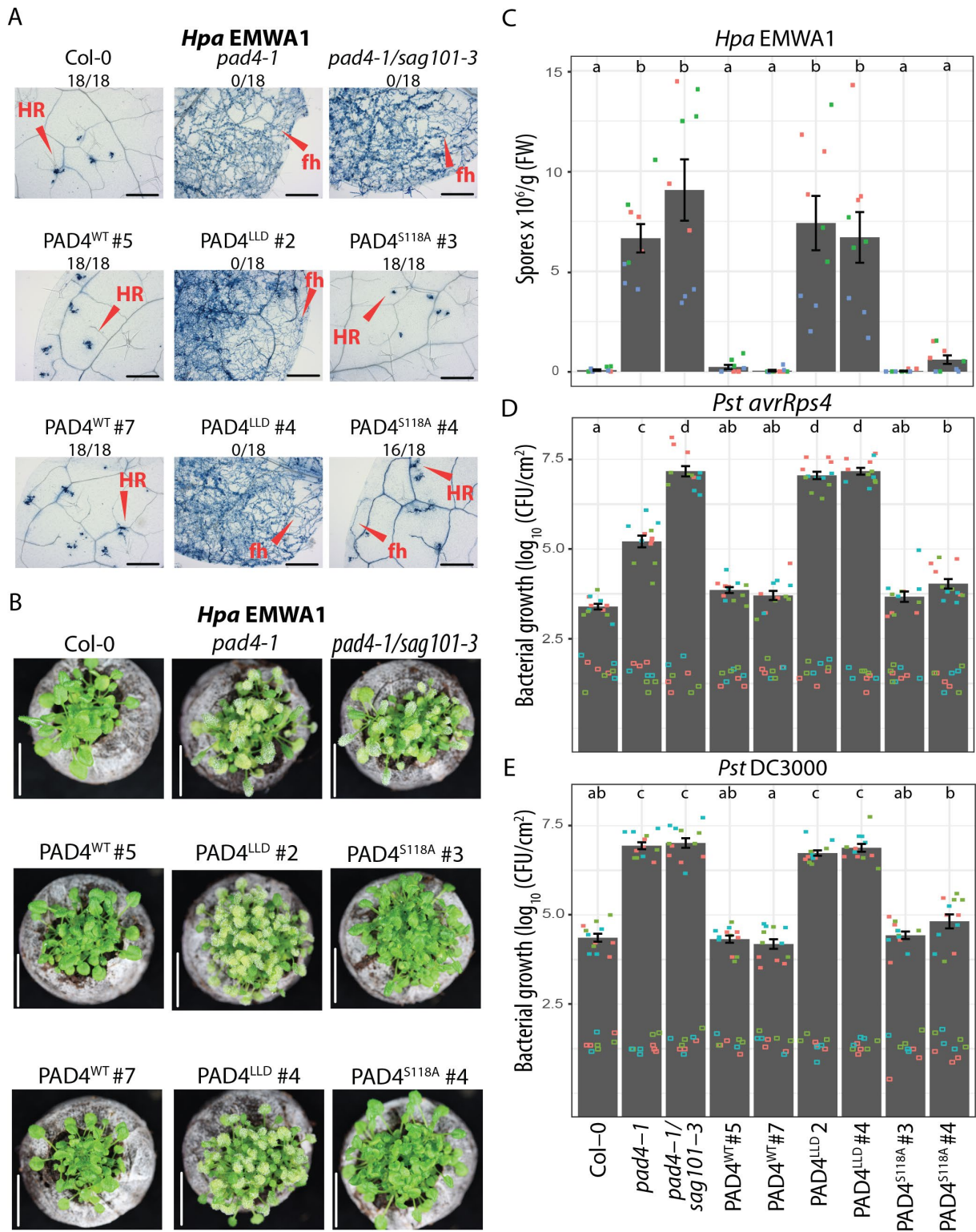


Figure 1.9. PAD4^{LLD} is not functional in *Arabidopsis* basal immunity and ETI.

A. Microscopic immunity phenotypes of 3-week-old *Arabidopsis* lines, as indicated, at 6 dpi with *Hpa* isolate EMWA1 (recognized by TNL RPP4). Col-0 (resistant), *pad4-1* (susceptible) and *pad4-1/sag101-3* (susceptible) functioned as controls. Trypan blue-stained leaves showing free hyphae (fh) and hypersensitive cell death (Hypersensitive Response (HR)). Black bars represent 500 μ m. Fractions (e.g. 18/18) indicate numbers of resistant leaves/total plants tested. Pictures are representative from three independent experimental replicates, > 6 leaves per replicate and > 30 infection sites per genotype. *Figure legend continues on next page.*

In addition, I tested PAD4^{LLD} function in basal immunity to virulent *Pst* DC3000, and in TNL (RRS1-S/RPS4) ETI to *Pst avrRps4*. In basal immunity, *pad4-1* was as susceptible as *pad4-1/sag101-3* while in ETI, *pad4-1* displays intermediate susceptibility between Col-0 and *pad4-1/sag101-3* (Figure 1.9D&E) (Feys *et al.*, 2005; Wagner *et al.*, 2013). In both basal immunity and ETI, PAD4^{S118A} was as resistant as Col-0 and PAD4^{WT}, which is consistent with previous findings that the PAD4 S-D-H predicted catalytic triad is not required for pathogen immunity (Figure 1.9D&E) (Louis *et al.*, 2012a; Wagner *et al.*, 2013). In contrast to GPA resistance, PAD4^{LLD} lines were fully susceptible to *Pst* DC3000 and *Pst avrRps4*, showing similar bacterial growth to *pad4-1/sag101-3* (Figure 1.9D&E). This indicates that PAD4^{LLD} is unable to activate basal immunity and ETI. Moreover, this suggests that PAD4 relies on its EP domain for immune functions. To determine the contribution of PAD4^{LLD} in immune signalling, I quantified the expression of defence marker genes 24 hpi with *Pst avrRps4*. This showed that PAD4^{LLD}, similar to *pad4-1/sag101-3*, is unable to induce defence marker gene expression (Figure 1.10). This indicates that PAD4^{LLD} is unable induce TNL-ETI signalling.

In conclusion, EDS1-family proteins required their EP domain for stable heterodimer formation, and did not only exclusively rely on their LLDs (Figure 1.1-5). Furthermore, this analysis of the Arabidopsis PAD4^{LLD} demonstrates a domain-specific partitioning of defence functions. The PAD4^{LLD} was necessary and sufficient for limiting GPA infestation (Figure 1.7), while the PAD4 EP domain (with the LLD) mediated pathogen immunity signalling (Figure 1.8&9). This indicated that the PAD4 EP domain plays a critical role in these immune responses. In the next chapter I investigated the role of the PAD4 EP domain in ETI and basal immunity.

Figure 1.9. PAD4^{LLD} is not functional in Arabidopsis basal immunity and ETI (continued).

B. *Hpa* EMWA1-inoculated plants of the same lines as in A. Resistant plants look healthy at 6 dpi, whereas susceptible plants produce conidiospores and leaf chlorosis. White bars correspond to 2 cm. **C.** TNL (RPP4) ETI assay in Arabidopsis independent transgenic lines with wild-type and mutant controls, as in A. *Hpa* EMWA1 conidiospores on leaves were quantified at 6 dpi in three independent experiments (squares; n=9). Squares of the same color represent three biological replicates in an independent experiment. Bars represent the mean of three experimental replicates \pm SE. Differences between genotypes were determined using ANOVA (Tukey-HSD, p <0.01), letters indicate significance class. **D.** TNL (RRS1-S/RPS4) ETI assay in the same Arabidopsis independent transgenic and control lines as in A. Four-week old Arabidopsis plants were syringe infiltrated with *Pst avrRps4* (OD₆₀₀ = 0.0005) and bacterial titers were determined at 0 dpi (empty squares; n=8-9) and 3 dpi (filled squares; n=11-12). Squares of the same color represent 2-3 (day 0) or 3-4 (day 3) biological replicates in an independent experiment. **E.** Infection assay was performed with basal immunity triggering *Pst* DC3000 (OD₆₀₀ = 0.0005). Experimental set-up as in D and statistical analysis as in C.

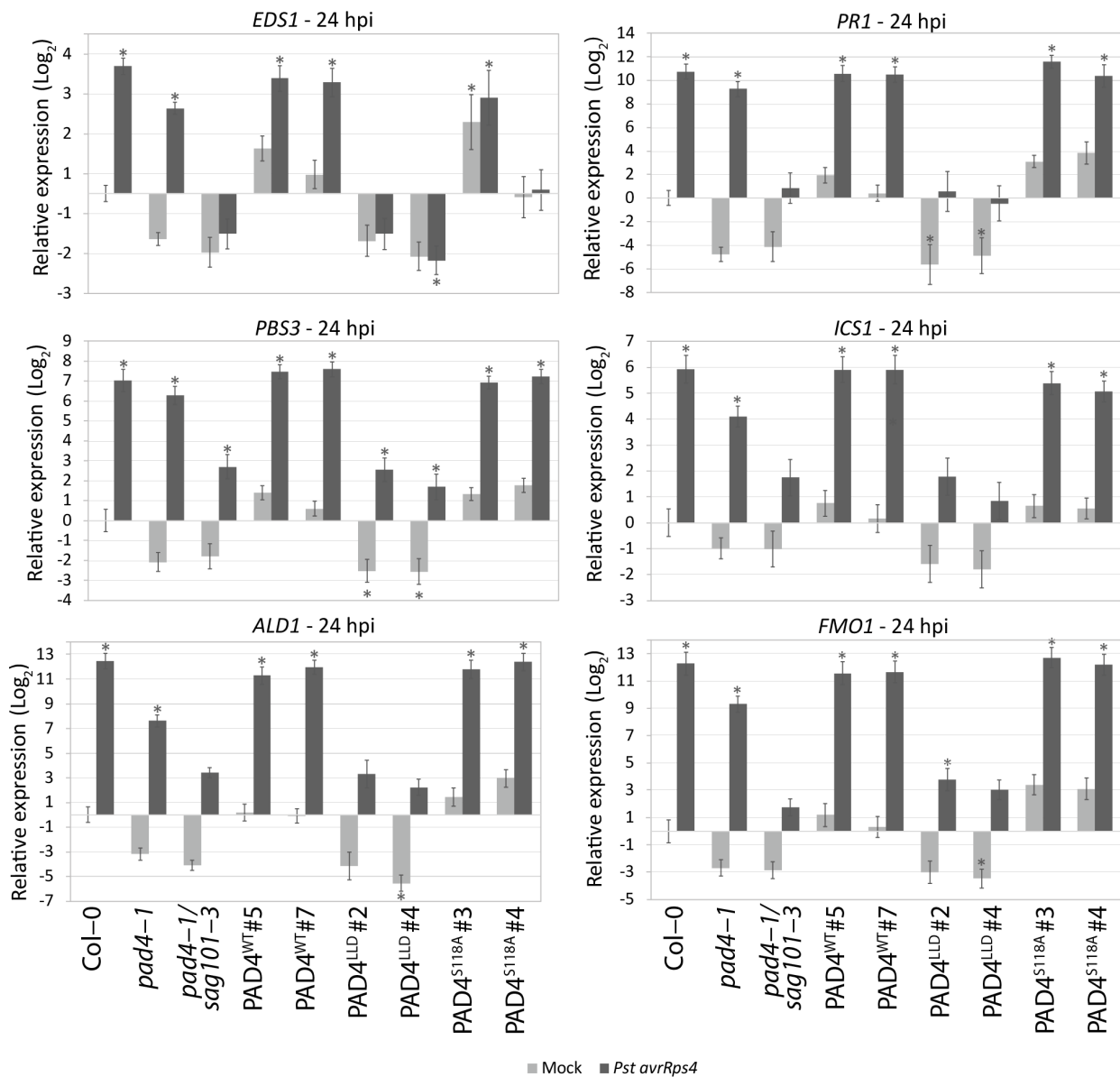


Figure 1.10. PAD4^{LLD} is not able to induce immune marker genes during *Pst avrRps4* triggered ETI. Transcript abundance determined by qRT-PCR in 4-week old Arabidopsis plants syringe-infiltrated with either buffer (mock, grey bars) or *Pst avrRps4* (black bars) (24 hpi). Data are pooled from three independent experiments, with two to three biological replicates per experiment (n = 6–9). *EDS1*, *AVRPPHB SUSCEPTIBLE 3* (*PBS3*), *AGD2-LIKE DEFENSE RESPONSE PROTEIN 1* (*ALD1*), *PATHOGENESIS RELATED1* (*PR1*), *ISOCHORISMATE SYNTHASE1* (*ICS1*), and *FLAVIN MONOOXYGENASE1* (*FMO1*) transcript abundances were measured relative to *ACTIN2* (*ACT2*). Relative expression and significance level is set to Col-0 mock-treated samples. Differences between genotypes were determined using ANOVA (Tukey-HSD), asterisks indicate $p < 0.01$.

Chapter 2: Arabidopsis PAD4 EP domain cavity plays an essential role in immunity

Chapter one shows that PAD4^{LLD} is sufficient for GPA resistance, but is insufficient for pathogen immunity, indicating PAD4 EP domain functions in pathogen immunity. Certain Arabidopsis and Tomato EDS1 EP domain residues are essential for immunity, *e.g.* *AtEDS1*^{R493} (Figure 2.1) (Bhandari *et al.*, 2019; Gantner *et al.*, 2019; Lapin *et al.*, 2019). Mutating the equivalent *AtEDS1*^{R493} residue in *AtPAD4* (R420A) does not inhibit PAD4 function (Bhandari *et al.*, 2019). Given that essential EDS1 EP domain residues reside at the EP domain cavity, while *AtPAD4*^{R420} does not, suggests that certain PAD4 EP domain cavity residues are essential for PAD4 immune signalling (Figure 2.1) (Bhandari *et al.*, 2019). Based on these observations I hypothesized that certain residues of the PAD4 EP domain EP domain cavity are also required for PAD4 immune signalling function.

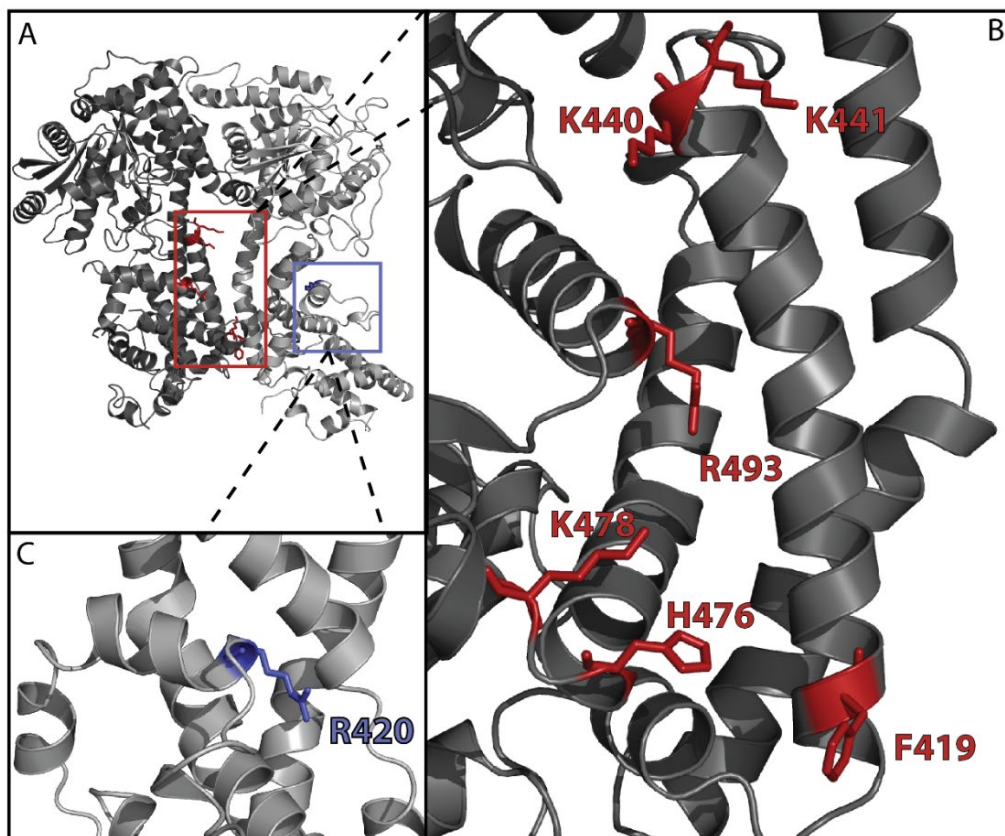
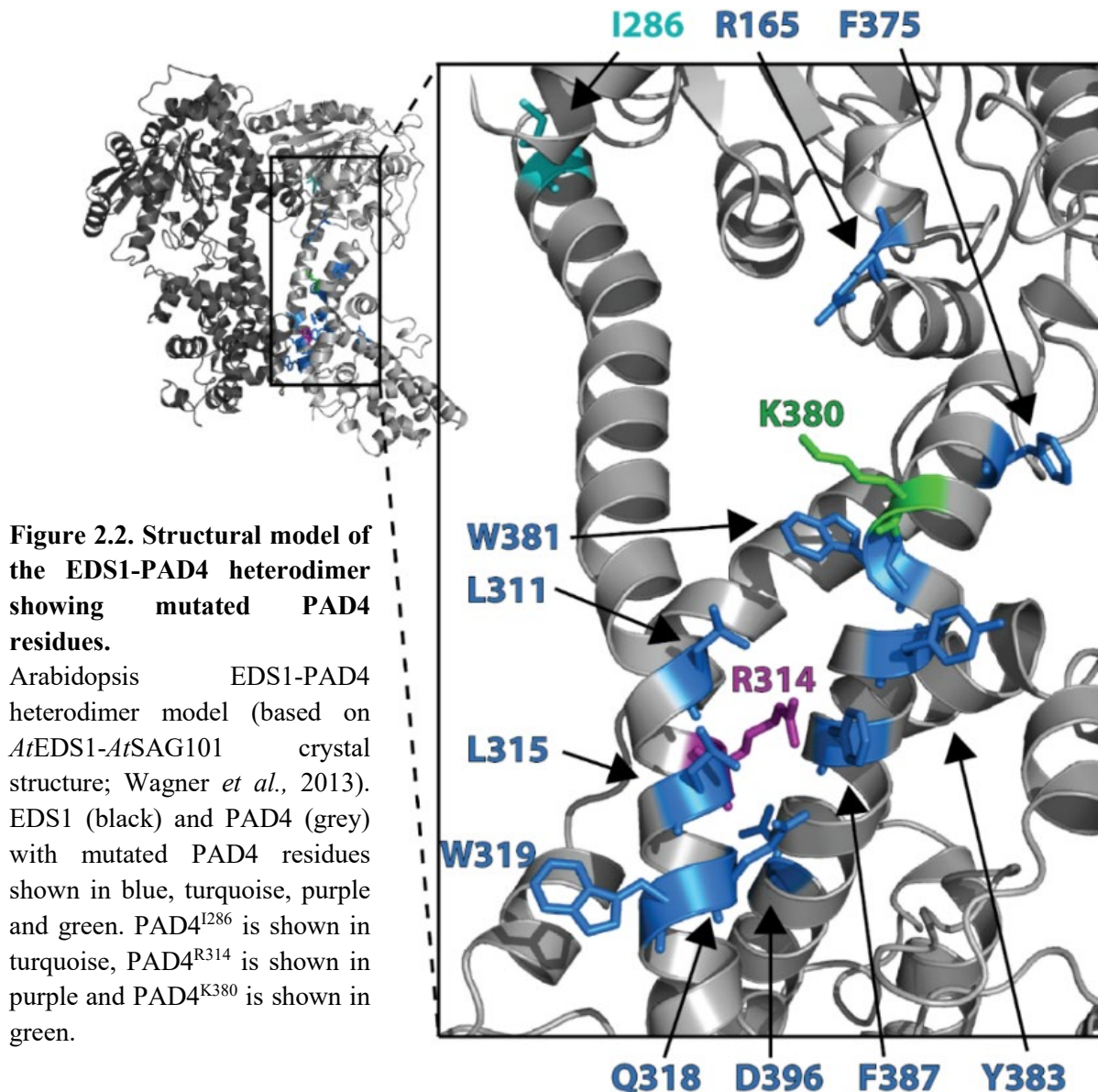


Figure 2.1. EDS1 and PAD4 EP domain residues that were mutated previously.

Arabidopsis EDS1-PAD4 heterodimer model (based on *AtEDS1-AtSAG101* crystal structure; Wagner *et al.*, 2013). EDS1 (black) PAD4 (grey) with residues previously mutated in EDS1 highlighted in red, and in *AtPAD4* residues shown in blue (Bhandari *et al.*, 2019; Lapin *et al.*, 2019). **A.** EDS1-PAD4 heterodimer model (Wagner *et al.*, 2013). Red box highlights the EDS1-PAD4 EP domain cavity and blue box highlights PAD4^{R420}. **B.** EDS1-cavity residues mutated previously are highlighted in red. **C.** PAD4^{R420} is not located in the cavity.

Selection of PAD4 EP domain cavity variants

To determine investigate the contribution of PAD4 EP domain cavity residues to immunity, I mutated several residues to an Alanine (A) (Figure 2.2). These sites were chosen based on three main criteria: i) the residue is solvent-exposed, ii) the residue is located in the EP domain cavity, and iii) the residue should at least be conserved within the Brassicaceae family (Figure 2.3; Supplemental Figure 2.1). As a control, I also mutated PAD4^{D396}, which is located in the EP domain, but not located in the cavity (Figure 2.2). This residue is also part of the EPLDIA motif, a motif of unknown function that is conserved in the EDS1-family (Figure 2.3; Wagner *et al.*, 2013). Another control I included was PAD4^{I286}, which is also solvent accessible (Figure 2.2), conserved within Brassicaceae, but is not located in the EP domain cavity (Figure 2.3; Supplemental Figure 2.1). This constituted to a set of 13 PAD4 variants that I screened for their contribution to pathogen immunity.



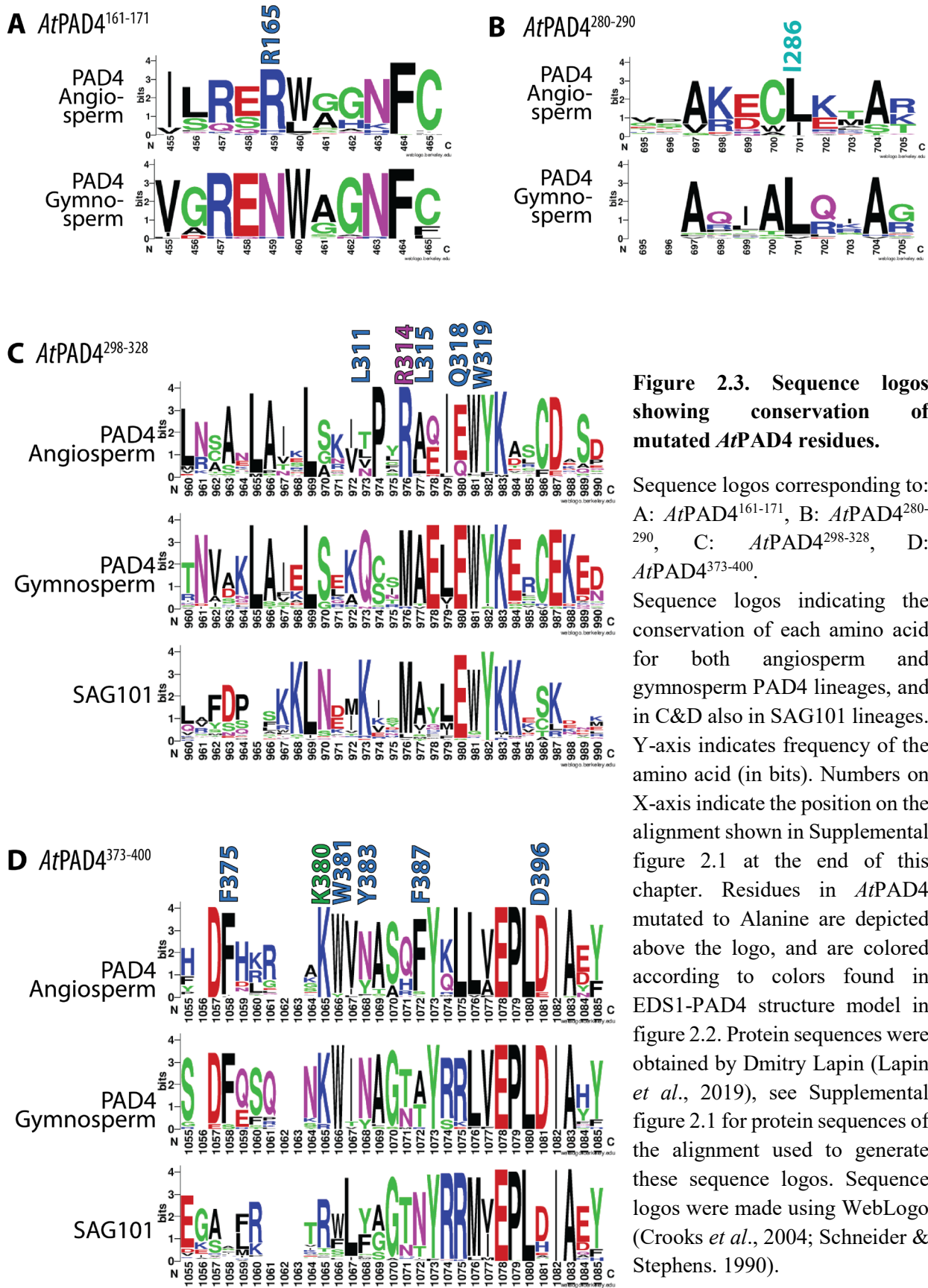


Figure 2.3. Sequence logos showing conservation of mutated *At*PAD4 residues.

Sequence logos corresponding to: A: *At*PAD4¹⁶¹⁻¹⁷¹, B: *At*PAD4²⁸⁰⁻²⁹⁰, C: *At*PAD4²⁹⁸⁻³²⁸, D: *At*PAD4³⁷³⁻⁴⁰⁰.

Sequence logos indicating the conservation of each amino acid for both angiosperm and gymnosperm PAD4 lineages, and in C&D also in SAG101 lineages. Y-axis indicates frequency of the amino acid (in bits). Numbers on X-axis indicate the position on the alignment shown in Supplemental figure 2.1 at the end of this chapter. Residues in *At*PAD4 mutated to Alanine are depicted above the logo, and are colored according to colors found in EDS1-PAD4 structure model in figure 2.2. Protein sequences were obtained by Dmitry Lapin (Lapin *et al.*, 2019), see Supplemental figure 2.1 for protein sequences of the alignment used to generate these sequence logos. Sequence logos were made using WebLogo (Crooks *et al.*, 2004; Schneider & Stephens. 1990).

Screening PAD4 EP domain cavity T1 mutants for susceptibility to *Hpa* EMWA1

I introduced the cPAD4 variants into *Arabidopsis pad4-1/sag101-3* mutants (as *pPAD4::StreptII-YFP-cPAD4*). To assess whether these cPAD4 variants are able to function in immunity, I inoculated 3 week-old T1 transformants with TNL triggering *Hpa* EMWA1. Out of all cPAD4 variants tested, only cPAD4^{R314A} and cPAD4^{K380A} showed susceptible disease phenotypes similar to *pad4-1/sag101-3* and *eds1-2*, based on microscopic *Hpa* colonisation phenotypes (Figure 2.4). The remaining cPAD4 variants showed resistance phenotypes similar to Col-0 and cPAD4^{WT}. This initial observation suggested that PAD4^{R314} and PAD4^{K380} are required for signalling in immunity.

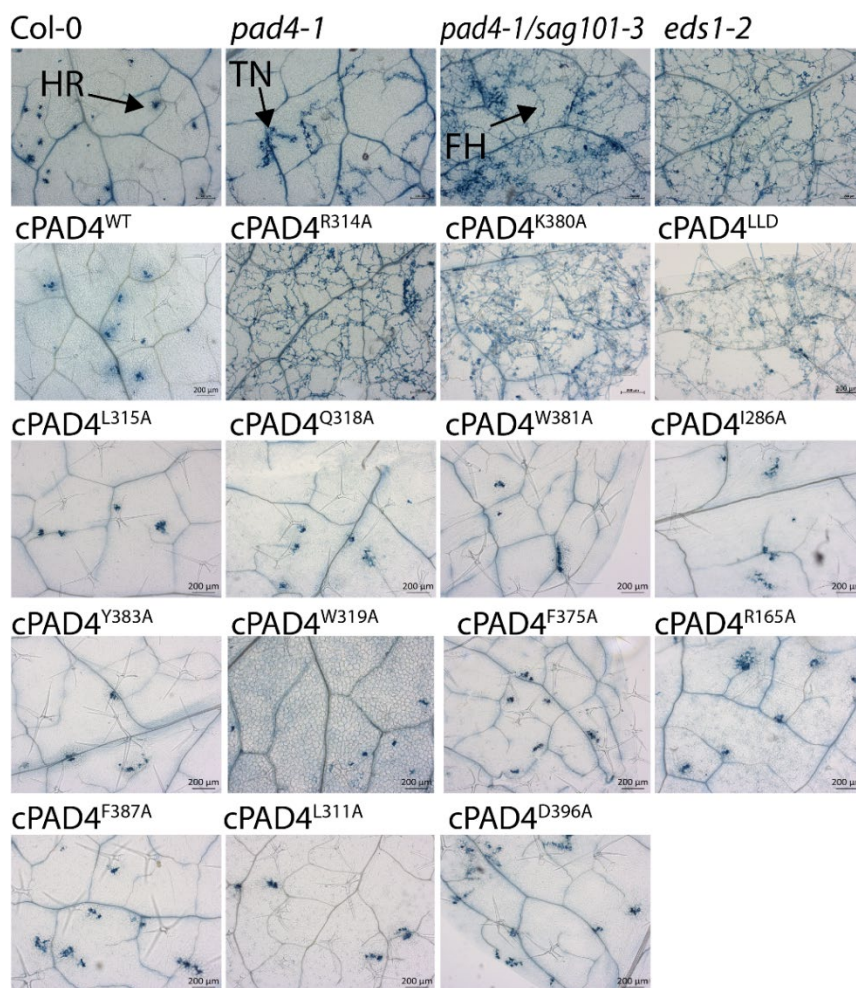


Figure 2.4. T1 complementation assay on PAD4 variants in Arabidopsis ETI against *Hpa* EMWA1. Microscopic immunity phenotypes of 3-week-old Arabidopsis lines, as indicated, at 6 dpi with *Hpa* isolate EMWA1 (recognized by TNL RPP4). Col-0 (resistant), *pad4-1* (susceptible) and *pad4-1/sag101-3* and *eds1-2* (susceptible) functioned as controls. Trypan blue-stained leaves showing free hyphae (FH), trailing necrosis (TN) and hypersensitive cell death (Hypersensitive Response (HR)). Black bars represent 200 µm. Over 12 independent T1 plants were tested per cPAD4 variant, and showed similar resistance phenotypes. Results were obtained from two independent experimental replicates except for cPAD4^{R314A} and cPAD4^{W319A}.

All PAD4 variants interact with EDS1 *in planta*, except PAD4^{I286A}

In chapter one, I showed that the interaction between PAD4 and EDS1 does not solely rely on the PAD4^{LLD}, but also required the PAD4 EP domain. Perhaps PAD4^{R314A} and PAD4^{K380A} susceptibility is caused protein instability or by the inability of these variants to interact with EDS1. To test this hypothesis, I transiently co-expressed EDS1 with each of the PAD4 variants in *N. benthamiana* leaves. Most PAD4 variants showed protein levels similar to PAD4^{WT}, though some variants accumulated to lower levels than PAD4^{WT} (Figure 2.5).

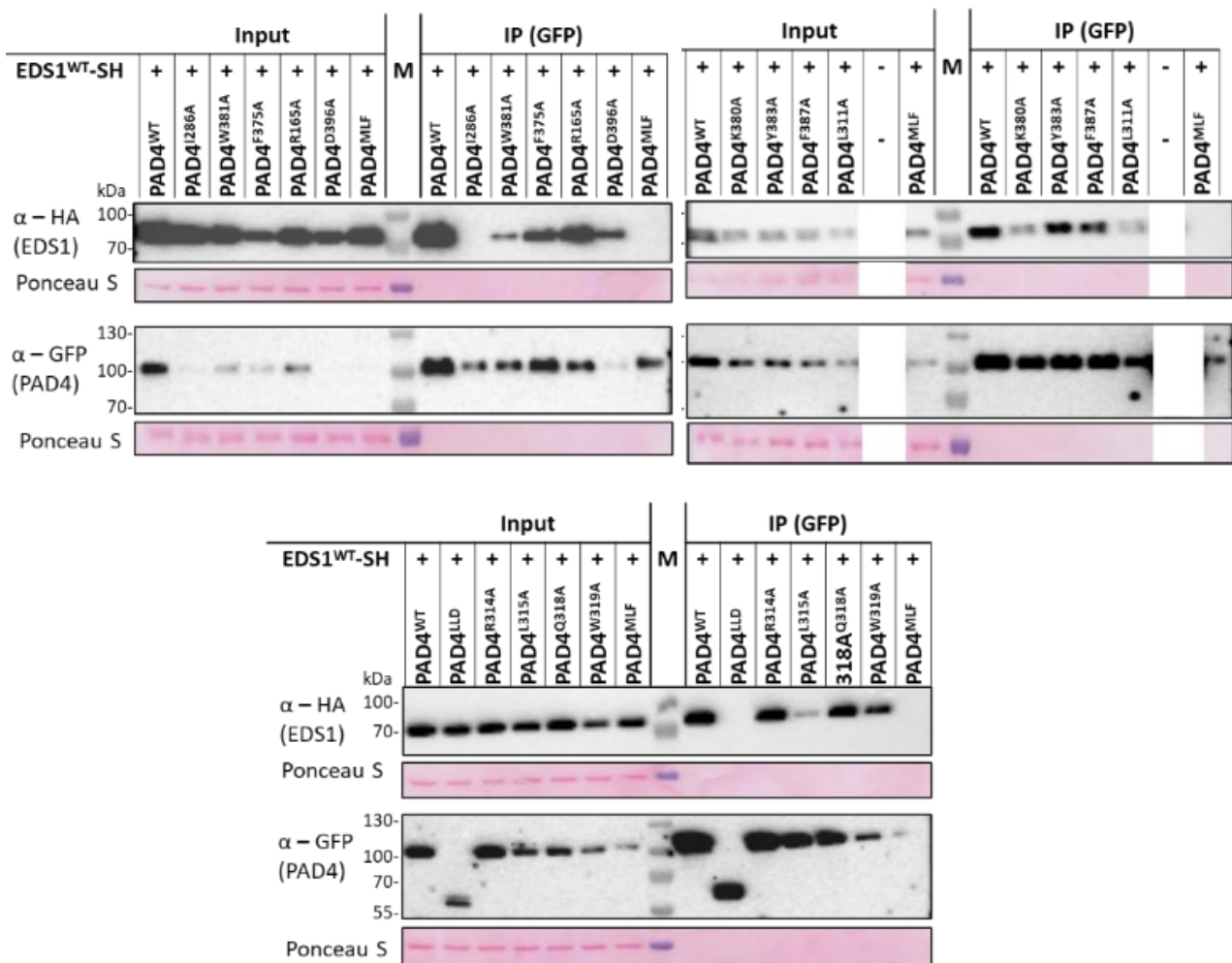


Figure 2.5. All cPAD4 variants interact with EDS1, except PAD4^{I286A}.

Transiently expressed PAD4 (as *pPAD4::StreptII-YFP-cPAD4*) variants co-expressed with EDS1 (as *35S::cEDS1-SH*) and in *N. benthamiana* leaf tissue. GFP-Trap (Chromotek) co-IP performed on tissue harvested 3 days post-infiltration. Wild-type PAD4 is used as a positive control, and PAD4^{MLF} and PAD4^{LLD} as negative controls. Similar results were obtained in two independent biological replicates. For PAD4^{I286A} this was repeated in two more independent biological replicates. For PAD4^{R314A} and PAD4^{K380A} this result was repeated in three more independent biological replicates. Blanked out parts in blots are from an unrelated co-IP sample.

All PAD4 variants were able to interact with EDS1, except PAD4^{I286A} (Figure 2.5), which is located in the LLD, but not at the EDS1 interface (Figure 2.2). Since cPAD4^{I286A} does not show a loss-of-function phenotype (Figure 2.4), these data suggest that a (strong) interaction between PAD4 and EDS1 is not required for immune signalling. Furthermore, these co-IP data indicate that none of the PAD4 variants in the EP domain cavity are required for the interaction with EDS1. Moreover, this suggests that the loss-of-function phenotype observed in *Arabidopsis* cPAD4^{R314A} and cPAD4^{K380A} cannot be explained by a loss of interaction with EDS1. To confirm that PAD4^{R314A} and PAD4^{K380A} indeed do interact with EDS1, split-LUC assays were performed. This showed that there is no significant decrease in binding between EDS1 and PAD4^{R314A}, and EDS1 and PAD4^{K380A} compared to PAD4^{WT} (Figure 2.6). Lastly, I determined cellular localisation of all PAD4 variants in *N. benthamiana* leaves, which showed nucleocytoplasmic localisation similar to PAD4^{WT} (Figure 2.7). In conclusion, based on these transient assays in *N. benthamiana* the PAD4^{R314A} and PAD4^{K380A} susceptibility phenotypes are not caused by protein instability, a diminished interaction with EDS1, or by mislocalisation.

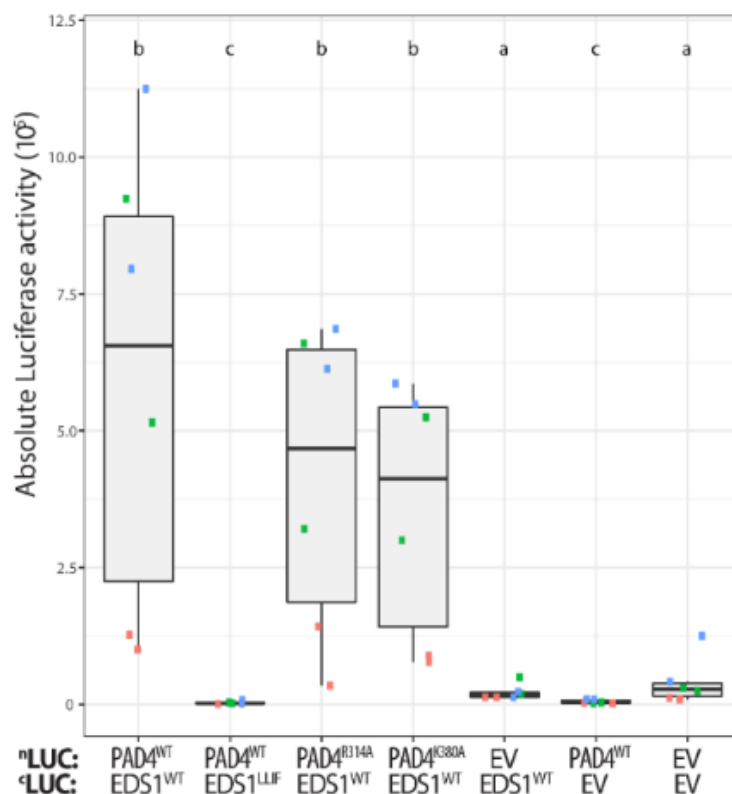


Figure 2.6. PAD4^{R314A} and PAD4^{K380A} interact with EDS1.

Absolute luciferase (LUC) activity from transiently co-expressed ^NLUC or ^CLUC constructs (35S promoter) in *N. benthamiana*. Data are pooled from three independent experiments with two biological replicates per experiment (n = 6). Letters indicate statistical significance as determined by one-way ANOVA with multiple testing correction using Tukey-HSD; $p < 0.01$. Data generated by Lucas Dijkgraaf.

PAD4^{R314A} and PAD4^{K380A} are stable and nucleocytoplasmic proteins in Arabidopsis

Previously, cDNA constructs of EDS1^{R493A} (cEDS1^{R493A}) were shown to accumulate less protein than cEDS1^{WT} (Bhandari *et al.*, 2019). To show that the susceptibility phenotype of these lines is not due to low protein levels, the authors generated genomic DNA (gDNA) constructs of EDS1^{R493A} (gEDS1^{R493A}) (Bhandari *et al.*, 2019). These gEDS1^{R493A} lines were as susceptible as cEDS1^{R493A}, but in contrast to cEDS1^{R493A}, gEDS1^{R493A} accumulated to a similar level as cEDS1^{WT} levels. This indicated that the phenotype of cEDS1^{R493A} is not due to low protein levels (Bhandari *et al.*, 2019). Since this same issue was likely to occur for the cPAD4 variants, I decided to generate gDNA lines for PAD4^{R314A} and PAD4^{K380A}.

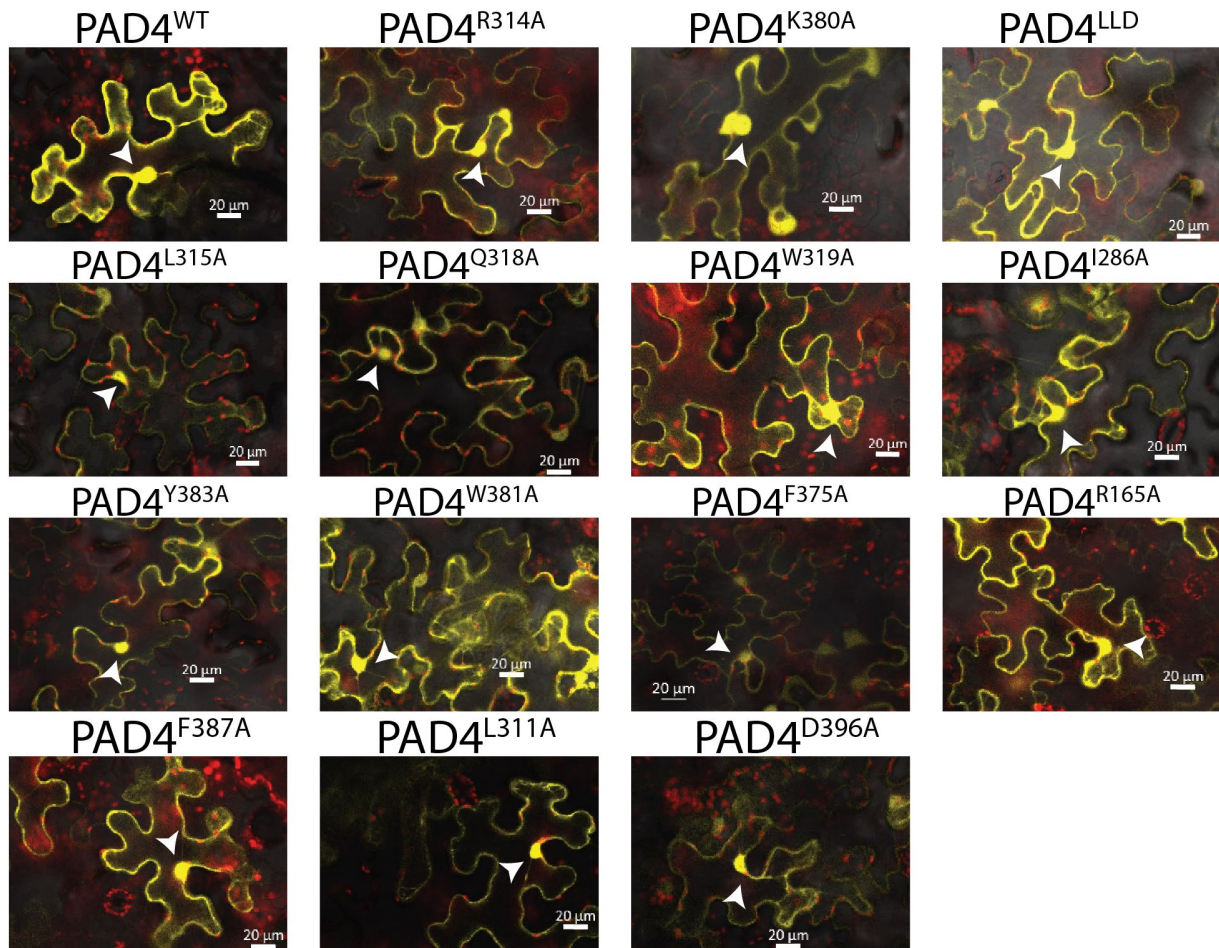


Figure 2.7. PAD4 variants maintain (WT-like) nucleocytoplasmic localisation in *N. benthamiana*. PAD4 variants transiently expressed as *pPAD4::StrepII-YFP-cPAD4* in *N. benthamiana* leaves. To determine PAD4 variant localisation, confocal microscope sensitivity was enhanced to enable its detection. Yellow channel = YFP-PAD4, red channel = Chlorophyll A, and white channel = PMT (bright field). White arrowheads indicate nuclei and white bars correspond to 20 μm . >40 cells per PAD4 variant were assessed for PAD4 cellular localisation. Data from one experimental replicate.

Typically, gDNA constructs contain the upstream intergenic region, UTRs, exons and introns. Within the *Arabidopsis* genus, *PAD4* upstream intergenic region and intron are conserved (Figure 2.8). Moreover, in *AtPAD4* leaves, these regions form an open chromatin region (Figure 2.8; Zhang *et al.*, 2016). This suggests that the promoter and intron contain *cis*-elements that regulate *AtPAD4* expression, and consequently *AtPAD4* levels. Recent evidence indicates that (conserved) downstream intergenic regions can also affect gene expression (Weber *et al.*, 2016; Zicola *et al.*, 2019). Since the downstream intergenic region of *AtPAD4* is conserved within most Brassicaceae *PAD4* orthologues (Figure 2.8), I decided to clone g*PAD4* constructs containing this downstream intergenic region.

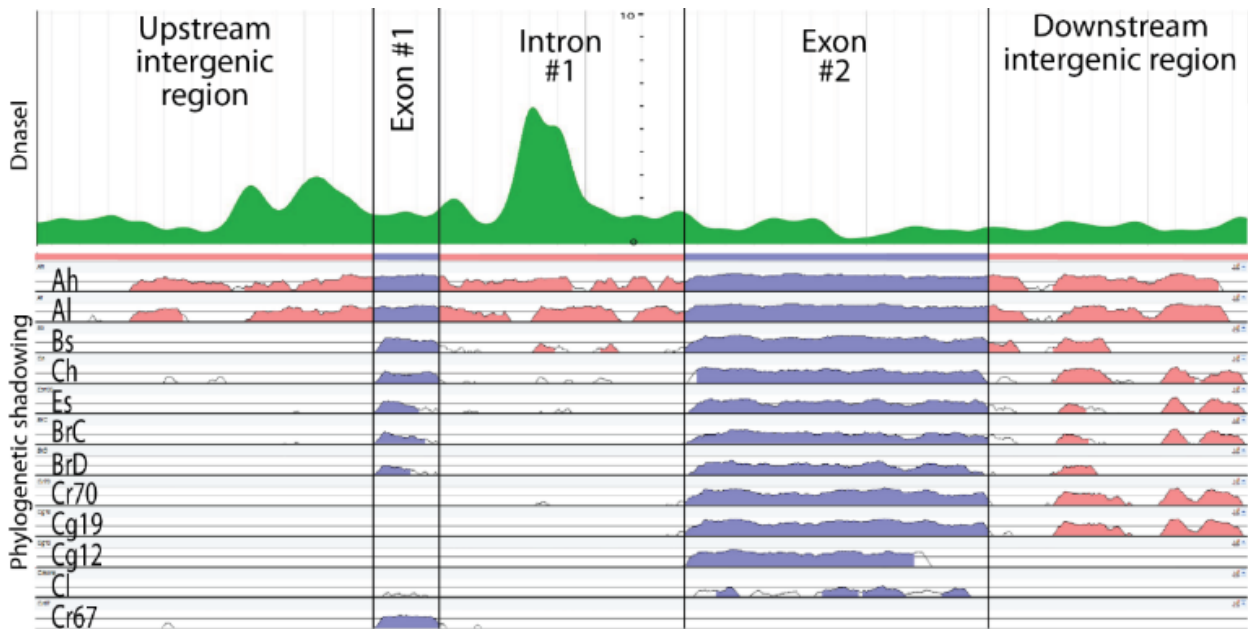


Figure 2.8. *PAD4* contains open chromatin regions and a conserved intron and downstream intergenic region.

Chromatin accessibility (DNaseI: top panel) and conservation level (Phylogenetic shadowing: bottom panel) at the *PAD4* locus. Chromatin accessibility at the *AtPAD4* locus from published leaf DNaseI-seq data (PlantDHS.org; Top panel) (Zhang *et al.*, 2016). Phylogenetic shadowing showing the level of sequence homology of *AtPAD4* in relation to selected Brassicales species (mVISTA; bottom panel). Red indicates intergenic regions, UTRs and introns, and blue highlights exons. Edouard Severing (Coupland Group) obtained genomic sequences from publicly available databases, *i.e.* Phytozome and Genomevolution.org. Species and loci as depicted in bottom panel: Ah: *A. halerii* (*g28366.t1*), Al: *A. lyrata* (*AL5G33080.t1*), Bs: *Boechera stricta* (*Bostr.29094s0001.1*), Ch: *Cardamine hirsuta*, Es: *Eutrema salsugineum*, BrC: *Brassica rapa* (*Brara.C04416.1.p*), BrD: *B. rapa* (*Brara.D00590.1.p*), Cr70: *Capsella rubella* (*Carubv10016970m*), Cg19: *Capsella grandiflora* (*Cagra.1952s0033.1.p*), Cg12: *C. grandiflora* (*Cagra.12401s0001.1.p*), Cl: *Cleoma* (*Tarenaya hassleriana*) and Cr67: *C. rubella* (*Carubv10016967m*).

For protein localisation and immune-detection purposes I introduced YFP with a Linker-peptide (Linker: Gly + 9x Ala peptide) in front of the PAD4 start codon. I generated gPAD4^{WT}, gPAD4^{R314A} and gPAD4^{K380A} constructs (*pPAD4::YFP-Linker-gPAD4::dsPAD4*) and introduced these into *Arabidopsis* (*pad4-1/sag101-3*).

To test whether PAD4^{R314A} and PAD4^{K380A} accumulate stably in *Arabidopsis*, I immunodetected PAD4 protein in *Hpa* EMWA1 infected leaves of T3 homozygous lines. cPAD4^{R314A} and cPAD4^{K380A} accumulated to lower levels than cPAD4^{WT} (Figure 2.9), while all tested gPAD4^{WT}, gPAD4^{R314A} and gPAD4^{K380A} accumulated to similar levels as cPAD4^{WT} (Figure 2.9). Furthermore, certain cPAD4^{I286A} and cPAD4^{L315A} lines showed low protein accumulation compared to PAD4^{WT}, whilst still being fully functional in *Hpa* EMWA1 resistance (Figure 2.4&9). These observations indicate the loss-of-function phenotype of PAD4^{R314A} and PAD4^{K380A} are not due to low protein levels. Next, I tested for PAD4 localisation in *Arabidopsis* leaves infected with *Pst avrRps4*. In line with the observations in *N. benthamiana*, both gDNA and cDNA lines of PAD4^{R314A} and PAD4^{K380A} showed wild-type-like nucleocytoplasmic localisation (Figure 2.10). These observations indicate that PAD4^{R314A} and PAD4^{K380A} are stable proteins located in the nucleus and cytoplasm.

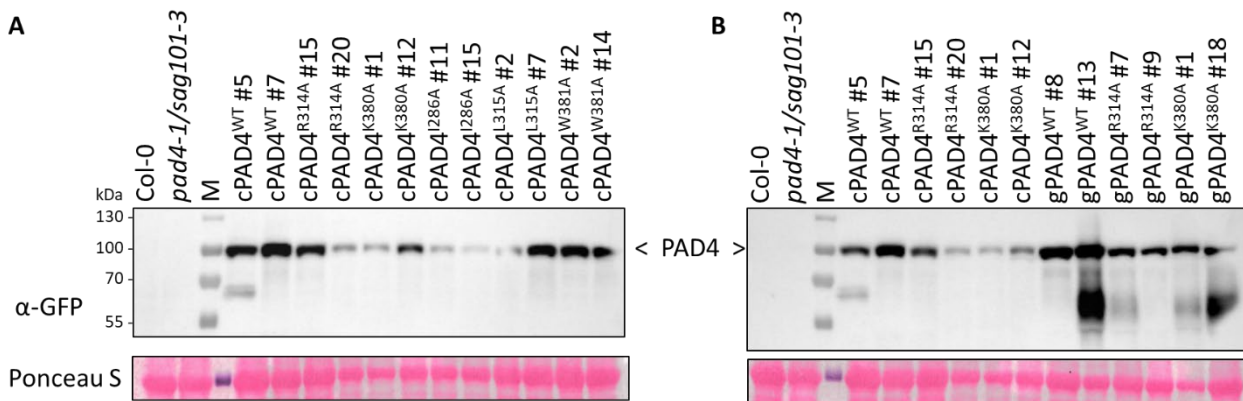


Figure 2.9. cPAD4 and gPAD4 variants accumulate in *Arabidopsis*.

PAD4 accumulation in independent stable transgenic *Arabidopsis* lines expressing StrepII-YFP-cPAD4 or YFP-gPAD4 and probed for PAD4 by Western blotting using α -GFP antibody. Samples were harvested from 3 week-old plants infected with *Hpa* EMWA1 (5 dpi). Col-0 and *pad4-1/sag101-3* as negative controls. Representative images from three independent experiments are shown. **A.** cPAD4^{R314A} and cPAD4^{K380A} accumulation relative to cPAD4^{WT}, cPAD4^{I286A}, cPAD4^{L315A} and cPAD4^{W381A} **B.** cPAD4^{R314A}, cPAD4^{K380A} and cPAD4^{WT} accumulation relative to gPAD4^{WT}, gPAD4^{R314A} and gPAD4^{K380A}.

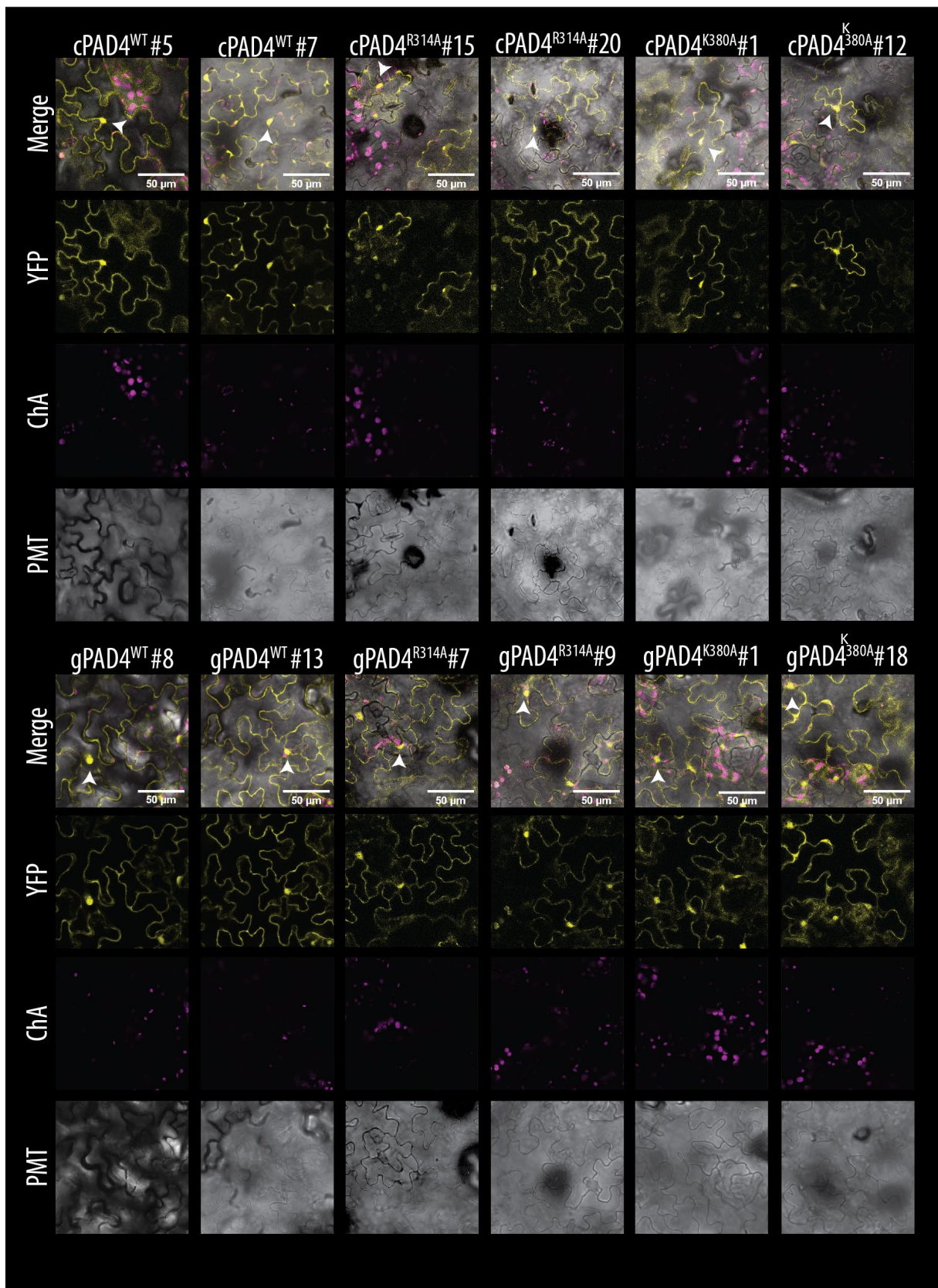


Figure 2.10. PAD4^{R314A} and PAD4^{K380A} cellular localisation in Arabidopsis.
Figure legend continues on next page.

Figure 2.10. PAD4^{R314A} and PAD4^{K380A} cellular localisation in Arabidopsis. (See previous page) Nucleocytoplasmic localisation of PAD4^{WT}, PAD4^{R314A} and PAD4^{K380A} as cDNA constructs (*pPAD4::StrepII-YFP-cPAD4*) or as gDNA constructs (*pPAD4::YFP-gPAD4-dsPAD4*) in Arabidopsis transgenic T3 lines (24 hpi, *Pst avrRps4*). I enhanced the confocal microscope sensitivity to determine PAD4 localisation. White arrowhead = nuclei; white bar = 50 µm. Similar results were obtained in two independent replicates in two biological replicates (n=4). ChA: chlorophyll A (auto-fluorescence); PMT: photon multiplier tube (bright field). Data generated together with Eva Penner.

Basal immunity and TNL-ETI require PAD4^{R314} and PAD4^{K380}

In the T1 complementation assay (Figure 2.4), cPAD4^{R314A} and cPAD4^{K380A} were susceptible to TNL-ETI triggering *Hpa* EMWA1 (RPP4). To verify this result, the assay was repeated on homozygous T3 cPAD4 lines and gPAD4 lines. These lines include cPAD4^{I286A}; as it was unable to bind to EDS1, and cPAD4^{L315A} and cPAD4^{W381A}; as these residues are adjacent to PAD4^{R314} and PAD4^{K380}, respectively. Col-0, cPAD4^{WT}, cPAD4^{I286A}, cPAD4^{L315A} and cPAD4^{W381A} were resistant to *Hpa* EMWA1, as measured by conidiospore production, and based on macroscopic disease and microscopic *Hpa* colonisation phenotypes (Figure 2.11). In contrast, cPAD4^{R314A} and cPAD4^{K380A} were susceptible, similar to *pad4-1/sag101-3*. For the genomic lines I observed a similar trend, Col-0 and gPAD4^{WT} lines were resistant, whilst gPAD4^{R314A} and gPAD4^{K380A} lines were susceptible, resembling *pad4-1/sag101-3* (Figure 2.11).

In addition, I investigated PAD4^{R314A} and PAD4^{K380A} function in basal immunity and TNL-ETI against, respectively, virulent *Pst* DC3000, avirulent *Pst avrRps4* (Figure 2.12). This showed that Col-0, cPAD4^{WT} and gPAD4^{WT} are resistant to both virulent and avirulent pathogens. In contrast, both cDNA and gDNA lines of PAD4^{R314A} and PAD4^{K380A} were as susceptible as *pad4-1/sag101-3* (Figure 2.12). This suggests that PAD4^{R314} and PAD4^{K380} are required for immune signalling. To test this hypothesis, I quantified the expression of defence marker genes 24 hpi with *Pst avrRps4*. This showed that cPAD4^{R314A} and cPAD4^{K380A} are unable to induce defence marker gene expression, like *pad4-1/sag101-3* (Figure 2.13). This indicates that PAD4^{R314A} and PAD4^{K380A} are unable induce TNL-ETI signalling. Taken together, these results indicate that PAD4^{R314} and PAD4^{K380} are required for basal immunity and TNL-ETI.

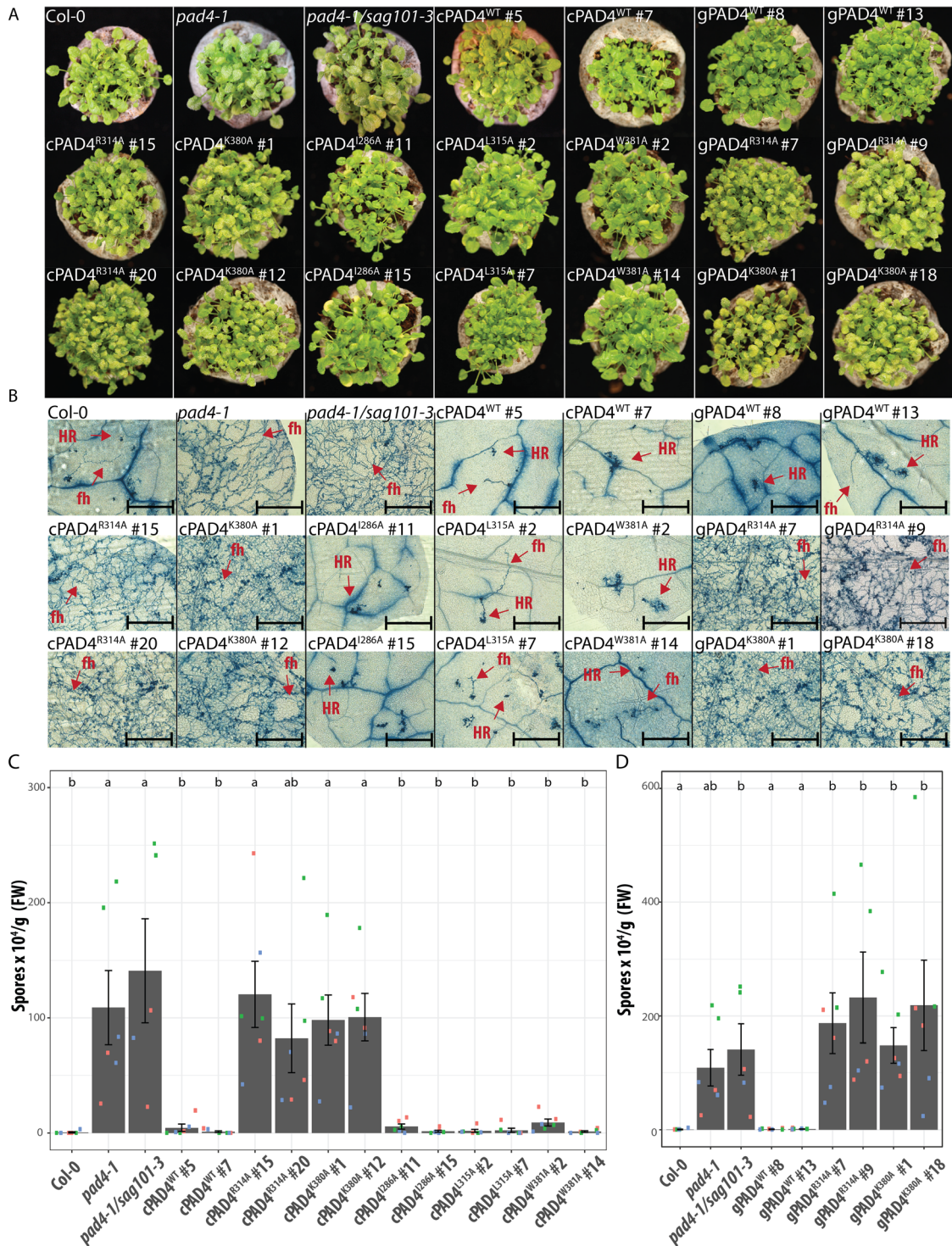


Figure 11. PAD4^{R314A} and PAD4^{K380A} are not functional in Arabidopsis ETI against *Hpa* EMWA1.

A. Macroscopic immunity phenotypes of 3-week-old Arabidopsis lines, as indicated, at 6 dpi with *Hpa* isolate EMWA1 (recognized by TNL RPP4). Col-0 (resistant), *pad4-1* (susceptible) and *pad4-1/sag101-3* (susceptible) functioned as controls. Resistant plants look healthy at 6 dpi, whereas susceptible plants produce conidiospores and leaf chlorosis. *Figure legend continues on next page.*

Figure 2.11. PAD4^{R314A} and PAD4^{K380A} are not functional in Arabidopsis ETI against *Hpa* EMWA1 (continued).

B. Trypan blue-stained leaves of *Hpa* EMWA1 infected plants at 5 dpi of the same lines as in A. Trypan blue-stained leaves showing free hyphae (fh) and hypersensitive cell death (Hypersensitive Response (HR)). Black bars represent 500 μ m. Pictures are representative from three independent experimental replicates, > 6 leaves per replicate and > 30 infection sites per genotype. **C-D.** TNL (RPP4) ETI assay in Arabidopsis independent transgenic lines with wild-type and mutant controls, as in A. *Hpa* EMWA1 conidiospores on leaves were quantified at 6 dpi in three independent experiments (squares; n=9). Squares of the same color represent three biological replicates in an independent experiment. Bars represent the mean of three experimental replicates \pm SE. Differences between genotypes were determined using ANOVA (Tukey-HSD, $p < 0.05$), letters indicate significance class. Data generated together with Eva Penner.

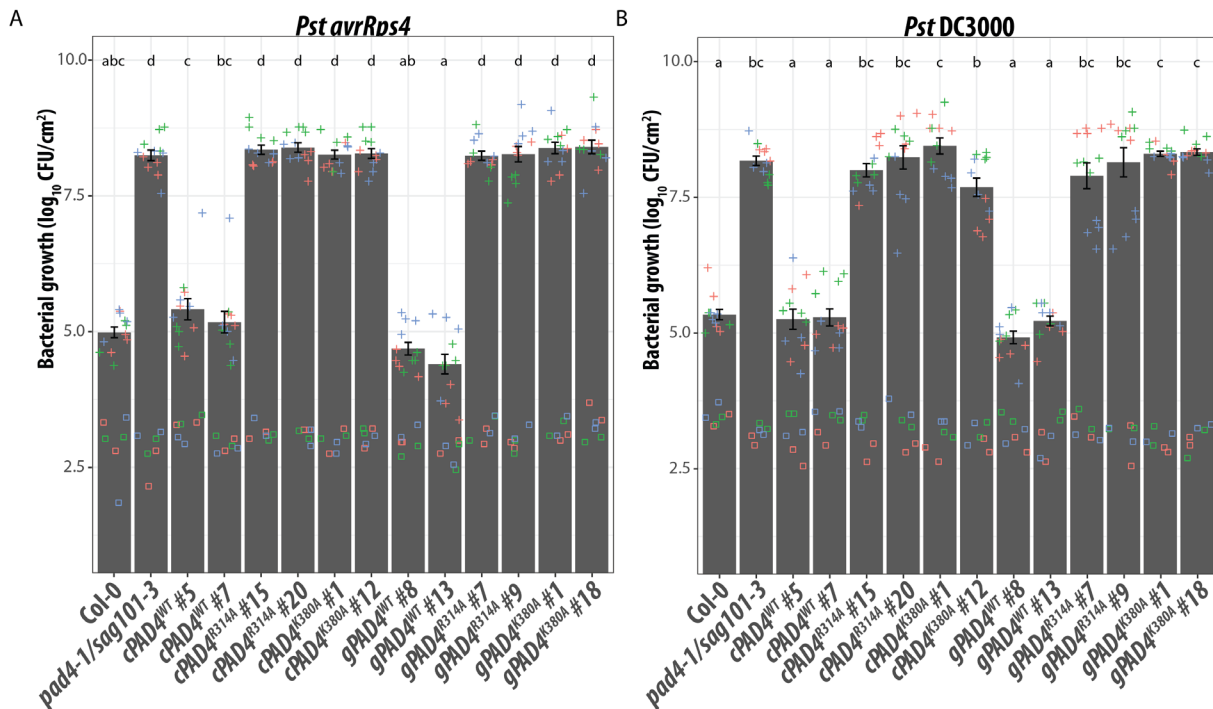


Figure 2.12. PAD4^{R314A} and PAD4^{K380A} are not functional in Arabidopsis ETI and basal immunity.

A. TNL (RRS1-S/RPS4) ETI assay in Arabidopsis independent transgenic and control lines as indicated. Four-week old Arabidopsis plants were syringe infiltrated with *Pst avrRps4* (OD₆₀₀ = 0.0005) and bacterial titers were determined at 0 dpi (empty squares; n=6) and 3 dpi (plus signs; n=12). Symbols of the same color represent 2 (day 0) or 4 (day 3) biological replicates in an independent experiment. Bars represent the mean of three experimental replicates \pm SE. Differences between genotypes were determined using ANOVA (Tukey-HSD, $p < 0.01$), letters indicate significance class. **B.** Infection assay was performed with basal immunity triggering *Pst* DC3000 (OD₆₀₀ = 0.0005). Experimental set-up and statistical analysis as in B. Data generated together with Eva Penner.

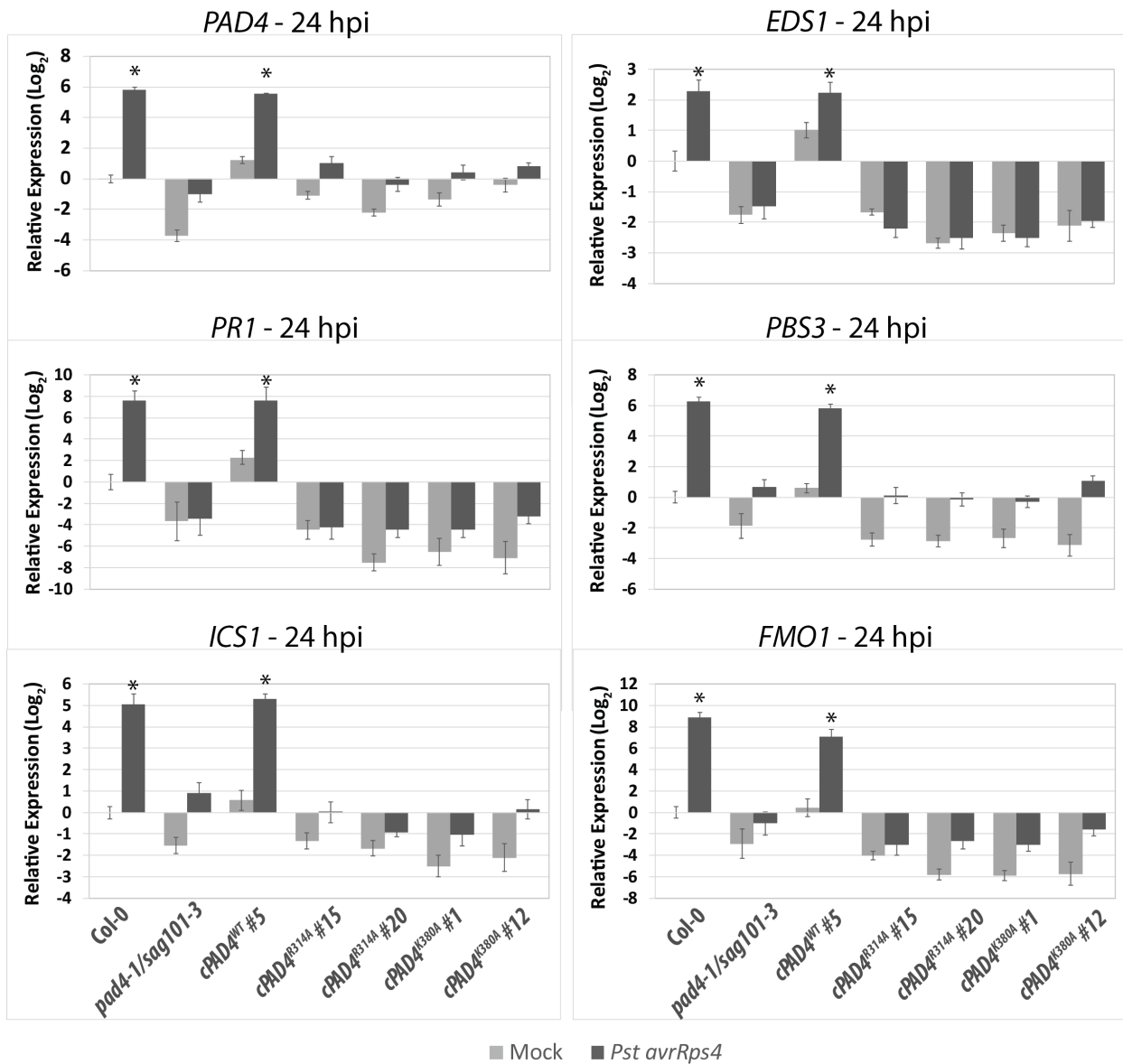


Figure 2.13. PAD4^{LLD} is not able to induce immune marker genes during *Pst avrRps4* triggered ETI. Transcript abundance determined by qRT-PCR in 4-week old *Arabidopsis* plants syringe-infiltrated with either buffer (mock, grey bars) or *Pst avrRps4* (black bars; OD₆₀₀ = 0.005) (24 hpi). Data are pooled from three independent experiments, with two to three biological replicates per experiment (n = 6–9). *PAD4*, *EDS1*, *PATHOGENESIS RELATED1* (*PR1*), *AVRPPHB SUSCEPTIBLE 3* (*PBS3*), *ISOCHORISMATE SYNTHASE1* (*ICS1*), and *FLAVIN MONOOXYGENASE1* (*FMO1*) transcript abundances were measured relative to *ACTIN2* (*ACT2*). Relative expression and significance level is set to Col-0 mock-treated samples. Differences between genotypes were determined using ANOVA (Tukey-HSD), asterisks indicate $p < 0.05$.

PAD4^{R314A} and PAD4^{K380A} susceptibility is independent of *Pst* DC3000-produced coronatine

Pst DC3000 produces a mimic of the phytohormone JA-Ile, called coronatine (Brooks *et al.*, 2005; Katsir *et al.*, 2008; Zheng *et al.*, 2012). Coronatine over-stimulates JA-signalling, leading to the repression of several immune pathways, including the EDS1 immune pathway (Brooks *et al.*, 2005; Cui *et al.*, 2018; Mine *et al.*, 2017b). Mutations in the EDS1 EP domain cavity render plants (partially) susceptible to coronatine-producing *Pst* strains, *i.e.* EDS1^{K478R} and EDS1^{R493A}. In contrast, these EDS1 variants are fully functional against certain coronatine deficient *Pst* strains, indicating coronatine represses EDS1 EP domain cavity signalling (Bhandari *et al.*, 2019). Since EDS1^{K478} and EDS1^{R493} are positively charged and located within the EDS1-PAD4 EP domain cavity, like PAD4^{R314} and PAD4^{K380}, I hypothesized that

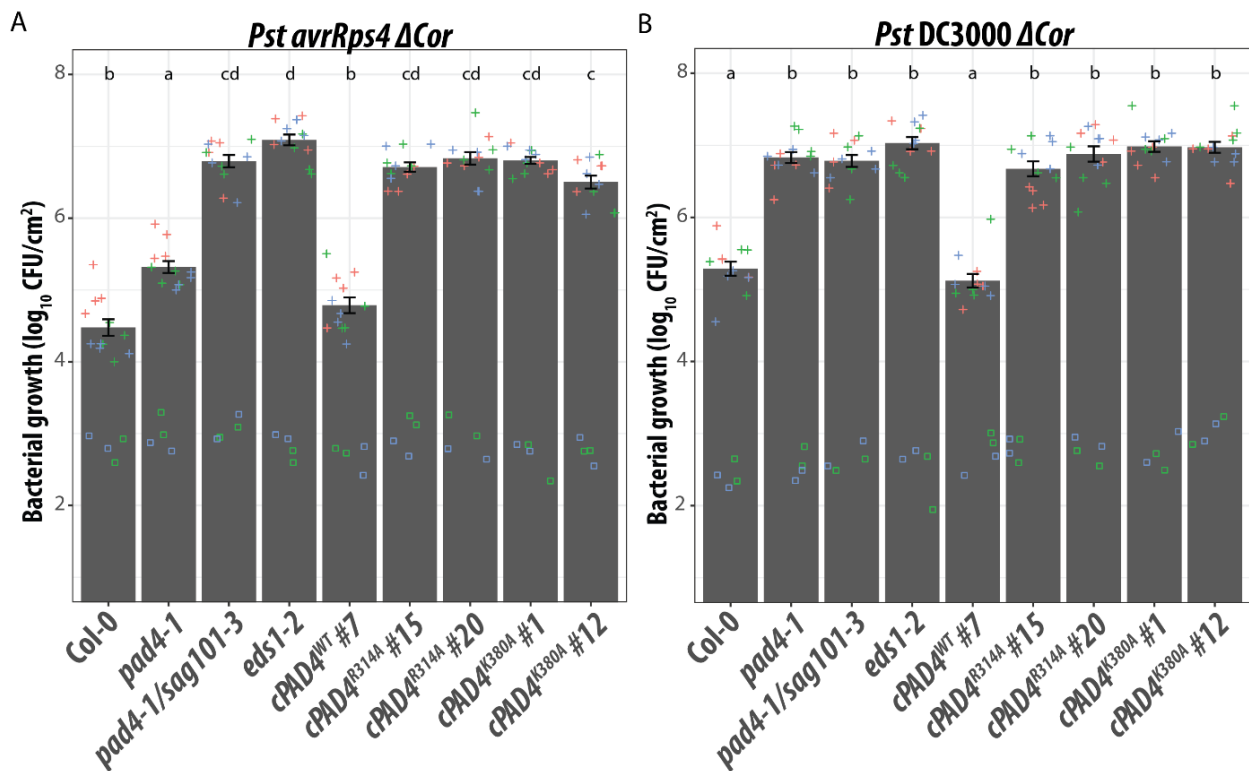


Figure 2.14. PAD4^{R314A} and PAD4^{K380A} susceptibility does not depend on *Pst* DC3000-produced coronatine.

A. TNL (RRS1-S/RPS4) ETI assay in Arabidopsis independent transgenic and control lines as indicated. Four-week old Arabidopsis plants were syringe infiltrated with *Pst avrRps4* Δ Cor (OD₆₀₀ = 0.0005) and bacterial titers were determined at 0 dpi (empty squares; n=4) and 3 dpi (plus signs; n=12). Symbols of the same color represent 2 (day 0) or 4 (day 3) biological replicates in an independent experiment. Bars represent the mean of three experimental replicates \pm SE. Differences between genotypes were determined using ANOVA (Tukey-HSD, p < 0.01), letters indicate significance class. **B.** Infection assay performed with basal immunity triggering *Pst* DC3000 Δ Cor (OD₆₀₀ = 0.0005). Experimental set-up and statistical analysis as in A.

PAD4^{R314A} and PAD4^{K380A} susceptibility to *Pst* is exacerbated by the virulence factor coronatine.

To test this hypothesis, I measured the virulence of coronatine deficient (ΔCor) *Pst* strains on cPAD4^{R314A} and cPAD4^{K380A} against Col-0 and PAD4^{WT} were resistant to virulent *Pst* DC3000 ΔCor and avirulent *Pst avrRps4* ΔCor . In contrast to EDS1^{K478R} and EDS1^{R493A} lines, PAD4^{R314A} and PAD4^{K380A} lines were susceptible and behaved similar to *pad4-1/sag101-3* and *eds1-2* (Figure 2.14; Bhandari *et al.*, 2019). This suggests that coronatine does not repress EDS1-PAD4 EP domain cavity immune functions, but rather that coronatine inhibits certain immune sectors downstream of EDS1 heterodimers, as previously proposed by Bhandari *et al.* (2019).

PAD4^{R314} and PAD4^{K380} are not required for resistance to GPA

PAD4 acts independently of EDS1 in GPA resistance (Pegadaraju *et al.*, 2007). This response depends on PAD4^{LLD} and specifically on the LLD located residues PAD4^{S118} and PAD4^{D178} (Figure 1.8; Louis *et al.*, 2012a). To test whether PAD4^{R314A} and PAD4^{K380A} are still functional proteins, I tested whether these PAD4 variants are sufficient to restrict aphid population growth. Consistent with previously published data (Louis *et al.*, 2012a; Pegadaraju *et al.*, 2007), *pad4-1*, *pad4-1/sag101-3* and PAD4^{S118A} (in *pad4-1/eds1-2/EDS1^{SDH}*; Wagner *et al.*, 2013) showed a significant increase in aphid population size compared to Col-0 in a no-choice bioassay (Figure 2.15). The PAD4^{R314A} and PAD4^{K380A} lines harboured a GPA population at 11 dpi similar to PAD4^{WT}, Col-0, PAD4^{LLD} and the *eds1-2* mutant. Thus, indicating that PAD4^{R314A} and PAD4^{K380A} are stable proteins with an *in planta* activity, which are sufficient for resistance to GPA infestation. Thus, highlighting that PAD4^{R314A} and PAD4^{K380A} are partial loss-of-function mutants that are specifically impaired in pathogen immunity signalling.

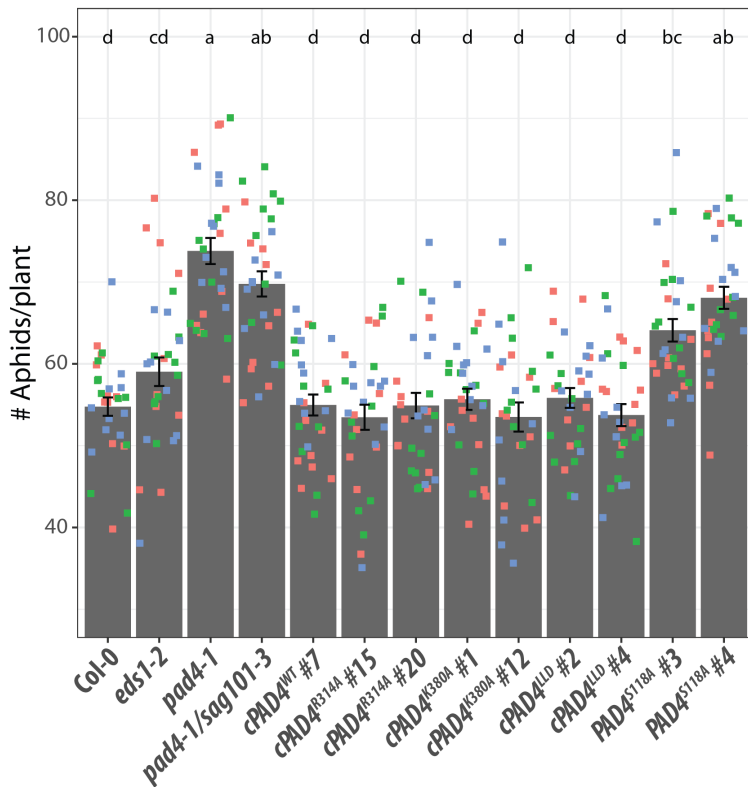


Figure 2.15. PAD4^{R314A} and PAD4^{K380A} is not required for GPA resistance

Number of green peach aphids (GPA) per plant at 11 days post-infestation in a no-choice assay. Data are pooled from three independent experiments each with ten biological replicates per experiment (n = 30). Squares of the same color represent ten biological replicates in an independent experiment. Bars represent the mean of three experimental replicates ± SE. Differences between genotypes were determined using ANOVA (Tukey-HSD, *p* < 0.01), letters indicate significance class. Data generated by Monika Patel, Lani Archer and Jyoti Shah (University of North Texas).

In conclusion, this chapter builds on the observations from chapter one, where I proposed that in *Arabidopsis* the PAD4^{LLD} is necessary and sufficient for GPA resistance, while the EP domain is required for immunity. Here, I show that the highly conserved PAD4 EP domain cavity residues PAD4^{R314} and PAD4^{K380} were dispensable for GPA resistance, but were essential in pathogen immunity (Figure 2.3&11-15; Supplemental figure 2.1). Similarly, *Arabidopsis* immunity signalling also depends on EDS1 EP domain cavity residues (Figure 2.1; Bhandari *et al.*, 2019; Lapin *et al.*, 2019). Notably, these EDS1 residues are juxtaposed to PAD4^{R314} and PAD4^{K380} (Figure 2.1&2), suggesting that the EDS1-PAD4 EP domain cavity forms an immune signalling surface. However, what substrate binds this surface remains elusive. In contrast to PAD4, SAG101 mainly functions in TNL-ETI and host cell death (Rietz *et al.*, 2011; Lapin *et al.*, 2019). Recent insights in SAG101 suggest that differences between PAD4 and SAG101 signalling are determined by the characteristics of their EP domain cavities (Lapin *et al.*, 2019). Future studies should therefore determine which SAG101 EP domain cavity residues are required for SAG101 immune function in *Arabidopsis*, and whether this overlaps with the PAD4 residues identified in this chapter (Figure 2.3). Taken together, the results discussed in this chapter highlight the EDS1-PAD4 EP domain cavity as an essential signalling surface in pathogen immunity.

	480	700
Ach Achinensis_prT_AA_24904/1-533	GPARDCLRTAI
Ach Achinensis_prT_AA_26621/1-537	GPARECLRTAV
Aco Acoerulea_prT_AA_29401/1-626	ILFRERWGGNFM	QQARNCLMEAR
Aip Aipaensis_prT_AA_11177/1-632	IFRERWGSNFC	TPAMECLKTTR
Aip Aipaensis_prT_AA_33463/1-523	ILKERWGANFI	EPAKECLKEAR
Aly Alyrata_prT_AA_28775/1-542	ISRSRLAHNFC	VLVKECIETAT
Ath Athaliana_prT_AA_19963/1-541	ISRSRLAHNFC	VLVKECIETAT
Bdi Bidistachyon_prT_AA_18350/1-655	ILFRERWGGNFC	TTVRHWLKASK
Bol Bol005033_locusScaffold000309_247874_252062_+_translate_table_standard/1-549	ISQSHVAQNF C	VSAKECIETAT
Bol Bol009127_locusScaffold000238_435243_439447_+_translate_table_standard/1-543	ISRSRLAHNFC	VSAKEIEAAT
Bol Bol025038_locusScaffold000089_313039_317033_+_translate_table_standard/1-548	VSRSLRAHKFC	VSVKECIETAT
Bol Bol025040_locusScaffold000089_326718_328959_+_translate_table_standard/1-442	VSRSLRAYKFC	VLVKECIETAT
Bra G24607/1-644	ILFRERWGGNFC	-RLEDCLKIAR
Bra Brapa_prT_AA_14296/1-543	ISRSRLAHNFC	VSAKEIEAAT
Bra Brapa_prT_AA_9817/1-549	ISRSRVAQNF C	VSAKECIETAT
Bst Bstricta_prT_AA_1560/1-539	ISRSRLAHNFC	VSVKECVERAT
Bvu Bvulgaris_prT_AA_7708/1-627	LLRQRWAANFC	KQAEDSLKMOVK
Cca Cc02_g33900_Putative_alpha_beta-Hydrolases_superfamily_protein/1-514	ILQERWGGNFC	GPAKDCLKLAK
Col Colementina_prT_AA_2765/1-631	ILFRERWGGNFC	TAAKDCLKMAR
Cgr Cgrandiflora_prT_AA_4434/1-541	ISRSRLAHNFC	VSVKECIERAT
Cmo Cmollissima_prT_AA_13389/1-506	VLFRERWGGNFC	RPVKDCLKTAR
Cpa Cpapaya_prT_AA_14314/1-602	IIRERWAANFC	GAARDCLKMAR
Cru Crubella_prT_AA_1485/1-541	ISRSRLAHNFC	VSVKECIERAT
Cru Crubella_prT_AA_51/1-543	ISRSRLAHNFC	VLVKECIERAT
Csa Csativus_prT_AA_19232/1-596	ILQERWGGNFC	QIAEHLRTAS
Csl Csinensis_prT_AA_18446/1-619	ILFRERWGGNFC	TAAKDCLKMAR
Egg Eggplant_prT_AA_46462/1-584	ILQQRWPGHFC	EDAKEALKKAK
Esa Esalsugineum_prT_AA_24752/1-606	ISRSRLAHNFC	VSAKECIETST
Fve Fvesca_prT_AA_57/1-649	ILFRERWGGNFC	GPAVDCLKMAR
Gra Graumondii_prT_AA_33534/1-624	IRRRQWGNFC	VMAKECLQMAQ
Lus Lusitansimum_prT_AA_10194/1-683	ILAQRWGSNFC	RSQKECLKLAK
Lus Lusitansimum_prT_AA_26064/1-671	ILTRWAGNFC	RSQKECLKLAK
Mac Macuinata_prT_AA_19665/1-610	VLFRERWGGNFC	VEARECLET - -
Mac Macuinata_prT_AA_21215/1-603	ILFRERWGGNFC	MEAREWLEM - -
Mdo Mdomestica_prT_AA_27627/1-517	ILFRERWGGNFC	APAKECLKIAR
Mgu Myuttatus_prT_AA_27337/1-628	ILQERWCGNFC	GVGKDCIVMAR
Ntr Ntruncatula_prT_AA_15437/1-634	ISREKWGGNFC	IPAKECLKSAR
N/1-609	ILQERWAGHFC	EDAKKALKEAK
Osa Osativa_prT_AA_38565/1-659	ILFRERWAGNFC	APARQWTKTSK
Pab Pabies_prT_AA_10447/1-604	VGRENWAGNFC	-G - - - - -
Pab Pabies_prT_AA_11175/1-613	VGRENWAGNFC	- - ARTALRRAR
Pab Pabies_prT_AA_12615/1-691	VGRENWAGNFC	- - ARIALQRAV
Pab Pabies_prT_AA_14937/1-611	VGRENWAGNFC	- - AQITLQKAG
Pab Pabies_prT_AA_17054/1-617	VGRENWAGNFC	- - APIALQLAR
Pab Pabies_prT_AA_1935/1-691	VGRENWGGNFC	- - AQLALRKAG
Pab Pabies_prT_AA_19622/1-561	VGRENWAGNFC	- - AQITLQKAG
Pab Pabies_prT_AA_21626/1-455	VGRENWGSNFC	- - AQIGLQIAR
Pab Pabies_prT_AA_24551/1-472	VGRENWGGNFC	- - AWLAVQEAG
Pab Pabies_prT_AA_3145/1-626	VGRENWANNFC	- - ARISLQKAR
Pab Pabies_prT_AA_4241/1-653	LGRENWGGNFC	- - AQFALRRAG
Pab Pabies_prT_AA_539/1-610	VGRENWAGNFC	- - QIALQVAG
Pda Pdactylifera_prT_AA_2603/1-532	VLFRERWCGNFC	TEARECLEMSK
Pda Pdactylifera_prT_AA_27259/1-500	VQREWCGNFC	-EARECLKMSK
Ppe Ppersica_prT_AA_3793/1-519	ILFRERWGGNFC	EPAKECLKIAR
Pta Ptadea_prT_AA_10739/1-581	VGRENWGGNFC	- - AERALRKAG
Pta Ptadea_prT_AA_12528/1-496	VDRQNWAGNFC	- - ARTALLRVR
Pta Ptadea_prT_AA_14011/1-777	VGRENWAGNFC	- - APIALQIAR
Pta Ptadea_prT_AA_14157/1-625	VARENWAAANFC	- - AQIALQIAG
Pta Ptadea_prT_AA_23346/1-560	VGRENWAGNFC	- - ALIALQIAG
Pta Ptadea_prT_AA_25461/1-626	VARENWGSNFC	- - AQIALQIAG
Pta Ptadea_prT_AA_25463/1-697	VARENWAGNFC	- - AQIALQIAG
Pta Ptadea_prT_AA_25933/1-613	- - - - -	- - AQLALRKAG
Pta Ptadea_prT_AA_27859/1-583	VGRENWGGNFC	- - LGCALRSAG
Pta Ptadea_prT_AA_27860/1-606	VGRENWAGNFC	- - ARSALRTAG
Pta Ptadea_prT_AA_27861/1-731	IGREHWGGNFC	- - VKLALLSHE
Pta Ptadea_prT_AA_28290/1-632	VARENWAGNFC	- - AQIALQRAA
Pta Ptadea_prT_AA_32513/1-641	VGRENWAGNFC	- - AQIALQIAR
Pta Ptadea_prT_AA_32951/1-624	VGRENWAGNFC	- - APIALQMAK
Pta Ptadea_prT_AA_3397/1-613	IDRENWGGNFC	- - AGPALRSAS
Pta Ptadea_prT_AA_7803/1-488	VGRENWGTGNFC	- - AQIAFERAR
Pth Pthocarpa_prT_AA_22089/1-623	ILFRERWGGKFC	GRAKDCLKAAR
Pth Pthocarpa_prT_AA_28900/1-611	ILREKWGGKFC	GPAKDCLKAAR
Pvu Pvulgaris_prT_AA_26451/1-642	IFRERWGGNFC	TSAKECLKKTR
Pvu Pvulgaris_prT_AA_5620/1-617	ILKERWGGNFC	- - AKECLKLTR
Rco Rcommunis_prT_AA_25575/1-484	ILRQRWGANFC	RPAKDCLKLAR
SIN_1002055/1-599	ILQERWGGNFC	GTAVNCLATAR
SIN_1025448/1-636	ILQERWGGNFC	GTRNCLAMAR
Sbi Sbicolor_prT_AA_20484/1-670	ILFRERWGGNFC	STARQWTKTSK
Sit Sitalica_prT_AA_30531/1-664	ILFRERWGGNFC	STARQWLRTSR
Sly Slycopersicum_prT_AA_9259/1-578	ILQKRWAGHFC	EDAKEALKKAK
Stu Stuberosum_prT_AA_32565/1-578	ILQKRWAGHFC	EDAKEALKKAK
Tca Toacao_prT_AA_7250/1-607	ILFRERWGGNFC	IRAKDCLKMAR
Tca Toacao_prT_AA_9905/1-638	ILFRERWGGNFC	IMAKDCLKMAQ
Tpa Tparula_prT_AA_14685/1-548	ISRSRLAHNFC	VSAKECIETAT
Vvi Vvinifera_prT_AA_14582/1-629	ILFRERWAGNFC	GPAKDCLKMAK
Zu XP_015867358.1/1-628	ILFRERWGGNFC	IPAKECLKMAR
Zma Zmays_prT_AA_60322/1-655	ILFRERWGGNFC	STARQWTKTSK
Zma Zmays_prT_AA_6141/1-647	ILFRERWGGNFC	STARHWLTKTSK

Supplemental figure 2.1. Protein alignments of logos shown in figure 2.3.

Two alignments corresponding to the conservation logos shown in Figure 2.3. First alignment shows conservation within PAD4 (Figure 2.3A&B), and the second alignment spans two pages and displays conservation in PAD4 and SAG101 (Figure 2.3C&D). Mutated residues are indicated at the top of the alignment and correspond to the *At*PAD4 protein. Their colours correspond to the colours used in Figure 3.2 and 3.3. Alignment made using ClustalW and visualised using Jalview. PAD4 and SAG101 sequences were obtained by Dmitry Lapin (Lapin *et al.*, 2019).

Supplemental figure 2.1. Protein Alignments of logos shown in figure 2.3.
 See description on before previous page

SAG101Ach Achinensis_prT_AA_2594/1-520	.VFDP-SKLLNEMKINMTYLEWYKKVSV--S	EGQFLH--PIWYSGTYRRMVEPLDAEY
SAG101Aha Ahalieri_prT_AA_10229/1-523	LRFDL-FKLLNDMKISMAYLEWYKKECRKV--	DISILK--RRFLSGNNYRRMIEPLDAEY
SAG101Aip Alpaensis_prT_AA_33048/1-587	.IFDP-TKLLNVKQVDMVQLLEWYKKDSRN-Q	EGAAFR--TRWYAGTNYRRMVEPLDAEY
SAG101Alj Allyrata_prT_AA_1537/1-526	LRFDL-FKLLNDMKISMAYLEWYKKECRKV--	DISILK--RRFLSGNNYRRMIEPLDAEY
SAG101Ath Athaliana_prT_AA_2284/1/1-537	LRFDMMF-SKLLNDMKISMAYLEWYKKECKEV--	DASILK--RRFLSGNNYRRMIEPLDAEY
SAG101Ath Atrichopoda_prT_AA_2605/1-508	.VFHP-SKLLNLMKMNMAQLEWYIKQCKD-L	TNVKLR--IAIFSGNTFRMVEPLDAEY
SAG101Bol Bol030417_locusScaffold000060_1199103	LRYPDQ-LKLLNDKIKSMIYLEWYKKSCKE--	EKSLK--TRFLSGNNYRRMVEPLDAEY
SAG101Bol Bol030418_locusScaffold000060_1210274	QRFDQ-LKLLDEVKISMAYLEWYKKSCKG--	EASLYK--KRCLESGNNYRRMVEPLDAEY
SAG101Bol Bol034308_locusScaffold000039_636347	QRFDQ-LKLLNEIKISMIYLEWYKKSCKME--	RKALLK--TRFLSGNNYRRMVEPLDAEY
SAG101Bol Bol034309_locusScaffold000039_640330	LRFDL-LIKLNDMKIKSMIYLEWYKKSCKE--	EKSLK--TRFLSGNNYRRMVEPLDAEY
SAG101Bol Bol034310_locusScaffold000039_645841	PRFDP-LIKLNDMKIKSMIYLEWYKKSCKM--	EKSLK--TRFLSGNNYRRMIEPLDAEY
SAG101Brae_G09721/1-597	.NSDS-DKLLNEMKVMAYLEWYKKSCKQ-R	EGAHFR--IRWYAGTNYRRMVEPLDAEY
SAG101Brae_G09723/1-1226	.NSDS-DKLLNEMKIMAYLEWYKKSCKA-R	EGAHFR--IRWYAGTNYRRMVEPLDAEY
SAG101Brae_G22274/1-598	KDSFS-DKLLNEMKICLALLEWYKKEANL-L	KGAHFG--VRWYAGTNYRRMVEPLDAEY
SAG101Bra Brapa_prT_AA_7129/1-520	LRYPDQ-LKLLNDKIKSMIYLEWYKKSCKME--	EKSLK--TRFLSGNNYRRMVEPLDAEY
SAG101Bra Brapa_prT_AA_7346/1-525	QRFDQ-LKLLNDKIKSMIYLEWYKKSCKGH--	EKSNLK--TRFLSGNNYRRMVEPLDAEY
SAG101Bra Brapa_prT_AA_8623/1-501	RRFDR-LQKLDIMKIKSMIYLEWYKKSCKL--	EKALFK--TRFLAANNYRRMVEPLDAEY
SAG101Bst Bstncta_prT_AA_8028/1-530	LRFDQ-LKLLNDMKIKSMIYLEWYKKSCKN--	EKSLK--TRFLSGNNYRRMIEPLDAEY
SAG101Can CA02y08B70_PREDICTED_senescence-ass	.AFDP-GKLLNEMKEMAWLEWYKKSCKVTLN--	EEAVFR--TRWYAGTNYRRMVEPLDAEY
SAG101Cca Ccanephora_prT_AA_13865/1-600	.IFDP-TKLLNDKIKSMIYLEWYKKSCKV--	EGLAFR--TRWYAGTNYRRMVEPLDAEY
SAG101Ccl Celemantina_prT_AA_9725/1-574	.GFDP-SKLLNEMKEDMAKLEWYKKSCKS-E	EEASFR--TRWYSGTNYRRMVEPLDAEY
SAG101Cgr Cgrandiflora_prT_AA_944/1/1-553	LRFDQ-LKLLNDMKIKSMIYLEWYKKSCKN--	EKSLK--TRFLSGNNYRRMIEPLDAEY
SAG101Cml Cmollisima_prT_AA_21683/1-465	.VFDP-SKLLNDMKINMAYLEWYKKSCKK--	EGASFR--TRWYAGTNYRRMIEPLDAEY
SAG101Cml Cmollisima_prT_AA_25580/1-426	.GFDP-SK--	EGASFR--
SAG101Cml Cmollisima_prT_AA_31624/1-453	.VFDP-STKLNQVQVHMALNLEWYKKSCKVAKD-K	VGASLR--TRWYSGTNYRRMIEPLDAEY
SAG101Cml Cmollisima_prT_AA_32766/1-454	.AFDP-TRGLNEKIKVLMAYLEWYKKSCKD-E	VGASLR--TRFLSGTNYRRMIEPLDAEY
SAG101Cml Cmollisima_prT_AA_32767/1-408	-----KLSK-D-E	VGASLR--TRFLSGTNYRRMIEPLDAEY
SAG101Cml Cmollisima_prT_AA_36572/1-527	.AFDP-TKGLNDKVVYMAYLEWYKKSCKD-E	VGAF LR--TRFLSGTNYRRMIEPLDAEY
SAG101Cml Cmollisima_prT_AA_5102/1-577	.AFDP-TRGLNDKVVYMAYLEWYKKSCKD-K	VGASLR--TRFLSGTNYRRMIEPLDAEY
SAG101Cml Cmollisima_prT_AA_6703/1-463	.QGNP-SKTLNEIKIRMAYLEWYKKSCKE-K	EGAFR--TRWYAGTNYRRMIEPLDAEY
SAG101Cpa Cpapaya_prT_AA_490/1-468	.VFDP-SKLLNEMKIMAYLEWYKKSCKD-R	EGASFR--TRWYAGTNYRRMIEPLDAEY
SAG101Csa Csaohivus_prT_AA_18453/1-583	.NTKL-AKTLNDVKIKMARLEWYKKSCKL-E	HGVPFD--TRWYAGTNYRRMIEPLDAEY
SAG101Csi Csinensis_prT_AA_23165/1-449	.GFDP-SKLLNEMKEDMAKLEWYKKSCKS-E	EEASFR--TRWYSGTNYRRMVEPLDAEY
SAG101Egg Egypplant_prT_AA_68769/1-647	.AFDP-GKLLNEMKEMAWLEWYKKSCKVTLN--	EEAARF--TRWYAGTNYRRMVEPLDAEY
SAG101Egg Sme2_5_1015B_1_g00003_1_TE/1-579	.DFDP-SK-ISISIKKSLSYLEWYKKSCKSLE--	ERRIRR--KRLYAVTNYRRMIEPLDAEY
SAG101Esa Esalsugineum_prT_AA_12115/1-511	VRFDQ-FKLLNDMKISMAKVVYIKESRNI--	DISILK--RRFLSGNYRRMIEPLDAEY
SAG101Esa Esalsugineum_prT_AA_21238/1-524	QRFDQ-LKLLNDKIKSMAKVVYIKESRND--	EKSVLK--TRFLSGNNYRRMIEPLDAEY
SAG101Esa Esalsugineum_prT_AA_22698/1-519	VRFDQ-FKLLNDMKIKSMAKVVYIKESRND--	DISILK--RRFLSGNNYRRMIEPLDAEY
SAG101Fve Fvesoa_prT_AA_9358/1-713	.NSDS-DKLLNEMKVMAYLEWYKKSCKQ-P	EGAHFR--IRWYAGTNYRRMVEPLDAEY
SAG101Gra Graumondii_prT_AA_3256/1-1587	.AFDP-AKLLNVIKIKMALEWYKKSCKA-N	QLVYLR--SRWYAGTNYRRMVEPLDAEY
SAG101Lus Lusitathissimum_prT_AA_17149/1-545	.AMEP-SRKLNEIKIKVYLGRYKQECRK-K	EGSHVR--VSWYSGTNYRRMVEPLDAEY
SAG101Lus Lusitathissimum_prT_AA_21999/1-607	.ATEQ-SRKKVQETKVKMAYLEWYKKSCKLNR	EGSFR--TRWYSGTNYRRMVEPLDAEY
SAG101Lus Lusitathissimum_prT_AA_31706/1-610	.ATEQ-SRKKVQETKVKMAYLEWYKKSCKLNR	EGSFR--TRWYSGTNYRRMVEPLDAEY
SAG101Lus Lusitathissimum_prT_AA_36339/1-464	.AMDQ-SRKLNDKIKIRMAYLEWYKKSCKK-K	EGSYIS--MMWYAGTNYRRMIEPLDAEY
SAG101Lus Lusitathissimum_prT_AA_8149/1-613	.AMEP-SRKLNEIKIKVYLGRYKQECRK-K	EGSHVR--VSWYSGTNYRRMVEPLDAEY
SAG101Mio Miomestica_prT_AA_16648/1-567	.VYSS-FWKLNEIKKYMAYLEWYKKSCKE-M	EGAXMR--TRFLSGTNYRRMIEPLDAEY
SAG101Mio Miomestica_prT_AA_16862/1-696	.VYSS-FWKLNEIKKYMAYLEWYKKSCKE-M	EGAXMR--TRFLSGTNYRRMIEPLDAEY
SAG101Mio Miomestica_prT_AA_19008/1-513	.VYSS-YLKLNEIKKYMAYLEWYKKSCKE-M	EGAXMR--TRFLSGTNYRRMIEPLDAEY
SAG101Mio Miomestica_prT_AA_3231/1-487	.AYSS-FLKLNEIKKYMAYLEWYKKSCKE-M	EGAXMR--TRFLSGTNYRRMIEPLDAEY
SAG101Mio Miomestica_prT_AA_35154/1-665	.VYSS-FWKLNEIKKYMAYLEWYKKSCKE-M	EGAXMR--TRFLSGTNYRRMIEPLDAEY
SAG101Mio Miomestica_prT_AA_39662/1-742	.VYSS-FLKLNEIKKYMAYLEWYKKSCKE-M	EGAXMR--TRFLSGTNYRRMIEPLDAEY
SAG101Mio Miomestica_prT_AA_44668/1-513	.VYSS-SLKLNEIKKYMAYLEWYKKSCKE-M	EGAXMR--TRFLSGTNYRRMIEPLDAEY
SAG101Mio Miomestica_prT_AA_49744/1-598	.VYSS-FWKLNEIKKYMAYLEWYKKSCKE-M	EGAXMR--TRFLSGTNYRRMIEPLDAEY
SAG101Mio Miomestica_prT_AA_5472/1/1-672	.VYSS-FWKLNEIKKYMAYLEWYKKSCKE-M	EGAXMR--TRFLSGTNYRRMIEPLDAEY
SAG101Mio Miomestica_prT_AA_60727/1-737	.VYSS-FXKLNEIKKYMAYLEWYKKSCKE-M	EGAXMR--TRFLSGTNYRRMIEPLDAEY
SAG101Mio Miomestica_prT_AA_61106/1-702	.VYSS-FXKLNEIKKYMAYLEWYKKSCKE-M	EGAXMR--TRFLSGTNYRRMIEPLDAEY
SAG101Mri Mtruncatula_prT_AA_39740/1-578	.KFDQ-SKLLNEMKIKMALEWYKKSCKN-R	EGASLR--TRWYSGTNYRRMVEPLDAEY
SAG101Mri Mtruncatula_prT_AA_40254/1-575	.SFPN-SNKKQEMKGGIAQVLEWYKKSCKTTN-L	EGAFR--TRWYSGTNYRRMVEPLDAEY
SAG101Mri Mtruncatula_prT_AA_42027/1-577	.SFPD-SKLLNEMKIKMALEWYKKSCKN-L	EGAFR--TRWYSGTNYRRMVEPLDAEY
SAG101Mri Mtruncatula_prT_AA_42271/1-501	.SFPD-SKLLNEMKIKMALEWYKKSCKN-L	EGAFR--TRWYSGTNYRRMVEPLDAEY
SAG101Mri Mtruncatula_prT_AA_42540/1-578	.SFPD-SKLLNEMKIKMALEWYKKSCKN-L	EGAFR--TRWYSGTNYRRMVEPLDAEY
SAG101Mri Mtruncatula_prT_AA_4305/1-581	.LFDQ-SKLLNDKIKVDMADLEWYKKSCKN-E	EGAFR--TRWYAGTNYRRMVEPLDAEY
SAG101N/1-514	.VFDP-SKLLSTLKKSMSYLEWYKKSCKSLE--	-----ERWYAGTNYRRMVEPLDAEY
SAG101Niben101Scf00271g02011.1/1-561	.VFDP-SKLLSTLKKSMSYLEWYKKSCKSSE--	EGRSLR--KRWYAGTNYRRMVEPLDAEY
SAG101Niben101Scf01300g01009.1/1-582	.AFDP-GKLLSKIKEDMAYLEWYKKSCKTLN--	EEAARF--TRWYSGTNYRRMVEPLDAEY
SAG101Niben101Scf09577g01001.1/1-554	.AFDP-GKLLSKIKEDMAYLEWYKKSCKTLN--	RKQLF--
SAG101Ppe Ppersica_prT_AA_11978/1-614	.TSNA-AKLLNDIKVSMVYLEWYKKSCKG-R	EGTAFR--TRWYAGTNYRRMVEPLDAEY
SAG101Ppe Ppersica_prT_AA_15456/1-617	.TSNA-AKLLNDIKVSMVYLEWYKKSCKG-R	EEAALR--TRWYAGTNYRRMVEPLDAEY
SAG101Ppe Ppersica_prT_AA_90/1-589	.ASNA-AKLLNDKIKVSMVYLEWYKKSCKD-R	EGAALR--TRWYAGTNYRRMVEPLDAEY
SAG101Pth Pthocarpa_prT_AA_35562/1-464	.GIDG-IEKLNRIKIKMALEWYKKSCKA-K	EGAYMR--ETWYAGTNYRRMVEPLDAEY
SAG101Pth Pthocarpa_prT_AA_6089/1-596	.AIDP-NEKLNRIKIKMALEWYKKSCKA-K	EGAFMR--ETWYAGTNYRRMVEPLDAEY
SAG101Pth Pthocarpa_prT_AA_6950/1-605	.TRGS-ENLNRIKIKMALEWYKKSCKA-K	EGAFIR--AAWYAGTNYRRMVEPLDAEY
SAG101Pth Pthocarpa_prT_AA_6967/1-640	.TMDP-RKRLNQIKIKMALEWYKKSCKA-K	EGAFIR--GTWYAGTNYRRMVEPLDAEY
SAG101Pvu Pvulgans_prT_AA_15632/1-569	.KFDQ-SKLLNEMKIKMALEWYKKSCKG-Q	EEAARF--IRWYAGTNYRRMVEPLDAEY
SAG101Rco Rcommunis_prT_AA_11606/1-600	.ALNP-SRKLNEIKIKMALEWYKKSCKK--	EGSFR--GTWYAGTNYRRMVEPLDAEY
SAG101Sly Slyopersicum_prT_AA_1122/1-581	.LFDQ-SK-ISKTKSMSYLEWYKKSCKSLE--	EGSTR--KRLYAATNYRRMVEPLDAEY
SAG101Sly Slyopersicum_prT_AA_9810/1-567	.AFDP-GKLLNEMKEMAWLEWYKKSCKTLK--	EEAVFR--TRWYAGTNYRRMVEPLDAEY
SAG101Stu Stuberosum_prT_AA_3306/1/1-576	.AFDP-GKLLNEMKEMAWLEWYKKSCKTLK--	EEAARF--TRWYAGTNYRRMVEPLDAEY
SAG101Stu Stuberosum_prT_AA_34228/1-576	.VFDP-FK-ISVTKKSLTNLEWYKKSCKSLE--	EGKIRR--KRLYAATNYRRMVEPLDAEY
SAG101Tca Tcaaoa_prT_AA_22116/1-592	.VFDP-AKLLNDKIKMALEWYKKSCKA-E	EG--VR--TRWYAGTNYRRMVEPLDAEY
SAG101Tpa Tparula_prT_AA_20214/1-526	LRFDQ-LKLLNEMKIKMALEWYKKSCKE-A	DISMLT--TRWYAGTNYRRMVEPLDAEY
SAG101Tpa Tparula_prT_AA_20215/1-741	LRFDQ-LKLLNDKIKMALEWYKKSCKD--	EKSVLK--TRFLSGNNYRRMVEPLDAEY
SAG101Vvi Vvinifera_prT_AA_21819/1-404	.KASD-AKLLNDKIKMALEWYKKSCKD-L	EGAFR--TRWYSGTNYRRMVEPLDAEY
SAG101Vvi Vvinifera_prT_AA_23718/1-458	.KVSQ-AKLLNDKIKMALEWYKKSCKD--	EGAFR--TRWYAGTNYRRMVEPLDAEY
SAG101Vvi Vvinifera_prT_AA_23718/1-521	.KASD-AKLLNDKIKMALEWYKKSCKD--	EGAFR--TRWYAGTNYRRMVEPLDAEY
SAG101Zju ZjuSAG101a XP_015879235.1/1-588	.LFDQ-SKLLNDKIKVYVLEWYKKSCKN-D	EGASFR--IRWYAGTNYRRMVEPLDAEY
SAG101Zju ZjuSAG101b XP_015879187.1/1-591	.SFPN-SKLLNDKIKVYVLEWYKKSCKD-Q	EGASLR--TRWYAGTNYRRMVEPLDAEY
SAG101Zju ZjuSAG101c XP_015879209.1/1-615	.QFDP-SKLLNDKIKVYVLEWYKKSCKD-Q	EGASLR--SRWYAGTNYRRMVEPLDAEY

Chapter 3: Identification of active PAD4 protein complexes during *Pst avrRps4* infection

The previous chapters described that PAD4^{LLD}, PAD4^{R314A} and PAD4^{K380A} were unable to function in basal immunity and ETI, and do not transcriptionally activate immune-related genes in ETI. This evidence highlights the EDS1-PAD4 EP domain cavity as an essential immune signalling surface, as previously proposed by Bhandari *et al.* (2019) and Lapin *et al.*, (2019). I hypothesise that during immune signalling the EDS1-PAD4 heterodimer cavity needs to interact with a key molecule, which could be a metabolite or a protein. The metabolite might be a signalling molecule: *e.g.* an NAD⁺-derived compound produced by activated TIR domains (Horsefield *et al.*, 2019; Wan *et al.*, 2019). Although the EP domain cavity might bind a signalling intermediate, eventually EDS1-PAD4 are likely to interact with one or more proteins to regulate the immune response and transcriptional reprogramming. To identify proteins that interact with PAD4 during the immune response, I performed IP coupled to nano-scale liquid chromatographic tandem mass spectrometry (IP nLC-MS/MS). In this chapter, I will discuss the results of this IP nLC-MS/MS analysis and subsequent experiments I performed to validate putative PAD4 interactors identified by IP nLC-MS/MS.

Experimental outline and rationale

To identify proteins that associate to actively signalling PAD4, I compared the interactomes of pathogen-challenged PAD4^{WT} with PAD4^{K380A}. This allowed me to investigate which proteins interact with non-signalling (inactive) PAD4^{K380A} and signalling (active) PAD4^{WT}. By focusing on proteins that were exclusively bound by PAD4^{WT}, I was able to identify interactors that exclusively engage with actively signalling PAD4 complexes. Besides PAD4^{K380A}, I also performed IP on PAD4^{LLD}, however, due to limited insights gained from PAD4^{LLD} I will not discuss these results here. For results that are more reliable, I used PAD4 lines accumulating similar PAD4 levels, *i.e.* cPAD4^{WT} #5 and cPAD4^{K380A} #12. These lines showed similar protein levels in preliminary experiments out of the cPAD4^{WT}, cPAD4^{R314A} and cPAD4^{K380A} lines discussed in chapter 2. I only used PAD4^{K380A} for this experiment, and not PAD4^{R314A}, since performing IP on four PAD4 lines would not have been feasible experimentally. Lastly, as a negative control I used a 35S::StrepII-YFP line that expresses the same tag as the cPAD4 lines, thereby eliminating any proteins that have affinity for StrepII-YFP (Lapin *et al.* 2019).

To detect PAD4 interactors during ETI signalling, I sampled RRS1-S/RPS4 TNL-ETI activated leaves. Four-week-old plants were vacuum infiltrated with *Pst avrRps4* at OD₆₀₀ = 0.1 for synchronous ETI activation, and samples were harvested at 4 and 6 hpi (Figure 3.1A). I chose these time-points since upon infection with *Pst avrRps4* EDS1 accumulates in the nucleus from 3 hpi and initial EDS1-dependent transcriptional changes occur at 3 hpi, which is followed by major transcriptional changes at 8 hpi (Bartsch *et al.*, 2006; Bhandari *et al.*, 2019; Garcia *et al.*, 2010). Thus, suggesting EDS1-PAD4 signalling complexes will have formed at 4 and 6 hpi. Samples were immunoprecipitated and delivered to the MPIPZ mass spectrometry group for processing (Dr. Sara Stolze and Anne Harzen; Dr. Hirofumi Nakagami Group). For both time-points, the LFQ (Label-free quantification) values were highly similar between all three genotypes and four experimental replicates, showing a Pearson's correlation (ρ) between 0.719 and 0.976, indicating these data were suitable for further analysis. For initial comparisons, I selected putative interactors based on an FDR of 0.05 and a *p*-value cut-off of <0.05 (two-sample t-test). At this threshold, I identified 311 putative interactors for PAD4^{WT}, with only 16 proteins shared between the two time-points (Figure 3.1B). EDS1 and PAD4 were among these 16 proteins, suggesting the IP was successful. Moreover, this indicates that EDS1 and PAD4 form a signalling complex in Arabidopsis upon infection with *Pst avrRps4*. Only 5% of identified proteins overlapped between 4 and 6 hpi samples, suggesting that PAD4 immune complexes are highly dynamic (Figure 3.1B).

GO-Term analysis

Gene Ontology (GO) term analysis showed that many of the identified interactors are predicted to localise to nuclear (32%) and cytosolic (50%) compartments, like PAD4 (Figure 3.1C). However, many proteins were predicted to localise to other cellular compartments (Figure 3.1C). These proteins were annotated to have diverse molecular functions (Figure 3.1D) and function in various biological processes (Figure 3.1E). However, this did not highlight a particular molecular function or biological process. Although certain proteins binned to GO-terms such as "cell death" and "response to biotic stimulus", there was no significant enrichment of a specific group of GO-terms. On the contrary, there were 89 Biological Process GO-terms and 20 Molecular Function GO-terms significantly enriched for the 311 PAD4 interactors (PANTHER Overrepresentation Test; released 20190711; Arabidopsis genome; Biological processes and Molecular Function; Fisher Exact with Bonferroni correction). Taken together, this GO-term analysis did not reveal which protein function or process is working in concert with PAD4 during immune signalling.

Chapter 3:
Identification of active PAD4 protein complexes during Pst avrRps4 infection

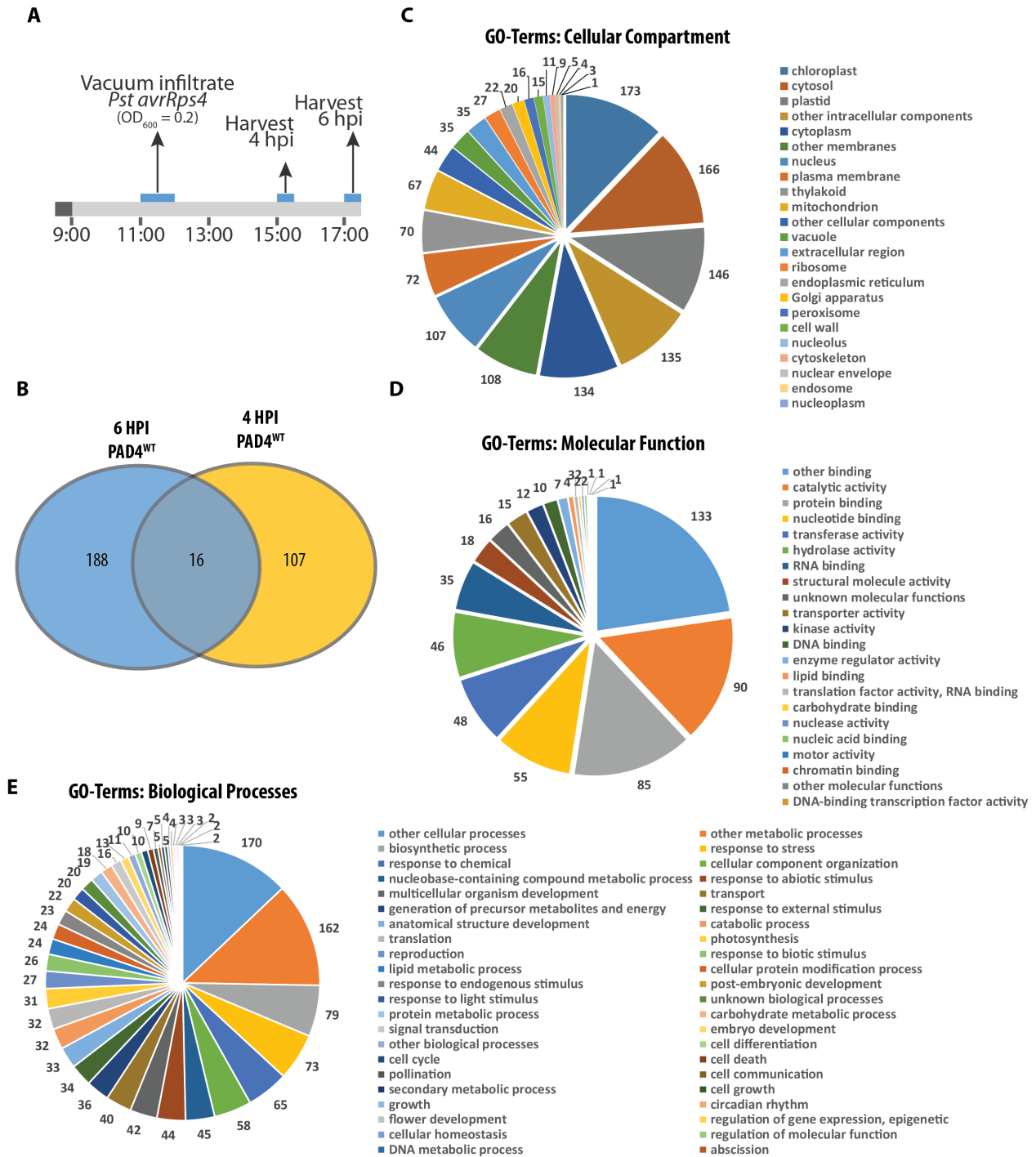


Figure 3.1. Summary of IP nLC-MS/MS on $PAD4^{WT}$ at four and six hpi.

A. Experimental set-up of IP-nLC-MS/MS experiment. Dark bar indicates nighttime, light bar indicates daytime, blue bars indicate duration of activity. **B.** Venn diagram showing the number of unique and overlapping identified interactors of $PAD4$ at four and six hpi at $FDR = 0.05$ and $p < 0.05$ (two-sample t -test). **C.** TAIR Predicted GO-terms in the category “cellular compartment” found for all $PAD4$ interactors at four and six hpi combined. **D.** As in C, but on GO-term “molecular functions.” **E.** As in C, but on GO-term “biological processes.”

Differential interactors of PAD4^{WT} and PAD4^{K380A} at 4 and 6 hpi

To identify relevant PAD4 interactors during ETI signalling, I compared interactomes of PAD4^{WT} and PAD4^{K380A} at 4 and 6 hpi (Figure 3.2). For each of the putative interactors I looked up the TAIR curated descriptions, browsed through publications on the protein (if any), and based on this information I determined whether a protein is potentially involved in immune signalling. For each protein, I manually binned these in different categories, *i.e.* cell death, immunity, transcription regulation, jasmonic acid, calcium signalling, nuclear trafficking and protein homeostasis (Figure 3.2). Inevitably, this approach created a bias in the proteins I selected. For example, I was sceptical of selecting chloroplast- and metabolism-related proteins since I deemed them unlikely to function in PAD4-dependent immune signalling. Consequently, there are putative interactors that perhaps do contribute to PAD4 immunity, which were not discussed here. Besides manually binning proteins in separate categories, I also included ASPARTIC PROTEASE IN GUARD CELL 1 (ASPG1; AT3G18490) in Figure 3.2. Recently, ASPG1-related ASPG2 was linked to EDS1-PAD4 function (Baggs *et al.*, 2019). This is based on *in silico* analyses where EDS1-PAD4 and ASPG2 have been co-lost in aquatic angiosperm species, and where *AtASPG2* is downregulated upon pathogen infection (Baggs *et al.*, 2019). This suggests antagonistic role of ASPG1 in EDS1-PAD4 immune responses, however, the role ASPGs remains unclear. From the manually curated list of proteins I selected three proteins to study further, *i.e.* METHYL ESTERASE 10 (MES10), Suppressor of G2 allele of SKP1 (SGT1b) and TOPLESS (TPL) RELATED 1 (TPR1). In the next paragraphs, I will discuss the proteins I found relevant to include in Figure 3.2, and why I chose to focus on MES10, SGT1b and TPR1.

The first proteins I discuss are relevant for both cell death and immunity. These include, besides EDS1 and PAD4, EUKARYOTIC TRANSLATION INITIATION FACTOR 5A-2 (ELF5A-2) and ACCELERATED CELL DEATH 2 (ACD2) (Figure 3.2). ELF5A-2 functions in protein translation, and knockdown lines of *ELF5A-2* show enhanced resistance to *Pst* DC3000 (Hopkins *et al.*, 2008). ACD2 is a chloroplast localised protein that relocates to the cytoplasm, mitochondria, and heterochromatic regions in the nucleus during basal immunity triggered by *P. syringae* *pv.* *maculicola* (*Psm*) (Mach *et al.*, 2001; Yao & Greenberg, 2006). Furthermore, ACD2 was reported to inhibit cell death execution and enhance resistance outputs (Greenberg *et al.*, 1994; Mach *et al.*, 2001; Yao & Greenberg, 2006). Based on these publications and since both proteins interacted with PAD4^{WT} and not PAD4^{K380A}, I hypothesise that ELF5A-2 and ACD2 are relevant putative interactors of PAD4 in immunity.

PAD4^{WT} immunoprecipitated several enzymes capable of regulating JA (-precursor) levels, *i.e.* ALLENE OXIDASE CYCLASE 2 (AOC2), LIPOXYGENASE 1 (LOX1) and METHYL ESTERASE 10 (MES10) (Figure 3.2). AOC2 performs an essential step in the JA-biosynthesis pathway, producing the oxylipin 12-oxo-phytodienoic acid (OPDA) (Wasternack & Song, 2017). LOX1 produces a specific group of oxylipins functioning in basal immunity, but not CNL-ETI (*Pst avrRpm1*) (Montillet *et al.*, 2013; Vicente *et al.*, 2012). MES10 and its family members MES1/2/3/9/16 harbour methyl-JA (MeJA) esterase activity *in vitro* (Yang *et al.*, 2008). In contrast to its family members, MES10 specifically shows esterase activity to MeJA, but not to methyl Indole-acetic acid, Me-SA, Me-Giberellin₄ and Me-Giberellin₆ (Yang *et al.* 2008). Remarkably, MES10 was one of three proteins that immunoprecipitated with both PAD4^{WT} and PAD4^{K380A} at both time-points (Figure 3.2). Since there is a clear link between

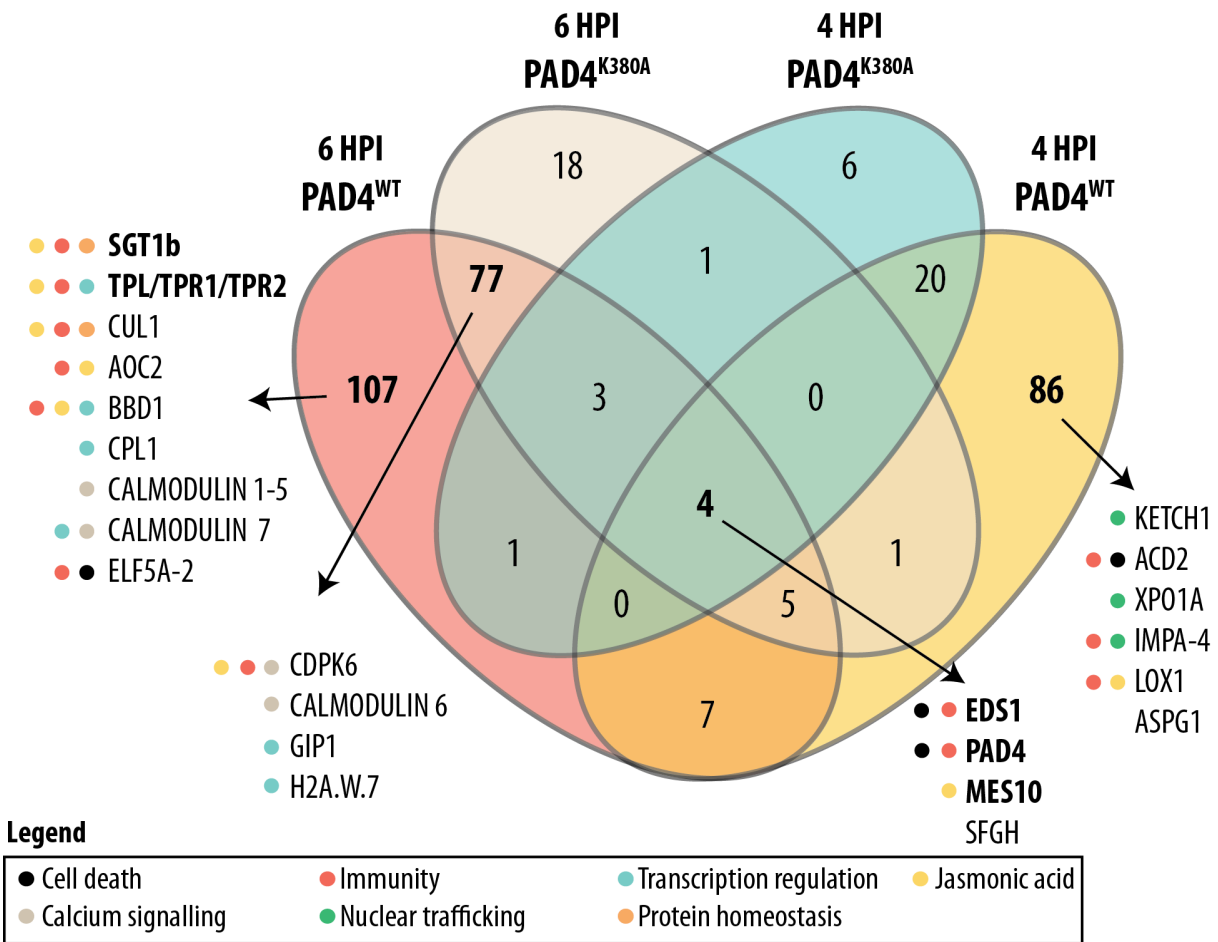


Figure 3.2. PAD4^{WT} and PAD4^{K380A} interactors at 4 and 6 hpi.

PAD4^{WT} and PAD4^{K380A} interactors as identified by IP nLC-MS/MS at 4 and 6 hpi with *Pst avrRps4* (FDR=0.05; $p < 0.05$). At certain overlaps in the Venn diagram I pointed out putative PAD4 interactors that could potentially be relevant in immune signalling. For each of these proteins a coloured dot indicates which process(es) the protein has been shown to function in. References for these annotations are mentioned in the main text.

EDS1 heterodimers and dampening of JA-signalling (Cui *et al.*, 2018), I questioned whether PAD4 is able to regulate MES10, and consequently affect JA-signalling. For this reason, I interrogated MES10 in more detail, which I will discuss in the next section of this chapter. Interestingly, the only other protein that was immunoprecipitated at both time-points by both PAD4 variants, besides MES10 and EDS1, was S-FORMYLGLUTATHIONE HYDROLASE (SFGH; AT2G41530) (Figure 3.2). In bacteria, mammals and yeast, this highly conserved protein functions in formaldehyde detoxification. In Arabidopsis, one gene encodes for SFGH, which has been shown to harbour hydrolase, thioesterase and carboxyesterase activity (Kordic *et al.*, 2002). *SFGH* transcripts are downregulated in autoimmune 35S::*RPS4* plants relative to Col-0 (>2-fold, $p < 0.01$; GEO: GSE40216, Genevestigator v7.5.1, Hruz *et al.*, 2008), suggesting an EDS1-dependent repression of *SFGH* expression. Whether SFGH functions in immunity is unknown.

Another group of proteins that stood out were related to calcium signalling, *i.e.* CALMODULIN (CAM) 1-7 and CALCIUM DEPENDENT PROTEIN KINASE 3 (CPK3/CDPK6; AT4G23650) (Figure 3.2). CAM 1-7 were only bound by PAD4^{WT} at six hpi, of which only CAM6 is also bound PAD4^{K380A}, suggesting only active PAD4 is able to recruit these CAMs. CAMs bind immunity-regulating TFs, such as the immune regulator CALMODULIN BINDING PROTEIN 60-LIKEg (CBP60g) (Reddy *et al.*, 2011; Wang *et al.*, 2009&2011; Zhang *et al.*, 2010). However, these CAMs are common contaminants in IP nLC-MS/MS experiments, and could therefore be false positives (van Leene *et al.*, 2015). Another putative interactor of PAD4 is CPK3. This is a calcium-regulated kinase tethered to the plasma membrane and vacuole by myristoylation of its N-terminus (Mehlmer *et al.*, 2010). CPK3 promotes the expression of the JA-responsive gene *PLANT DEFENSIN1.2* (*PDF1.2*), but not *VEGETATIVE STORAGE PROTEIN 1* (*VSP1*), and can phosphorylate certain TFs *in vitro*, such as the JA/Ethylene inducible ETHYLENE RESPONSE FACTOR 1 (ERF1), and the wound inducible SALT-INDUCIBLE ZINC FINGER 2 (SZF2; Kanchiswamy *et al.*, 2010). This suggests CPK3 activates the immunity and ABA branch of JA-signalling against necrotrophic pathogens (Pieterse *et al.*, 2012). Since EDS1-PAD4 functions antagonistically to JA (Cui *et al.*, 2018), and we detected several genes related to JA-biosynthesis and -signalling (Figure 3.2), I postulate that CPK3 plays a role in EDS1-PAD4 immune signalling.

Another set of proteins that stood out were related to nuclear shuttling, *i.e.* EXPORTIN 1A (XPO1A), IMPORTIN ALPHA ISOFORM-4 (IMPA-4; close relative of MODIFIER OF SUPPRESSOR OF NPR1-1 CONSTITUTIVE 1 (SNC1) 6 (MOS6)/IMPA-3) and

KARYOPHERIN ENABLING THE TRANSPORT OF THE CYTOPLASMIC HYL1 (KETCH1) (Contreras *et al.*, 2019; Roth *et al.*, 2017; Stankovic *et al.*, 2015; Xiong *et al.*, 2020; Zhang *et al.*, 2017a). Notably, these proteins only associated at 4 hpi with PAD4^{WT}, when EDS1 accumulates in the nucleus (Figure 3.2) (Garcia *et al.*, 2010), suggesting PAD4 is transported into the nucleus at 4 hpi with *Pst avrRps4*. In the nucleus, EDS1 binds proteins involved in transcriptional reprogramming (Bhandari *et al.*, 2019; Bhattacharjee *et al.*, 2011; Garcia *et al.*, 2010; Stuttmann *et al.*, 2016). Strikingly, PAD4^{WT} associated to several nuclear proteins related to transcriptional regulation at six hpi with *Pst avrRps4*, *i.e.* TPL/TPR1/TPR2, BIFUNCTIONAL NUCLEASE IN BASAL DEFENSE RESPONSE 1 (BBD1), C-TERMINAL DOMAIN PHOSPHATASE-LIKE 1 (CPL1), GBF-INTERACTING PROTEIN 1 (GIP1) and the histone variant H2A.W.7 (Figure 3.2).

For TPL/TPR1/TPR2, one peptide was identified, which was insufficient to differentiate between the three TPL family members. The Arabidopsis TPL-family proteins function in JA-signalling, among other hormone pathways (Long *et al.*, 2006; Lynch *et al.*, 2017; Oh *et al.*, 2014; Wasternack & Song, 2017). *TPR1* functions redundantly with *TPL* and *TPR4* in basal immunity and TNL-ETI, but not CNL-ETI (Zhu *et al.*, 2010). However, I decided to focus on TPR1, since autoimmunity caused by an auto-active allele of the TNL *sncl* is suppressed by *pad4* and *tpr1*, but only weakly by *tpl* (Zhu *et al.*, 2010). Furthermore, autoimmunity caused by *TPR1*-overexpression is dependent on *PAD4* and *EDS1* (Zhu *et al.*, 2010). Moreover, previous work in the Parker Lab has uncovered a functional link between TPR1 and EDS1-PAD4 dependent immune activation (unpublished work from T. Griebel - Parker Lab). Taken together, TPR1 was a promising interactor of PAD4 in immunity.

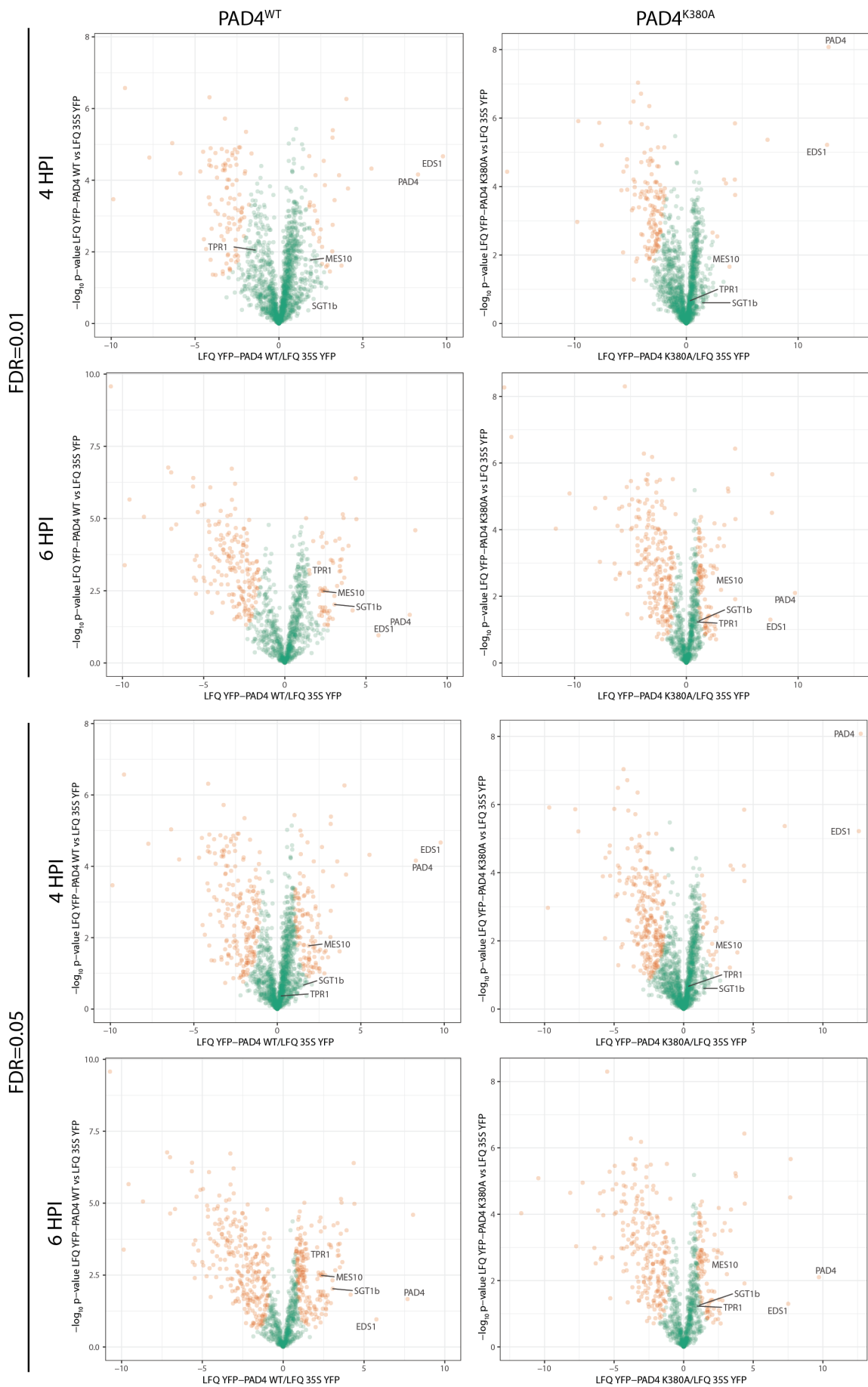
BBD1 is also an interesting putative interactor since it is required for resistance to necrotrophic *Botrytis cinerea*, specifically binds JA response *cis*-elements (JARE), and it is able to interact with the JA-signalling components JAZ1 and JAZ4 (Seo *et al.*, 2013; You *et al.*, 2010). Another interesting putative interactor is CPL1, as it is required for GPA induced leaf senescence, like PAD4 (Thatcher *et al.*, 2018; Pegadaraju *et al.*, 2005). Furthermore, this protein stimulates nonsense-mediated decay of certain mRNAs, a process that also negatively regulates ETI signalling by reducing NLR transcript levels post-transcriptionally (Cui *et al.*, 2016; Jung *et al.*, 2020). GIP1 interacted with PAD4 at 6 hpi with *Pst avrRps4*, and functions as a transcriptional coactivator together with the TF G-BOX BINDING FACOR (GBF1) that promotes *PAD4* expression during PTI (Giri *et al.*, 2017; Lee *et al.*, 2014; Shaikhali, 2015). Lastly, H2A.W.7 is a plant specific Histone H2A variant that enhances chromatin condensation, which is correlated

with inhibiting gene expression (Kawashima *et al.*, 2015; Yelagandula *et al.*, 2014). In conclusion, I consider the identified PAD4 interactors TPR1, BBD1, CPL1, GIP1 and H2A.W.7 as potentially important for PAD4 nuclear functions.

The last set of proteins that are worth considering are CULLIN1 (CUL1) and SGT1b, since they purified with PAD4^{WT} specifically at six hpi, and regulate protein homeostasis and immunity (Figure 3.2). CUL1 is a component of SKP-CULLIN-F-box (SCF) E3 Ligase complexes, and regulates many processes, including JA-signalling (Yan *et al.*, 2013; Pieterse *et al.*, 2012). Furthermore, CUL1 can negatively regulate NLR protein levels, as was shown for the TNL SNC1 (Cheng *et al.*, 2011). Similar to CUL1, *AtSGT1b* antagonizes NLR accumulation, *e.g.* the TNL SNC1 and the CNL RPS5, (Holt *et al.*, 2005; Li *et al.*, 2010). In monocots and dicots, SGT1 functions as a protein chaperone involved in NLR-mediated resistance and in Arabidopsis SGT1b functionally overlaps with PAD4 in TNL-ETI signalling (Austin *et al.*, 2002; Azevedo *et al.*, 2002&2006; Feys *et al.*, 2005; Kim *et al.*, 2012; Tor *et al.*, 2002). In Arabidopsis, *SGT1b* and *PAD4* are required to sustain the autoimmunity phenotypes of *chilling sensitive 1-2 (chs1-2)*, *chs3-1* and *senescence-associated e3 ubiquitin ligase 1 (saull)* (Lee *et al.*, 2016; Yang *et al.*, 2010; Wang *et al.*, 2013; Zhang *et al.*, 2017b). By contrast, Arabidopsis *chs3-2D* and *chs2* (an *rpp4* mutant allele) autoimmunity does not depend on *PAD4*, but does depend on *EDS1* and *SGT1b*, suggesting SGT1b can also function with EDS1-SAG101 (Xu *et al.*, 2015; Huang *et al.*, 2010). As was discussed for several putative interactors mentioned above, *AtSGT1b* also stimulates JA-signalling, by stabilising the JA receptor COI1 (Zhang *et al.*, 2015). Lastly, *NbSGT1* is required for leaf chlorosis induced by the GPA effector Mp10, while GPA induced leaf chlorosis in Arabidopsis depends on *AtPAD4* (Bos *et al.*, 2010; Pegadaraju *et al.*, 2005). Taking all of the above data together, I consider SGT1b as a promising candidate interactor of PAD4 in immunity, which is why I studied SGT1b in more detail in the next section of this chapter.

In conclusion, based on published data described above MES10, TPR1 and SGT1b are relevant putative interactors of PAD4 in immune signalling. By quantitatively assessing these interactions one can see that MES10 was significantly co-purified at FDR=0.05 by PAD4^{WT} and PAD4^{K380A} at 4 and 6 hpi with *Pst avrRps4* (Figure 3.3). Furthermore, at FDR=0.01 and FDR=0.05, TPR1 and SGT1b associated exclusively with PAD4^{WT}, not PAD4^{K380A}, at six hpi, but not at 4 hpi (Figure 3.3). In the next paragraphs, I investigated the role of MES10 in immunity and I aimed to corroborate the interaction between PAD4 and TPR1 and SGT1b.

Chapter 3:
 Identification of active PAD4 protein complexes during
Pst avrRps4 infection



MES10 T-DNA mutants are resistant to *Hpa* EMWA1

MES10 purified with PAD4^{WT} and PAD4^{K380A} at 4 and 6 hpi, as only one out of three proteins (Figure 3.2&3). Since MES10 shows *in vitro* MeJA esterase activity, I investigate whether MES10 is involved in immunity. Four Arabidopsis T-DNA insertion lines located at the *MES10* locus (AT3G50440) were obtained from the NASC stock centre (Figure 3.4A). After selecting lines that were homozygous for the T-DNA insertion, we determined whether *MES10* contributes to TNL-ETI by challenging plants with *Hpa* EMWA1. All *mes10* mutants were as resistant as Col-0 to *Hpa* EMWA1, based on conidiospore production, macroscopic disease symptoms and microscopic *Hpa* colonisation (Figure 3.4B&C). In contrast, the negative controls *pad4-1* and *pad4-1/sag101-3* were susceptible.

Since *mes10* mutants did not show a susceptibility phenotype to *Hpa* EMWA1, we questioned whether other data point to a *MES10* contribution to immunity. Therefore, I mined publicly available datasets using Genevestigator (Hruz *et al.*, 2008; v7.5.1) and found *MES10* transcripts to be significantly ($p < 0.05$; $\text{Log}_2 > 1.5$) altered in immune-related contexts (Table 3.1). For example, *MES10* is down regulated in Arabidopsis leaf tissues during basal immunity, TNL-ETI, CNL-ETI, 35S:RPS4 autoimmunity and after SA application (Table 3.1). On the other hand, *MES10* is significantly upregulated in *sid2* (*ics1*), *ald1*, and *pad4-1* relative to Col-0, in 35S:RPS4/*eds1-2* plants relative to 35S:RPS4, and in MeJA-treated plants (Table 3.1). These data indicate that EDS1, PAD4 and ICS1-produced SA negatively regulate *MES10* expression, while MeJA induces *MES10* expression. Notably, *MES10* expression is significantly down regulated upon *B. cinerea* infection, while being upregulated upon *Alternaria brassicicola* infection (Table 3.1). These contrasting transcriptional changes are counterintuitive, since resistance to these necrotrophic pathogens depends on JA-signalling. (Glazebrook, 2005). Since JA functions antagonistically to SA and EDS1-PAD4 (Glazebrook, 2005; Cui *et al.*, 2018), I hypothesize that MES10 enhances JA-levels, and thereby negatively regulates EDS1-PAD4 immunity. Future experiments should reveal whether *mes10* mutants show enhanced resistance to virulent *Pst* DC3000 and avirulent *Pst avrRps4*, and enhanced susceptibility to necrotrophic pathogens.

Figure 3.3. Volcano plots for PAD4^{WT} and PAD4^{K380A} (See previous page).

Volcano plots of proteins identified by IP nLC-MS/MS in PAD4^{WT} and PAD4^{K380A} at 4 and 6 hpi with *Pst avrRps4*. Orange dots indicate significantly immunoprecipitated proteins at FDR=0.01 (Top panel) or FDR=0.05 (Bottom panel) and green dots indicate non-significantly immunoprecipitated proteins. X-axis indicates label-free quantification (LFQ) values; a measure of protein abundance relative to 35S:YFP (negative control), and Y-axis indicates *p*-value.

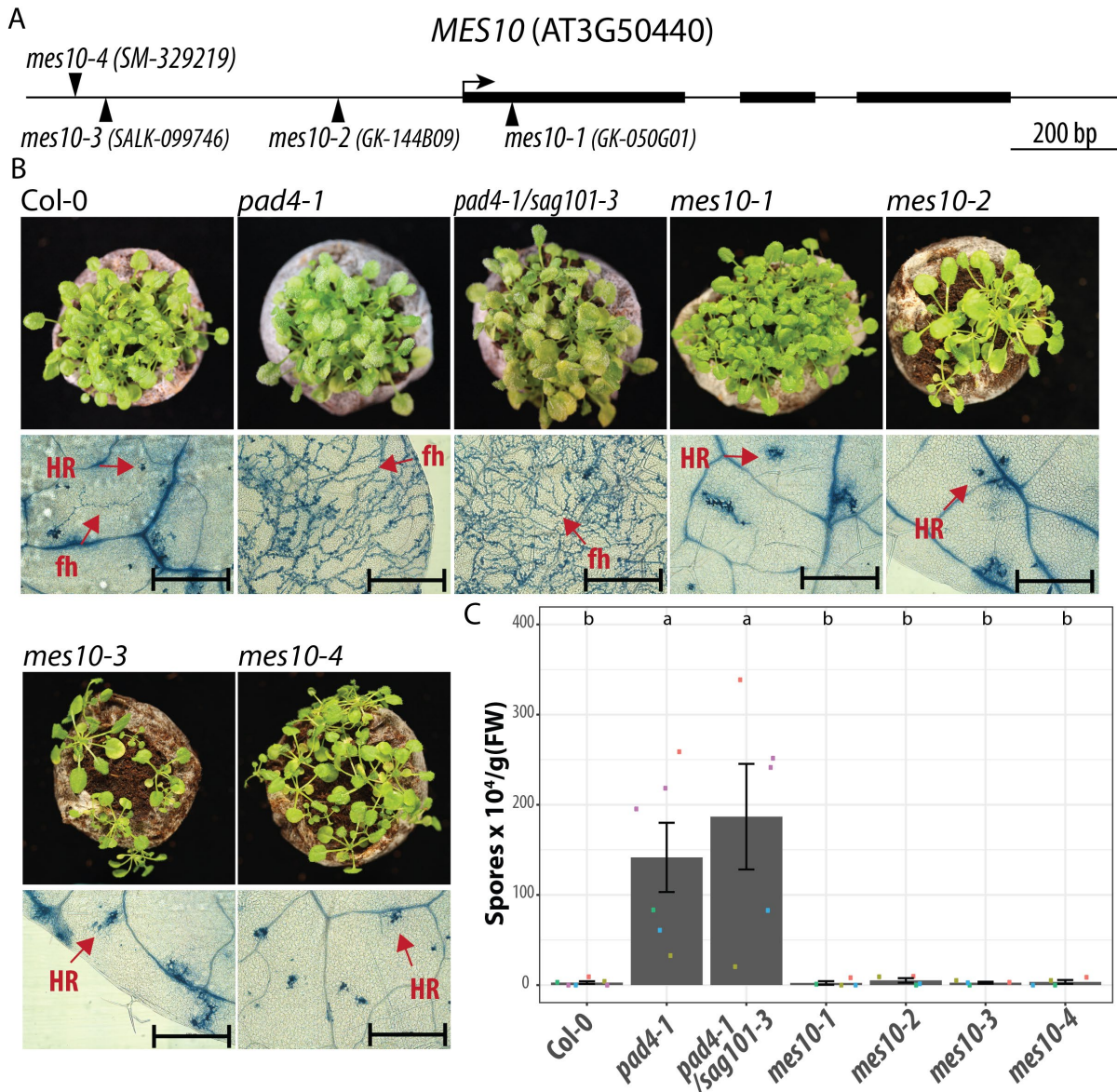


Figure 3.4. *mes10* mutants are resistant against TNL-ETI triggering *Hpa* EMWA1. **A.** *MES10* gene model showing the T-DNA insertion sites in the different *mes10* mutants. **B.** Macro- and microscopic immunity phenotypes of 3-week-old Arabidopsis lines, as indicated, at 6 dpi with *Hpa* isolate EMWA1 (recognized by TNL RPP4). Col-0 (resistant), *pad4-1* (susceptible) and *pad4-1/sag101-3* (susceptible) functioned as controls. Resistant plants look healthy at 6 dpi, whereas susceptible plants produce conidiospores. *Hpa* EMWA1 infected trypan blue-stained leaves of plants at 5 dpi showing free hyphae (fh) and hypersensitive cell death (Hypersensitive Response (HR)). Black bars represent 500 μ m. Pictures are representative from two independent experimental replicates, > 6 leaves per replicate and > 30 infection sites per genotype. **C.** TNL (RPP4) ETI assay in Arabidopsis independent transgenic lines with wild-type and mutant controls, as in A. *Hpa* EMWA1 conidiospores on leaves were quantified at 6 dpi in >3 independent experiments (squares; n=3-6), as indicated by coloured squares. Bars represent the mean of three experimental replicates \pm SE. Differences between genotypes were determined using ANOVA (Tukey-HSD, $p < 0.05$), letters indicate significance class. Data generated together with Eva Penner; T-DNA lines were selected by Jaqueline Bautor.

Chapter 3:
Identification of active PAD4 protein complexes during Pst avrRps4 infection

Table 3.1. *MES10* transcript changes in various genotypes, conditions and treatments (Perturbations) taken from publicly available datasets using Genevestigator (Hruz *et al.*, 2008; v7.5.1).

Perturbations	Log ₂ -ratio	p-value	Experiment	Publication	Data Repository & Sample ID
<i>A. brassicicola</i> (Ler) / untreated leaf disc samples (Ler)	2.6	0.00366	Microarray	-	GEO: GSE17464
<i>sid2-1</i> / Col-0	2.5	4.5E-05	RNA-seq	Bernsdorff <i>et al.</i> , 2015	ArrayExpress: E-MTAB-4151
35S:RPS4-HS <i>eds1-2</i> / 35S:RPS4-HS	2.3	3.2E-05	Microarray	Heidrich <i>et al.</i> , 2013	GEO: GSE50019
<i>ald1-T2</i> / Col-0	2.2	0.00255	RNA-seq	Bernsdorff <i>et al.</i> , 2015	ArrayExpress: E-MTAB-4151
MeJa study 5 (Ler) / untreated leaf disc samples (Ler)	1.3	0.01297	Microarray	-	GEO: GSE17464
<i>pad4-1</i> / Col-0	0.8	0.03814	Microarray	-	GEO: GSM469776
<i>P. syringae</i> pv. tomato study 19 (DC3000 <i>avrRps4</i> ; 6hpi) / <i>P. syringae</i> pv. tomato study 19 (DC3000; 6hpi)	-0.8	0.04125	RNA-seq	Howard <i>et al.</i> , 2013	ArrayExpress: E-MTAB-4450
shift 28°C to 19°C (35S:RPS4-HS <i>eds1-2</i>) / 28°C (35S:RPS4-HS <i>eds1-2</i>)	-0.9	0.00482	Microarray	Heidrich <i>et al.</i> , 2013	GEO: GSE50019
<i>P. syringae</i> pv. tomato study 3 (DC3000) / mock inoculated leaf samples (24h)	-1.2	0.00746	Microarray	Kemmerling <i>et al.</i> , 2007	AtGenExpress: A13ATGEN231_24H_DC3000
salicylic acid study 4 (Col-0) / silwet L77 treated Col-0 leaf samples (4h)	-1.2	0.00594	Microarray	Van Leeuwen <i>et al.</i> , 2007	ArrayExpress: E-TABM-51
<i>P. syringae</i> pv. tomato study 2 (DC3000 <i>avrRpm1</i>) / mock inoculated leaf samples (6h)	-1.4	0.00829	Microarray	-	TAIR Accession: 1007966202
<i>P. syringae</i> pv. maculicola (Col-0) / mock treated leaf samples (Col-0)	-1.4	0.00231	Microarray	-	GEO: GSE18978
<i>P. syringae</i> pv. tomato study 10 (DC3000) / mock inoculated leaf samples	-1.5	0.0191	Microarray	-	TAIR Accession: 1007966204
salicylic acid study 3 / mock treated seedlings	-1.7	0.0232	Microarray	-	GEO: GSE14961
<i>B. cinerea</i> study 2 (Col-0) / mock inoculated rosette leaf samples (Col-0)	-1.9	4.7E-05	RNA-seq	Liu <i>et al.</i> , 2015	GEO: GSE66290
<i>P. syringae</i> pv. maculicola study 2 (Col-0) / mock inoculated Col-0 rosette leaf samples	-2.2	0.00034	RNA-seq	Bernsdorff <i>et al.</i> , 2015	ArrayExpress: E-MTAB-4151
35S:RPS4-HS / Col-0	-4.1	7.4E-06	RNA-seq	-	GEO: GSE40216
shift 28°C to 19°C study 2 (35S:RPS4-HS) / 28°C (35S:RPS4-HS)	-4.8	7.4E-06	Microarray	Heidrich <i>et al.</i> , 2013	GEO: GSE50019
shift 28°C to 19°C study 5 (35S:RPS4-HS) / 28°C study 2 (35S:RPS4-HS)	-5.5	7.4E-06	RNA-seq	-	GEO: GSE40216

TPR1 and SGT1b do not interact with PAD4 in *N. benthamiana*

TPR1 and SGT1b only purified with PAD4^{WT} specifically at 6 hpi with *Pst avrRps4* (Figure 3.2&3). Both proteins have been implicated in TNL-ETI, suggesting that PAD4 functions together with TPR1 and SGT1b in ETI (Austin *et al.*, 2002; Azevedo *et al.*, 2002; Feys *et al.*, 2005; Kim *et al.*, 2012; Tor *et al.*, 2002; Xu *et al.*, 2015; Yang *et al.*, 2010; Zhu *et al.*, 2010; Zhang *et al.*, 2015). To confirm that these proteins interact with PAD4, targeted IP assays were performed. However, by transiently co-expressing PAD4 with TPR1 and SGT1b in *N. benthamiana*, no interaction above the level of the YFP negative control was observed (Figure 3.5). Since PAD4 functions in a heterodimer with EDS1, I postulated that EDS1 is required for PAD4-TPR1 and PAD4-SGT1b interaction. Co-expression of EDS1 also did not show an interaction between these proteins above the YFP negative control level (Figure 3.5). In these experiments, PAD4 did bind EDS1, indicating that the co-IP was successful (Figure 3.5).

In the IP nLC-MS/MS experiment we only detected one peptide for TPR1 and two (unique) peptides for SGT1b, suggesting that the interaction between PAD4 and TPR1 and SGT1b occurs transiently after pathogen induction. Since such transient interactions are easily washed away during co-IP processing, I decided to try split-LUC assays. In split-LUC assays, ^NLUC and ^CLUC can only catabolise the luciferin substrate, producing luminescence, if both proteins are in close proximity to one another (Gehl *et al.*, 2011). For this reason, ^NLUC was N- and C-terminally tagged to PAD4 were used, *i.e.* ^NLUC-PAD4 and PAD4-^NLUC. In this way, the stoichiometry between PAD4 and TPR1 and SGT1b does not interfere with ^CLUC- and ^NLUC luciferase activity.

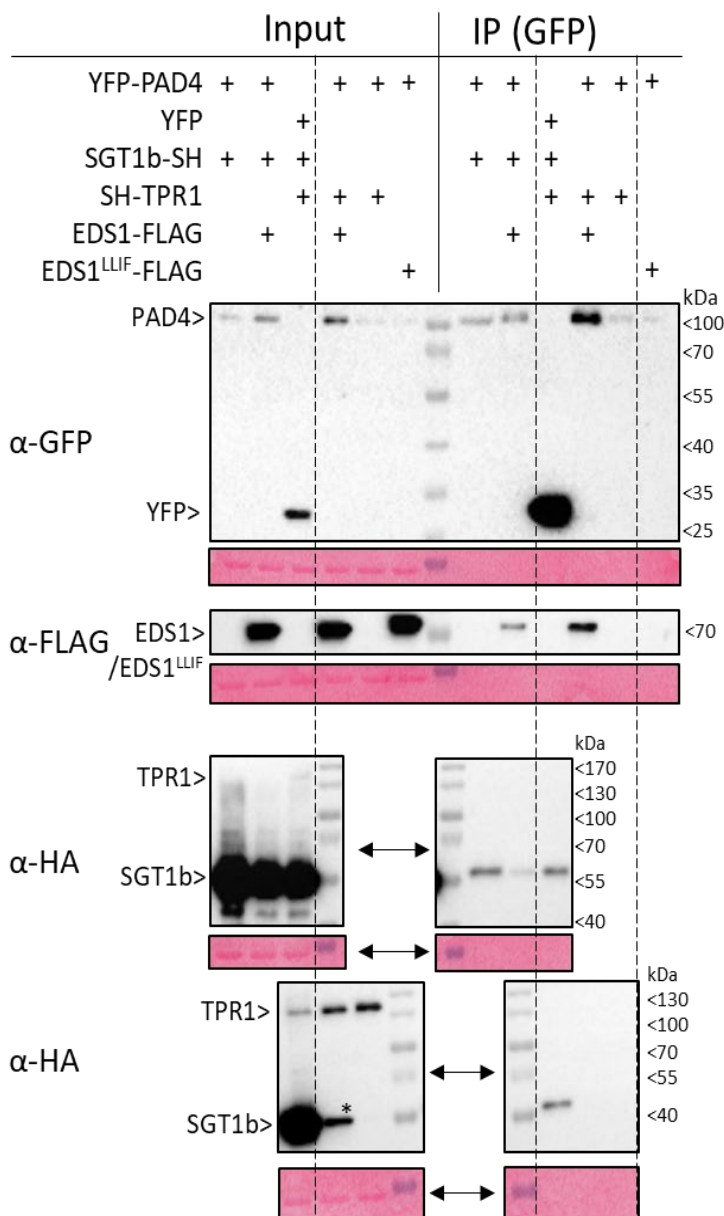


Figure 3.5. TPR1 and SGT1b do not co-IP with PAD4 in *N. benthamiana*.

Co-immunoprecipitation (GFP-trap) of StrepII-YFP-PAD4 with SH-TPR1 and SGT1b-SH, co-expressed with and without EDS1^{WT}. PAD4-EDS1 functioned as a positive control. YFP and EDS1^{LLIF}-3xFLAG functioned as negative controls. All proteins were transiently co-expressed in *N. benthamiana* leaves under the 35S promoter, except for PAD4, which was expressed under the native *pPAD4* promoter. Left: all proteins are expressed in the input. Right: in the IP fraction only EDS1^{WT} co-immunoprecipitates with PAD4^{WT} (positive control). The non-interacting variant EDS1^{LLIF} and does not co-IP with PAD4. PAD4 does not IP TPR1 and PAD4 does not IP more SGT1b than the YFP negative control. *= SGT1b is highly expressed and some sample flowed into the neighboring lane while loading the gel. Similar results obtained in 3 independent experiments. Data obtained by Lucas Dijkgraaf.

EDS1^{WT} and PAD4 produced a strong LUC signal indicating the assay functioned properly (Figure 3.6). However, neither PAD4 with TPR1, nor PAD4 with SGT1b showed a significant difference in LUC signal compared to the negative controls PAD4-EDS1^{LLIF} and PAD4-empty vector (EV) (Figure 3.6). Since EDS1 might be required for the interaction between PAD4 and TPR1 and SGT1b, we also co-expressed EDS1. However, the EDS1-PAD4 positive control did not show a higher luciferase activity than the negative controls, indicating the LUC assay does not work when co-infiltrating three plasmids at once (data not shown). We speculate that this led to below-threshold accumulation of ^NLUC and ^CLUC, and consequently weak luciferase activity. This is likely since the ^NLUC and ^CLUC vectors contain a weak 35S promoter and a low copy-number origin of replication, allowing *Agrobacterium* to transfer only few T-DNAs to *N. benthamiana* cells, resulting in low protein accumulation (Gehl *et al.*, 2011).

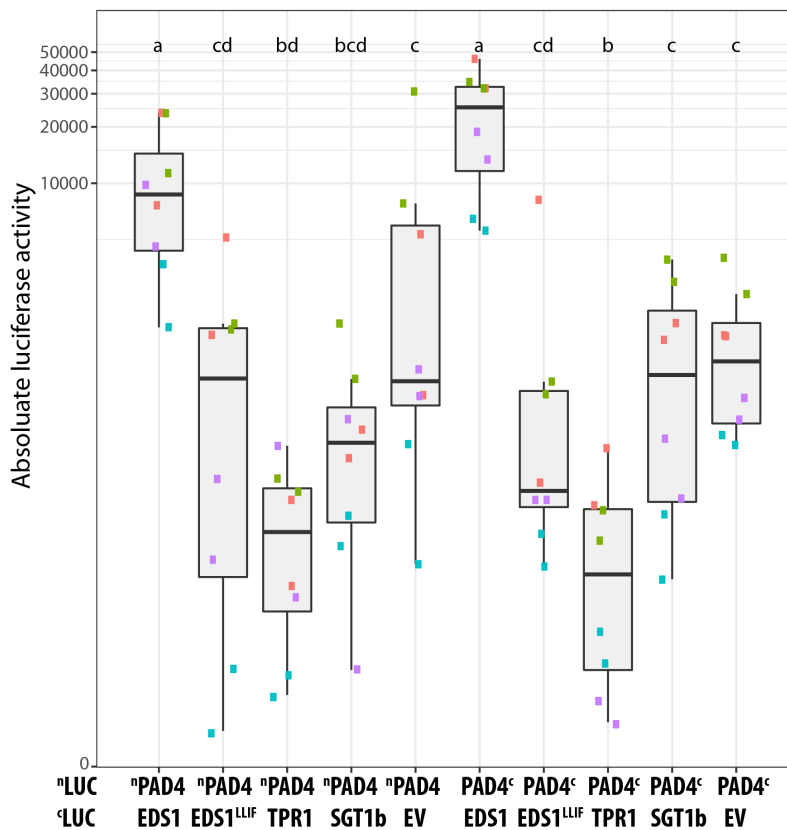


Figure 3.6. TPR1 and SGT1b do not interact with PAD4 using split-luciferase in *N. benthamiana*. Absolute luciferase (LUC) activity from transiently co-expressed ^NLUC or ^CLUC constructs (35S promoter) in *N. benthamiana*. ^NPAD4 is N-terminally tagged PAD4, and PAD4^C is C-terminally tagged PAD4. Data are pooled from four independent experiments with two biological replicates per experiment (n = 8). Colors indicate samples from one independent experiment. Letters indicate statistical significance as determined by one-way ANOVA with multiple testing correction using Tukey-HSD; *p* < 0.01. Data generated by Eva Penner.

In conclusion, I identified putative interactors of PAD4 in *Pst avrRps4* infected Arabidopsis leaves at 4 and 6 hpi. This showed a marginal overlap between the time-points, suggesting PAD4 engages in transient interactions during the immune response (Figure 3.1). Several of these putative interactors were already implicated in PAD4 dependent immunity (Figure 3.2). Out of the putative PAD4 interactors, I selected MES10, TPR1 and SGT1b to study in more detail. MES10 was one of the core interactors of PAD4 (Figure 3.2). However, *mes10* mutants did not exhibit a loss of *RPP4* (TNL) resistance to *Hpa* EMWA1, which has been shown to genetically depend on *PAD4*. *MES10* is negatively regulated by SA, *EDS1* and *PAD4*, and is therefore likely to function antagonistically to EDS1-PAD4, thereby repressing immunity (Table 3.1). Future experiments should determine if *mes10* mutants' show enhanced resistance to virulent pathogens, such as *Pst* DC3000, and on the other hand if MES10 is required for resistance to necrotrophic pathogens. PAD4^{WT} associated with TPR1 and SGT1b, but not with PAD4^{K380A}, suggesting a PAD4 EP domain cavity specific interaction. However, the interaction between PAD4^{WT} and TPR1 and SGT1b could not be corroborated using targeted co-IP and split-LUC assays. I postulate that this is due to the nature of these interactions. The association of PAD4 with TPR1 and SGT1b were only observed in Arabidopsis at six hpi with *Pst avrRps4* (Figure 3.2&3). Future studies should therefore focus on performing targeted co-IP on pathogen challenged Arabidopsis stable transformants expressing tagged PAD4 and TPR1, and PAD4 and SGT1b. Alternatively, using epitope-tagged lines of TPR1 and SGT1b one could replicate the IP nLC-MS/MS experiment as described here for PAD4. If these experiments were to co-purify PAD4, this would be an independent confirmation that the interaction of PAD4 with TPR1 and SGT1b occurs in Arabidopsis TNL-ETI signalling.

Chapter 4: Cytoplasmic-enriched PAD4 causes autoimmunity in Arabidopsis

Arabidopsis PAD4 is a nucleocytoplasmic protein and associates to several nuclear- and cytosolic-localised proteins (Figure 3.1). However, where PAD4 exerts immune functions is still unknown. For *AtEDS1* there is evidence indicating it functions mainly in the nucleus during basal immunity and ETI (Cui *et al.*, 2018; Garcia *et al.*, 2010; Stuttmann *et al.*, 2016). *EDS1* accumulated in the nucleus at three hpi when infected with ETI-triggering *Pst avrRps4* (Garcia *et al.*, 2010). Moreover, nuclear export signal (NES) tagged *EDS1* (*EDS1-NES*) transgenic lines displayed a partial loss-of-function phenotype due to depletion of nuclear *EDS1* (Garcia *et al.*, 2010). In contrast, nuclear localisation signal (NLS) tagged *EDS1*-NLS (*EDS1-NLS*) lines displayed autoimmunity due to over-accumulation of *EDS1* in the nucleus (Stuttmann *et al.*, 2016). These results indicate that Arabidopsis *EDS1* functions mainly in the nucleus for the examined TNL and basal immunity responses. Information on the main intracellular site of PAD4-activity was lacking. I therefore investigated the function of PAD4 when it was directed mainly to the cytoplasmic or nuclear compartment, respectively, using NES or NLS tags.

Nuclear- and cytoplasmic-enriched PAD4 lines are resistant to *Hpa* EMWA1

To study the nuclear and cytoplasmic functions of PAD4, I generated PAD4 lines with nuclear-enriched and cytoplasm enriched PAD4 levels. I cloned gPAD4 lines, with an NLS, NES, mutated NES (*nes*), or mutated NLS (*nls*) in between the linker and the PAD4 start codon (*pPAD4::YFP-Linker-NLS/NES/nls/nes-gPAD4*; Figure 2.8), and introduced these into *pad4-1/sag101-3* mutants (Garcia *et al.*, 2010; Stuttmann *et al.*, 2016). T2 transformants were tested for complementation of the *pad4-1/sag101-3* phenotype by spraying with *Hpa* EMWA1, inducing TNL-ETI (Figure 4.1). All of these PAD4 lines behaved similar to Col-0 and gPAD4^{WT} and did not show macroscopic disease phenotypes, such as chlorosis or sporulation (Data not shown). This indicates that these nuclear and cytoplasmic-enriched PAD4 lines function in ETI. However, certain *nesgPAD4*, *NLSgPAD4* and *nlsPAD4* lines showed weak free hyphal growth, when compared to Col-0 (Figure 4.1). Although these phenotypes were weak compared *pad4-1* and *pad4-1/sag101-3*, this does indicate that certain lines did not fully complement the *pad4-1/sag101-3* mutant phenotype.

Cytoplasm-enriched PAD4 induces autoimmunity in Arabidopsis

Notably, while taking these nuclear-enriched and cytoplasm-enriched PAD4 lines forward to the T3 generation, some of the NESgPAD4 lines displayed developmental defects, reminiscent of autoimmunity. To assess whether these plants displayed autoimmunity, homozygous T3 plants were grown under controlled conditions. Indeed, NESgPAD4 lines #5 and #15 showed dwarfism, shrivelled leaves and chlorosis; characteristic of autoimmunity (Figure 4.2A) (Heidrich *et al.*, 2013; Huang *et al.*, 2010; Lee *et al.*, 2016; Yang *et al.*, 2010). Notably, the veins of NESgPAD4 plants were particularly chlorotic (Figure 4.2A). In contrast, gPAD4^{WT} and nesgPAD4 lines did not show any of these phenotypes, except for a smaller rosette compared to Col-0 and *pad4-1/sag101-3*. For many autoimmune genotypes ambient temperature can modulate the severity of the autoimmune phenotype, and even abolish it (Heidrich *et al.*, 2013; Huang *et al.*, 2010; Lee *et al.*, 2016; Yang *et al.*, 2010). Indeed, when grown at 26 °C, NESgPAD4 lines did not display dwarfism, shrivelled leaves or chlorosis (Figure 4.2B).

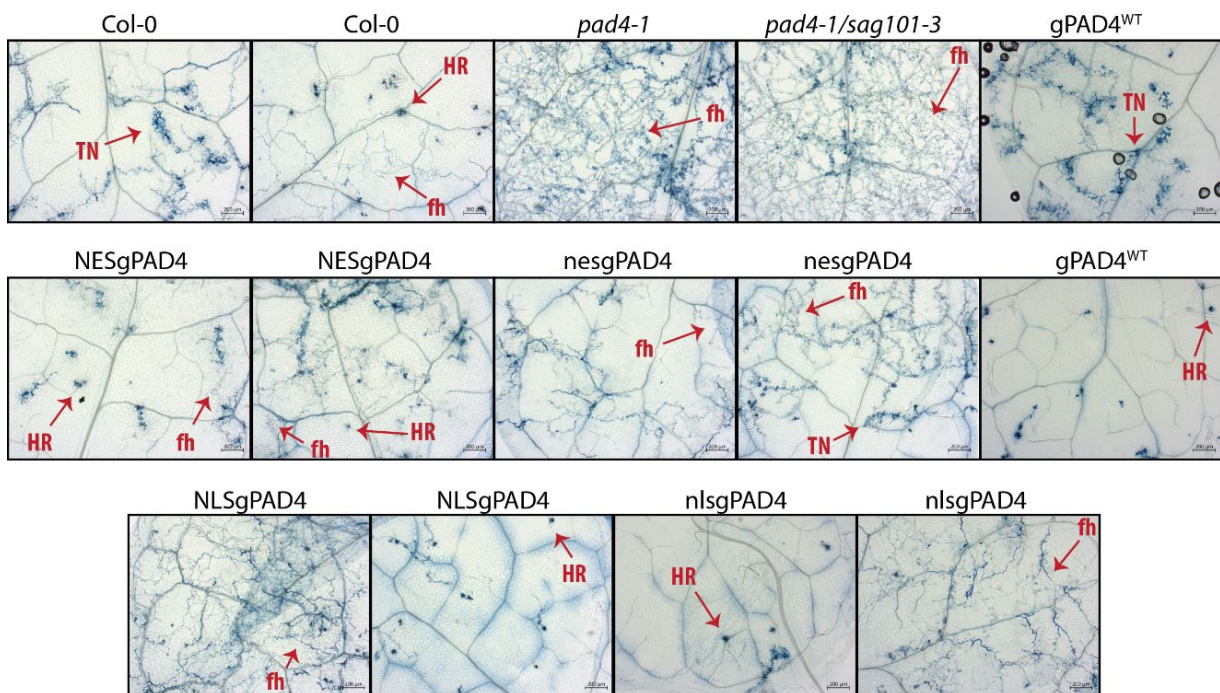


Figure 4.1. Nuclear- and cytoplasmic-enriched PAD4 in Arabidopsis ETI against *Hpa* EMWA1. Microscopic immunity phenotypes of 3-week-old Arabidopsis lines, as indicated, at 4 dpi with *Hpa* isolate EMWA1 (recognized by TNL RPP4). Col-0 (resistant), *pad4-1* (susceptible) and *pad4-1/sag101-3* (susceptible) functioned as controls. Trypan blue-stained leaves showing free hyphae (fh), trailing necrosis (TN) and hypersensitive response (HR). Black bars in bottom right indicate 200 μ m. Over eight independent T2 transformants were tested per genotype. Due to the large variation in phenotypes I decided to show two pictures for all genotypes to display the variation in infection phenotypes, except for *pad4-1* and *pad4-1/sag101-3*. Data generated with Lucas Dijkgraaf.

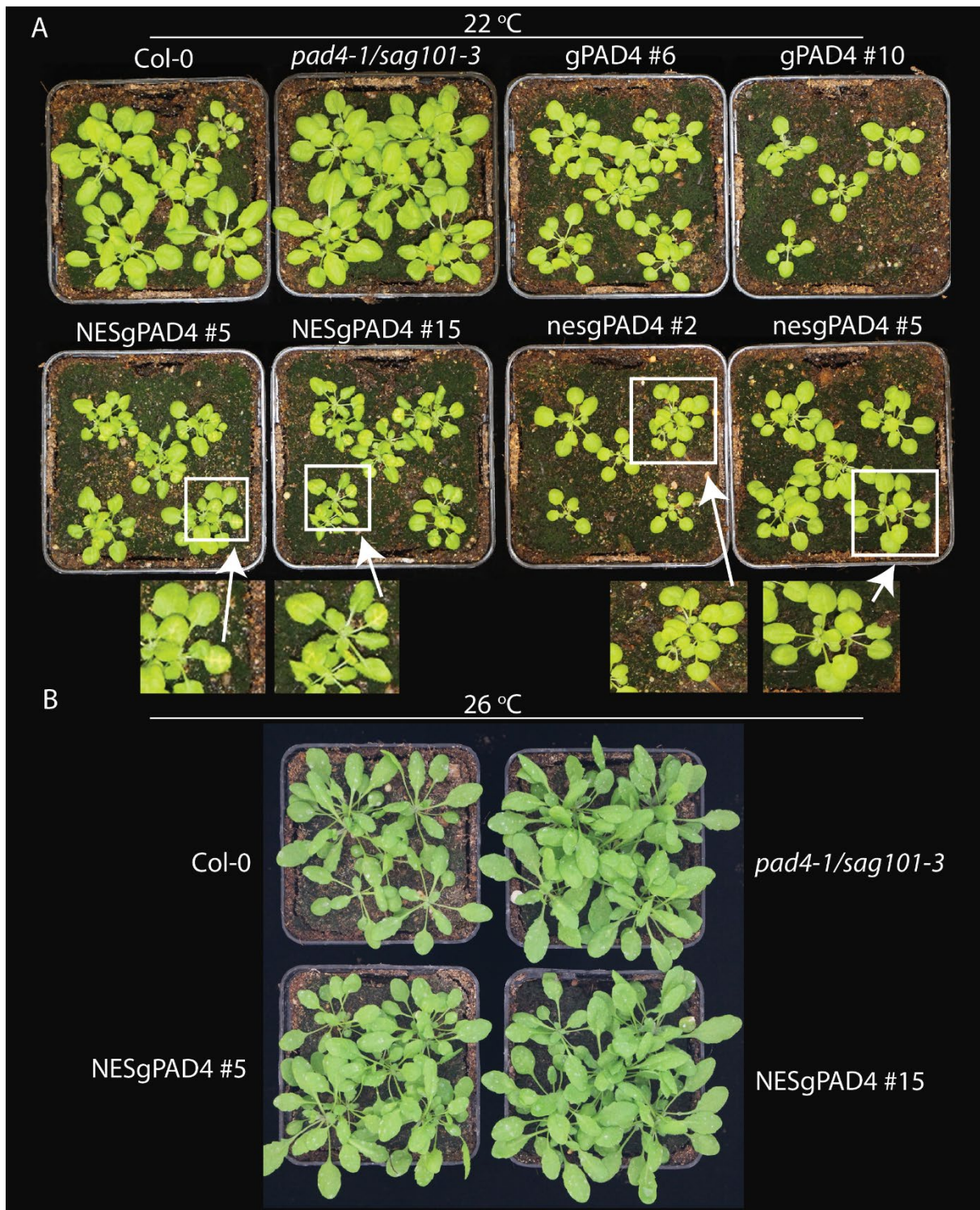


Figure 4.2. NESgPAD4 show temperature-dependent autoimmunity.

Plants grown for 23 days in SD conditions at A) 22° and B) 26 °C. **A.** Close-ups show chlorosis on the veins for NESgPAD4 lines, while chlorosis is absent on nesgPAD4 lines. **B.** NESgPAD4 do not display autoimmunity at 26 °C. Similar phenotypes observed in three independent experiments. All pots are 9 cm x 9 cm. Data generated with Lucas Dijkgraaf.

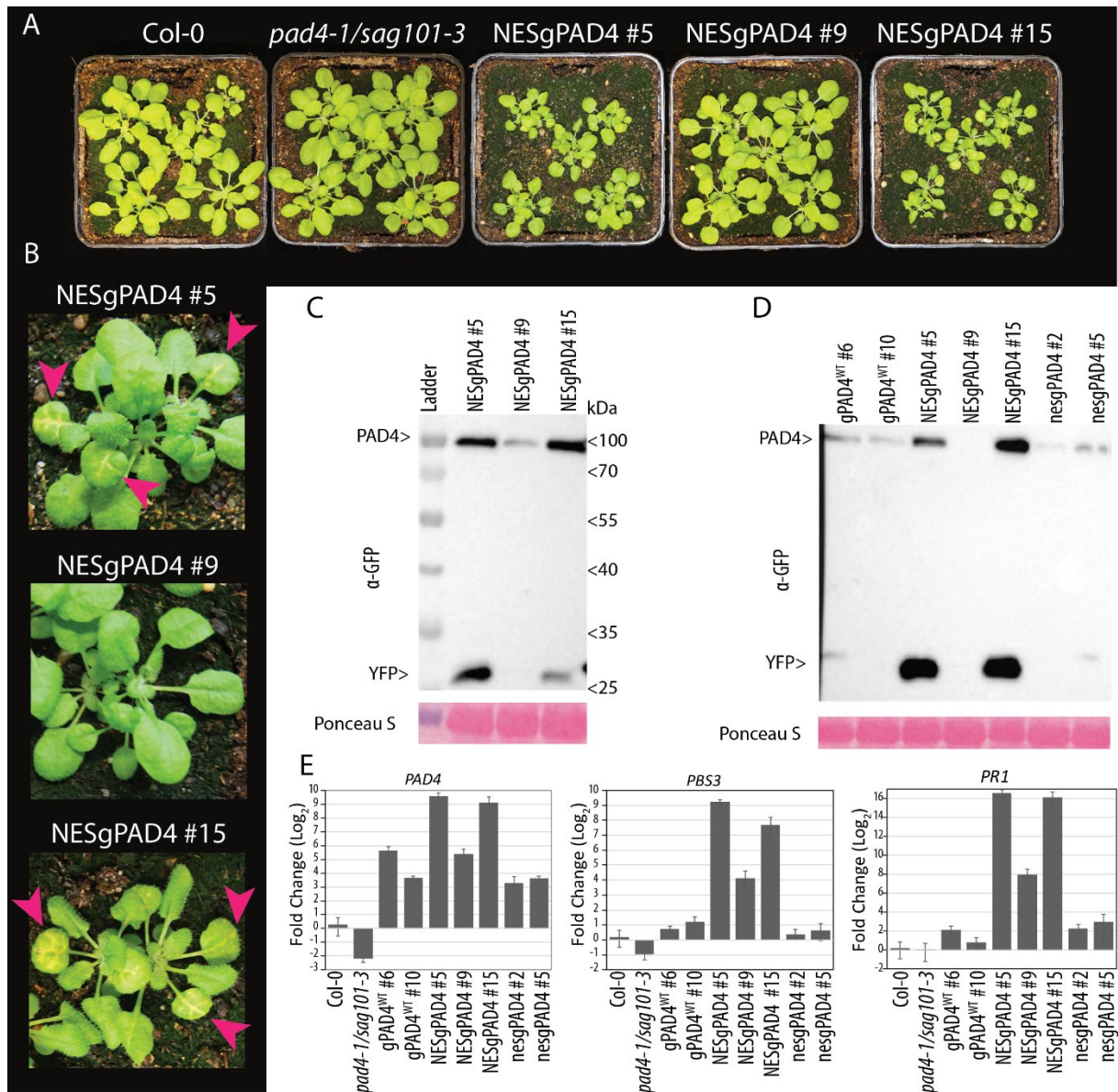


Figure 4.3. NESgPAD4 autoimmunity is protein level dependent and correlates with high *PAD4*, *PBS3* and *PR1* expression.

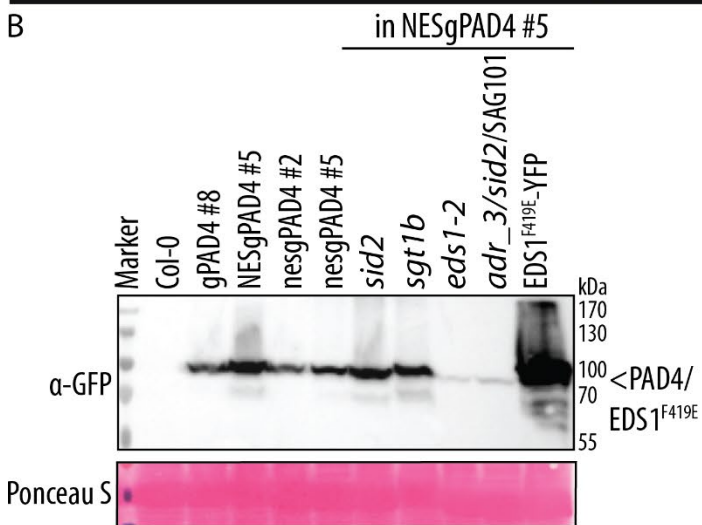
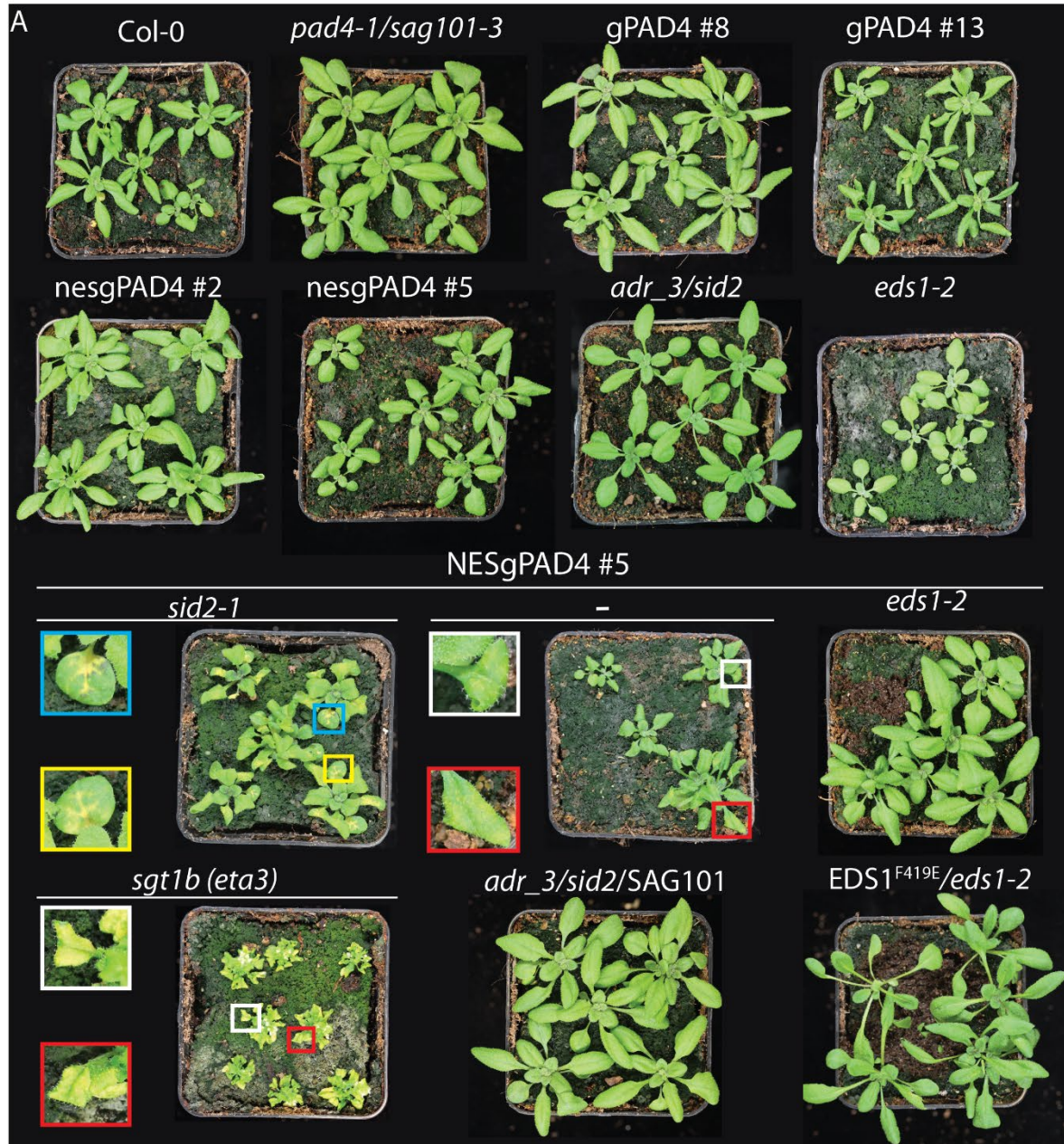
A. Plants grown for 23 days in SD conditions at 22 °C. **B.** Close-up of NESgPAD4 lines, pink arrow indicates leaves with chlorosis along the veins. **C.** PAD4 accumulation in 21 day-old LD grown plants. **D.** PAD4 accumulation of samples in **A.** **E.** Transcript abundance determined by qRT-PCR in plants shown in **A.** Data are pooled from one independent experiment with three biological replicates (n = 3). Similar results were obtained for Col-0, *pad4-1/sag101-3*, NESgPAD4 #5/#9/#10/#15 in another experimental replicate. *PAD4*, *PATHOGENESIS RELATED 1 (PR1)*, *AVRPPHB SUSCEPTIBLE 3 (PBS3)* transcript abundances were measured relative to *ACT2*. Relative expression is set to Col-0 samples. I did not apply statistics here, since the number of data points is not sufficient for statistical analysis. All pots are 9 cm x 9 cm. Data generated with Lucas Dijkgraaf.

Not all NESgPAD4 lines displayed autoimmunity (Figure 4.3A&B). This is reminiscent of EDS1-NLS autoimmunity, where only EDS1-NLS lines accumulating high protein levels showed autoimmunity (Stuttman *et al.*, 2016). This suggests that NESgPAD4 protein accumulation in non-autoimmune lines could be lower than in autoimmune lines. Indeed, NESgPAD4 #9 did not display autoimmunity and showed lower PAD4 accumulation than the autoimmune NESgPAD4 lines #5 and #15 (Figure 4.3C). Furthermore, NESgPAD4 lines #5 and #15 displayed higher protein accumulation than gPAD4^{WT} and nesgPAD4 lines (Figure 4.3D). Moreover, transcript abundance of *PAD4* and its downstream target genes *PR1* and *PBS3* were higher in NESgPAD4 autoimmune lines than non-autoimmune plants (Figure 4.3E). These results suggest that NESgPAD4 autoimmunity phenotype is dependent on PAD4 accumulation. Taken together, based on the data presented here, PAD4 has specific immune-related functions in the cytoplasm.

NESgPAD4 autoimmunity depends on *EDS1* but not *ICS1*-generated SA

To identify downstream signalling components necessary for NESgPAD4 autoimmunity, I crossed NESgPAD4 #5 (in *pad4-1/sag101-3*) with several relevant immune-related mutants. This indicated that NESgPAD4 autoimmunity is EDS1-dependent, since NESgPAD4 #5 in the *eds1-2* (in Col-0; Bartsch *et al.*, 2006) mutant background fully repressed the autoimmunity phenotype (Figure 4.4). However, NESgPAD4 protein levels were reduced in the *eds1-2* background (Figure 4.4B), indicating that EDS1 *cis*- and/or *trans*-regulation of PAD4 is required to maintain autoimmunity, and not signalling *per se* (Bartsch *et al.* 2006; Bhandari *et al.*, 2019; Rietz *et al.*, 2011; Wagner *et al.*, 2013). Furthermore, NESgPAD4 #5 crossed with the EDS1 EP domain mutant *EDS1*^{F419E} (in Col-0/*eds1-2*; Figure 2.1; Lapin *et al.*, 2019) did not show autoimmunity (Figure 4.4A). However, in the lines, I could not differentiate between *EDS1*^{F419E}-YFP and YFP tagged NESgPAD4 bands by immune-detection, making it impossible to assess if NESgPAD4 or *EDS1*^{F419E} accumulated (Figure 4.4B). Taken together, EDS1 is at least indirectly required to maintain NESgPAD4 autoimmunity.

In Arabidopsis immunity, PAD4 functionally overlaps with the ADR1 helper NLR family and partially overlaps with ICS1-produced SA (Bonardi *et al.*, 2011; Cui *et al.*, 2017; Lapin *et al.*, 2019; Tsuda *et al.*, 2009). To determine their contribution to NESgPAD4 autoimmunity, I crossed NESgPAD4 #5 (in *pad4-1/sag101-3*) into the *adr1-1/adr1-L1/adr1-L2-4/sid2-1* mutant (referred to hereafter as *adr_3/sid2*) (Bonardi *et al.*, 2011; Wildermuth *et al.*, 2001; unpublished cross from X. Sun – Parker lab). The *sid2* (*ics1* mutant allele) allele partially suppressed



NESgPAD4 induced dwarfism, while showing more pronounced chlorosis on the veins (Figure 4.4A). This line showed similar NESgPAD4 levels in NESgPAD4 #5, suggesting ICS1-generated SA did not alter NESgPAD4 levels, but instead suppressed immune pathways downstream of PAD4. NESgPAD4 #5 in *pad4-1/sag101-3/adr_3/sid2* has not yet been obtained, since *SAG101* (AT5G14930) and *ADR1-L2* (AT5G04720) are genetically linked (~3 Mb apart).

Nonetheless, NESgPAD4 in *pad4-1/adr_3/sid2/SAG101* suppressed autoimmunity, indicating that *adr_3* and/or *SAG101* suppress the NESgPAD4/*sid2* phenotype (Figure 4.4A). However, NESgPAD4 levels were lower in this line than in NESgPAD4 #5 and NESgPAD4/*sid2*, making it difficult to dissect if the autoimmunity suppression is due to the absence of PAD4-dependent signalling or reduced NESgPAD4 levels, similar to NESgPAD4 in *eds1-2* (Figure 4.4). To dissect the roles of *adr_3* and *SAG101* in NESgPAD4 autoimmunity, I aim to obtain NESgPAD4/*pad4-1* in the following backgrounds: *adr_3/sid2/sag101-3*, *adr_3/SID2/sag101-3* and *ADR_3/SID2/SAG101*. With this material, I will determine the precise contribution of each of these immune components alone and in relation to each other in NESgPAD4 autoimmunity. If *SAG101* suppresses NESgPAD4 autoimmunity, this would be the first indication that *SAG101* competes with PAD4 for EDS1 interaction in Arabidopsis immune signalling.

As discussed in chapter three, the protein chaperone SGT1b is a putative interactor of PAD4. Both are required for several immune responses in Arabidopsis, suggesting their roles in immunity partially overlap (Austin *et al.*, 2002, Kim *et al.*, 2012; Tor *et al.*, 2002; Xu *et al.*, 2015; Yang *et al.*, 2010; Zhang *et al.*, 2015). To determine if *SGT1b* is also required for NESgPAD4 autoimmunity, I crossed NESgPAD4 #5 (in *pad4-1/sag101-3*) with *sgt1b* (*eta3*; Gray *et al.*, 2003). These plants still showed autoimmunity, in fact, NESgPAD4/*sgt1b* plants were smaller, more chlorotic and had more curled leaves than NESgPAD4 #5 (Figure 4.4). NESgPAD4 levels were not elevated in the *sgt1b* mutant background (Figure 4.4B). Notably, NESgPAD4 ran consistently higher on western blots, suggesting NESgPAD4 is

Figure 4.4. NESgPAD4 autoimmunity in various mutant backgrounds (See previous page).

A. Plants grown for 21-25 days in speed breeding conditions (22h light - 2h dark at 22°C). All transgenic PAD4 lines are in *pad4-1/sag101-3* mutant background, except NESgPAD4#5/*adr_3/sid2/SAG101*, which is in the *pad4-1* background. Close-ups show chlorosis on the leaves as indicated by corresponding coloured boxes. All pots are 9 cm x 9 cm. **B.** PAD4 and EDS1^{F419E} accumulation in independent stable transgenic Arabidopsis lines expressing various PAD4 variants as YFP-(NES/nes)-gPAD4 and gEDS1^{F419E}-YFP probed by western blotting using α -GFP antibody of plants depicted in A. Col-0 as negative control. Representative image from 2 independent experiments are shown. Higher NESgPAD4 band in *sgt1b* background was observed in both replicates. Crosses were genotyped by Jaqueline Bautor.

modified post-translationally in the *sgt1b* mutant background. Moreover, this suggests that these post-translational modifications enhance PAD4 activity. Taken together, these data indicate that NESgPAD4 autoimmunity depends on *EDS1*, while *SGT1b* and ICS1-produced SA enhance NESgPAD4 autoimmunity phenotypes.

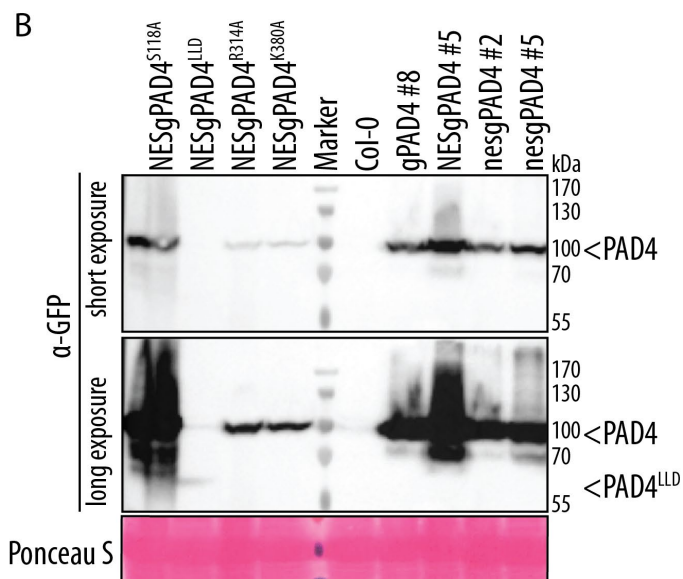
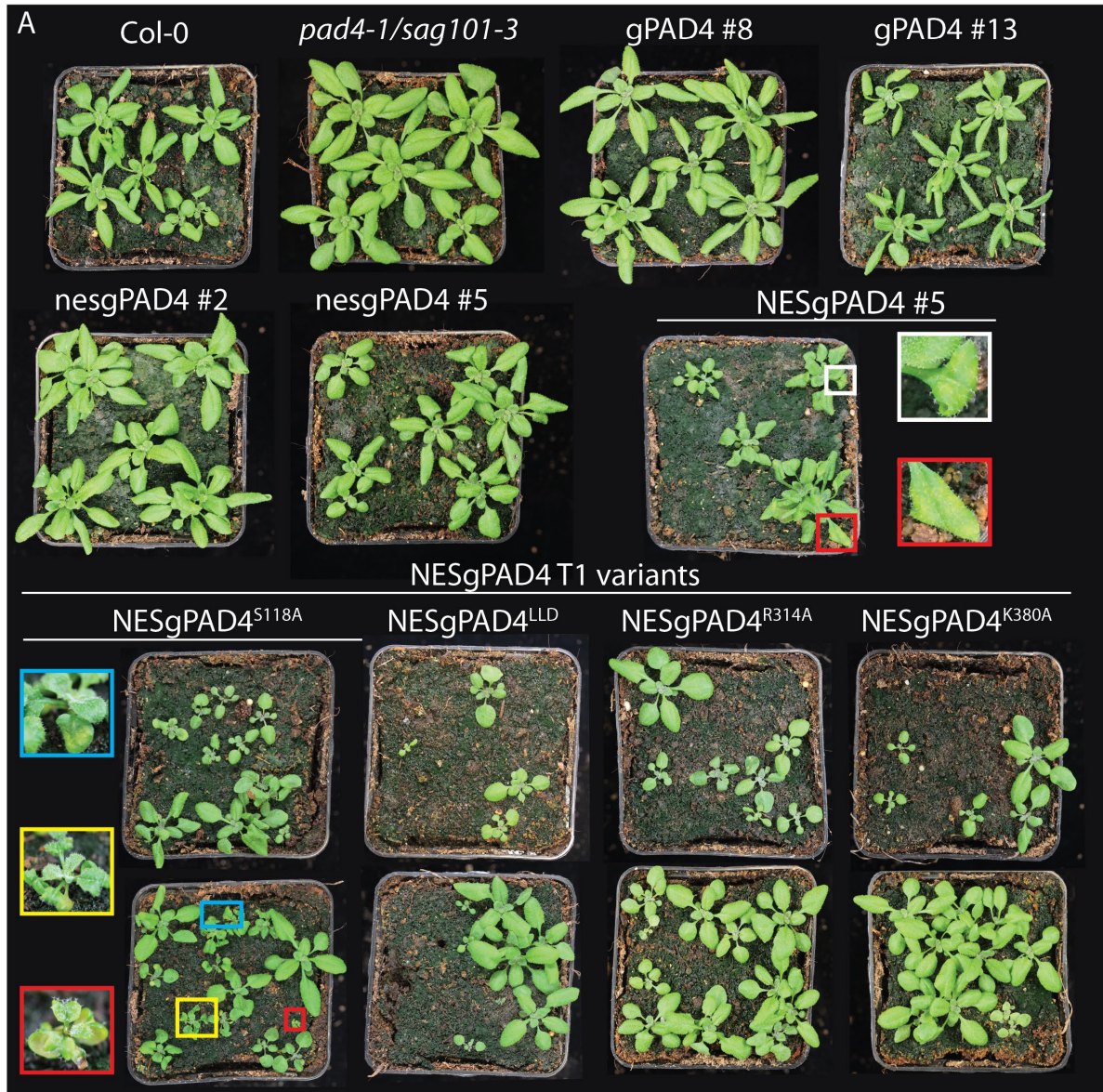
NESgPAD4 autoimmunity does not depend on PAD4^{S118}

This study and previously published studies have shed light on PAD4 structural features in specific resistance pathways (Dongus *et al.*, 2020; Louis *et al.*, 2012a; Neubauer *et al.*, 2020; Wagner *et al.*, 2013). Here, I applied that knowledge to identify PAD4 structural features necessary for NESgPAD4 autoimmunity. In Chapters 1 and 2, I showed that PAD4^{LLD}, PAD4^{R314A} and PAD4^{K380A} were sufficient for GPA resistance, but were unable to function in immunity. Conversely, PAD4^{S118A} functioned in immunity, but not in GPA resistance (Figure 1.7-8; Louis *et al.*, 2012a; Wagner *et al.*, 2013). I combined these insights to test which PAD4 resistance pathway is over-activated in NESgPAD4 autoimmunity: pathogen immunity or GPA resistance.

Instead of determining which residue(s) render NESgPAD4 non-autoimmune, I focused on mutations that allow autoimmunity to persist. My reasoning behind this was the following: NESgPAD4 phenotype depends on PAD4 accumulation (Figure 4.3), and mutations in PAD4 lead to reduced PAD4 levels (Figure 1.7&2.9). Therefore, if a certain NESgPAD4 mutant does not retain autoimmunity, this might be due to NESgPAD4 accumulating below a critical threshold. This makes it difficult to determine whether the absence of autoimmunity is caused by the inactivation of a resistance pathway or diminished PAD4 levels. Hence, I focused on determining mutations that allow NESgPAD4 autoimmunity to persist. This would indicate whether a residue and its corresponding role in resistance are dispensable for NESgPAD4 autoimmunity.

Figure 4.5. NESgPAD4 autoimmunity in various PAD4 mutants (See next page).

A. Plants grown for 21-25 days in speed breeding conditions (22h light-2h dark at 22°C). All transgenic PAD4 lines are in *pad4-1/sag101-3* mutant background. Close-ups show chlorosis on the leaves as indicated by corresponding coloured boxes. T1 NESgPAD4 mutant variant seeds were harvested a week before, and because of that did not germinate synchronously. This explains why there are several small, but healthy, plants in all the NESgPAD4 variant pots. In NESgPAD4^{S118A}, many plants show chlorosis and dwarfism. All pots are 9 cm x 9 cm. **B.** PAD4 accumulation in independent stable transgenic Arabidopsis lines expressing various PAD4 variants as YFP-(NES/nes)gPAD4 probed by western blotting using α -GFP antibody of plants depicted in A. Col-0 as negative control. A representative image from 2 independent experiments is shown. Col-0 shows a weak aspecific band at ~100 kDa in the long exposure blot, which is also visible in NESgPAD4^{LLD}. NESgPAD4^{LLD} runs between 55 and 70 kDa.



I generated NESgPAD4^{S118A}, NESgPAD4^{LLD}, NESgPAD4^{R314A} and NESgPAD4^{K380A} constructs and introduced these as stable transgenes into *pad4-1/sag101-3*. Preliminary results from T1 generation plants revealed that NESgPAD4^{LLD}, NESgPAD4^{R314A} and NESgPAD4^{K380A} did not show signs of autoimmunity (Figure 4.5A). Although these plants did look smaller, this was likely due to asynchronous germination of the freshly harvested seeds. Furthermore, these NESgPAD4 variants accumulated lower PAD4 levels than the control lines gPAD4, nesgPAD4 and NESgPAD4 (Figure 4.5B). This made it difficult to discern whether the lack of autoimmunity is due to the mutation in PAD4 or due to below-threshold PAD4 accumulation. In contrast, NESgPAD4^{S118A} protein accumulated to similar levels as NESgPAD4 and retained autoimmunity phenotypes as observed for NESgPAD4 #5, *i.e.* dwarfism, chlorosis and severe curling of leaves (Figure 4.5). These preliminary results indicate that PAD4^{S118} is not required for NESgPAD4 autoimmunity, suggesting that the PAD4 GPA resistance pathway is dispensable for NESgPAD4 autoimmunity.

In conclusion, the experiments discussed in this chapter indicated that perturbations in PAD4 nucleocytoplasmic balance does not alter TNL-ETI against *Hpa* EMWA1 (RPP4). Enriching PAD4 in the cytoplasm induced autoimmunity in a protein level dependent manner (Figure 4.2&3). NESgPAD4 autoimmunity did not depend on PAD4 GPA resistance activity, but on PAD4 pathogen immune activity (Figure 4.4&5). Mutations in *sgt1b* and *sid2* enhanced NESgPAD4 autoimmunity, without enhancing NESgPAD4 accumulation (Figure 4.4), indicating ICS1-produced SA and SGT1b repress certain PAD4 immune pathways. Taken together, these results suggests that PAD4 has immune activating functions in the cytoplasm.

Discussion

In this thesis, I studied Arabidopsis PAD4 structure-function in plant resistance. In Arabidopsis, PAD4 controls defences against (hemi-) biotrophic pathogens and Green Peach Aphid (GPA). PAD4 plays a major role with EDS1 in basal and effector-triggered immunity, and independently of EDS1, PAD4 controls GPA resistance (Bhandari *et al.*, 2019; Cui *et al.*, 2017; Cui *et al.*, 2018; Dongus *et al.*, 2020; Glazebrook *et al.*, 1997; Lapin *et al.*, 2019; Louis *et al.*, 2012a; Pegadaraju *et al.*, 2007; Rietz *et al.*, 2011; Wagner *et al.*, 2013). In chapter 1 and 2, I investigated the contribution of the PAD4^{LLD} and the PAD4 EP domain cavity residues PAD4^{R314} and PAD4^{K380} to these different defence outputs (Figure D.1). PAD4^{LLD}, PAD4^{R314A} and PAD4^{K380A} conferred GPA resistance (Figure 1.8&2.15), but were non-functional in resistance to *Hpa* and *Pst* pathogens (Figure 1.9&2.11&12). These data indicate that Arabidopsis PAD4 has domain specific functions (Figure D.1). Moreover, the PAD4 EP domain cavity is also required for immune signalling, like in EDS1, suggesting that the EDS1-PAD4 heterodimer cavity functions as a signalling surface. In chapter 3, I studied PAD4 complexes during ETI signalling by IP nLC-MS/MS, which showed that PAD4 complexes are very dynamic (Figure 3.1-3). I identified several putative interactors, of which TPR1, SGT1b and MES10 are most promising, and subsequently studied these three proteins in more detail (Figure 3.3-6). Lastly, in chapter 4 I observed that lines expressing cytoplasmic-enriched PAD4 display autoimmunity (Figure 4.2). Both genetic and protein-structure analyses suggest this autoimmune phenotype depends on PAD4 immune function (Figure 4.3-4). Taken together, this thesis highlights PAD4 as a central regulator in Arabidopsis resistance, and reveals new insights in PAD4 structure-function in GPA resistance and pathogen immunity (Figure D.1).

PAD4 is unlikely to function as a hydrolase

Chapter 1 shows that PAD4^{LLD} is sufficient to function in GPA resistance. However, the underlying molecular mechanism remains elusive. GPA resistance in Arabidopsis depends on the PAD4^{LLD} located S-D-H triad residues S¹¹⁸ and D¹⁷⁸, but not H²²⁹. Notably, Arabidopsis resistance against the hemi-biotrophic pathogen *Fusarium graminearum*, also depends on PAD4^{S118}, suggesting a common resistance mechanism (Makandar *et al.*, 2015). PAD4^{LLD} resembles the α/β hydrolase-fold family that catalyses a variety of enzymatic reactions using their core S-D-H catalytic triad, such as esterification, hydrolysis and acyl transfer (Rauwerdink & Kazlauskas, 2015). In the PAD4 structural model, the predicted S-D-H catalytic triad is solvent-accessible (Figure 1.8), suggesting hydrolase activity, however, this is only the case in

Brassicaceae PAD4 (Wagner *et al.*, 2013). Beyond the Brassicaceae clade, PAD4 contains an insertion extending from β -sheet scaffold. In *AtEDS1*, this insertion forms a helical loop that covers the S-D-H triad like a lid, rendering it inaccessible to the solvent (Wagner *et al.*, 2013). Such helical loop structures regulate the enzymatic activity of inactive-state triacylglycerol lipases (Khan *et al.*, 2017). Thus, although the PAD4 S-D-H triad is highly conserved, it is possible that the PAD4 S-D-H triad functions differently outside the Brassicaceae clade (Wagner *et al.*, 2013). Nonetheless, PAD4 is unlikely to function as hydrolase activity since the PAD4 S-D-H triad mutant, PAD4^{H229A}, still functions in PAD4-mediated GPA resistance in *Arabidopsis*. Since all three residues in the catalytic S-D-H triad are required for hydrolase function, this indicates that PAD4 does not rely in hydrolase activity in GPA resistance (Louis

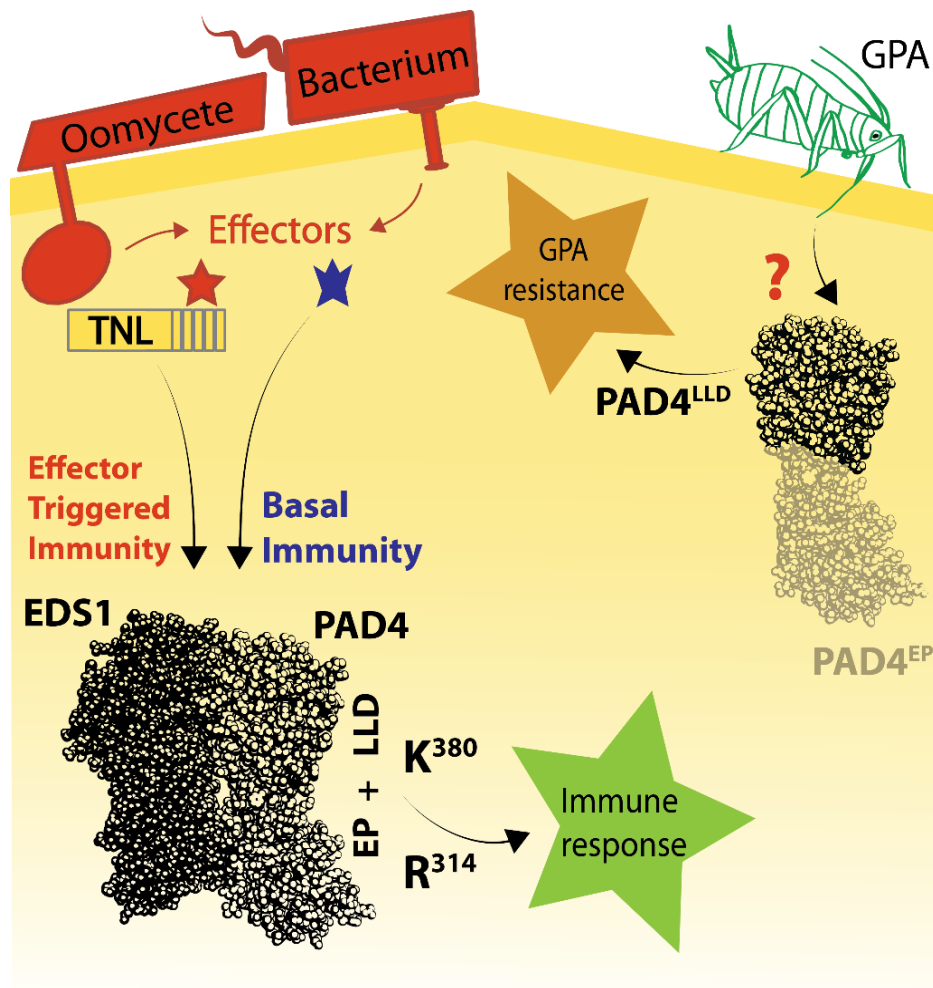


Figure D.1. Model of PAD4 signalling in pathogen immunity and GPA resistance.

Schematic showing separable pathogen immunity and GPA resistance activities of PAD4. Upon infection by bacteria or oomycetes, the EDS1-PAD4 heterodimer is activated via TNLs in ETI or by other signals in basal immunity. PAD4 LLD and EP domain are required to activate the immune response, and specifically the EP domain cavity located R³¹⁴ and K³⁸⁰ play an essential role in downstream signalling. In resistance to green peach aphids (GPA), *PAD4* expression is upregulated through an unknown mechanism. Independent of EDS1, PAD4^{LLD} is necessary and sufficient to restrict aphid infestation.

et al., 2012a; Rauwerdink & Kazlauskas, 2015). Moreover, a recent study on the *AtEDS1* monomer structure concludes that *AtEDS1* is a pseudo-enzyme (Voss *et al.*, 2019). It is therefore unlikely that GPA resistance requires a PAD4 canonical hydrolase activity.

Alternatively, the PAD4 S-D-H triad could function as a ligand-binding receptor, a feature commonly found in α/β hydrolase fold proteins (Mindrebo *et al.*, 2016). For example, the Arabidopsis karrikin receptor *AtKAI2* (KARRIKIN INSENSITIVE 2) and the gibberellin (GA) receptors Rice (*Oryza sativa*; *Os*) *OsGID1* & *AtGID1* (GA INSENSITIVE DWARF1) use their catalytically inactive S-D-H and S-D-V triads, respectively, for ligand recognition (Guo *et al.*, 2013; Murase *et al.*, 2008; Shimada *et al.*, 2008). Notably, this indicates that the Histidine in the S-D-H triad is not required *per se* for ligand binding, while this Histidine is essential for hydrolase activity (Murase *et al.*, 2008; Rauwerdink & Kazlauskas, 2015; Shimada *et al.*, 2008). Upon ligand binding, *AtGID1* undergoes a conformational change resulting in the assembly of an SCF^{GID1} complex. Subsequently, SCF^{GID1} induces proteasomal degradation of DELLA proteins by the 26S proteasome and activation of downstream signalling (Murase *et al.*, 2008). Notably, an unknown stearic acid-derived compound stimulates GPA resistance, which partially depends on PAD4 and the enzymatically active α/β hydrolase-fold lipase MYZUS PERSICAE-INDUCED LIPASE1 (MPL1; Louis *et al.*, 2010a&b). This indicates there is a lipid-derived molecule that functions in GPA resistance. Taken together, these examples highlight the possibility that PAD4^{LLD} and its S-D-H triad could function as a stearic acid-derived ligand-binding surface in a protein-signalling complex, rather than as a lipase.

In conclusion, further insights are required to determine whether PAD4^{LLD} functions as a lipase or as a receptor in GPA resistance. Furthermore, PAD4^{LLD} does not interact with EDS1, nor does it contain the EP domain required for immunity, and is therefore a suitable tool to specifically study PAD4 functions in GPA resistance (Figure 1.9). For example, future studies could perform IP-MS/MS to identify proteins and metabolites that associate to PAD4^{LLD} during GPA resistance.

PAD4 S-D-H triad-independent GPA activities

Besides GPA resistance, Arabidopsis PAD4 also functions in GPA anti-xenosis (aphid deterrence) and GPA-induced senescence (Pegadaraju *et al.*, 2005). In choice-assays, GPA prefers to settle on *pad4* mutants to Col-0, suggesting PAD4 stimulates anti-xenosis. During GPA infestation, PAD4 induces leaf senescence, chlorophyll degradation and the expression of a specific set of senescence-associated genes, *i.e.* *SAG13/21/27* (Pegadaraju *et al.*, 2005&2007). These PAD4 functions are independent of its S-D-H triad, which is required for GPA resistance (Louis *et al.*, 2012a). This indicates that other PAD4 surface(s) are functioning in GPA anti-xenosis and GPA-induced senescence. I postulate that these GPA responses are activated by the PAD4 EP domain cavity through the transcriptional regulation of a specific set of genes (Figure D.2).

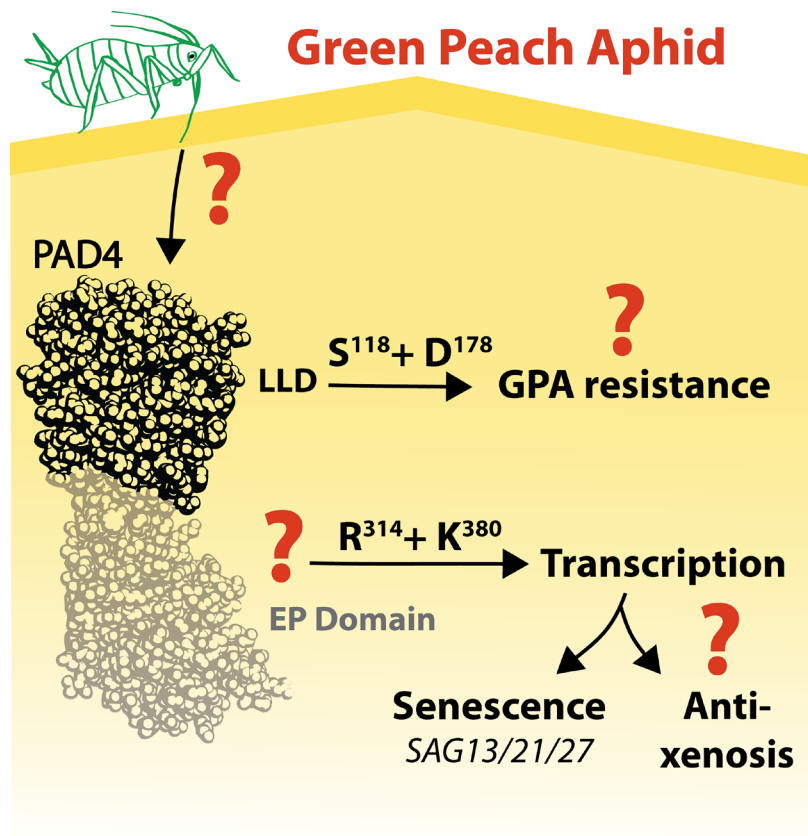


Figure D.2. Model of PAD4 structure-function in GPA defence responses. GPA induces the expression *PAD4* via an unknown mechanism. *AtPAD4* monomer structure model is based on *AtEDS1-AtSAG101* structure (Wagner *et al.*, 2013). $PAD4^{LLD}$ (black) and $PAD4^{S118/D178}$ are required for GPA resistance. GPA induced leaf senescence correlates with the upregulation of the senescence-associated genes *SAG13/21/27*, and depends on PAD4. Anti-xenosis (aphid-deterrence) depends on PAD4 (Pegadaraju *et al.*, 2005), however, it remains unclear whether it is under transcriptional control of PAD4. I postulate that $PAD4^{EP\ domain}$ (grey) located $PAD4^{R314}$ and $PAD4^{K380}$ are required for transcriptional changes, and are thus required for leaf senescence and anti-xenosis. Red question marks indicate open questions in the field.

Since PAD4^{LLD}, PAD4^{R314A} and PAD4^{K380A} were unable to induce immune gene expression upon *Pst avrRps4* infection, it is therefore possible that these PAD4 EP domain cavity mutants are also unable to upregulate *SAG13/21/27*, induce senescence and stimulate GPA anti-xenosis. Since the PAD4- and EDS1 EP domain cavity overlap in function, this would imply that EDS1 is also involved in these GPA responses (Bhandari *et al.*, 2019; Lapin *et al.*, 2019). However, EDS1 is not required for GPA resistance, *SAG13/21/27* upregulation and GPA induced senescence (Figure 2.15; Pegadaraju, 2005; Pegadaraju *et al.*, 2007). This indicates that EDS1 does not function in GPA defences. Nonetheless, future studies should determine if PAD4^{LLD}, PAD4^{R314A} and PAD4^{K380A} function in GPA induced senescence and anti-xenosis. These experiments will show if PAD4 has two functional surfaces, *e.g.* S-D-H triad and EP domain cavity, or if PAD4 contains more signalling surfaces (Figure D.2).

***PAD4* cis-regulation in plant resistance**

Many resistance pathways and metabolites induce *PAD4* expression. For example, *AtPAD4* transcripts accumulate in PTI, basal immunity and ETI, and upon application of MeJA, SA and nicotinamide (Baggs *et al.*, 2019; Bhandari *et al.*, 2019; Jirage *et al.*, 1999; Mine *et al.*, 2017a). Furthermore, upon infestation with the green peach aphid (GPA, *Myzus persicae* Sülzer) and trehalose treatment *PAD4* transcripts accumulate in Arabidopsis and Tomato (*Solanum lycopersicum*; *Sl*) (Couldridge *et al.*, 2007; Hodge *et al.*, 2013; Singh *et al.*, 2011; Singh & Shah, 2012; Pegadaraju *et al.*, 2005). *AtPAD4* expression depends on EDS1, PAD4, SAG101, ADF3, LIPOXYGENASE 5 (LOX5) and TPS11 (Bhandari *et al.*, 2019; Dongus *et al.*, 2020, Giri *et al.*, 2017; Mondal *et al.*, 2018; Nalam *et al.*, 2013). In contrast, BOTRYTIS-INDUCED KINASE 1 (BIK1), a PTI signalling component, and the phytohormone ABA repress *PAD4* expression (Baggs *et al.*, 2019; Lei *et al.*, 2014).

PAD4 expression dynamics are conserved in the Brassicaceae family. Upon treatment of the MAMP flg22, a peptide derived from bacterial flagellin, and upon MeJA-treatment, *PAD4* transcripts increase in Arabidopsis and in related Brassicaceae species *Arabidopsis lyrata*, *Capsella rubella*, and *Eutrema salsugineum* (Mine *et al.*, 2017a). However, when comparing the *AtPAD4* locus to these Brassicaceae species, mainly *AtPAD4*'s downstream (intergenic) region shows highly conserved regions, while its intron, and especially its upstream (intergenic) region, only contain small and weakly conserved regions (Figure 2.8). This suggests that the *AtPAD4* downstream region is important for *PAD4* transcription regulation.

Certain TFs have been found to regulate *PAD4* expression. For example, the JA and ABA regulated TFs *AtMYC2/3/4* repress flg22-induced *AtPAD4* expression (Mine *et al.*, 2017a&b; Pieterse *et al.*, 2012). However, MYC2 does not bind the *AtPAD4* promoter G-Box after flg22 and MeJA treatment (Mine *et al.*, 2017a), suggesting MYC2 binds the conserved *AtPAD4* downstream region rather than the promoter (Figure 2.8). Alternatively, MYC2 could bind a G-box in the *AtPAD4* intron. This G-box is located at the centre of an open chromatin site and locates close to a small conserved region, suggesting it contains *cis*-regulatory elements (Figure 2.8; Giri *et al.*, 2017; Zhang *et al.*, 2016). The bZIP class TF GBF1 binds this intronic G-Box, and stimulates basal immunity and CNL-ETI, in part by boosting *AtPAD4* expression (Giri *et al.*, 2017). Notably, in IP- nLC-MS/MS, PAD4 interacted with GIP1 that enhances GBF1 DNA-binding affinity *in vitro*, suggesting a PAD4-GIP-GBF1 module might enhance *PAD4* expression during TNL-ETI (Figure 1.7&3.2; Shaikhali, 2015). Furthermore, constructs containing the *AtPAD4* intron show higher *AtPAD4* expression than constructs without the *AtPAD4* intron (Giri *et al.*, 2017). Thus, indicating that the *PAD4* intron contains *cis*-elements important for *AtPAD4* regulation. Taken together, various triggers rapidly induce *AtPAD4* expression (Figure 1.9; Louis & Shah, 2015; Mine *et al.*, 2017a). Future studies should therefore investigate which regions regulate spatio-temporal *AtPAD4* expression. Moreover, by expressing *AtPAD4* under the control of tissue specific promoters, *e.g.* in guard cells, trichomes and phloem companion cells (Francia *et al.*, 2008; Stadler & Sauer, 1996; Szymanski *et al.*, 1998), one could dissect the contribution of *AtPAD4* in specific tissues in GPA defence responses, pathogen immunity and SAR.

PAD4^{R314A} and PAD4^{K380A} susceptibility is not dependent on *Pst*-produced coronatine

The JA-Ile phytohormone-mimic coronatine is a potent virulence factor produced by *Pst* DC3000, which represses several immune pathways, including the EDS1 immune pathway (Cui *et al.*, 2018; Brooks *et al.*, 2005; Zheng *et al.*, 2012). The EDS1 EP domain cavity mutants EDS1^{K478R} and EDS1^{R493A} show a coronatine-dependent susceptibility phenotype, indicating that the JA-pathway is negatively regulating EDS1 EP domain cavity functions (Bhandari *et al.*, 2019). Notably, juxtaposed to these EDS1 residues lie PAD4^{R314} and PAD4^{K380}. In contrast to EDS1^{K478R} and EDS1^{R493A}, PAD4^{R314A} and PAD4^{K380A} did not show a coronatine-dependent susceptibility phenotype (Figure 2.14). This indicates that these PAD4 variants are unable to function in immunity, similar to EDS1^{R493E} (Bhandari *et al.*, 2019).

Furthermore, these results highlight that coronatine is not specifically repressing SAG101 function. If coronatine was specifically affecting SAG101 function, then one would expect *pad4-1*, with *SAG101*, to be as resistant as Col-0 upon infection with *Pst* DC3000 Δ *Cor* and *Pst avrRps4* Δ *Cor*. However, *pad4-1* is still susceptible to these strains, showing similar degrees of susceptibility as in coronatine-producing *Pst* strains (Figure 1.9&2.14). This indicates that coronatine is not specifically affecting SAG101 functions. In conclusion, coronatine is not an inhibitor of EDS1-PAD4 EP domain cavity immune functions, but rather an inhibitor of processes downstream of EDS1 heterodimers, as previously proposed by Bhandari *et al.* (2019).

EDS1-family heterodimerisation is essential for immunity

EDS1-family heterodimer formation is essential for immune function in Arabidopsis and *N. benthamiana*. (Wagner *et al.*, 2013; Gantner *et al.*, 2019). Moreover, EDS1 and PAD4 are able to heterodimerise within their respective monocot and dicot species, suggesting EDS1-PAD4 heterodimerisation is a key feature adopted early on in EDS1-family evolution (Gantner *et al.*, 2019; Gao *et al.*, 2014; Lapin *et al.*, 2019). Moreover, this suggests a conserved function of EDS1-PAD4 heterodimers in seed plants. In Arabidopsis, previous reports suggest that EDS1-PAD4 heterodimerisation solely depends on their respective LLDs interacting, more specifically, on the EDS1^{LLIF} and the PAD4^{MLF} motifs (Wagner *et al.*, 2013). Here I show that Arabidopsis EDS1^{LLD}, PAD4^{LLD} and SAG101^{LLD} are not sufficient for heterodimer formation, suggesting the EP domain also contributes to heterodimerisation (Figure 1.1-5). Notably, all of the EDS1 and PAD4 EP domain cavity mutants generated thus far, are still able to interact with their respective partner (Bhandari, *et al.*, 2019; Gantner *et al.*, 2019; Lapin *et al.*, 2019; Neubauer *et al.*, 2020; Figure 1.1&2.5-6). This suggests that multiple residues in the EDS1 and PAD4 EP domain take part in heterodimer formation or stabilisation, by either directly binding its cognate partner, or indirectly via a yet unknown entity that functions as a glue.

*At*EDS1^{LLIF} does not function in immunity, which has been ascribed to its inability to interact with PAD4 and SAG101 (Wagner *et al.*, 2013). Although this is currently the most probable model, there are some observations that suggest this is not causality, but rather a correlation. In chapter two, I showed that PAD4^{L286A} still functions in ETI, yet is unable to interact with EDS1 (Figure 2.1-5&11). Similarly, J. Bautor and Dr. J. Qiu characterized residues in the PAD4 LLD, which upon mutation are unable to interact with EDS1, yet maintain their function in ETI (Unpublished data, Parker lab). This suggests that the EDS1-PAD4 interaction at the LLD is not essential for EDS1-PAD4 function in immunity. Moreover, this suggests that the EDS1^{LLIF} motif could have another function besides interacting with PAD4 and SAG101.

However, split-LUC data showed that EDS1^{LLIF}-PAD4 and EDS1^{LLIF}-SAG101 show a significant reduction in binding compared to non-interacting EDS1-PAD4^{LLD}/ EDS1-SAG101^{LLD} (Figure 1.1&2&5). This indicates that the EDS1^{LLIF} mutation has a stronger negative effect on EDS1-PAD4/-SAG101 heterodimer formation than the LLD truncations. In accordance with this observation, EDS1^{L262P}, located in the LLIF motif, no longer associates with PAD4, while EDS1^{L262P} still interacts with SAG101 (Rietz *et al.*, 2011). Consequently, EDS1^{L262P} only loses basal immunity functions, which depend on PAD4, but retains ETI functions, which depend on SAG101 (Rietz *et al.*, 2011). Similarly, five aliphatic residues in *NbSAG101b*^{LLD} have to be mutated to a negatively charged Glutamate before *NbSAG101b* fails to function with *NbEDS1* in ETI (Gantner *et al.*, 2019). These studies indicate that EDS1-family heterodimerisation is robust. Moreover, this suggests that EDS1 and PAD4 EP domain mutants described thus far are not sufficient to completely obstruct heterodimer formation (Chapter 2; Bhandari *et al.*, 2019; Gantner *et al.*, 2019; Lapin *et al.*, 2019). In conclusion, these data indicate that the EDS1-PAD4/-SAG101 interaction is robust and can withstand many perturbations before it fails to function in immunity.

Future studies should focus on quantifying Arabidopsis EDS1-PAD4/-SAG101 heterodimer binding strength. Not simply to determine which residues contribute to heterodimer formation, but to determine whether EDS1 prefers EDS1-PAD4 or EDS1-SAG101 heterodimers. This is relevant since recent findings show that in RRS1-S/RPS4-ETI, PAD4 functions mainly in resistance, while SAG101 functions mainly in cell death (Lapin *et al.*, 2019). Notably, the intensity of these outputs are anti-correlated between the accessions Col-0 and Ws-2 (Previously Ws-0), where Col-0 is more resistant than Ws-2, while, Col-0 shows weaker cell death than Ws-2 (Feys *et al.*, 2005; Saucet *et al.*, 2015). This suggests that processes downstream of effector recognition orchestrate the balance between cell death and resistance. Insights in EDS1-family heterodimer stoichiometry would yield insight in the default EDS1 complex pre-activation. Although it is still unclear how the immune network decides which pathway to prefer over the other, it is clear that EDS1 heterodimers are a paramount signalling hub on this bifurcation point.

TIR-NADase activity and the EDS1-family EP domain cavity

Previous studies have highlighted the importance of the EDS1 EP domain cavity in immunity (Bhandari *et al.*, 2019; Gantner *et al.*, 2019; Lapin *et al.*, 2019). In chapter 2, I show that the *At*PAD4 EP domain cavity contains PAD4^{R314} and PAD4^{K380} that are essential for *At*PAD4 immune function (Figure D.3). Nearly all of these EDS1 and PAD4 EP domain cavity residues are polar and positively charged, suggesting a negatively charged entity binds the EP domain cavity (Figure D.3; Bhandari *et al.*, 2019; Lapin *et al.*, 2019). However, this observation could be due to an experimental bias. Namely, all of these residues were identified by mutation to a non-polar Alanine, therefore, positively charged (polar) residues were more affected than non-polar residues. In contrast, non-polar EDS1^{F419} (Lapin *et al.* 2019) has been identified through mutation to a negatively charged (polar) glutamic acid (E), suggesting more disruptive mutations are required to determine the contribution of non-polar residues in immunity.

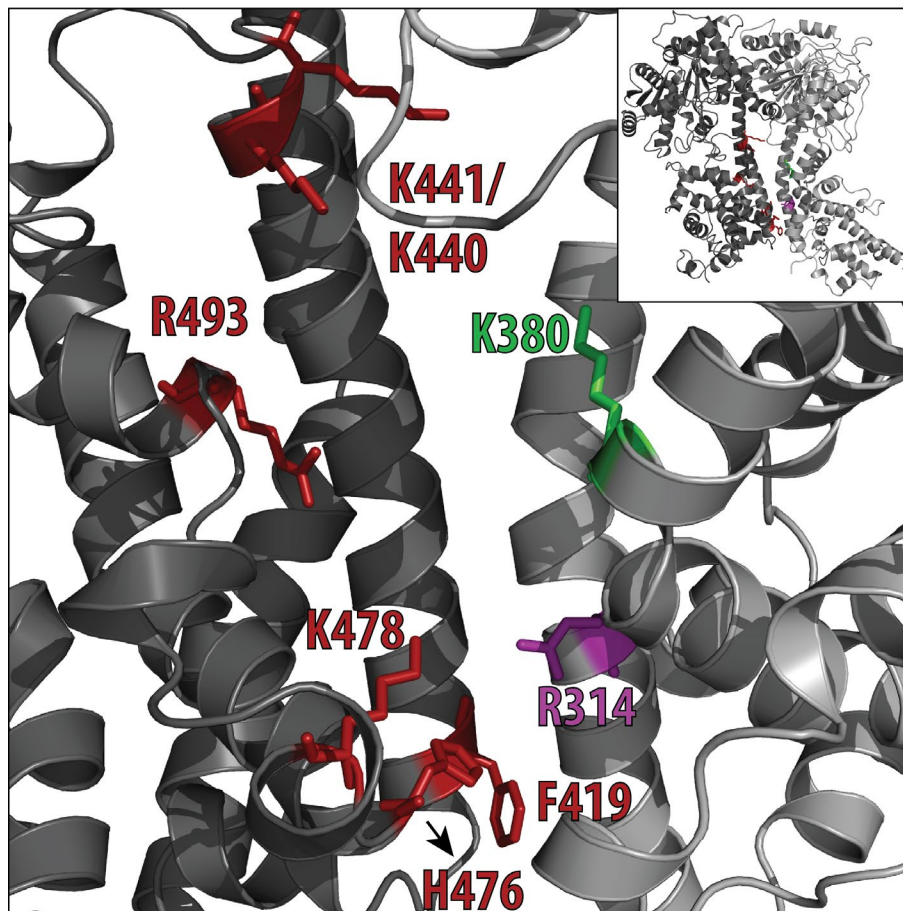


Figure D.3. EDS1-PAD4 EP domain cavity forms a (positively charged) signalling surface.

Arabidopsis EDS1-PAD4 heterodimer model in top right corner, based on Arabidopsis EDS1-SAG101 structure (Wagner *et al.*, 2013). EDS1 EP domain cavity residues that contribute to immunity are shown in red, and PAD4 EP domain cavity residues that contribute to immunity are shown in purple (R314) and green (K380). Two major questions remain unsolved, 1) are the same sites as in PAD4 required for SAG101 function (See figure 2.2)? and 2) what protein or signalling molecule fits in the EDS1-PAD4 EP domain cavity?

Recent findings suggest that the EP domain cavity-located *AtSAG101* residues between amino acids 289-308 play an essential role in *AtSAG101* cell death function in *N. benthamiana* (Lapin *et al.*, 2019). This suggests that, besides the EDS1-PAD4 EP domain cavity, EDS1-SAG101 EP domain cavity also forms a signalling surface in Arabidopsis. Functional differences in Arabidopsis between EDS1-PAD4 and EDS1-SAG101 are therefore likely determined by the characteristics of their EP domain cavities. This suggests that the EDS1 EP domain cavity side is not the selective component that discriminates between interacting entities. I postulate that the EDS1 EP domain cavity forms a more promiscuous interacting surface, in contrast to the PAD4 and SAG101 EP domain cavity sides, which are likely more discriminating.

This hypothesis is supported by observations made expressing EDS1 and PAD4 from Tomato and Grapevine (*Vitis aestivalis*; *Va*) in Arabidopsis. *SlEDS1* and *VaEDS1* function with *AtPAD4* in Arabidopsis immunity, while *SlPAD4* and *VaPAD4* do not function with, respectively, *AtEDS1*, and *AtEDS1* and *VaEDS1* (Gao *et al.*, 2010&2014; Lapin *et al.*, 2019). This suggests incompatibility between Arabidopsis signalling components and *SlPAD4* and *VaPAD4*. Strikingly, co-expressed *SlEDS1-SlPAD4* do function in Arabidopsis TNL-ETI, suggesting a compensatory effect of *SlEDS1* on *SlPAD4* and Arabidopsis signalling components (Lapin *et al.*, 2019). The incompatibility between *AtEDS1* and *SlPAD4* and *VaPAD4* might be due to the absence of the helper NLR *SlADR1* and *VaADR1*, respectively. In Tobacco, *AtEDS1-AtSAG101* co-expression does not confer resistance in absence of the helper NLR *AtNRG1* (Lapin *et al.*, 2019). Hence, *VaPAD4* and *SlPAD4* possibly do not function in Arabidopsis immunity without the presence of ADR1 from their respective species. In summary, based on these reports it is likely that PAD4 and SAG101 are the components in the EDS1 heterodimer that specify which specific substrate binds the EP domain cavity. Based on literature, prime candidates to interact with EDS1-family EP domain cavities are NAD⁺-derived compounds, and the helper NLR family proteins NRG1 and ADR1 (Horsefield *et al.*, 2019; Lapin *et al.*, 2019; Jubic *et al.*, 2019; Wu *et al.*, 2019; Wan *et al.*, 2019).

Plant TIR domain NADase activity is essential for cell death *in planta* (Horsefield *et al.*, 2019; Wan *et al.*, 2019). Moreover, TNL NADase-induced cell death fully depends on EDS1 *in planta* (Horsefield *et al.*, 2019; Wan *et al.*, 2019). EDS1-family proteins are essential for TNL-ETI signalling, where EDS1 and PAD4 interact with TNLs (Bhattacharjee *et al.*, 2011; Heidrich *et al.*, 2011; Kim *et al.*, 2012). This suggests that EDS1 heterodimers (in-) directly recognise NAD⁺ depletion or the presence of an NAD⁺-derived product, *e.g.* cyclic ADP-ribose (cADPR),

for immune activation (Horsefield *et al.*, 2019; Wan *et al.*, 2019). A candidate recognition surface is the EDS1-PAD4/-SAG101 EP domain cavity. The residues in the EDS1-PAD4 EP domain cavity that function in immunity are between ~5 and ~23 Å apart, indicating that NAD⁺ (~22 Å wide; PubChem CID: 925) and cADPR (~13 Å wide; PubChem CID:123847) principally would fit inside (Figure D.3&2.1-2&4; Bhandari *et al.*, 2019; Lapin *et al.*, 2019). However, to determine if these compounds could interact with the EDS1-PAD4 EP domain cavity would require extensive modelling. If biochemical *in vitro* assays confirm this takes place, this would indicate that certain NAD⁺-derived products bind the EDS1-PAD4 EP domain cavity to induce resistance, while others bind the EDS1-SAG101 EP domain cavity to induce cell death.

Alternatively, the helper NLR families ADR1 and NRG1 could function as receptors of NAD⁺-derived products. In Arabidopsis, ADR1 & PAD4, and NRG1 & SAG101 functionally overlap in immunity, suggesting they function together in, respectively, resistance and cell death (Bonardi *et al.*, 2011; Castel *et al.*, 2019; Lapin *et al.*, 2019; Wu *et al.*, 2019). ADR1 and NRG1 could bind NAD⁺-derived compounds using their NB domain, which upon ligand recognition, could induce immune signalling by associating to the EDS1-PAD4 and EDS1-SAG101 EP domain cavities, respectively. This model is in line with the observations that *Nb*NRG1 interacts with and signals via *Nb*EDS1 (Peart *et al.*, 2005; Qi *et al.*, 2018). Notably, *At*EDS1 has not been found to interact with *At*NRG1 *in planta* (Lapin *et al.*, 2019; Wu *et al.*, 2019). Similarly, I did not detect any *At*ADR1 peptides in IP nLC-MS/MS on *At*PAD4 at 4 and 6 hpi with *Pst avrRps4*. Thus, suggesting EDS1-PAD4-ADR1 complexes are not formed in Arabidopsis, or that their association takes place at a different time-point during *Pst avrRps4* infection. In conclusion, TNL-NADase activity, ADR1 function and NRG1 function are linked to EDS1-family signalling in Arabidopsis, however, the underlying molecular mechanism is not well understood.

Taken together, the exact molecular function of the EDS1-family EP domain cavity remains elusive. However, these results suggest that Arabidopsis EDS1-PAD4 and EDS1-SAG101 form two similar cavities, which are functionally different, and are therefore likely to interact with two different, yet similar, molecular entities.

Perspectives on CC-NLR structure-function and signalling via EDS1-PAD4

In Arabidopsis, RPS2/RPM1 CNL-ETI depends on EDS1, PAD4 and SA for resistance, and partially for cell death execution (Cui *et al.*, 2017; Feys *et al.*, 2005), indicating EDS1-PAD4 and SA can integrate CNL-ETI signals. Recently, cryo-EM revealed the oligomeric structure of the Arabidopsis CNL ZAR1 (Wang *et al.*, 2019a&b). Post-activation, ZAR1 forms a circular pentameric structure (resistosome), where the N-terminal α 1-helices together form a funnel-shaped structure or pore that associates to the plasma membrane. This membrane association and α 1-helix formed pore are essential for ZAR1 cell death and resistance function (Wang *et al.*, 2019a&b). Like ZAR1, the CNL receptor pair RPS2/RPM1 are CNLs that can associate to the plasma membrane in Arabidopsis and could therefore function similar to ZAR1 (Boyes *et al.*, 1998; Axtell & Staskawicz, 2003). In contrast to RPS2/RPM1-ETI, ZAR1-ETI does not depend on any known basal immunity and ETI signalling component, including EDS1, PAD4, ICS1-produced SA and NON RACE-SPECIFIC DISEASE RESISTANCE 1 (NDR1) (Lewis *et al.*, 2010). This indicates that ZAR1-ETI is not representative for RPS2/RPM1-ETI, which suggests that the ZAR1 structure model is not representative for RPS2/RPM1 structure function. Thus, the molecular mechanisms described for ZAR1, may not be helpful to understand CNL-ETI signal integration by EDS1-PAD4 and SA.

The ZAR1 α 1-helix contains a conserved MADA-motif at its N-terminus, which is present in several monocot and dicot CNLs (Adachi *et al.*, 2019; Wang *et al.*, 2019a&b). For the helper NLR and CNL *Nb*NRC4 (NLR REQUIRED FOR CELL DEATH 4) this MADA-motif is essential for its immune function in *N. benthamiana*, suggesting the MADA-motif is required for MADA-motif containing CNLs, like the pore forming *At*ZAR1 (Adachi *et al.*, 2019). The RNLs NRG1 and ADR1 do not contain this MADA-motif, suggesting they do not form a funnel-shaped structure (Adachi *et al.*, 2019). However, recent evidence suggests that RNLs can oligomerise and that their CC_R domains potentially form a pore (Li *et al.*, 2020).

The Arabidopsis RNL HR4 oligomerises *in planta* with the CNL RPP7 during immune signalling (Li *et al.*, 2020). Arabidopsis HR4, NRG1 and ADR1 CC_R domains show similarity to MLKL and HeLo/HELL domains from mammals and fungi, which can form membrane pore forming toxins (Collier *et al.*, 2011; Li *et al.*, 2020; Mahdi *et al.*, 2019; Petrie *et al.*, 2018; Jubic *et al.*, 2019). Similar to mammalian MLKLs, *At*MLKLs are hypothesised to form pores, since *At*MLKL is membrane-localised and forms oligomers that structurally resemble mammalian pore-forming MLKLs. Moreover, *At*MLKLs are required for immunity against filamentous

biotrophic pathogens in Arabidopsis, suggesting pore-formation is required for certain immune responses (Mahdi *et al.*, 2019). Taken together, these data suggest that Arabidopsis RNLs NRG1 and ADR1 can oligomerise and function as membrane pore forming domains (Jubic *et al.*, 2019). This is particularly likely for NRG1, since *AtNRG1* has already been shown to localise to the cytoplasmic endomembrane in stable Arabidopsis transgenic lines, and in *N. benthamiana* pre- and post-TNL-ETI activation (Wu *et al.*, 2019). Whether ADR1 and NRG1 form a pore and how such a pore links to EDS1-family signalling remains unknown.

Immune signalling components downstream of NLRs and EDS1-PAD4

Although the described processes above would molecularly explain EDS1-PAD4/-SAG101 heterodimer activation, they do not explain how activated EDS1 heterodimers regulate immunity downstream of NLRs. In chapter 3, I aimed to identify such downstream components by comparing functional PAD4^{WT} interactomes with that of non-functional PAD4^{K380A} at 4 and 6 hpi with *Pst avrRps4*. This showed that PAD4 always immunoprecipitated EDS1, indicating that PAD4 forms complexes with EDS1 during pathogen invasion (Figure 3.1). Furthermore, 95% of the identified proteins did not associate to PAD4^{WT} at both time-points, indicating that PAD4 complexes change rapidly over time (Figure 3.1).

PAD4^{WT} interacted with TPR1/TPL/TPR2 at 6 hpi with *Pst avrRps4* (Figure 3.2-3). TPR1 has been shown to function in Arabidopsis basal immunity and TNL-ETI, like EDS1 and PAD4 (Feys *et al.*, 2005; Zhu *et al.*, 2010). TPR1 is a transcriptional regulator acting as a docking station for transcription factors and chromatin modifiers, such as the basal immunity activator HISTONE DEACETYLASE 19 (HDA19) (Kim *et al.*, 2008; Long *et al.*, 2006; Lynch *et al.*, 2017; Oh *et al.*, 2014; Zhu *et al.*, 2010). Recently, the SUMO (small ubiquitin-like modifier) E3 ligase SIZ1 was proposed to repress immunity by disrupting the interaction between HDA19 and TPR1 through SUMOylation of TPR1 (Niu *et al.*, 2019). Notably, an *AtTPR1* orthologue, *NbTPL4*, stimulates resistance in Tobacco against the Tobacco Mosaic Virus (Zhang *et al.*, 2019). Moreover, *NbTPL4* was found to interact with the TNL *NbN*, suggesting a conserved role of TPL-family proteins in TNL-ETI (Zhang *et al.*, 2019).

In uninfected Arabidopsis leaves, EDS1 interacts with the transcriptional regulator SUPPRESSOR OF RPS4-RLD (SRFR1) (Bhattacharjee *et al.*, 2011). In contrast to TPR1, SRFR1 represses TNL-ETI responses in Arabidopsis (Kim *et al.*, 2009; Kwon *et al.* 2009; Li *et al.*, 2010). Like EDS1, SRFR1 interacts with the TNLs SNC1, RPS4 and RPS6, but not with

the CNL RPM1, suggesting SRFR1 represses TNL-ETI specifically (Bhattacharjee *et al.*, 2011; Heidrich *et al.*, 2011). It is therefore plausible that upon TNL activation, SRFR1 releases EDS1, thereby allowing TPR1 to interact with EDS1-PAD4, which results in the formation of an immunity-activating transcription complex. In my IP nLC-MS/MS analysis, I did not analyse the PAD4 interactome pre-infection, but only at 4 and 6 hpi with *Pst avrRps4*. Future studies should therefore analyse EDS1, PAD4 and SAG101 complexes in triggered and non-triggered tissues to determine differences between pre- and post-activation complexes of EDS1-family proteins.

Interaction between EDS1-family proteins and phytohormone processing enzymes

MES10 was immunoprecipitated by PAD4^{WT} and PAD4^{K380A} at 4 and 6 hpi with *Pst avrRps4* (Figure 3.2-3). MES10 is one out of 20 methyl-esterases encoded by the Arabidopsis genome and belongs to the α/β hydrolase superfamily (Yang *et al.*, 2008). MES10 groups in a separate clade compared to its family members, and is the only MES in Arabidopsis that shows exclusive MeJA methyl-esterase activity *in vitro* (Yang *et al.* 2008). Furthermore, *At*MES10 does not show any SA-binding affinity or SA-esterase activity, unlike its family members *Nb*SA-BINDING PROTEIN 2 (*Nb*SABP2) and *At*MES1/2/7/9 (Vlot *et al.*, 2008; Yang *et al.* 2008). Thus far, it remains unclear if MES10 functions in plant resistance, although transcriptome data suggest MES10 functions antagonistically to EDS1 and PAD4 in basal immunity and ETI (Table 3.1; Figure 3.4). Further analyses on *mes10* mutants should reveal its role in plant immunity against biotrophic and necrotrophic pathogens.

MES10 was not the first phytohormone-processing enzyme to associate to an EDS1-family protein. Recently, the SA-processing enzyme PBS3 has been shown to interact with EDS1 (Chang *et al.*, 2019). In the cytosol, PBS3 catalyses the reaction from isochorismate (IC) to IC-9-Glutamate, the before-last and essential step in chorismate-derived SA biosynthesis (Ding & Ding, 2020; Rekhter *et al.*, 2019; Torrens-Spence *et al.*, 2019). Notably, PBS3 competes for EDS1 interaction with the SA receptors and CUL3 adaptors NPR3/4 (Chang *et al.*, 2019). The SCF component CUL3 and NPR3/4 stimulate poly-ubiquitination of EDS1, resulting in EDS1 degradation by the 26S proteasome (Chang *et al.*, 2019). Remarkably, PBS3 interaction with EDS1 inhibits this process, indicating PBS3 limits EDS1 degradation besides stimulating SA accumulation. If PBS3 regulates PAD4-accumulation is unknown. Taken together, PBS3 has a dual role in immunity and functions as a moonlighting protein, where it stimulates SA biosynthesis on the one hand, and stimulates EDS1 protein levels on the other (Chang *et al.*,

2019). As a mirror image of EDS1-PBS3, MES10 could possibly function as a moonlighting protein too by stimulating JA-levels and possibly limiting PAD4 accumulation. Future studies should therefore investigate the role of MES10 in immunity against biotrophic and necrotrophic pathogens, and PAD4 accumulation in *mes10* mutants.

NESgPAD4 phenocopies EDS1-NLS

Cytoplasmic-enriched PAD4 induces autoimmunity in a protein level dependent manner (Figure 4.2&3). Preliminary results suggest that this autoimmune response depends on the EDS1 and PAD4 EP domain cavity, and not on PAD4 GPA resistance activity (Figure 4.3&4). EDS1-NLS induces autoimmunity, which is suppressed by *dangerous mix 2h (dm2h)*, a TNL expressed from the *RPP1-like* gene cluster from Landsberg *erecta* (*Ler*) (Stuttman *et al.*, 2016). This suggests that DM2h is guarding EDS1, and is sensing over-accumulation of nuclear EDS1, rather than the alternative hypothesis where enhanced nuclear EDS1 levels stimulate EDS1-nuclear activity. Similarly, I hypothesise that NESgPAD4 does not induce cytosolic PAD4 activities. Instead, I postulate that PAD4 is also guarded by a TNL that senses over-accumulation of cytoplasmic PAD4, which induces autoimmunity in NESgPAD4 lines.

Notably, NESgPAD4 phenocopies EDS1-NLS (Dr. J. Stuttmann, personal communication), suggesting that these phenotypes are caused by the same underlying molecular mechanism. If this is indeed true, than one of two scenarios is causal for autoimmunity in EDS1-NLS and NESgPAD4 lines. In the first scenario a high PAD4:EDS1 ratio in the cytoplasm triggers autoimmunity. In this scenario, NESgPAD4 lines show high cytoplasmic PAD4 levels, thus, a high PAD4:EDS1 ratio in the cytoplasm, which results in autoimmunity. In the same scenario, EDS1-NLS causes autoimmunity, since low cytosolic EDS1 levels result in a high PAD4:EDS1 ratio in the cytoplasm. Conversely, in the second scenario, a high EDS1:PAD4 ratio in the nucleus triggers autoimmunity. In this scenario, EDS1-NLS lines show high nuclear EDS1 levels, thus, a high EDS1:PAD4 ratio in the nucleus, which results in autoimmunity. In the same scenario, NESgPAD4 causes autoimmunity, since low nuclear PAD4 levels result in a high EDS1:PAD4 ratio in the nucleus. Thus far, it remains unclear, which of these scenarios is causal for the EDS1-NLS and NESgPAD4 autoimmune phenotypes. In addition, whether NESgPAD4 autoimmunity is caused by an erroneously activated NLR, or due to a hyperactive EDS1 or PAD4, remains unclear. Nonetheless, it is clear that perturbations in EDS1 and PAD4 subcellular localisation activates the immune system.

Taken together, these results show that our understanding of nuclear and cytosolic functions of PAD4 are rudimentary. Future research should study PAD4 subcellular localisation dynamics during pathogen infection and GPA infestation. Furthermore, one could make EDS1, PAD4 or SAG101 protein fusions that tether the protein to the cytosolic side of various membranes, *e.g.* vacuole, chloroplast, mitochondrion, plasma membrane and ER, but also the inner nuclear envelope. This would yield insight in EDS1-family cytosolic, nuclear and membrane-associated functions, not only in ETI and GPA defences, but also in PTI. Such experiments would gain insight in the relation between EDS1-family proteins and membrane tethered proteins. This is particularly relevant since recent reports highlight crosstalk between PTI and ETI signalling, and various reports indicate that certain ETI signalling components locate to a membrane (Cui *et al.*, 2015; Jubic *et al.*, 2019; Mahdi *et al.*, 2019; Ngou *et al.*, 2020; Yuan *et al.*, 2020; Wang *et al.*, 2019a&b).

SGT1b in NESgPAD4 autoimmunity

SGT1b is a protein chaperone that can antagonizes and stimulate protein accumulation of NLRs *in planta* (Azevedo *et al.*, 2006; Holt *et al.*, 2006; Li *et al.*, 2010). PAD4^{WT} associated with SGT1b specifically at 6 hpi with *Pst avrRps4*, but not with the non-signalling PAD4 variant PAD4^{K380A} (Figure 3.2&3). In Arabidopsis, SGT1b and PAD4 are required for several NLR signalling pathways, suggesting PAD4 and SGT1b engage in ETI signalling (Austin *et al.*, 2002; Feys *et al.*, 2005; Kim *et al.*, 2012; Lee *et al.*, 2016; Tor *et al.*, 2002; Yang *et al.*, 2010; Wang *et al.*, 2013; Zhang *et al.*, 2017b). NESgPAD4 autoimmunity was enhanced in *sgt1b* mutants, without enhancing NESgPAD4 protein levels, suggesting *SGT1b* suppresses NESgPAD4 downstream signalling (Figure 4.4). Notably, NESgPAD4 protein in the *sgt1b* mutant ran higher on western blot, suggesting NESgPAD4 is post-translationally modified in the absence of SGT1b (Figure 4.4B). These modifications could lead to enhanced NESgPAD4 activity. Future studies should identify if, and where, such modifications are placed on NESgPAD4. Mutagenesis of these sites can determine whether they are required for NESgPAD4 autoimmunity and PAD4 immune function.

As mentioned above, NESgPAD4 autoimmunity could depend on an NLR, like EDS1-NLS depends on the TNL *DM2h* (Stuttman *et al.*, 2016). Therefore, the enhanced NESgPAD4/*sgt1b* autoimmunity phenotype could be attributed to enhanced NLR levels, leading to enhanced NLR auto-activity, as was previously observed for RPS4 and SNC1 (Cheng *et al.*, 2011; Heidrich *et*

al., 2013). Future studies could therefore determine if TNL levels in NESgPAD4/*sgt1b* are elevated using native antibodies, such as α -SNC1 (Li *et al.*, 2010).

Alternatively, reduced JA-signalling could be causal for the enhanced NESgPAD4/*sgt1b* autoimmunity phenotype. JA antagonizes EDS1-PAD4 immunity signalling and *vice versa* (Bhandari *et al.*, 2019; Cui *et al.*, 2018). In contrast, SGT1b stimulates JA-signalling through stabilisation of the JA receptor COI1 (Zhang *et al.*, 2015). Therefore, NESgPAD4/*sgt1b* are likely to contain lower COI1 levels and consequently reduced JA-signalling activity. This relieves JA-mediated inhibition of EDS1-PAD4 signalling, leading to enhanced NESgPAD4 activity and autoimmunity. This hypothesis could be tested by comparing the expression of JA-marker genes *PDF1.2* and *VSP1* in NESgPAD4 and NESgPAD4/*sgt1b* lines (Pieterse *et al.*, 2012). Furthermore, NESgPAD4 should be crossed with *coil* to determine if this phenocopies NESgPAD4/*sgt1b*. Taken together, SGT1b regulates various immune pathways that converge on EDS1-PAD4 signalling, and is therefore a relevant interactor of PAD4 in TNL-ETI signalling.

ICS1-produced SA in NESgPAD4 autoimmunity

ICS1-produced SA functions in parallel to PAD4 in basal immunity and ETI (Cui *et al.*, 2017; Wildermuth *et al.*, 2001; Zhou *et al.*, 1998). Notably, NESgPAD4/*sid2* (*ics1*) mutants showed enhanced leaf chlorosis along the veins (Figure 4.4), indicating that ICS1-produced SA can inhibit certain PAD4 pathways. Intuitively, one would expect vein-chlorosis to depend on PAD4 GPA resistance function, since GPA feed from the phloem along the vasculature (Pegadaraju *et al.*, 2005&2007). However, using structure-guided mutagenesis I showed that this GPA resistance function is not required to induce leaf chlorosis (Figure 4.5). This suggests that ICS1-produced SA inhibits a vein-specific immune activity of NESgPAD4.

The SAR pathway might be one of the EDS1-PAD4 pathways that is upregulated in NESgPAD4/*sid2*. EDS1-PAD4 induce the expression of *ALD1* and *FMO1*, which catalyse essential steps in the biosynthesis of the SAR-stimulating compound NHP (Bhandari *et al.*, 2019; Dongus *et al.*, 2020; Hartmann & Zeier, 2019). Although it is unclear which cell-types in the leaf produce NHP, one would expect cells along the veins to produce NHP. Possibly, NESgPAD4 leaf chlorosis depends on the over-expression of *ALD1* and *FMO1*, leading to over-accumulation of NHP in the vasculature. Future studies should determine gene expression of *ALD1* and *FMO1* in NESgPAD4 and NESgPAD4/*sid2* to determine if these genes are over-

expressed in the NESgPAD4/*sid2* lines. Furthermore, to determine if *ALDI* and *FMO1* contribute to leaf chlorosis, one should cross NESgPAD4/*sid2* with *ald1* and *fmol* mutants.

NESgPAD4-induced vein chlorosis highlights an important, but often overlooked dimension in plant immunity: space. Recently, spatio-temporal changes in the promoter activity of *PRI* (SA marker gene) and *VSP1* (JA marker gene) were monitored upon pathogen infection (Betsuyaku *et al.*, 2018). This revealed that the promoters were activated in distinct zones around the infection site. Such approach should also be used to identify where and when certain immune pathways are activated upon infection, *e.g.* *PAD4* and *ADR1*-family for basal immunity; *SAG101* and *NRG1*-family for TNL-ETI; *PBS3* and *ICSI* for SA production; and *FMO1* and *ALDI* for NHP production. To monitor their expression activities one should use a clearly visible fluorophore that is enriched in the nucleus, *e.g.* 3xVenus-NLS. Furthermore, for a high and representative spatio-temporal expression pattern, these constructs should be under the control of the full genomic locus, including, upstream- and downstream intergenic regions, UTRs, but excluding the exons, to eliminate post-translational regulation of the fluorophore.

Concluding remarks and outlook

My analysis of Arabidopsis PAD4 demonstrates a domain-specific partitioning of resistance functions. The PAD4^{LLD} is necessary and sufficient for limiting GPA infestation, while the PAD4 EP domain cavity residues R³¹⁴ and K³⁸⁰ are essential for resistance against *Pst* and *Hpa* (Figure D.1). This study and previous reports highlight the EDS1-PAD4 EP domain cavity as a signalling surface in immunity (Bhandari *et al.*, 2019; Lapin *et al.*, 2019; Wagner *et al.*, 2019). Recent insights indicate that the *AtSAG101* EP domain is also required for immune signalling (Lapin *et al.*, 2019). *AtPAD4*^{R314} and *AtPAD4*^{K380} are highly conserved in, respectively, angiosperm, and angiosperm & gymnosperm lineages, but are not present in *SAG101* lineages (Figure 2.3). Thus, suggesting a conserved function of PAD4^{R314} and PAD4^{K380} in angiosperm immunity, which is distinct from *SAG101* (Ke *et al.*, 2014). Future studies should determine which *SAG101* EP domain cavity residues contribute to *SAG101* signalling function, and whether the same sites as in PAD4 are required for *SAG101* signalling function.

Nearly all of the EDS1 and PAD4 EP domain cavity residues, which previously have been characterised to function in immunity, are positively charged (Figure 2.2&4; Bhandari *et al.*, 2019; Gantner *et al.*, 2019; Lapin *et al.*, 2019). This suggests that the EP domain cavity signalling-surface interacts with a negatively charged entity. Based on literature, NAD⁺-derived

molecules and the helper NLR family ADR1 are prime candidates for EDS1-PAD4 EP domain cavity interaction (Figure D.4) (Horsefield *et al.*, 2019; Lapin *et al.*, 2019; Wan *et al.*, 2019; Wu *et al.*, 2019). Future studies should determine if EDS1-PAD4 interacts with ADR1 and/or NAD⁺-derived compounds *in vitro*, and if such interaction leads to the formation of a higher-order complex (Figure D.4). Subsequently, one should obtain a crystal/cryo-EM structure to determine the precise stoichiometry of such EDS1-PAD4 complexes.

Although the suggested *in vitro* experiments above would yield insight in EDS1-PAD4 activation, this does not explain how the heterodimer induces transcriptional reprogramming in the nucleus. Recently, TNL *NbN* interactors were captured using TurboID coupled to nLC-MS/MS (Zhang *et al.*, 2019). This proximity-based labelling method allowed for the identification of *NbN* interactors during the first 12 hours of ETI signalling in Tobacco. Although my IP nLC-MS/MS on *AtPAD4* yielded several interesting interactors (Figure 3.2), these were all captured at one specific moment in time, thus only showed a snapshot of PAD4 interactors. Moreover, weak interactions can be washed away during IP sample preparation, while TurboID can capture those weak and transient interactions (Zhang *et al.*, 2019). Future studies should therefore focus on identifying interactors of EDS1, PAD4 and SAG101 during TNL-ETI by TurboID coupled to nLC-MS/MS. By comparing the common and unique interactors of these proteins, one can start to build EDS1-PAD4 and EDS1-SAG101 immune signalling pathways. To properly define these pathways, this would also require a thorough transcriptomic analysis that characterises the quantitative and qualitative differences between PAD4- and SAG101-dependent transcriptional reprogramming. By combining these transcriptomic and proteomic approaches, one can start to dissect which PAD4 and SAG101 signalling components contribute to quantitative and qualitative differences in PAD4- and SAG101-dependent transcriptional reprogramming pathways and ultimately resistance.

Figure D.4. Hypothetical model of EDS1-PAD4-ADR1 and EDS1-SAG101-NRG1 signalling in pathogen immunity. (See next page)

Upon infection by virulent *Pst avrRps4*, *avrRps4* and other effectors are secreted in to the plant cell. “Unrecognised” effectors trigger basal immunity, possibly through weak-NLR activation. RRS1-S/RPS4 recognises *avrRps4*, enzymatically active RPS4 TIR domain produces NAD⁺-derived compounds, which triggers ETI in and EDS1 dependent manner. NAD⁺-derived compounds possibly bind the EDS1-PAD4 and EDS1-SAG101 EP domain cavities (highlighted by a red circle), which could lead to the formation of an oligomer with ADR1 and NRG1, respectively. *Figure legend continues on next page.*

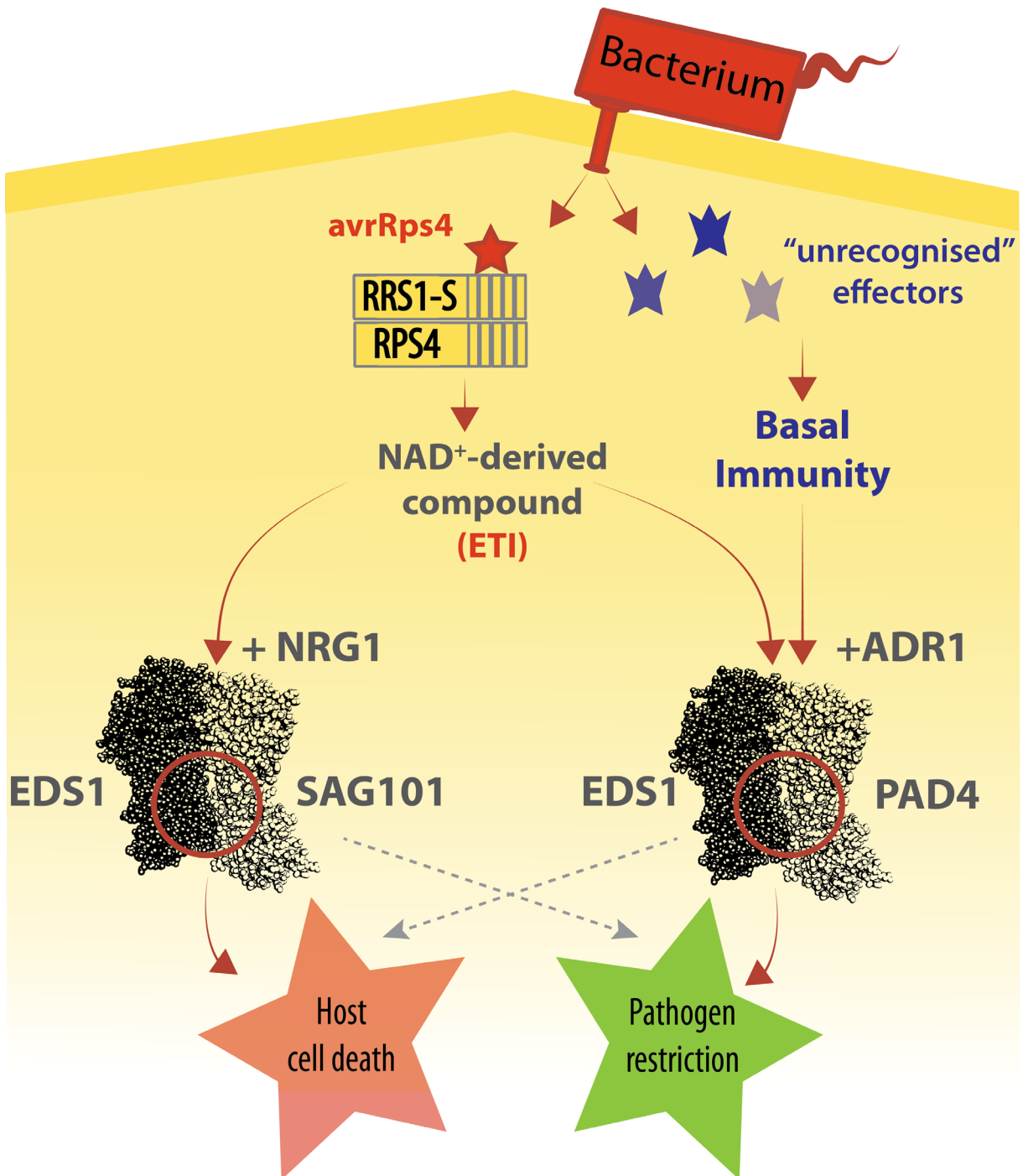


Figure D.4. Hypothetical model of EDS1-PAD4-ADR1 and EDS1-SAG101-NRG1 signalling in pathogen immunity (continued).

Alternatively, the ADR1 and NRG1 NB domains possibly bind NAD^+ -derived compounds, which might trigger a conformational change in ADR and NRG1 that would allow, respectively, EDS1-PAD4 and EDS1-SAG101 to bind and form an oligomer. EDS1-SAG101-NRG1 (mainly) induces host cell death. EDS1-PAD4-ADR1 is activated by basal immunity or through ETI, which then (mainly) induces the restriction of pathogen growth. Model is based on model proposed in Lapin *et al.* (2019).

Materials and Methods

Materials and methods are divided into two sections. The first section, “Materials” consists of a list of materials used in this work including plant lines, pathogen and bacterial strains, antibodies, chemicals, enzymes, media, etc. Experimental procedures and other experimental details are described in the second section “Methods.”

Materials

Plant Materials

The *Arabidopsis thaliana* lines used in this study are listed in Table 1.

Table 1 - *Arabidopsis thaliana* lines used in this work

Genotype	Accession	Reference
WT	Col-0	Dangl lab, University of North Carolina, NC, USA
<i>eds1-2</i>	Col-0/(Ler)*	Bartsch <i>et al.</i> 2006
<i>pad4-1</i>	Col-0	Glazebrook <i>et al.</i> , 1997
<i>pad4-1/sag101-3</i>	Col-0	Wagner <i>et al.</i> , 2013
<i>eds1-2/pad4-1/sag101-3</i>	Col-0	Wagner <i>et al.</i> , 2013
EDS1 ^{F419E} (<i>eds1-2</i>)	Col-0	Lapin <i>et al.</i> , 2019
<i>sgt1b (eta3)</i>	Col-0	Gray <i>et al.</i> , 2003
<i>sid2-1</i>	Col-0	Wildermuth <i>et al.</i> , 2001
<i>adr_3 (adr1-1/adr1-L1/adr1-L2-4)</i>	Col-0	Bonardi <i>et al.</i> , 2011
35S:StrepII-YFP	Col-0	Lapin <i>et al.</i> , 2019
<i>mes10-1</i> (GABI-KAT-050G01) <u>Primers</u> MES10: AC514+AC515; <i>mes10-1</i> : AC515+LN45	Col-0	NASC Stock Centre (N404777); Scholl <i>et al.</i> , 2000; Kleinboelting <i>et al.</i> , 2012
<i>mes10-2</i> (GABI-KAT-144B09) <u>Primers</u> MES10: AC514+AC515; <i>mes10-2</i> : AC514+LN45	Col-0	NASC Stock Centre (N413749); Scholl <i>et al.</i> , 2000; Kleinboelting <i>et al.</i> , 2012

<i>mes10-3</i> (SALK-099746) <u>Primers</u> MES10: AC516+AC517; <i>mes10-3</i> : AC516+LBb1.3	Col-0	NASC Stock Centre (N599746); Scholl <i>et al.</i> , 2000; Alonso <i>et al.</i> , 2003
<i>mes10-4</i> (SM-329219) <u>Primers</u> MES10: AC516+AC517; <i>mes10-3</i> : AC517+M149	Col-0	NASC Stock Centre (N115546); Scholl <i>et al.</i> , 2000; Tissier <i>et al.</i> , 1999

* *Ler eds1-2* allele introgressed into Col-0 background, 8th backcrossed generation, referred to as "*eds1-2*" in this work (Bartsch *et al.*, 2006).

For *Agrobacterium tumefaciens* dependent transient expression assays I used *Nicotiana benthamiana 310A* plants from the seed stock of MPIPZ, Cologne, GER.

Pathogen/Pest Strains

Throughout this work, *Hyaloperonospora arabidopsidis* (*Hpa*) EMWA1 was used as an avirulent filamentous biotrophic pathogen (Van der Biezen *et al.*, 2002; Asai *et al.*, 2018). *Pseudomonas syringae* pv. *tomato* DC3000 (*Pst*) was used as a virulent hemi-biotrophic pathogen strain. To generate *Pst avrRps4*, *Pst* was transformed with *pVSP61* carrying *avrRPS4*, an effector gene from *Pseudomonas syringae* pv. *pisi* (Hinsch *et al.* 1996). The coronatine deficient strain *Pst* DC3000 Δ *Cor* was obtained from Renier van der Hoorn (MPIPZ). To generate *Pst avrRPS4* Δ *Cor*, the *pVSP61-avrRPS4* plasmid was transformed into *Pst* Δ *Cor*.

For aphid fecundity/resistance, assays Green peach aphid (*Myzus persicae* Sülzer) was used (Specimen number 194 deposited with Kansas State University Museum of Entomological and Prairie Arthropod Research) (Nalam *et al.*, 2018.)

Bacterial Strains

An overview of bacteria used in this study is given in table 2.

Table 2 - Bacterial strains used in this work

Species	Strain	Genotype
E.coli	DB3.1	F- <i>gyrA462 endA</i> Δ (<i>sr1-recA</i>) <i>mcrB mrr hsdS20</i> (rB- mB-) <i>supE44 ara14 galK2</i> <i>lacY1 proA2 rpsL20</i> (StrR) <i>xyl5</i> λ - <i>leu mtl1</i>

E.coli	DH5 α	F- Φ 80 <i>lacZ</i> Δ M15 Δ (<i>lacZYA-argF</i>) U169 <i>deoR recA1 endA1 hsdR17</i> (rk -, mk+) <i>phoA supE44</i> λ - <i>thi-1 gyrA96 relA1</i>
E.coli	DH10b	F- <i>mcrA</i> Δ (<i>mrr-hsdRMS-mcrBC</i>) Φ 80 <i>lacZ</i> Δ M15 Δ <i>lacX74 deoR recA1 endA1 ara</i> Δ 139 Δ (<i>ara, leu</i>)7697 <i>galU galK</i> λ - <i>rpsL</i> (StrR) <i>nupG</i>
A. tumefaciens	GV3101	<i>pMP90 / PMP90RK</i> (Deak <i>et al.</i> 1986)

Antibiotics

Table 3 shows antibiotics used in this study. Aqueous stocks were sterile filtered before use.

Table 3 - Antibiotic stock solutions

Name	stock concentration (mg/ml)	working concentration (μ g/ml)	solved in
Ampicillin	100	100	ddH ₂ O
Carbenicillin	100	50	ddH ₂ O
Kanamycin	50	25	ddH ₂ O
Gentamycin	25	25 (<i>Pst</i>)/15 (<i>Agrobac.</i>)	ddH ₂ O
Rifampicin	40	100	DMSO
Spectinomycin	100	100	ddH ₂ O
Chloramphenicol	300	30	Ethanol

Antibodies

Antibodies used in this study are listed in table 4.

Table 4 - Antibodies

Antibody	Source	Dilution	Supplier	Group
α -flag	rabbit polyclonal	1:5000	Sigma-Aldrich	primary
α -GFP (rabbit)	rabbit monoclonal	1:5000	Cell Signalling Technology	primary
α -GFP (mouse)	mouse monoclonal	1:2500	Roche (Sigma-Aldrich)	primary
α -HA	rabbit monoclonal	1:5000	Cell Signalling Technology	primary

α-myc	rabbit monoclonal	1:5000	Cell Signalling Technology	primary
α-mouse IgG-HRP	goat polyclonal	1:5000	Sigma-Aldrich	secondary
α-rabbit IgG-HRP	goat polyclonal	1:5000	Sigma-Aldrich	secondary
α-mouse IgG-HRP	goat polyclonal	1:5000	Cell Signalling Technology	secondary

Chemicals

All chemicals met laboratory use purity and were obtained by various laboratory suppliers including Merck (Darmstadt, GER), Roth (Karlsruhe, GER), SERVA (Heidelberg, GER), Sigma-Aldrich (Hamburg, GER), ThermoFisher (MA, USA), and VWR (Langenfeld, GER).

Enzymes

Restriction Enzymes

For DNA digestion, restriction enzymes from either New England Biolabs (NEB, Frankfurt, GER) or ThermoFisher Scientific (MA, USA) were used according to the manufacturer's recommendations.

DNA Polymerases

Different DNA Polymerases were used according to cloning purpose and complexity. An overview is given in table 5.

Table 5 - DNA Polymerases used in this work

Name	Purpose	Supplier
Phire II	standard PCR	ThermoFisher
Pfu Polymerase	HF, proofreading for cloning	ThermoFisher
Phusion HF	HF, proofreading for cloning	ThermoFisher

Other enzymes

Other enzymes used include T4 DNA ligase (Roche), Alkaline phosphatase (Roche), RevertAid H Minus First Strand cDNA Synthesis kit (ThermoFisher), Gateway® pENTR™/D-TOPO™ Kit (ThermoFisher), Gateway® LR Clonase® II Enzyme Mix (ThermoFisher).

Oligonucleotides

Oligonucleotides and primers are shown in table 6. For regular oligo design primer3 (<http://bioinfo.ut.ee/primer3/>) was used while SDM primer were created by the primerX (<http://www.bioinformatics.org/primerx>). Oligonucleotides were ordered at Sigma-Aldrich (Hamburg, GER). Lyophilised primer were suspended in ddH₂O to 100 µM stock concentration and diluted 1:10 to reach a working concentration of 10 µM.

Table 6 - Oligonucleotides used in this work

Name	Description	Oligo Sequence(5' to 3')	Orientation	Purpose
DB136	PAD4_1- 300_STOP_F	CCTATTCTGAGGTAAGCTGAGTTAG CC	fw	cloning
DB137	PAD4_1- 300_STOP_R	GGCTAACTCAGCTTACCTCAGAATA GG	rv	cloning
DB138	PAD4_R314 A_F	GTCTTGCCAGCAgcACTCGAGATTC AATG	fw	cloning
DB139	PAD4_R314 A_R	CATTGAATCTCGAGTgcTGCTGGCA AGAC	rv	cloning
DB140	PAD4_L315 A_F	CTTGCCAGCAAGAgcCGAGATTCAA TGG	fw	cloning
DB141	PAD4_L315 A_R	CCATTGAATCTCGgcTCTTGCTGGCA AG	rv	cloning
DB142	PAD4_Q318 A_F	CAAGACTCGAGATTgcATGGTACAA AGATC	fw	cloning
DB143	PAD4_Q318 A_R	GATCTTTGTACCATgcAATCTCGAGT CTTG	rv	cloning
DB144	PAD4_W319 A_F	CTCGAGATTCAAgcGTACAAAGATC GTTG	fw	cloning
DB145	PAD4_W319 A_R	CAACGATCTTTGTACgcTTGAATCTC GAG	rv	cloning

DB146	PAD4_K380 A_F	CATTAGGAAAGgcATGGATTTACG C	fw	cloning
DB147	PAD4_K380 A_R	GCGTAAATCCATgcCTTTCCTAAATG	rv	cloning
DB148	PAD4_I286A _F	GTCAAAGAATGTgcAGAAACAGCTA C	fw	cloning
DB149	PAD4_I286A _R	GTAGCTGTTTCTgcACATTCTTTGAC	rv	cloning
DB150	PAD4_Y383 A_F	GAAAGAAATGGATTgcCGCATCTCA ATT	fw	cloning
DB151	PAD4_Y383 A_R	AATTGAGATGCGgcAATCCATTTCTT TC	rv	cloning
DB152	PAD4_W381 A_F	TTTAGGAAAGAAAgcGATTTACGCA TCTC	fw	cloning
DB153	PAD4_W381 A_R	GAGATGCGTAAATCgcTTTCTTTCCT AAA	rv	cloning
DB154	PAD4_F375 A_F	GTTACCTTTTGATgcTCATTTAGGAA AG	fw	cloning
DB155	PAD4_F375 A_R	CTTTCCTAAATGAgcATCAAAAGGT AAC	rv	cloning
DB156	PAD4_R165 A_F	CAATTTACGATCAgcTTTAGCACAC AAC	fw	cloning
DB157	PAD4_R165 A_R	GTTGTGTGCTAAAgcTGATCGTGAA ATTG	rv	cloning
DB158	PAD4_F387 A_F	CGCATCTCAAgcTTATCAACTCTTAG	fw	cloning
DB159	PAD4_F387 A_R	CTAAGAGTTGATAAgcTTGAGATGC G	rv	cloning
DB160	PAD4_L307 A_F	GTTAGCCAATGAGgcTGCTAGTGTCT TG	fw	cloning
DB161	PAD4_L307 A_R	CAAGACACTAGCAgcCTCATTGGCT AAC	rv	cloning
DB162	PAD4_L311 A_F	GCTTGCTAGTGTCgcGCCAGCAAGA CTC	fw	cloning
DB163	PAD4_L311 A_R	GAGTCTTGCTGGCgcGACACTAGCA AGC	rv	cloning

JAD009	PAD4_1- L331_STOP_ F	GAAGAGCAGCTA ^{taa} GGTTACTACGA T	fw	cloning
JAD010	PAD4_1- L331_STOP_ R	ATCGTAGTAAC ^{tta} TAGCTGCTCTTC	rv	cloning
JAD011	PAD4_1- T408_STOP_ F	GATATAAAGACT ^{taa} GGCGGGCATT C	fw	cloning
JAD012	PAD4_1- T408_STOP_ R	GTAATGCCCGCC ^{tta} AGTCTTTATATC	rv	cloning
JAD013	PAD4_1- S470_STOP_ F	GAAAAGAGAGT ^{taa} AGTGATCCCCA G	fw	cloning
JAD014	PAD4_1- S470_STOP_ R	CTGGGGATCACT ^{tta} ACTCTCTTTTC	rv	cloning
JAD015	SAG101_1- S303_STOP_ F	CATGAAGATATCG ^{taa} ATGGCTTATA TA	fw	cloning
JAD016	SAG101_1- S303_STOP_ R	TATATAAGCCAT ^{tta} CGATATCTTCAT G	rv	cloning
JAD017	SAG101_1- I319_STOP_ F	GAGGTCAAGATC ^{taa} GGTTACTACGA T	fw	cloning
JAD018	SAG101_1- I319_STOP_ R	ATCGTAGTAAC ^{tta} GATCTTGACCTC	rv	cloning
JAD019	SAG101_1- R398_STOP_ F	GAGGGTCGG ^{taa} AAAGAGTATCG	fw	cloning
JAD020	SAG101_1- R398_STOP_ R	CGATACTCTTT ^{tta} CCGACCCTC	rv	cloning

JAD021	SAG101_1- G463_STOP_ F	CAACTGTGGGGtaaATGAGAGACG	fw	cloning
JAD022	SAG101_1- G463_STOP_ R	CGTCTCTCATttaCCCCACAGTTG	rv	cloning
JAD025	PAD4_L307 E_F	GTTAGCCAATGAGgaaGCTAGTGTCT TG	fw	cloning
JAD026	PAD4_L307 E_R	CAAGACACTAGCttcCTCATTGGCTA AC	rv	cloning
JAD037	gPAD4_I_F	ATGCCAAGTTTGTACAAAAAAGCA GGCTTCaattagggtttatcagattaaagagatttact gatttcaatc	fw	cloning
JAD038	gPAD4_I_R	GCCCACTTTGTACAAGAAAGCTGGG TCCTAatctctctcgctcttcttagtctatcggaatac	rv	cloning
FA19	pDONR201 PIPE-PCR	TAGGACCCAGCTTTTCTGTACAAAG TGG	fw	cloning
FA20	pDONR201 PIPE-PCR	GAAGCCTGCTTTTTTGTACAAACTT GGC	rev	cloning
JAD039	YFP-NLS- gPAD4_I_F	gttctgcaactcttactcgatatccaatcATGGTGA GCAAGGGCGAGGAGC	fw	cloning
JAD040	YFP-NLS- gPAD4_I_R	TCCTCCAACCTTTCTCTTCTTCTTAG GAGCCGCAGCAGCGGCAGCCGCTG CCGCGCCCTTGTACAGCTCGTCCAT GCCG	rv	cloning
JAD041	YFP-NLS- gPAD4_V_F	GCTCCTAAGAAGAAGAGAAAGGTT GGAGGAATGGACGATTGTTCGATTC GAGAC	fw	cloning
JAD042	YFP-NLS- gPAD4_V_R	GGTGAACAGCTCCTCGCCCTTGCTC ACCATgattggatcagtagagagttgcagaac	rv	cloning
JAD043	YFP- gPAD4_I_R	AGCCGCAGCAGCGGCAGCCGCTGC CGCGCCCTTGTACAGCTCGTCCATG CCG	rv	cloning
JAD044	YFP- gPAD4_V_F	GGCGCGGCAGCGGCTGCCGCTGCT GCGGCTATGGACGATTGTTCGATTTCG AGAC	fw	cloning

JAD061	YFP-nls- gPAD4_I_R	TCCTCCAACCTTTCTCTTCgTCTTAG GAGCCGCAGCAGCGGCAGCCGCTG CCGCGCCCTTGTACAGCTCGTCCAT GCCG	rv	cloning
JAD062	YFP-nls- gPAD4_V_F	GCTCCTAAGAcGAAGAGAAAGGTTG GAGGAATGGACGATTGTCTGATTCTG AGAC	fw	cloning
JAD063	YFP-NES- gPAD4_I_R	AATATCAAGTCCAGCCA ACTTAAGA GCAAGAGCCGCAGCAGCGGCAGCC GCTGCCGCGCCCTTGTACAGCTCGT CCATGCCG	rev	cloning
JAD064	YFP-NES- gPAD4_V_F	GCTCTTGCTCTTAAGTTGGCTGGAC TTGATATTATGGACGATTGTCTGATT CGAGAC	rw	cloning
JAD065	YFP-nes- gPAD4_I_R	AgcATCAgcTCCAGCCgcCTTAAGAGC AAGAGCCGCAGCAGCGGCAGCCGC TGCCGCGCCCTTGTACAGCTCGTCC ATGCCG	rev	cloning
JAD066	YFP-nes- gPAD4_V_F	GCTCTTGCTCTTAAGgcGGCTGGAgc TGATgcTATGGACGATTGTCTGATTCTG AGAC	fw	cloning
JAD067	Vector_FW_ R314A	AATGAGCTTGCTAGTGTCTTGCCAG CAGCACTCGAGATTCAATGGTACAA AGATCGTTG	fw	cloning
JAD068	Insert_REV_ R314A	ACGATCTTTGTACCATTGAATCTCG AGTGCTGCTGGCAAGACACTAGCA AGCTC	rev	cloning
JAD069	Vector_FW_ K380A	TTACCTTTTGATTTTCATTTAGGAAA GGCATGGATTTACGCATCTCAATTT TATCAACTCTTAG	fw	cloning
JAD070	Insert_REV_ K380A	TTGATAAAATTGAGATGCGTAAATC CATGCCTTTCCTAAATGAAAATCAA AAGGTA ACTCATTCG	rev	cloning
JAD071	PAD4_H229 A_fw	CAAAATACCGAGGAAgcTCAGAGGT ACGGAC	fw	cloning
JAD072	PAD4_H229 A_rev	GTCCGTACCTCTGAgcTTCCTCGGTA TTTTG	rev	cloning

JAD073	PAD4_D178 A_fw	GTCTCCATCCACGcCCTCGTTCCTAG AAG	fw	cloning
JAD074	PAD4_D178 A_rev	CTTCTAGGAACGAGGgCGTGGATGG AGAC	rev	cloning
JAD091	Vector_FW_ S118A	GGTAAAAAGCTGGTGGTGATAACC GGCCATGCAACCGGCGGCATTG GCCGCTTTC	fw	cloning
JAD092	Insert_REV_ S118A	TGCGGTGAAAGCGGCCAATGCGCC GCCGGTTGCATGGCCGGTTATCACC ACCAGCTT	rv	cloning
JAD093	Vector_FW_ 1-300stop	ACAAGAATTGTTTCGGGCTCCTATTC TGAGGTAAGCTGAGTTAGCCAATG AGCTTGCTAG	fw	cloning
JAD094	Insert_REV_ 1-300stop	GACACTAGCAAGCTCATTGGCTAAC TCAGCTTACCTCAGAATAGGAGCCC GAACAATTCT	rv	cloning
JAD095	Vector_FW_ R314I	AATGAGCTTGCTAGTGTCTTGCCAG CAattCTCGAGATTCAATGGTACAAA GATCGTTG	fw	cloning
JAD096	Insert_REV_ R314I	CAACGATCTTTGTACCATTGAATCT CGAGaatTGCTGGCAAGACACTAGCA AGCTCATT	rv	cloning
JAD097	Vector_FW_ R314K	AATGAGCTTGCTAGTGTCTTGCCAG CAaaaCTCGAGATTCAATGGTACAAA GATCGTTG	fw	cloning
JAD098	Insert_REV_ R314K	ACGATCTTTGTACCATTGAATCTCG AGtttTGCTGGCAAGACACTAGCAAG CTC	rv	cloning
JAD099	Vector_FW_ K380R	TTACCTTTTGATTTTCATTTAGGAAA GagaTGGATTTACGCATCTCAATTTT ATCAACTCTTAG	fw	cloning
JAD100	Insert_REV_ K380R	TTGATAAAATTGAGATGCGTAAATC CAtctCTTTCCTAAATGAAAATCAAA AGGTAACTCATTCG	rv	cloning

JAD101	Vector_FW_ R314M	AATGAGCTTGCTAGTGTCTTGCCAG CAatgCTCGAGATTCAATGGTACAAA GATCGTTG	fw	cloning
JAD102	Insert_REV_ R314M	CAACGATCTTTGTACCATTGAATCT CGAGcatTGCTGGCAAGACACTAGCA AGCTCATT	rv	cloning
JAD103	SAG101_R37 3K_fw	GATGCATCGATTCTCAAGAGAgcaTT TCTATTCTCGGGGAACAA	fw	cloning
JAD104	SAG101_R37 3K_rev	TTGTTCCCCGAGAATAGAAAAtgcTCT CTTGAGAATCGATGCATC	rv	cloning
JAD105	SAG101_R37 3A_fw	GATGCATCGATTCTCAAGAGAAAAaTT TCTATTCTCGGGGAACAA	fw	cloning
JAD106	SAG101_R37 3A_rev	TTGTTCCCCGAGAATAGAAAAtttTCTC TTGAGAATCGATGCATC	rv	cloning
JP Stock	ACT2	ATGGAAGCTGCTGGAATCCAC	fw	qRT-PCR
JP Stock	ACT2	TTGCTCATACGGTCAGCGATA	rv	qRT-PCR
JP Stock	qPAD4_F	GGTCTGTTCGTCTGATGTTT	fw	qRT-PCR
JP Stock	qPAD4_R	GTTCCCTCGGTGTTTTGAGTT	rev	qRT-PCR
JP Stock	qEDS1_F	CGAAGACACAGGGCCGTA	fw	qRT-PCR
JP Stock	qEDS1_R	AAGCATGATCCGCACTCG	rev	qRT-PCR
JP Stock	qPBS3_F	ACACCAGCCCTGATGAAGTC	fw	qRT-PCR
JP Stock	qPBS3_R	CCCAAGTCTGTGACCCAGTT	rev	qRT-PCR
JP Stock	qICS1_F	TTCTGGGCTCAAACACTAAAAC	fw	qRT-PCR
JP Stock	qICS1_R	GGCGTCTTGAAATCTCCATC	rev	qRT-PCR
JP Stock	qFMO1_F	GTTCGTGGTTGTGTGTACCG	fw	qRT-PCR
JP Stock	qFMO1_R	TGTGCAAGCTTTTCCTCCTT	rev	qRT-PCR
JP Stock	qPR1_F	TTCTTCCTCGAAAGCTCAA	fw	qRT-PCR
JP Stock	qPR1_R	AAGGCCACCAGAGTGTATG	rev	qRT-PCR
JP Stock	qALD1_F	TGGCCTTAAGGAGATACGGT	fw	qRT-PCR
JP Stock	qALD1_R	ACCTGAGCCTGGTACTGTTA	rev	qRT-PCR
JP Stock	pad4-1_F (PAD4 Bsmfl sensitive)	GCGATGCATCAGAAGAG	fw	Genotyping
JP Stock	pad4-1_R (PAD4 Bsmfl sensitive)	TTAGCCCCAAAAGCAAGTATC	rev	Genotyping

JP Stock	SAG101_F	GCGGCCTCCTCTCTACTTCT	fw	Genotyping
JP Stock	SAG101_R	CTTCTTGAAACCATCGAACC	rev	Genotyping
JP Stock	sag101-3_F (GABI-KAT)	ATATTGACCATCATACTCATTGC	fw	Genotyping
JP Stock	sag101-3_R	TTGTGACTTACCATAACTCTCG	fev	Genotyping
JP Stock	EDS1_F	ACACAAGGGTGATGCGAGACA	fw	Genotyping
JP Stock	eds1-2_F	CAAACGTCAAGAGAGCTGAG	fw	Genotyping
JP Stock	eds1- 2/EDS1_R	GTGGAAACCAAATTTGACATTAG	rev	Genotyping
MS4	<i>sid2-1</i> (ICS1_ MunI sensitive)	GCAGTCCGAAAGACGACCTCGAG		Genotyping
MS5	<i>sid2-1</i> (ICS1_ MunI sensitive)	CTATCGAATGATTCTAGAAGAAGC		Genotyping
Y226	sgt1b_eta3 (SGT1b AluI sensitive)	aggatgagaagcttgatggagatgcacc	fw	Genotyping
Y227	dC_eta3 (SGT1b AluI sensitive)	cgcccattcgactctgctgtcaaagc	rev	Genotyping
DL483	adr1 (SAIL_842_ B05)	CTCAACAGCCAGATTTTGCTC	fw	Genotyping
DL484	adr1 (SAIL_842_ B05)	TCCTCGTCAATATCATGCCTC	rev	Genotyping
DL485	adr1-L1 (SAIL_302_ C06)	CGTGCTTGTTGCTTTAGGAAG	fw	Genotyping
DL486	adr1-L1 (SAIL_302_ C06)	AAGTTCCTCAGCTCCTCAAG	rev	Genotyping
DL487	adr1-L2-4 (SALK_1264 22)	ATTCGCTCCGACTCTAAAG	fw	Genotyping

DL488	adr1-L2-4 (SALK_1264 22)'	ATCGGTTGTCACCATCTCAAC	rev	Genotyping
AC514	mes10-1/- 2_LP	TGGTCCATTTTAAATGGCTTTAG	fw	Genotyping
AC515	mes10-1/- 2_RP	GGGTGTTCTAATCCTTCCTCG	rev	Genotyping
AC516	mes10-3/- 4_LP	GACTCGAAAAAGTTGCAATGG	fw	Genotyping
AC517	mes10-3/- 4_RP	TCAGGGCACATAGTTTTCTGG	rev	Genotyping
M160 (dSpm11)	For SAIL lines	GCCTTTTCAGAAATGGATAAATAGC CTTGCTTCC	-	Genotyping
LBb1.3	For SALK lines	ATTTTGCCGATTTTCGGAAC	-	Genotyping
M149	For SM lines	GGTGCAGCAAAACCCACACTTTTAC TTC	-	Genotyping
LN45	For GABI- KAT (GK) lines	ATATTGACCATCATACTCATTGC	-	Genotyping

Vectors

Vectors used or generated in this work are listed in table 7.

Table 7 - Vectors

Vector	Notes
pDONR201	Gateway® donor vector used for taking up DNA fragments for cloning
pDONR207	Gateway® donor vector used for taking up DNA fragments for cloning
pENTRy D-PAD4	Gateway® entry plasmid that contains CDS of PAD4 with stop codon from <i>Ler</i> (Wagner <i>et al.</i> , 2013)
pENTR-PAD4 no stop	Gateway® entry plasmid that contains CDS of PAD4 without stop codon from <i>Ler</i> (Wagner <i>et al.</i> , 2013)
pENTR/D-SAG101	Gateway® entry plasmid that contains CDS of SAG101 with stop codon from <i>Ler</i> (Wagner <i>et al.</i> , 2013)
pENTR/D-SGT1b no stop	Gateway® entry plasmid that contains CDS of SGT1b without stop codon (Witte <i>et al.</i> , 2004)

pDONR207-TPR1	Gateway® entry plasmid that contains CDS of TPR1 with stop codon, made by reverse BP reaction (Zhu <i>et al.</i> , 2010)
p-D1	Binary Gateway® destination vector for expression of a fusion protein under control of PAD4 native promoter with an N-terminal StrepII (Witte <i>et al.</i> , 2004) and YFP tag (Bhandari <i>et al.</i> , 2019)
pENSG-smGFP-GW (NME10)	Binary Gateway® destination vector for expression of a fusion protein under control of 35S promoter with an N-terminal smGFP tag
pAlligator2 (pAL2)	Binary Gateway® destination vector for Agrobacterium mediated transformation (Bensmihen <i>et al.</i> , 2004); used for genomic PAD4 clones
pAL2- Genomic PAD4	Binary Gateway® destination vector (pAlligator2) for expression of PAD4 under control of its native promoter with an N-terminal YFP tag and as a Linker Gly-9x-Ala, including UTRs, introns and up- and downstream intergenic regions. NLS/NES/nls/nes (Garcia <i>et al.</i> , 2010; Stuttmann <i>et al.</i> , 2016) tag were placed in between linker and PAD4 start codon
pXCPEDS1gEDS1-3xFLAG	Binary Gateway® destination vector for expression of genomic EDS1 under control of native EDS1 promoter with a C-terminal 3x FLAG tag
pXCPEDS1gEDS1 LLIF-3xFLAG	Binary Gateway® destination vector for expression of genomic EDS1 under control of native EDS1 promoter with a C-terminal 3x FLAG tag
pJ2B-3xFLAG-EDS1 1-384	Binary Gateway® destination vector for expression of EDS1 under control of 35S promoter with an N-terminal 3x FLAG tag (Wagner <i>et al.</i> , 2013)
pDEST-NLUC-GW	Binary Gateway® destination vector for expression of a fusion protein under control of 35S promoter with an N-terminal ^N LUC tag (Gehl <i>et al.</i> , 2011)
pDEST-CLUC-GW	Binary Gateway® destination vector for expression of a fusion protein under control of 35S promoter with an N-terminal ^C LUC tag (Gehl <i>et al.</i> , 2011)
pDEST-GW-NLUC	Binary Gateway® destination vector for expression of a fusion protein under control of 35S promoter with a C-terminal ^N LUC tag (Gehl <i>et al.</i> , 2011)
pDEST- GW-CLUC	Binary Gateway® destination vector for expression of a fusion protein under control of 35S promoter with a C-terminal ^C LUC tag (Gehl <i>et al.</i> , 2011)
pXCSG-GFP	Binary Gateway® destination vector for expression of GFP under control of 35S promoter tagged with a C-terminal StrepII tag
pENS-EDS1-SH	Binary Gateway® destination vector for expression of EDS11 under control of 35S promoter with an C-terminal StrepII-3xHA tag

Media

All media were sterilised by autoclaving at 121 °C for 20 min. Heat sensitive additives such as antibiotics were added once the media cooled down to approximately 50 °C.

Agrobacterium tumefaciens media

YEB

Beef extract 5.0 g/L	1M MgSO ₄ 2.0 ml/l
Yeast extract 1.0 g/l	pH 7.2
Peptone 5.0 g/l	For YEB agar plates:
Sucrose 5.0 g/l	1.5 % (w/v) agar

Escherichia coli media

LB (Luria-Bertani) broth

Tryptone 10.0 g/l	pH 7.0
Yeast extract 5.0 g/l	For LB agar plates:
NaCl 5.0 g/l	1.5 % (w/v) agar

Pseudomonas syringae media

NYG broth

Peptone 5.0 g /l	pH 7.0
Yeast extract 3.0 g/l	For NYG agar (NYGA) plates:
Glycerol 20 ml/l	1.5 % (w/v) agar

Buffers and Solutions

Buffers and their components used in this thesis are summarised in table 8.

Table 8 - Buffers and Components

Application	Buffer	Components
Plant DNA extraction	DNA extraction buffer	200 mM Tris pH 7.5, 250 mM NaCl, 25 mM EDTA pH 7.5, 0.5 % SDS
Fast plant DNA extraction	Sucrose DNA extraction buffer	50 mM Tris pH 7.5, 300 mM NaCl, 300 mM sucrose
DNA solvent solution	TE Buffer	10 mM Tris-HCl, pH 8.0, 1 mM EDTA
PCR clean-up	PEG 8000 solution	30% PEG 8000, 30 mM MgCl ₂
DNA electrophoresis	10x TAE running buffer	0.4 M Tris, 0.2 M acetic acid, 10 mM EDTA, pH 8.5
	6x DNA loading buffer	40 % (w/v) sucrose, 0.5 M EDTA, 0.2 % (w/v) bromophenol blue
	DNA ladder	10 % (v/v) 6× loading buffer, 5 % (v/v) 1 kb DNA ladder (ThermoFisher)
SDS-PAGE	10x Tris-glycine running buffer	250 mM Tris, 1.92 M glycine, 1 % (w/v) SDS
	2x SDS sample buffer (Lämmli buffer)	60 mM Tris pH 6.8, 4 % (w/v) SDS, 200 mM DTT, 20 % (v/v) glycerol, 0.2 % (w/v) bromophenol blue
Immunoblotting	TBS (T) buffer	10 mM Tris pH 7.5, 150 mM NaCl, (0.1 % (v/v) Tween 20)
	10x transfer buffer	250 mM Tris pH 9.2, 1.92 M glycine, 1 % (w/v) SDS, 20 % (v/v) Methanol
	Ponceau S	Dilution of ATX Ponceau concentrate (Fluka) 1:5 in ddH ₂ O

Protein extraction	Extraction buffer	50 mM Tris pH7.5, 150 mM NaCl, 10 % (v/v) Glycerol, 2 mM EDTA, 5 mM DTT, Protease inhibitor (Roche, 1 tablet per 50 mL), 0.1 % Triton
Wash buffer: co-IP	Co-IP wash buffer	50 mM Tris pH7.5, 150 mM NaCl, 10 % (v/v) Glycerol, 2 mM EDTA, 5 mM DTT, 0.1 % Triton
Wash buffer: IP for mass spectrometry	IP-MS wash buffer	20 mM Tris pH7.5, 150 mM NaCl, 10 % (v/v) Glycerol, 2 mM EDTA
<i>N. benthamiana</i> transient expression	infiltration solution	10 mM MES, 10 mM MgCl ₂ , pH5.6, 0.15 mM acetosyringone
<i>Pst</i> infection (syringe infiltration)	infiltration solution	10 mM MgCl ₂
<i>Pst</i> infection (vacuum infiltration)	infiltration solution	10 mM MgCl ₂ , 0.005 % Silwet-77
<i>Pst</i> leaf extraction	extraction solution	10 mM MgCl ₂ , 0.01 % Silwet-77

Methods

Plant methods

Maintenance and propagation of *Arabidopsis thaliana* plants

All *Arabidopsis* plants were grown on potting soil supplemented with 10 mg/l Confidor® WG 70 (Bayer, GER). For synchronous germination, *Arabidopsis* seeds were imbibed in water, or sown on moist soil prior to stratification in the dark for 48 h at 4 °C. Pots were covered with a propagator lid and placed in growth chambers set to the following conditions: 10 h light, 14 h dark, 100-150 $\mu\text{mol m}^{-2} \text{s}^{-1}$, 22 °C, 65 % humidity. For short generation time and crossings, I used speed-breeding settings, *i.e.* 22 h light, 2 h dark, 100-150 $\mu\text{mol m}^{-2} \text{s}^{-1}$, 22 °C, 65 % humidity. Propagator lids were removed seven days after placing the seeds to light. To collect seeds, mature inflorescences were wrapped in a breathable plastic/paper bag and harvested once the plants had dried out completely.

***Agrobacterium tumefaciens* mediated stable transformation of Arabidopsis**

Arabidopsis plants were transformed using a simplified method (Logemann *et al.*, 2006) of floral dip (Clough & Bent, 1998). After bolting, Arabidopsis inflorescences were cut once to increase the number of inflorescences. After axillary meristems produced multiple inflorescences, plants were dipped in 5 % sucrose, 0.01 % Silwet L-77 solution containing *A. tumefaciens* (OD₆₀₀ = 1.0-1.5). Inflorescences were submerged for 45 sec with gentle agitation and covered in plastic bags for 24 h without direct exposure to light. After this, plastic bags were removed and plants were transferred to the greenhouse to set seed.

Agrobacterium tumefaciens* mediated transient expression assays in *N. benthamiana

N. benthamiana plants were grown for 4-6 weeks in the greenhouse in the following conditions: 16 h light, 8 h dark and ~24 °C. Non-flowering and healthy plants were transferred to the lab for infiltration with *A. tumefaciens* (OD₆₀₀ = 0.2-0.6; depending on the expression efficiency of the plasmid). Bacteria were grown for 2-3 days on YEB agar plates with their respective antibiotics, dissolved in infiltration solution, and hand infiltrated using a needle-less syringe. Per plant, two mature leaves were selected and infiltrated on the abaxial side of the leaf directly, or by first making a hole in the leaf with a needle. Samples were taken 2-3 days post-infiltration, snap frozen in liquid nitrogen, and stored at -80 °C waiting for downstream application.

Crossing of Arabidopsis plants

Arabidopsis plants were grown until inflorescence emergence, to cross genetically defined backgrounds. Young flowers with fully developed stigmata, but immature anthers, were emasculated and received donor pollen by applying donor stamen onto each stigma. Cross-pollinated stigmata were kept away from other flowers by wrapping the flower in paper bags and were kept in there to collect the seeds. Progeny was analysed for the presence of the desired allele(s) by PCR, genotyping by sequencing, seed coat fluorescence and/or BASTA resistance.

***Pseudomonas* pathogen growth assays in Arabidopsis**

Pst DC3000 or *Pst* DC3000 with *avrRps4* (in pV316-1a; *Pst avrRps4*) were syringe-infiltrated into leaves at OD₆₀₀=0.0005 in 10 mM MgCl₂. After infiltration, lids were kept on trays for 3 h. Bacteria were isolated at 0 dpi (3 hpi) from 4 to 6 leaf discs (6 mm diameter) making 2-3 technical replicates and at 3 dpi from 12 leaf discs (6 mm diameter) distributed over 4 technical replicates). Dilutions were plated onto NYGA plates supplemented with rifampicin 100 mg/l, and kept overnight at 28°C and at RT for the subsequent night. For statistical analysis, bacterial titre from independent experiments (biological replicates) were combined. Normality of residuals distribution and homoscedasticity was checked visually (by Q-Q plot) and with formal

Shapiro-Wilcoxon test ($\alpha=0.05$). Collected titre data were considered suitable for ANOVA and Tukey's HSD test.

Hyaloperonospora arabidopsidis (Hpa) EMWA1 infection assays

Arabidopsis seedlings were grown on Jiffy pots potting soil as discussed in "Maintenance and propagation of Arabidopsis thaliana plants." After 16-21 days, plants were sprayed with *Hpa* EMWA1 by spray inoculation (40 conidiospores/ μ l dH₂O) as described in Stuttmann *et al.* (2011). *Hpa* colonisation was determined at 4-6 dpi post spray depending on the disease progression on the susceptible control plants, *i.e.* *pad4-1*, *pad4-1/sag101-3*, and/or *eds1-2*. For macroscopic phenotypes, leaves were photographed using a Canon EOS D mirror-reflex camera with a Macro lens. For microscopic phenotypes leaves were stained with lactophenol Trypan blue (TB) (Koch & Slusarenko, 1990; Muskett *et al.*, 2002) by boiling leaves for 1 min in TB solution (1:1 diluted with 100% ethanol) and destaining with chloral hydrate (2.5g/ml dH₂O) for >24 hours. *Hpa* colonisation, hypersensitive response and trailing necrosis (disease phenotypes) were documented using a Zeiss Axio Imager microscope. Oomycete fitness was quantified by counting conidiospores on leaves. In statistical analysis, counts were normalized per mg of fresh weight (average of 2 counts per data point/technical replicate) and these counts from independent experiments (biological replicates) were combined. Significance of difference in spore counts was assessed by ANOVA and Tukey's HSD test.

Aphid no-choice bioassay

Monika Patel & Lani Archer performed aphid assays in the lab of Prof. Dr. J. Shah at the University of North Texas (USA). For each biological replicate five one-day-old nymphs were released onto the centre of a 17-day-old plant. The total number of aphids (adult + nymphs) per biological replicate were counted 11 days post-infestation. Each independent experimental replicate consisted of 10 biological replicates per genotype (Nalam *et al.*, 2018).

Bacterial methods

Escherichia coli

E. coli laboratory strains were grown at 37 °C in LB medium supplemented with their respective antibiotic to ensure plasmid maintenance. Transformation of chemically competent *E. coli* cells was performed by thawing 50 μ l of competent cells on ice and incubating 2 - 50 ng of plasmid for 5-10 min on ice. The mixture was heat-shocked for 1 min in a thermo-mixer set to 37-42 °C, after which samples were transferred to ice for 2 min. 500 μ l LB medium was added to the

mixture and were subsequently incubated at 37 °C (200-700 rpm) for ~1 h to allow expression of the resistance cassette. Generally, only 10% of the reaction mixture was plated on selective LB media plates, in case of an anticipated high cloning and/or transformation efficiency. For cases with low efficiency cloning/transformation, cells were pelleted (21000 x g, 1 min), its supernatant discarded, pellet resuspended remaining supernatant (in ~50 µl) and then plated.

Agrobacterium tumefaciens

A. tumefaciens cells were grown in liquid or solid YEB or LB medium with respective antibiotic resistance at 28 °C for 2-3 days. *A. tumefaciens* cells were transformed via electroporation. Electro-competent cells were thawed on ice and were incubated with 10-80 ng plasmid DNA for 10 min on ice before being transferred to a precooled electroporation cuvette (1 mm, Eurogentec, BE). The BioRad Gene Pulser Xcell™ was used for electroporation with the following settings: 25 µF, 2.5 kV, 5 ms, and 400 Ω. Immediately after pulsing, cells were mixed in 500 µl LB medium and incubated at 28 °C, 200-700 rpm for 2 h to allow for the expression of the resistance cassette. To obtain single colonies, 50 µl of cells were plated on selective LB media plates. For *Nicotiana benthamiana* infiltration *Agrobacteria* were grown on YEB plates overnight and resuspended in infiltration medium with an adjusted OD₆₀₀ = 0.2 - 0.6. A needleless syringe was used to infiltrate the abaxial side of mature leaves.

Pseudomonas syringae

P. syringae strains were grown on selective NYGA plates at 28 °C for 2 days. Stock plates were kept for a maximum of 3 weeks at 4 °C before being re-streaked from the -80 °C stock. Before each infection experiments, bacteria were streaked on fresh selective NYGA plates and grown overnight. Bacteria were suspended in infiltration medium, and the abaxial leaf side was subsequently infiltrated using a needleless syringae. Pathological infection assays were performed by infiltrating *Pst* with an OD₆₀₀ = 0.0005 and samples were taken at 3 hpi (day 0) or 3 dpi. For qRT-PCR, confocal microscopy and determining protein levels plants were infiltrated with *Pst* with an OD₆₀₀ = 0.005. For nLC-MS/MS analysis bacterial OD₆₀₀ was adjusted to 0.1 and bacteria were dissolved in vacuum-infiltration solution (10mM MgCl₂; 0.005% Silwet-77) samples were taken at 4 and 6 hpi. After infiltration, plants were covered with a propagator lid for 6 h to ensure high humidity. In general, plants were always infiltrated between 9 to 12 a.m. to avoid the circadian clock creating distortion in the data.

Biochemical methods

Total protein extraction for immunoblot analysis

Plant tissue was collected and snap frozen in liquid nitrogen, followed by homogenisation with the Qiagen TissueLyser II (Qiagen, Hilden, GER). Per sample, 50 - 100 μ l Lämmli Buffer was added to the sample, vortexed, boiled at 95 °C for 10 min, and centrifuged at 21 000 x g at RT for 1 min. Supernatant was used for immunoblot analysis and was stored at -20 °C.

Immunoprecipitation of transiently expressed protein

For immunoprecipitation of proteins expressed in *N. benthamiana* leaves, 4-8 leaf discs (7 mm diameter, depending on expected protein accumulation) were sampled and homogenised using a Qiagen TissueLyser II (Qiagen, Hilden, GER). Samples were resuspended in 1.5 mL protein extraction buffer and were incubated on ice for 5 min with interspersed vortexing before being centrifuged for 20 min, 4 °C, 21 000 x g. 50 μ l supernatant was taken as input sample. For immunoprecipitation, 3 mL co-IP wash buffer and 10 μ l of GFP-Trap beads/ Magnetic Agarose (MA) GFP-Trap (Chromotek, Martinsried, GER) or ANTI-FLAG® M1 Gel (Sigma-Aldrich) were added to the supernatant and gently mixed on a rotating mixer for 2.5 h at 4 °C. After incubation, beads were spun down at 2500 x g at 4 °C for 2 min, or incubated for 1 min in a magnetic rack, and washed 4 times with 1 ml co-IP wash buffer. To elute the protein, 100 μ l of Lämmli buffer was added to the beads and heated to 96 °C for 10 min with 3 vortex steps. Finally, the eluted beads were collected at the bottom by centrifugation (21 000 x g, 4 °C, 1 min) and supernatant was used for immunoblot analysis and stored at -20 °C.

SDS-polyacrylamide gel electrophoresis (SDS-PAGE)

Proteins were separated based on their size using the Mini-PROTEAN 3 SDS-PAGE system (BioRad). Samples were boiled in Lämmli buffer at 95 °C for 10 min to extract proteins. Samples were loaded on discontinuous, 1.5 mm wide self-cast polyacrylamide gels (10 % for running gel, see table 9, and 6 % for stacking gel, see table 10). Electrophoresis took place in 1x Running buffer at 80 or 100 V for 20 min, followed by 120 V for 60 - 80 min. Per each gel 3 μ l of the PageRuler™ Prestained Protein Ladder (ThermoFisher) was loaded as a marker.

Table 9 - Composition SDS PAGE gels (for 4 1.5 mm gels)

Component	10 % running gel
ddH₂O	15.7 ml
1.5 M Tris-HCl pH 8.8	10 ml
10 % SDS (Protein quality - Biorad)	400 µl
30 % Acrylamide/Bis solution 29:1 (Biorad)	13.3 ml
10 % APS	400 µl
TEMED	25 µl

Table 10 - Composition SDS-PAGE stacking gel (for 4 1.5 mm gels)

Component	6 % stacking gel
ddH₂O	9 ml
0.5 M Tris-HCl pH 6.8	4 ml
10 % SDS (Protein quality - Biorad)	160 µl
30 % Acrylamide/Bis solution 29:1 (Biorad)	2.6 ml
10 % APS	160 µl
TEMED	25 µl

Immunoblot analysis

After proteins were successfully separated on SDS-PAGE, proteins were transferred to a Hybond™-ECL™ nitrocellulose membrane (GE Healthcare, Freiburg, GER) by western blotting using the BioRad Mini Trans-Blot® cell system. Gels were submerged in cold (4 °C) 1x transfer buffer and transfer cassettes were assembled according to the manufacturer's instructions. Transfer was performed at 110 V for 70 min at 4 °C. Membranes were blocked (5 % (w/v) low-fat milk (Biorad) TBST solution) for 60 min at RT on a shaker (40-60 rpm), to avoid high background signal during exposure. Blocked membranes were incubated with the primary antibody (2 % (w/v) low-fat milk (Biorad) in TBST solution) between 12-80 h at 4 °C on a shaker (50 rpm) (See Table 4 for antibody dilutions). In the morning, membranes were washed 3 times for 10 min each with TBST. Subsequently, membranes were incubated with secondary antibody (2 % (w/v) low-fat milk (Biorad) in TBST solution) at RT for 60 - 120 min at 50 rpm. Primary antibodies bound by protein of interest were detected with the secondary

antibody, which is conjugated with horseradish peroxidase (HRP). After 3 washes with TBST of 10 min each, membranes were gently dried on a piece of kitchen paper, placed on a plastic foil and supplied with 150 μ l of substrate (Biorad Clarity™/Clarity Max™ Western ECL). For highly abundant proteins Clarity substrate were sufficient to detect proteins, however, for low abundance proteins a 1:1 ratio of Clarity™:Clarity Max™ or pure Clarity Max™ was used. Chemiluminescence was detected using the BioRad ChemiDoc™ XRS+ system.

Split-Luciferase Assay

For each assay, all tested co-expression constructs (^NLUC; N-Terminal Luciferase and ^CLUC; C-terminal Luciferase) shown in one figure were transiently expressed on the same leaf (Gehl *et al.*, 2011). Three leaf disks (4 mm diameter) from three independent leaves from 1 plant were pooled per biological replicate and processed in reporter lysis buffer (Promega; E1500, + 150 mM Tris; pH 7.5). Samples were mixed in a 1:1 ratio with Luciferin substrate (Promega; E1531) and luminescence was measured using a luminescence microplate reader (Centro XS; Berthold Technologies). Absolute luminescence, *i.e.* absolute luciferase activity was used as a proxy for protein-protein interaction intensity.

Immunoprecipitation for nLC-MS/MS

Immunoprecipitation (IP) for nLC-MS/MS analysis was performed with tissue from stable transgenic Arabidopsis plants cPAD4^{WT} #5, cPAD4^{K380A} #12, cPAD4^{LLD} #2 and 35S::StrepII-YFP (Lapin *et al.*, 2019). For the infiltration process, please see “Bacterial methods; *P. syringae*”. The 4 hpi and 6 hpi samples were immunoprecipitated and analysed by nLC-MS/MS on different times (1.5 months apart), and can therefore not directly be compared using statistics. For each sample >4 g of leaf tissue was collected, snap frozen and stored at -80 °C. Subsequently, 2g of tissue was ground by hand for 2 min using a pestle and mortar. For optimal and replicable sample homogenisation, the sample was mechanically ground using the Precellys® Evolution Homogeniser (3x 7500 rpm, 10 sec) (VWR, Darmstadt, GER). The samples was then suspended in 4 ml protein extraction buffer for 40 min by vortexing every 10 min. After centrifugation (4000 x g at 4 °C for 2 min), 2 mL supernatant was transferred to a new tube (Protein Lo-bind, Eppendorf), which was centrifuged again (21 000 x g at 4 °C, 20 min). 200 μ l of supernatant was kept as input control and 1.45 mL supernatant was transferred to a new tube to which 20 μ l Magnetic Agarose (MA) GFP-Trap (Chromotek, Martinsried, GER) was added per sample. Beads were carefully mixed using a rotating mixer for 3 h at 4 °C. Beads were collected by placing the tubes in a magnetic rack for 1 min at 4 °C, and were washed

with IP-MS wash buffer 4 times. After the final wash, samples were stored at -20 °C until further processing by the Mass spectrometry facility (MPIPZ)

nLC-MS/MS analysis (By Sara Stolze and Anna Harzen – H. Nakagami Lab – MPIPZ)

Sample preparation and LC-MS/MS data acquisition. Proteins (from GFP-trap enrichment) were submitted to an on-bead digestion. In brief, dry beads were re-dissolved in 25 µL digestion buffer 1 (50 mM Tris, pH 7.5, 2M urea, 1mM DTT, 5 µg/µL trypsin) and incubated for 30 min at 30 °C in a Thermomixer at 400 rpm. Next, beads were pelleted and the supernatant was transferred to a fresh tube. Digestion buffer 2 (50 mM Tris, pH 7.5, 2M urea, 5 mM CAA) was added to the beads, after mixing the beads were pelleted, the supernatant was collected and combined with the previous one. The combined supernatants were then incubated overnight at 32 °C in a Thermomixer with 400 rpm; samples were protected from light during incubation. The digestion was stopped by adding 1 µL TFA and desalted with C18 Empore disk membranes according to the StageTip protocol (Rappsilber *et al.*, 2003). Dried peptides were re-dissolved in 2% ACN, 0.1% TFA (10 µL) for analysis and measured without dilution in case of on-bead digested samples. Samples were analysed using an EASY-nLC 1200 (Thermo Fisher) coupled to a Q Exactive Plus mass spectrometer (Thermo Fisher). Peptides were separated on 16 cm frit-less silica emitters (New Objective, 0.75 µm inner diameter), packed in-house with reversed-phase ReproSil-Pur C18 AQ 1.9 µm resin (Dr. Maisch). Peptides were loaded on the column and eluted for 115 min using a segmented linear gradient of 5% to 95% solvent B (0 min : 5%B; 0-5 min -> 5%B; 5-65 min -> 20%B; 65-90 min ->35%B; 90-100 min -> 55%; 100-105 min ->95%, 105-115 min ->95%) (solvent A 0% ACN, 0.1% FA; solvent B 80% ACN, 0.1%FA) at a flow rate of 300 nL/min. Mass spectra were acquired in data-dependent acquisition mode with a TOP15 method. MS spectra were acquired in the Orbitrap analyzer with a mass range of 300–1750 m/z at a resolution of 70,000 FWHM and a target value of 3×10^6 ions. Precursors were selected with an isolation window of 1.3 m/z. HCD fragmentation was performed at a normalized collision energy of 25. MS/MS spectra were acquired with a target value of 10^5 ions at a resolution of 17,500 FWHM, a maximum injection time (max.) of 55 ms and a fixed first mass of m/z 100. Peptides with a charge of +1, greater than 6, or with unassigned charge state were excluded from fragmentation for MS², dynamic exclusion for 30s prevented repeated selection of precursors.

Data analysis. Raw data were processed using MaxQuant software (version 1.5.7.4, <http://www.maxquant.org/>) (Cox & Mann, 2008) with label-free quantification (LFQ) and iBAQ enabled (Tyanova *et al.*, 2016). MS/MS spectra were searched by the Andromeda search

engine against a combined database containing the sequences from *A. thaliana* (TAIR10_pep_20101214;ftp://ftp.arabidopsis.org/home/tair/Proteins/TAIR10_protein_lists/) and sequences of 248 common contaminant proteins and decoy sequences. Trypsin specificity was required and a maximum of two missed cleavages allowed. Minimal peptide length was set to seven amino acids. Carbamidomethylation of cysteine residues was set as fixed, oxidation of methionine and protein N-terminal acetylation as variable modifications. Peptide-spectrum-matches and proteins were retained if they were below a false discovery rate of 1%.

Statistical analysis of the MaxLFQ values was carried out using Perseus (version 1.5.8.5, <http://www.maxquant.org/>). Quantified proteins were filtered for reverse hits and hits “identified by site” and MaxLFQ values were log₂ transformed. After grouping samples by condition only those proteins were retained for the subsequent analysis that had two valid values in one of the conditions. Two-sample *t*-tests were performed using a permutation-based FDR of 5%. Alternatively, quantified proteins were grouped by condition and only those hits were retained that had 3 valid values in one of the conditions. Missing values were imputed from a normal distribution (2.0 downshift, separately for each column). The Perseus output was exported and further processed using Excel.

Molecular biological methods

Confocal laser scanning microscopy

For confocal laser scanning microscopy using the Zeiss LSM 780 I used: 20x water objective (W Plan-Apochromat 20x/1.0DIC D=0.17 M27 70 mm), Argon Laser intensity of 1-5% (maximum 10%), YFP excitation at 514nm, detection between 520-590 nm, and auto-fluorescence of Chlorophyll A (ChA) detection between 630-735 nm. For confocal laser scanning microscopy using the Leica SP8 I used: 20x water objective (HC PL APO CS2 20x, 0.75 IMM), Argon Laser intensity of 2-10% (maximum 20%), YFP excitation at 514nm, detection between 518-530 nm, and auto-fluorescence of Chlorophyll A (ChA) detection between 695-737 nm .

Isolation of genomic DNA

Fresh leaf material (ca. 0.5 cm²) was collected in a tube and crushed with a pestle, or with beads using a TissueLyser II (Qiagen). 400 µl DNA extraction buffer was added to the tube and vortexed. The mixture was cleared by centrifugation at 21 000 x g at RT for 2 min. 300 µl supernatant were transferred to a new tube and DNA was precipitated by adding 300 µl 100% high-grade isopropanol and tubes were inverted several times. Tubes were centrifuged at 21

000 x g, RT, 5 min, supernatant was removed and washed in 600 µl 70 % EtOH and dried at 40 °C for 5 - 10 min. Dried DNA was suspended in 50 µl ddH₂O and samples were kept at 4 °C or -20 °C for longer storage.

Fast isolation of genomic DNA

For large-scale DNA isolation, I used a method based on a high sucrose solution that allows DNA extraction in a 96 well plate format (Berendzen *et al.*, 2005). Few mg of leaf material was collected in collection tubes (Qiagen) containing one metal bead. 200 µl Sucrose DNA extraction buffer was added to each tube and samples were homogenised with a TissueLyser II (Qiagen). Tubes were centrifuged at 1000 g, RT, for 1 min and then placed in a water bath for 15 min at 97 °C. After this, samples were placed on ice for 30 min, and centrifuged again at 1000 g, RT, for 1 min. Per PCR reaction 1 µl of solution was used. DNA was kept at 4 °C for a maximum of 7 days, but are not suitable for long-term storage at -20°C.

Isolation of total RNA

Total RNA was extracted from Arabidopsis leaves using the Plant RNA Kit (Bio-Budget, Krefeld, GER) according to the provided instructions. In case of mature leaves, 10% extra extraction buffer was added per sample to enhance the extraction efficiency. Briefly, samples were homogenised in extraction buffer, loaded on DNA binding columns to remove gDNA, precipitated, loaded on RNA binding columns, washed, dried and eluted into collection tubes. Immediately after RNA extraction, either RNA was processed or RNA was stored at -20 °C.

Polymerase Chain Reaction (PCR)

For genotyping or colony PCRs non-proofreading Phire II DNA polymerase (ThermoFisher) was used. For cloning purposes, proofreading Phusion HF polymerase (ThermoFisher) or Pfu Polymerase (ThermoFisher) was used (See Table 5). PCR reaction mixtures were identical for all polymerases (Table 11). The thermal cycling program was adjusted to each polymerase (Table 12). For PIPE-PCR, there are some slight differences to a regular PCR, for more information see section below.

Table 11 - PCR reaction mix

Component	Volume	Volume (PIPE-PCR)
10x PCR buffer	2 μ l	7.5 μ l (15 μ l HF Buffer - ThermoFisher)
dNTP mix (2.5 mM)	1.6 μ l	6 μ l
forward primer (10 μM)	1 μ l	1,5 μ l
reverse primer (10 μM)	1 μ l	1.5 μ l
template DNA	0.2 - 10 ng	200-500 ng
polymerase	0.2 - 0.5 μ l	0.8 μ l
ddH₂O	Up to 20 μ l	Up to 75 μ l

Table 12 - Thermo-cycling programs

Stage	Temperature (°C)	Phire Pol. Time	Phusion Pol. Time	PIPE-PCR Phusion Pol. Time	Cycles
Initiation	98	30 sec	5 min	5 min	1x
Denaturation	98	10 sec	10 sec	10 sec	30 - 35x (PIPE-PCR 20x)
Annealing	55 - 60	15 sec	30 sec	30 sec	
Elongation	72	15 sec/kb	30 sec/kb	30 sec/kb	
Final extension	72	5	5	NO EXTENSION	1x

Site-directed Mutagenesis by PCR

To mutate selected nucleotides in the sequence of a plasmid of interest, site-directed mutagenesis was performed with minor alterations according to the instructions of the QuickChange Site-Directed Mutagenesis Kit (Agilent, Waldbronn, GER). See table 11 for PCR mix details, and table 12 for the thermo-cycling program. A maximum of 20 cycles was used in order to avoid PCR induced sequence mistakes. To remove the plasmid template from the reaction mix post-PCR, I used the restriction enzyme DpnI (NEB), which specifically digests methylated-DNA, *i.e.* plasmid DNA, but not PCR-DNA. Per 20 μ l PCR mix, 1 μ l DpnI was

added and this was incubated for 1 h at 37 °C. 5 µl of the digested PCR mix was used for Dh10b heat-shock transformation.

PIPE-PCR

To cut and paste different DNA pieces together without overhangs, digestion sites or Golden Gate domestication, PIPE-PCR was used and is described here (Klock & Lesley, 2009). Two independent PCR reactions are performed to create an insert and a vector fragment. This means one requires 4 unique oligos. Each oligo consists of 2 parts, 1) a primer-section required for binding and elongation during PCR, and 2) an overhang used by *E. coli* for ligation *in vivo*. This overhang can also contain a FLAG-tag or a peptide linker for protein fusions, but it is required to overlap with the DNA sequence you want to glue together. The primer-section should be at least 24 base pairs long, and should not have an annealing temperature below 70 °C. The overhang section has to have an overlap of at least 30 base pairs with the other PCR product. Meaning that these oligos are at least 54 base pairs long, but can be much longer. To remove the plasmid template from the reaction mix post-PCR, I used the restriction enzyme DpnI (1 µl + 6 µl CutSmart buffer NEB), which specifically digests methylated-DNA, *i.e.* plasmid DNA, but not PCR-DNA. To wash out salts and enzymes from the mixture, DNA was cleaned-up using PEG 8000 DNA clean up. A DNA clean up kit is not suitable for this. To each 82 µl PIPE-PCR mixture 250 µl TE buffer was added, and mixed by inverting, before adding 150 µl PEG 8000 solution. After homogenising the samples by inverting, DNA was pelleted by centrifugation at 10 000 x g, RT, for 20 min. After removing the supernatant, DNA pellet was dissolved in 50 µl TE buffer. The two PCR products were combined in a 1:1, 1:5, 1:10, 5:1 or 10:1 ratio, with at least 10 fmol PCR fragment per PCR fragment. A 10-fold volume of *E. coli* DH10b was incubated with the PCR products for 10 min on ice before performing heat-shock.

cDNA Synthesis

Total RNA was isolated as described above and 250 - 1000 ng were used for cDNA synthesis. I used cDNA Synthesis SuperMix (Bimake) following manufacturer's instructions and diluted cDNA 1:1 when using 250 ng total RNA and 1:5 when using 1000 ng total RNA. cDNA was stored at -20 °C.

Quantitative reverse-transcription PCR (qRT-PCR)

qRT-PCR was performed using a BioRad CFX96 Touch™ Real-Time PCR Detection System. For details see table 13 and table 14. Primer sequences can be found in table 6. For data analysis, CFX Maestro™ Software (BioRad) was used. Data were further analysed in Excel and R-studio. Normality of residuals distribution and homoscedasticity was checked visually (by Q-

Q plot) and with formal Shapiro-Wilcoxon test ($\alpha=0.05$). Collected titre data were considered suitable for ANOVA and Tukey's HSD test.

Table 13 - qRT-PCR reaction mix

Component	Volume
SYBR® Green Supermix	5 μ l
forward primer (10 μM)	0.5 μ l
reverse primer (10 μM)	0.5 μ l
template cDNA	1 μ l
ddH₂O	to 10 μ l

Table 14 - qRT-PCR thermo-cycling program

Stage	Temperature (°C)	Time	Cycles
Initiation	95	30 sec	1x
Denaturation	95	10 sec	40x
Annealing	55	15 sec	
Elongation	72	10 sec	
Melt Curve	60 - 95	5 sec per 0.5 °C	1x

Plasmid DNA isolation from bacteria

For standard plasmid prep, the NucleoSpin® Plasmid Kit (Macherey-Nagel, Düren, GER) was used to the manufacturer's instructions. For prepping *A. tumefaciens*, the low copy-number protocol was used.

Restriction endonuclease digestion of DNA

DNA digestion was performed to the respective enzyme manufacturer's instructions. Typically, 1-8 μ l DNA (corresponding to 50-500 ng DNA) was mixed with 1 μ l reaction buffer, 0.2 μ l enzyme and brought to a final volume of 10 μ l. The reaction was incubated at the recommended temperature for 20 min up to 2 h and stored at 4 °C.

Agarose gel electrophoresis of DNA

If not pre-mixed (*e.g.* Phire polymerase reaction buffer), DNA was mixed with DNA loading dye and loaded on a 0.8 - 2 % (w/v) agarose gel in TAE buffer. Typically, agarose gels were

run at 100-200 V for 10 - 40 min. Agarose gels were supplemented with 0.2 mg/l ethidium bromide and visualised on a 312 nm UV trans-illuminator.

DNA purification from agarose gels

Separated DNA fragments were visualised by illuminating the DNA on a UV trans-illuminator. Using a clean razor blade PCR fragments were cut out and further processed using the PCR clean-up and gel extraction kit (Macherey-Nagel) according to the manufacturer's instructions.

Gateway® DNA cloning

The Gateway® system for DNA cloning (ThermoFisher) was used mainly in this study. Entry clones were obtained by performing a BP reaction with a previously produced expression clone containing attB sites and a pDONR (*e.g.* pDONR207) containing attP sites, according to the manufacturer's instructions. Alternatively, using PIPE-PCR a gene of interest and the pDONR201 vector were amplified and ligated *in vivo* by *E. coli*, see section on PIPE-PCR. To create expression clones, an LR reaction was performed by recombining an entry vector with a destination vector using Gateway LR Clonase II mix (ThermoFisher). Typically, LR reactions were incubated for 1 h at RT and transformed into *E. coli* (DH10b). For reaction mix, see table 15.

Table 15 - LR reaction mix

Component	Volume / Amount
Entry vector	25 - 75 ng
Destination vector	75 ng
ddH ₂ O	Up to 4 µl
LR Clonase II mix	1 µl

DNA sequencing

DNA sequencing was carried out by Eurofins Genomics (Ebersberg, GER) using their Mix2Seq kit. DNA sequencing samples were prepared according to the manufacturer's instructions.

In silico analyses

DNA/Protein sequence analysis

All Sanger DNA sequence data was analysed using the Seqman Pro software (DNA STAR). For phylogenetic protein alignment, protein sequences were obtained via the Phytozome database (<http://phytozome.jgi.doe.gov>), aligned using Clustal Omega (<https://www.ebi.ac.uk/Tools/msa/clustalo/>), and coloured using Jalview

(<https://www.jalview.org/>). Sequence Logo were created using WebLogo (<https://weblogo.berkeley.edu/logo.cgi>; Crooks *et al.*, 2004; Schneider & Stephens. 1990). Plant DHS was used to determine chromatin accessibility of Arabidopsis loci (<http://plantdhs.org/>; Zhang *et al.*, 2016). For phylogenetic shadowing, DNA sequences were obtained from the Phytozome database (<http://phytozome.jgi.doe.gov>) and the Genome Evolution database (<https://genomeevolution.org/coge/>). Phylogenetic shadowing was performed using mVista (<http://genome.lbl.gov/vista/mvista/submit.shtml>; Frazer *et al.*, 2004).

Data Analysis

All data analysis and data representation was performed in RStudio (v. 1.1.463; <https://rstudio.com>) using the following packages: ggplot2, plyr, multcompView, GGally, grid, futile.logger, VennDiagram and ggrepel. Pie charts and qRT-PCR bar plots were generated using Excel 2016. GO-term analyses were performed using the TAIR GO-Term analysis tool (https://www.arabidopsis.org/tools/go_term_enrichment.jsp), which runs on PANTHER (<http://www.pantherdb.org/>). Statistical GO-term Overrepresentation Test was performed on PANTHER (<http://www.pantherdb.org/>; released 20190711; Arabidopsis genome; Biological processes and Molecular Function; Fisher Exact with Bonferroni correction).

Protein structure visualisation

EDS1-SAG101 crystal structure and EDS1-PAD4 structure model (Wagner *et al.*, 2013) were visualised using PyMol (2.3.0; <https://pymol.org/2/>).

References

1. Adachi, H., Contreras, M.P., Harant, A., Wu, C.H., Derevnina, L., Sakai, T., Duggan, C., Moratto, E., Bozkurt, T.O., Maqbool, A., Win, J., Kamoun, S. 2019. An N-terminal motif in NLR immune receptors is functionally conserved across distantly related plant species. *eLife*. 8:e49956
2. Alonso, J.M., Stepanova, A.N., Leisse, T.J., Kim, C.J., Chen, H.M., Shinn, P., Stevenson, D.K., Zimmerman, J., Barajas, P., Cheuk, R., Gadrinab, C., Heller, C., Jeske, A., Koesema, E., Meyers, C.C., Parker, H., Prednis, L., Ansari, Y., Choy, N., Deen, H., Geralt, M., Hazari, N., Hom, E., Karnes, M., Mulholland, C., Ndubaku, R., Schmidt, I., Guzman, P., Aguilar-Henonin, L., Schmid, M., Weigel, D., Carter, D.E., Marchand, T., Risseeuw, E., Brogden, D., Zeko, A., Crosby, W.L., Berry, C.C., Ecker, J.R. 2003. Genome-wide insertional mutagenesis of *Arabidopsis thaliana*. *Science*. 301:653-657.
3. Asai, S., Furzer, O.J., Cevik, V., Kim, D.S., Ishaque, N., Goritschnig, S., Staskawicz, B.J., Shirasu, K., Jones, J.D.G. 2018. A downy mildew effector evades recognition by polymorphism of expression and subcellular localization. *Nature Communications*. 9:5192.
4. Austin, M.J., Muskett, P., Kahn, K., Feys, B.J., Jones, J.D., Parker, J.E. 2002. Regulatory role of SGT1 in early R gene-mediated plant defenses. *Science*. 295:2077-2080.
5. Axtell, M.J., Staskawicz, B.J. 2003. Initiation of RPS2-specified disease resistance in *Arabidopsis* is coupled to the AvrRpt2-directed elimination of RIN4. *Cell*. 112:369-377.
6. Azevedo, C., Sadanandom, A., Kitagawa, K., Freialdenhoven, A., Shirasu, K., Schulze-Lefert, P. 2002. The RAR1 interactor SGT1, an essential component of R gene-triggered disease resistance. *Science*. 295:2073-2076.
7. Azevedo, C., Betsuyaku, S., Peart, J., Takahashi, A., Noël, L., Sadanandom, A., Casais, C., Parker, J., Shirasu, K. 2006. Role of SGT1 in resistance protein accumulation in plant immunity. *EMBO Journal*. 25:2007-2016.
8. Baggs, E., Dagdas, G., Krasileva, K.V. 2017. NLR diversity, helpers and integrated domains: making sense of the NLR Identity. *Current Opinion in Plant Biology*. 38:59-67.
9. Baggs, E.L., Thanki, A.S., O'Grady, R., Schudoma, C., Haerty, W., Krasileva, K.V. 2019. Convergent loss of an EDS1/PAD4 signalling pathway in several plant lineages predicts new components of plant immunity and drought response. *bioRxiv* 572560. doi: <https://doi.org/10.1101/572560>.
10. Bartsch, M., Gobbato, E., Bednarek, P., Debey, S., Schultz, J.L., Bautor, J., Parker, J.E. 2006. Salicylic Acid-Independent ENHANCED DISEASE SUSCEPTIBILITY1 Signalling in *Arabidopsis* Immunity and Cell Death Is Regulated by the Monooxygenase FMO1 and the Nudix Hydrolase NUDT7. *The Plant Cell*. 18:1038-1051.
11. Bensmihen, S., To, A., Lambert, G., Kroj, T., Giraudat, J., Parcy, F. 2004. Analysis of an activated ABI5 allele using a new selection method for transgenic *Arabidopsis* seeds. *FEBS letters*. 561:127-131.
12. Berendzen, K., Searle, I., Ravenscroft, D., Koncz, C., Batschauer, A., Coupland, G., Somssich, I.E., Ulker, B. 2005. A rapid and versatile combined DNA/RNA extraction protocol and its application to the analysis of a novel DNA marker set polymorphic between *Arabidopsis thaliana* ecotypes Col-0 and Landsberg erecta. *Plant Methods*. 1:4.

13. Bernacki, M.J., Czarnocka, W., Szechyńska-Hebda, M., Mittler, R., Karpiński, S. 2019. Biotechnological Potential of LSD1, EDS1, and PAD4 in the Improvement of Crops and Industrial Plants. *Plants*. 8:290.
14. Bernoux, M., Ve, T., Williams, S., Warren, C., Hatters, D., Valkov, E., Zhang, X., Ellis, J.G., Kobe, B., Dodds, P.N. 2011. Structural and functional analysis of a plant resistance protein TIR domain reveals interfaces for self-association, signaling, and autoregulation. *Cell host & microbe*. 9:200-211.
15. Bernsdorff, F., Döring, A. C., Gruner, K., Schuck, S., Bräutigam, A., Zeier, J. 2016. Pipecolic Acid Orchestrates Plant Systemic Acquired Resistance and Defense Priming via Salicylic Acid-Dependent and -Independent Pathways. *The Plant Cell*. 28:102-129.
16. Betsuyaku, S., Katou, S., Takebayashi, Y., Sakakibara, H., Nomura, N., Fukuda, H. 2018. Salicylic Acid and Jasmonic Acid Pathways are Activated in Spatially Different Domains Around the Infection Site During Effector-Triggered Immunity in *Arabidopsis thaliana*. *Plant Cell & Physiology*. 59:439.
17. Bhandari, D.D., Lapin, D., Kracher, B., von Born, P., Bautor, J., Niefind, K., Parker, J.E. 2019. An EDS1 heterodimer signalling surface enforces timely reprogramming of immunity genes in *Arabidopsis*. *Nature Communications*. 10:772.
18. Bhattacharjee, S., Halane, M.K., Kim, S.H., Gassmann, W. 2011. Pathogen effectors target *Arabidopsis* EDS1 and alter its interactions with immune regulators. *Science*. 334:1405-1408.
19. Birker, D., Heidrich, K., Takahara, H., Narusaka, M., Deslandes, L., Narusaka, Y., Reymond, M., Parker, J.E., O'Connell, R. 2009. A locus conferring resistance to *Colletotrichum higginsianum* is shared by four geographically distinct *Arabidopsis* accessions. *Plant Journal*. 60:602-613.
20. Bonardi, V., Tang, S., Stallmann, A., Roberts, M., Cherkis, K., Dangl, J.L. 2011. Expanded functions for a family of plant intracellular immune receptors beyond specific recognition of pathogen effectors. *PNAS USA*. 108:16463-16468.
21. Bos, J.I., Prince, D., Pitino, M., Maffei, M.E., Win, J., Hogenhout, S.A. 2010. A functional genomics approach identifies candidate effectors from the aphid species *Myzus persicae* (green peach aphid). *PLoS Genetics*. 6:e1001216.
22. Boutrot, F., Zipfel, C. 2017. Function, Discovery, and Exploitation of Plant Pattern Recognition Receptors for Broad-Spectrum Disease Resistance. *Annual Review of Phytopathology*. 55:257-286.
23. Boyes, D.C., Nam, J., Dangl J.L. 1998. The *Arabidopsis thaliana* RPM1 disease resistance gene product is a peripheral plasma membrane protein that is degraded coincident with the hypersensitive response. *PNAS USA*. 95:15849-15854.
24. Brooks, D.M., Bender, C.L., Kunkel, B.N. 2005. The *Pseudomonas syringae* phytotoxin coronatine promotes virulence by overcoming salicylic acid-dependent defences in *Arabidopsis thaliana*. *Molecular Plant Pathology*. 6:629-639.
25. Castel, B., Ngou, P.M., Cevik, V., Redkar, A., Kim, D.S., Yang, Y., Ding, P., Jones, J.D.G. 2019. Diverse NLR immune receptors activate defence via the RPW8-NLR NRG1. *New Phytologist*. 222:966-980.
26. Cesari, S. 2017. Multiple strategies for pathogen perception by plant immune receptors. *New Phytologist*. 219:17-24.

27. Century, K.S., Holub, E.B., Staskawicz, B.J. 1995. NDR1, a locus of *Arabidopsis thaliana* that is required for disease resistance to both a bacterial and a fungal pathogen. *PNAS USA*. 92:6597-6601.
28. Chang, M., Zhao, J., Chen, H., Li, G., Chen, J., Li, M., Palmer, I.A., Song, J., Alfano, J.R., Liu, F., Fu, Z.Q. 2019. PBS3 Protects EDS1 from Proteasome-Mediated Degradation in Plant Immunity. *Molecular Plant*. 12:678688.
29. Cheng, Y.T., Li, Y., Huang, S., Huang, Y., Dong, X., Zhang, Y., Li, X. 2011. Stability of plant immune-receptor resistance proteins is controlled by SKP1-CULLIN1-F-box (SCF)-mediated protein degradation. *PNAS USA*. 108:14694-14699.
30. Clough, S.J., Bent, A.F. 1998 Floral dip: a simplified method for *Agrobacterium*-mediated transformation of *Arabidopsis thaliana*. *Plant Journal*. 16:735-43.
31. Collier, S.M., Hamel, L.P., Moffett, P. 2011. Cell death mediated by the N-terminal domains of a unique and highly conserved class of NB-LRR protein. *Molecular Plant Microbe Interactions*. 24:918-931.
32. Contreras, R., Kallemini, P., González-García, M.P., Lazarova, A., Sánchez-Serrano, J.J., Sanmartín, M., Rojo, E. 2019. Identification of Domains and Factors Involved in MINIYO Nuclear Import. *Frontiers in Plant Science*. 10:1044.
33. Couldridge, C., Newbury, H.J., Ford-Lloyd, B., Bale, J., Pritchard, J. 2007. Exploring plant responses to aphid feeding using a full *Arabidopsis* microarray reveals a small number of genes with significantly altered expression. *Bulletin of Entomological Research*. 97:523-532.
34. Cox, J., Mann, M. 2008. MaxQuant enables high peptide identification rates, individualized p.p.b.-range mass accuracies and proteome-wide protein quantification. *Nature Biotechnology*. 26:1367-21372.
35. Crooks, G.E., Hon G, Chandonia J.M., Brenner S.E. 2004. WebLogo: A sequence logo generator. *Genome Research*, 14:1188-1190.
36. Cui, H., Tsuda, K., Parker, J.E. 2015. Effector-Triggered Immunity: From Pathogen Perception to Robust Defense. *Annual Review of Plant Biology*. 66:487-511.
37. Cui, P., Chen, T., Qin, T., Ding, F., Wang, Z., Chen, H., Xiong, L. 2016. The RNA polymerase II C-terminal domain phosphatase-like protein FIERY2/CPL1 interacts with eIF4AIII and is essential for nonsense-mediated mRNA decay in *Arabidopsis*. *The Plant Cell*. 28:770-785
38. Cui, H., Gobbato, E., Kracher, B., Qiu, J., Bautor, J., Parker, J.E. 2017. A core function of EDS1 with PAD4 is to protect the salicylic acid defense sector in *Arabidopsis* immunity. *New Phytologist*. 213:1802-1817.
39. Cui, H., Qiu, J., Zhou, Y., Bhandari, D.D., Zhao, C., Bautor, J., Parker, J.E. 2018. Antagonism of Transcription Factor MYC2 by EDS1/PAD4 Complexes Bolsters Salicylic Acid Defense in *Arabidopsis* Effector-Triggered Immunity. *Molecular Plant*. 11:1053-1066.
40. Dangl, J.L., Horvath, D.M., Staskawicz, B.J. 2013. Pivoting the plant immune system from dissection to deployment. *Science*. 341:746-751.
41. Deslandes, L., Olivier, J., Peeters, N., Feng, D.X., Khounloham, M., Boucher, C., Somssich, I., Genin, S., Marco, Y. 2003. Physical interaction between RRS1-R, a protein conferring resistance to bacterial wilt, and PopP2, a type III effector targeted to the plant nucleus. *PNAS USA*. 100:8024-8029.

42. Ding, P., Ding, Y. 2020. Stories of Salicylic Acid: A Plant Defense Hormone. *Trends in Plant Science*. doi: 10.1016/j.tplants.2020.01.004
43. Dodds, P.N., Rathjen, J.P. 2010. Plant immunity: towards an integrated view of plant-pathogen interactions. *Nature Reviews Genetics*. 11:539-548.
44. Dong, O.X., Tong, M., Bonardi, V., Kasmi, F.E., Woloshen, V., Wünsch, L.K., Dangl, J.L., Li, X. 2016. TNL-mediated immunity in *Arabidopsis* requires complex regulation of the redundant ADR1 gene family. *New Phytologist*. 210:960-973.
45. Dongus, J.A., Bhandari, D., Patel, M., Archer, L., Dijkgraaf, L., Deslandes, L., Shah, J., Parker, J.E. 2020. *Arabidopsis* PAD4 lipase-like domain is sufficient for resistance to green peach aphid. *Molecular Plant-Microbe Interactions*. 33:328-335.
46. Dudareva, N., Negre, F., Nagegowda, D.A., Orlova, I. 2006. Plant Volatiles: Recent Advances and Future Perspectives. *Critical Reviews in Plant Sciences*. 25:417-440.
47. Feys, B.J., Moisan, L.J., Newman, M.A., Parker, J.E. 2001. Direct interaction between the *Arabidopsis* disease resistance signalling proteins, EDS1 and PAD4. *EMBO Journal*. 20:5400-5411.
48. Feys, B.J., Wiermer, M., Bhat, R.A., Moisan, L.J., Medina-Escobar, N., Neu, C., Cabral, A., Parker, J.E. 2005. *Arabidopsis* SENESCENCE-ASSOCIATED GENE101 stabilizes and signals within an ENHANCED DISEASE SUSCEPTIBILITY1 complex in plant innate immunity. *The Plant Cell*. 17:2601-2613.
49. Francia, P., Simoni, L., Cominelli, E., Tonelli, C., Galbiati, M. 2008. Gene trap-based identification of a guard cell promoter in *Arabidopsis*. *Plant Signaling & Behaviour*. 3:684-686.
50. Frazer, K.A., Pachter, L., Poliakov, A., Rubin, E.M., Dubchak, I. 2004. VISTA: computational tools for comparative genomics. *Nucleic Acids Research*. 32:273-279
51. Fu, Z.Q., Dong, X. 2013. Systemic acquired resistance: turning local infection into global defense. *Annual Review of Plant Biology*. 64:839-63.
52. Gantner, J., Ordon, J., Kretschmer, C., Guerois, R., Stuttmann, J. 2019. An EDS1-SAG101 Complex is Essential for TNL-mediated Immunity in *Nicotiana benthamiana*. *The Plant Cell*. 31:2456-2474.
53. Garcia, A.V., Blanvillain-Baufumé, S., Huibers, R.P., Wiermer, M., Li, G., Gobbato E., Rietz, S., Parker, J.E. 2010. Balanced nuclear and cytoplasmic activities of EDS1 are required for a complete plant innate immune response. *PLoS Pathogens*. 6:e1000970.
54. Gao, F., Shu, X., Ali, M.B., Howard, S., Li, N., Winterhagen, P., Qiu, W., Gassmann, W. 2010. A functional EDS1 ortholog is differentially regulated in powdery mildew resistant and susceptible grapevines and complements an *Arabidopsis eds1* mutant. *Planta*. 231:1037-1047.
55. Gao, F., Dai, R., Pike, S. M., Qiu, W., Gassmann, W. 2014. Functions of EDS1-like and PAD4 genes in grapevine defenses against powdery mildew. *Plant Molecular Biology*. 86:381-393.
56. Gehl, C., Kaufholdt, D., Hamisch, D., Bikker, R., Kudla, J., Mendel, R.R., Hänsch, R. 2011. Quantitative analysis of dynamic protein-protein interactions in planta by a floated-leaf luciferase complementation imaging (FLuCI) assay using binary Gateway vectors. *Plant Journal*. 67:542-553.

57. Giri, M.K., Singh, N., Banday, Z.Z., Singh, V., Ram, H., Singh, D., Chattopadhyay, S., Nandi, A.K. 2017. GBF1 differentially regulates CAT2 and PAD4 transcription to promote pathogen defense in *Arabidopsis thaliana*. *Plant Journal*. 91:802-815.
58. Glazebrook, J., Zook, M., Mert, F., Kagan, I., Rogers, E.E., Crute, I.R., Holub, E.B., Hammerschmidt, R., Ausubel, F.M. 1997. Phytoalexin-deficient mutants of *Arabidopsis* reveal that PAD4 encodes a regulatory factor and that four PAD genes contribute to downy mildew resistance. *Genetics*.146:381-392.
59. Glazebrook, J. 2005. Contrasting mechanisms of defense against biotrophic and necrotrophic pathogens. *Annual Review Phytopathology*. 43:205-227.
60. Gray, W.M., Muskett, P.R., Chuang, H.W., Parker, J.E. 2003. *Arabidopsis* SGT1b is required for SCF(TIR1)-mediated auxin response. *The Plant Cell*, 15:1310-1319.
61. Greenberg, J. T., Guo, A., Klessig, D. F., Ausubel, F. M. 1994. Programmed cell death in plants: a pathogen-triggered response activated coordinately with multiple defense functions. *Cell*. 77:551-563.
62. Guo, Y., Zheng, Z., La Clair, J. J., Chory, J., Noel, J. P. 2013. Smoke-derived karrikin perception by the α/β -hydrolase KAI2 from *Arabidopsis*. *PNAS USA*. 110:8284-8289.
63. Hacquard, S., Spaepen, S., Garrido-Oter, R., Schulze-Lefert, P. 2017. Interplay Between Innate Immunity and the Plant Microbiota. *Annual Review of Phytopathology*. 55:565-589.
64. Hartmann, M., Zeier, J. 2019. N-hydroxypipicolinic acid and salicylic acid: a metabolic duo for systemic acquired resistance. *Current opinion in plant biology*. 50:44-57.
65. Heidrich, K., Wirthmueller, L., Tasset, C., Pouzet, C., Deslandes, L., Parker, J.E. 2011. *Arabidopsis* EDS1 connects pathogen effector recognition to cell compartment-specific immune responses. *Science*. 334:1401-1404.
66. Heidrich, K., Tsuda, K., Blanvillain-Baufumé, S., Wirthmueller, L., Bautor, J., Parker, J.E. 2013. *Arabidopsis* TNL-WRKY domain receptor RRS1 contributes to temperature-conditioned RPS4 auto-immunity. *Frontiers in Plant Science*. 4:403.
67. Hodge, S., Ward, J.L., Beale, M.H., Bennett, M., Mansfield, J.W., Powell, G. 2013. Aphid-induced accumulation of trehalose in *Arabidopsis thaliana* is systemic and dependent upon aphid density. *Planta*. 237:1057-1064.
68. Hogenhout, S.A., Bos, J.I. 2011. Effector proteins that modulate plant-insect interactions. *Current Opinion in Plant Biology*. 14:422-428.
69. Holt, B.F., Belkadir, Y., Dangl, J.L. 2005. Antagonistic control of disease resistance protein stability in the plant immune system. *Science*. 309:929-932.
70. Hopkins, M.T., Lampi, Y., Wang, T.W., Liu, Z., Thompson, J.E. 2008. Eukaryotic translation initiation factor 5A is involved in pathogen-induced cell death and development of disease symptoms in *Arabidopsis*. *Plant Physiology*. 148:479-489.
71. Horsefield, S., Burdett, H., Zhang, X., Manik, M.K., Shi, Y., Chen, J., Qi, T., Gilley, J., Lai, J. S., Rank, M.X., Casey, L.W., Gu, W., Ericsson, D.J., Foley, G., Hughes, R.O., Bosanac, T., von Itzstein, M., Rathjen, J.P., Nanson, J.D., Boden, M., Dry, I.B., Williams, S.J., Staskawicz, B.J., Coleman, M.P., Ve, T., Dodds, P.N., Kobe, B. 2019. NAD⁺ cleavage activity by animal and plant TIR domains in cell death pathways. *Science*. 365:793-799.
72. Howard, B.E., Hu, Q., Babaoglu, A.C., Chandra, M., Borghi, M., Tan, X., He, L., Winter-Sederoff, H., Gassmann, W., Veronese, P., Heber, S. 2013. High-throughput RNA

- sequencing of pseudomonas-infected Arabidopsis reveals hidden transcriptome complexity and novel splice variants. *Plos one*. 8:e74183.
73. Hruz, T., Laule, O., Szabo, G., Wessendorp, F., Bleuler, S., Oertle, L., Widmayer, P., Gruissem, W., Zimmermann, P. 2008. Genevestigator V3: a reference expression database for the meta-analysis of transcriptomes. *Advances in Bioinformatics*. 420747.
 74. Hu, Z., Yan, C., Liu, P., Huang, Z., Ma, R., Zhang, C., Wang, R., Zhang, Y., Martinon, F., Miao, D., Deng, H., Wang, J., Chang, J., Chai, J. 2013. Crystal structure of NLRC4 reveals its autoinhibition mechanism. *Science*. 341:172-75
 75. Huang, X., Li, J., Bao, F., Zhang, X., Yang, S. 2010. A gain-of-function mutation in the Arabidopsis disease resistance gene RPP4 confers sensitivity to low temperature. *Plant Physiology*. 154:798-809.
 76. Jacob, F., Vernaldi, S., Maekawa, T. 2013. Evolution and conservation of plant NLR functions. *Frontiers in Immunology*. 4:297.
 77. Jirage, D., Tootle, T.L., Reuber, T.L., Frost, L.N., Feys, B.J., Parker, J.E., Ausubel F.M., Glazebrook, J. 1999. Arabidopsis thaliana PAD4 encodes a lipase-like gene that is important for salicylic acid signalling. *PNAS USA*. 96:13583-13588.
 78. Jones, J.D., Vance, R.E., Dangl, J.L. 2016. Intracellular innate immune surveillance devices in plants and animals. *Science*. 354:aaf6395.
 79. Jones, J.D., Dangl, J.L. 2006. The plant immune system. *Nature*. 16:323-329.
 80. Jubic, L.M., Saile, S., Furzer, O.J., Kasmi, F.E., Dangl, J.L. 2019. Help wanted: Helper NLRs and plant immune responses. *Current Opinion in Plant Biology*. 50:82-94.
 81. Jung, H.W., Panigrahi, G.K., Jung, G.Y., Lee, Y.J., Shin, K.H., Sahoo, A., Choi, E.S., Lee, E., Kim, K.M., Yang, S.H., Jeon, J.S., Lee, S.C., Kim, S.H. 2020. Pathogen-associated Molecular Pattern-triggered Immunity Involves Proteolytic Degradation of Core Nonsense-mediated mRNA Decay Factors During the Early Defense Response. *The Plant Cell*. pii: tpc.00631.2019.
 82. Katsir, L., Schillmiller, A.L., Staswick, P.E., He, S.Y., Howe, G.A. 2008. COI1 is a critical component of a receptor for jasmonate and the bacterial virulence factor coronatine. *PNAS USA*. 105:7100-7105.
 83. Kawashima, T., Lorković, Z.J., Nishihama, R., Ishizaki, K., Axelsson, E., Yelagandula, R., Kohchi, T., Berger, F. 2015. Diversification of histone H2A variants during plant evolution. *Trends in Plant Science*. 20:419-425.
 84. Ke, Y., Liu, H., Li, X., Xiao, J., Wang, S. 2014. Rice OsPAD4 functions differently from Arabidopsis AtPAD4 in host-pathogen interactions. *The Plant Journal*. 7:619-631.
 85. Kemmerling, B., Schwedt, A., Rodriguez, P., Mazzotta, S., Frank, M., Qamar, S. A., Mengiste, T., Betsuyaku, S., Parker, J. E., Müssig, C., Thomma, B. P., Albrecht, C., de Vries, S. C., Hirt, H., Nürnberger, T. 2007. The BRI1-associated kinase 1, BAK1, has a brassinolide-independent role in plant cell-death control. *Current biology*. 17:1116-1122.
 86. Khan, F.I., Lan, D., Durrani, R., Huan, W., Zhao, Z., Wang, Y. 2017. The Lid Domain in Lipases: Structural and Functional Determinant of Enzymatic Properties. *Front. Bioeng. Biotech*. 5:16.
 87. Kim, K.C., Lai, Z., Fan, B., and Chen, Z. 2008. Arabidopsis WRKY38 and WRKY62 transcription factors interact with Histone Deacetylase 19 in basal defense. *The Plant Cell* 20:2357-2371.

88. Kim, S.H., Kwon, S.I. Saha, D., Anyanwu, N.C., Gassmann, W. 2009. Resistance to the *Pseudomonas syringae* effector HopA1 is governed by the TIR-NBS-LRR protein RPS6 and is enhanced by mutations in SRFR1. *Plant Physiology*. 150:1723-1732.
89. Kim, T.H., Kunz, H.H., Bhattacharjee, S., Hauser, F., Park, J., Engineer, C., Liu, A., Ha, T., Parker, J.E., Gassmann, W., Schroeder, J.I. 2012. Natural Variation in Small Molecule-Induced TIR-NB-LRR Signalling Induces Root Growth Arrest via EDS1- and PAD4-Complexed R Protein VICTR in *Arabidopsis*. *The Plant Cell*. 24:5177-5192.
90. Kleinboelting, N., Huep, G., Kloetgen, A., Viehoveer, P., Weisshaar, B. 2012 GABI-Kat SimpleSearch: new features of the *Arabidopsis thaliana* T-DNA mutant database. *Nucleic Acids Research*. 40:D1211-1215.
91. Klock, H.E., Lesley, S.A. 2009. The Polymerase Incomplete Primer Extension (PIPE) method applied to high-throughput cloning and site-directed mutagenesis. *Methods in Molecular Biology*. 498:91-103.
92. Koch, E., Slusarenko, A. 1990. *Arabidopsis* is susceptible to infection by a downy mildew fungus. *The Plant Cell*. 2:437-445.
93. Kordic, S., Cummins, I., Edwards, R. 2002. Cloning and characterization of an S-formylglutathione hydrolase from *Arabidopsis thaliana*. *Archives of Biochemistry and Biophysics*. 399:232-238.
94. Kwon, S.I., Kim, S.H., Bhattacharjee, S., Noh, J.J., Gassmann, W. 2009. SRFR1, a suppressor of effector-triggered immunity, encodes a conserved tetratricopeptide repeat protein with similarity to transcriptional repressors. *Plant Journal*. 57:109-119.
95. Lapin, D., Kovacova, V., Sun, X., Dongus, J.A., Bhandari, D.D., von Born, P., Bautor, J., Guarneri, N., Stuttmann, J., Beyer, A., Parker, J.E. 2019. A coevolved EDS1-SAG101-NRG1 module mediates cell death signalling by TIR-domain immune receptors. *The Plant Cell*. 31:2430-2455.
96. Lee, H.W., Park, J.H., Park, M.Y., Kim, J. 2014. GIP1 may act as a coactivator that enhances transcriptional activity of LBD18 in *Arabidopsis*. *Journal of Plant Physiology*. 17:14-18.
97. Lee, I.H., Lee, I.C., Kim, J., Kim J.H., Chung, E.H., Kim, H.J., Park, S.J., Kim, Y.M., Kang, S.K., Nam, H.G., Woo, H.R., Lim P.O. 2016. NORE1/SAUL1 integrates temperature-dependent defense programs involving SGT1b and PAD4 pathways and leaf senescence in *Arabidopsis*. *Physiologia Plantarum*. 158:180-199.
98. Lei, J., Finlayson, S., Salzman, R.A., Shan, L., Zhu-Salzman, K. 2014. BOTRYTIS-INDUCED KINASE1 modulates *Arabidopsis* resistance to green peach aphids via PHYTOALEXIN DEFICIENT4. *Plant Physiology*. 165:1657-1670.
99. Le Roux, C., Huet, G., Jauneau, A., Camborde, L., Tremousaygue, D., Kraut, A., Zhou, B., Levailant, M., Adachi, H., Yoshioka, H., Raffaele, S., Berthomé, R., Couté, Y., Parker, J.E., Deslandes, L. 2015. A receptor pair with an integrated decoy converts pathogen disabling of transcription factors to immunity. *Cell*. 161:1074-1088.
100. Lewis, J.D., Wu, R., Guttman, D.S., Desveaux, D. 2010. Allele-specific virulence attenuation of the *Pseudomonas syringae* HopZ1a type III effector via the *Arabidopsis* ZAR1 resistance protein. *PLOS Genetics*. 6:e1000894.
101. Li, Y., Li, S., Bi, D., Cheng, Y.T., Li, X., Zhang, Y. 2010. SRFR1 negatively regulates plant NB-LRR resistance protein accumulation to prevent autoimmunity. *PLoS Pathogens* 6:e1001111.

102. Li, L., Habring, A., Wang, K., Weigel, D. 2020. Atypical Resistance Protein RPW8/HR Triggers Oligomerization of the NLR Immune Receptor RPP7 and Autoimmunity. *Cell Host Microbe*. 27:405-417.
103. Liu, S., Kracher, B., Ziegler, J., Birkenbihl, R.P., Somssich, I.E. 2015. Negative regulation of ABA signalling by WRKY33 is critical for Arabidopsis immunity towards *Botrytis cinerea* 2100. *Elife*. 4:e07295.
104. Logemann, E., Birkenbihl, R.P., Ülker, B., Somssich, I.E. 2006. An improved method for preparing *Agrobacterium* cells that simplifies the Arabidopsis transformation protocol. *Plant Methods*. 2:16.
105. Long, J.A., Ohno, C., Smith, Z.R., Meyerowitz, E.M. 2006. TOPLESS regulates apical embryonic fate in Arabidopsis. *Science*. 312:1520-1523.
106. Louis, J., Leung, Q., Pegadaraju, V., Reese, J., Shah, J. 2010a. PAD4-dependent antibiosis contributes to the *ssi2*-conferred hyper-resistance to the green peach aphid. *Molecular Plant-Microbe Interactions*. 23:618-627.
107. Louis, J., Lorenc-Kukula, K., Singh, V., Reese, J.C., Jander, G., Shah, J. 2010b. Antibiosis against the green peach aphid requires the Arabidopsis *thaliana* MYZUS PERSICAE-INDUCED LIPASE1 gene. *Plant Journal*. 64:800-811.
108. Louis, J., Gobbato, E., Mondal, H.A., Feys, B.J., Parker, J.E., Shah, J. 2012a. Discrimination of Arabidopsis PAD4 Activities in Defense against Green Peach Aphid and Pathogens. *Plant Physiology*. 158:1860-1872.
109. Louis, J., Mondal, H.A., Shah, J. 2012b. Green peach aphid infestation induces Arabidopsis PHYTOALEXIN-DEFICIENT4 expression at site of insect feeding. *Plant Signalling & Behavior*. 7:1431-1433.
110. Louis, J., Shah, J. 2015. Plant defence against aphids: the PAD4 signalling nexus. *Journal of Experimental Botany*. 66:449-54.
111. Lynch, T.J., Erickson, B.J., Miller, D.R., Finkelstein, R.R. 2017. ABI5-binding proteins (AFPs) alter transcription of ABA-induced genes via a variety of interactions with chromatin modifiers. *Plant Molecular Biology*. 93:403-418.
112. Ma, Y., Guo, H., Hu, L., Martinez, P.P., Moschou, P.N., Cevik, V., Ding, P., Duxbury, Z., Sarris, P.F., Jones, J.D.G. 2018. Distinct modes of derepression of an Arabidopsis immune receptor complex by two different bacterial effectors. *PNAS USA*. 115:10218-10227.
113. Mahdi, L., Huang, M., Zhang, X., Nakano, T.R., Kopp, L.B., Saur, I.M.L., Jacob, F., Kovacova, V., Lapin, D., Parker, J.E., Murphy, J.M., Hofmann, K., Schulze-Lefert, P., Chai, J., Maekawa, T. 2019. Plant mixed lineage kinase domain-like proteins limit biotrophic pathogen growth. *bioRxiv*. 681015. doi: <https://doi.org/10.1101/681015>
114. Mach, J.M., Castillo, A.R., Hoogstraten, R., Greenberg, J.T. 2001. The Arabidopsis-accelerated cell death gene ACD2 encodes red chlorophyll catabolite reductase and suppresses the spread of disease symptoms. *PNAS USA* 98:771-776.
115. Makandar, R., Nalam, V.J., Chowdhury, Z., Sarowar, S., Klossner, G., Lee, H., Burdan, D., Trick, H.N., Gobbato, E., Parker, J.E., Shah, J. 2015. The Combined Action of ENHANCED DISEASE SUSCEPTIBILITY1, PHYTOALEXIN DEFICIENT4, and SENESCENCE-ASSOCIATED101 Promotes Salicylic Acid-Mediated Defenses to Limit *Fusarium graminearum* Infection in Arabidopsis *thaliana*. *Molecular plant-microbe interactions*. 28:943-953.

116. Mbow, C., Rosenzweig, C., Barioni, L.G., Benton, T.G., Herrero, M., Krishnapillai, M., Liwenga, E., Pradhan, P., Rivera-Ferre, M.G., Sapkota, T., Tubiello, F.N., Xu, Y. 2019: Food Security. In: *Climate Change and Land: an IPCC special report on climate change, desertification, land degradation, sustainable land management, food security, and greenhouse gas fluxes in terrestrial ecosystems* [P.R. Shukla, J. Skea, E. Calvo Buendia, V. Masson-Delmotte, H.-O. Pörtner, D.C. Roberts, P. Zhai, R. Slade, S. Connors, R. van Diemen, M. Ferrat, E. Haughey, S. Luz, S. Neogi, M. Pathak, J. Petzold, J. Portugal Pereira, P. Vyas, E. Huntley, K. Kissick, M. Belkacemi, J. Malley, (eds.)]. In press
117. Mehlmer, N., Wurzing, B., Stael, S., Hofmann-Rodrigues, D., Csaszar, E., Pfister, B., Bayer, R., Teige, M. 2010. The Ca(2+) -dependent protein kinase CPK3 is required for MAPK-independent salt-stress acclimation in Arabidopsis. *Plant Journal*. 63:484-498.
118. Milligan, S.B., Bodeau, J., Yaghoobi, J., Kaloshian, I., Zabel, P., Williamson, V.M. 1998. The Root Knot Nematode Resistance Gene Mi from Tomato Is a Member of the Leucine Zipper, Nucleotide Binding, Leucine-Rich Repeat Family of Plant Genes. *The Plant Cell*. 10:1307.
119. Mindrebo, J.T., Narthey, C.M., Seto, Y., Burkart, M.D., Noel, J.P. 2016. Unveiling the functional diversity of the alpha/beta hydrolase superfamily in the plant kingdom. *Current Opinion Struct. Biology*. 41:233-246.
120. Mine, A., Nobori, T., Salazar-Rondon, M.C. Winkelmüller, T.M., Anver, S., Becker, D., Tsuda, K. 2017a. An incoherent feed-forward loop mediates robustness and tunability in a plant immune network. *EMBO Reports*. 18:464-476.
121. Mine, A., Berens, M.L., Nobori, T., Anver, S., Fukumoto, K., Winkelmüller, T.M., Takeda, A., Becker, D., Tsuda, K. 2017b. Pathogen exploitation of an abscisic acid- and jasmonate-inducible MAPK phosphatase and its interception by Arabidopsis immunity. *PNAS. USA* 114:7456-7461.
122. Mondal, H.A., Louis, J., Archer, L., Patel, M., Nalam, V.J., Sarowar, S., Sivapalan, V., Root, D.D., Shah, J. 2018. Arabidopsis ACTIN-DEPOLYMERIZING FACTOR3 Is Required for Controlling Aphid Feeding from the Phloem. *Plant Physiology*. 176:879-890.
123. Montillet, J.L., Leonhardt, N., Mondy, S., Tranchimand, S., Rumeau, D., Boudsocq, M., Garcia, A.V., Douki, T., Bigeard, J., Laurière, C., Chevalier, A., Castresana, C., Hirt, H. 2013. An abscisic acid-independent oxylipin pathway controls stomatal closure and immune defense in Arabidopsis. *PLOS Biology*. 11:e1001513.
124. Moran, P.J., Thompson, G.A. 2001. Molecular responses to aphid feeding in Arabidopsis in relation to plant defence pathways. *Plant Physiology* 125:1074-1085.
125. Murase, K., Hirano, Y., Sun, T.P., Hakoshima, T. 2008. Gibberellin-induced DELLA recognition by the gibberellin receptor GID1. *Nature*. 456:459-463.
126. Muskett, P.R., Kahn, K., Austin, M.J., Moisan, L.J., Sadanandom, A., Shirasu, K., Jones, J.D.G., Parker, J.E. 2002. Arabidopsis RAR1 Exerts Rate-Limiting Control of R Gene-Mediated Defenses against Multiple Pathogens. *The Plant Cell*. 14:979-992.
127. Nalam, V.J., Keereetawee, J., Shah, J. 2013. The green peach aphid, *Myzus persicae*, acquires a LIPOXYGENASE5-derived oxylipin from Arabidopsis thaliana, which promotes colonization of the host plant. *Plant Signalling & Behaviour*. 8:e22735.

128. Nalam, V., Louis, J., Patel, M., Shah, J. 2018. Arabidopsis-Green Peach Aphid Interaction: Rearing the Insect, No-choice and Fecundity Assays, and Electrical Penetration Graph Technique to Study Insect Feeding Behavior. *Bio-protocol*. 8:e2950.
129. Narusaka, M., Shirasu, K., Noutoshi, Y., Kubo, Y., Shiraishi, T., Iwabuchi, M., Narusaka, Y. 2009. RRS1 and RPS4 provide a dual resistance-gene system against fungal and bacterial pathogens. *Plant Journal*. 60:218-226.
130. Neubauer, M., Serrano, I., Rodibaugh, N., Bhandari, D.D., Bautor, J., Parker, J.E., Innes, R.W. 2020. Arabidopsis EDR1 Protein Kinase Regulates the Association of EDS1 and PAD4 to Inhibit Cell Death. *Molecular plant-microbe interactions*. 33:693-703.
131. Ngou, B.P.M., Ahn, H., Ding, P., Jones, J.D.G. 2020. Mutual Potentiation of Plant Immunity by Cell-surface and Intracellular Receptors. *bioRxiv* .04.10.034173. doi: <https://doi.org/10.1101/2020.04.10.034173>
132. Niu, D., Lin, X.L., Kong, X., Qu, G.P., Cai, B., Lee, J., Jin, J.B. 2019. SIZ1-Mediated SUMOylation of TPR1 Suppresses Plant Immunity in Arabidopsis. *Molecular Plant* 12:215-228.
133. Oh, E., Zhu, J.Y., Ryu, H., Hwang, I., Wang, Z.Y. 2014. TOPLESS mediates brassinosteroid-induced transcriptional repression through interaction with BZR1. *Nature Communications*. 5:4140.
134. Pajuelo, D., Gonzalez-Juarbe, N., Tak, U., Sun, J., Orihuela, C.J., Niederweis, M. 2018. NAD(+) depletion triggers macrophage necroptosis, a cell death pathway exploited by mycobacterium tuberculosis. *Cell Reports*. 24:429-440.
135. Parker, J.E., Holub, E.B., Frost, L.N., Falk, A., Gunn, N.D., Daniels, M.J. 1996. Characterization of eds1, a mutation in Arabidopsis suppressing resistance to *Peronospora parasitica* specified by several different RPP genes. *The Plant Cell*. 8:2033-2046.
136. Peart, J.R., Mestre, P., Lu, R., Malcuit, I., Baulcombe, D.C. 2005. NRG1, a CC-NB-LRR protein, together with N, a TIR-NB-LRR protein, mediates resistance against tobacco mosaic virus. *Current Biology*. 15:968-973.
137. Pegadaraju, V. 2005. PhD dissertation: Molecular insights into arabidopsis response to *Myzus persicae* sulzer (green peach aphid). <http://hdl.handle.net/2097/129>
138. Pegadaraju, V., Knepper, C., Reese, J., Shah, J. 2005. Premature leaf senescence modulated by the Arabidopsis PHYTOALEXIN DEFICIENT4 gene is associated with defense against the phloem-feeding green peach aphid. *Plant Physiology*. 139:1927-1934.
139. Pegadaraju, V., Louis, J., Singh, V., Reese, J.C., Bautor, J., Feys, B.J., Cook, G., Parker, J.E., Shah, J. 2007. Phloem-based resistance to green peach aphid is controlled by Arabidopsis PHYTOALEXIN DEFICIENT4 without its signalling partner ENHANCED DISEASE SUSCEPTIBILITY1. *Plant Journal*. 52:332-341.
140. Petrie, E.J., Czabotar, P.E., Murphy, J.M. 2018. The structural basis of necroptotic cell death signalling. *Trends in Biochemical Science*. 44:53-63.
141. Pieterse, C.M., Van der Does, D., Zamioudis, C., Leon-Reyes, A., Van Wees, S.C. 2012. Hormonal modulation of plant immunity. *Annual Review of Cell & Developmental Biology*. 28:489-521.
142. Qi, T., Seong, K., Thomazella, D.P.T., Kim, J.R., Pham, J., Seo, E., Cho, M.-J., Schultink, A., Staskawicz, B.J. 2018. NRG1 functions downstream of EDS1 to regulate TIR NLR-mediated plant immunity in *Nicotiana benthamiana*. *PNAS USA*. 115:E10979-E10987

143. Rashid, M.H., Khan, A., Hossain, M.T., Chung, Y.R. 2017. Induction of Systemic Resistance against Aphids by Endophytic *Bacillus velezensis* YC7010 via Expressing PHYTOALEXIN DEFICIENT4 in Arabidopsis. *Frontiers in Plant Science*. 8:211.
144. Rauwerdink, A., Kazlauskas, R.J. 2015. How the Same Core Catalytic Machinery Catalyzes 17 Different Reactions: the Serine-Histidine-Aspartate Catalytic Triad of α/β -Hydrolase Fold Enzymes. *ACS Catalysis*. 5:6153-6176.
145. Rappsilber, J., Ishihama, Y., Mann, M. 2003. Stop and go extraction tips for matrix-assisted laser desorption/ionization, nanoelectrospray, and LC/MS sample pretreatment in proteomics. *Analytical Chemistry*. 75:663-70.
146. Reddy, A.S.N., Ali, G.S., Celesnik, H., Day, I.S. 2011. Coping with Stresses: Roles of Calcium- and Calcium/Calmodulin-Regulated Gene Expression. *The Plant Cell*. 23:2010-2032.
147. Rekhter, D., Lüdke, D., Ding, Y., Feussner, K., Zienkiewicz, K., Lipka, V., Wiermer, M., Zhang, Y., Feussner, I. 2019. Isochorismate-derived biosynthesis of the plant stress hormone salicylic acid. *Science*. 365:498-502.
148. Rietz, S., Stamm, A., Malonek, S., Wagner, S., Becker, D., Medina-Escobar, N., Vlot, A.C., Feys, B.J., Niefind, K., Parker, J.E. 2011. Different roles of Enhanced Disease Susceptibility1 (EDS1) bound to and dissociated from Phytoalexin Deficient4 (PAD4) in Arabidopsis immunity. *New Phytologist*. 191:107-119.
149. Roberts, M., Tang, S., Stallmann, A., Dangl, J. L., Bonardi, V. 2013. Genetic requirements for signalling from an autoactive plant NB-LRR intracellular innate immune receptor. *PLoS genetics*. 9:e1003465.
150. Rossi, M., Goggin, F.L., Milligan, S.B., Kaloshian, I., Ullman, D.E., Williamson, V.M. 1998. The nematode resistance gene Mi of tomato confers resistance against the potato aphid. *PNAS USA*. 95:9750-9754.
151. Roth, C., Lüdke, D., Klenke, M., Quathamier, A., Valerius, O., Braus, G.H., Wiermer, M. 2017. The truncated NLR protein TIR-NBS13 is a MOS6/IMPORTIN- α 3 interaction partner and required for plant immunity. *Plant Journal*. 92:808-821.
152. Sarris, P.F., Duxbury, Z., Huh, S.U., Ma, Y., Segonzac, C., Sklenar, J., Derbyshire, P., Cevik, V., Rallapalli, G., Saucet, S., Wirthmuller, L., Menke, F., Sohn, K.H., Jones, J.D.G. 2015. A Plant Immune Receptor Detects Pathogen Effectors that Target WRKY Transcription Factors. *Cell*. 161:1089-1100.
153. Saucet, S.B., Ma, Y., Sarris, P.F., Furzer, O.J., Sohn, K.H., Jones, J.D. 2015. Two linked pairs of Arabidopsis TNL resistance genes independently confer recognition of bacterial effector avrRps4. *Nature Communications*. 6:6338.
154. Schneider, T.D., Stephens, R.M. 1990. Sequence Logos: A New Way to Display Consensus Sequences. *Nucleic Acids Res*. 18:6097-6100.
155. Scholl, R.L., May, S.T., Ware, D.H. 2000. Seed and molecular resources for Arabidopsis. *Plant Physiology*. 124:1477-1480.
156. Seo, J.S., Koo, Y.J., Jung, C., Yeu, S.Y., Song, J.T., Kim, J.K., Choi, Y., Lee, J.S., Do Choi, Y. 2013. Identification of a Novel Jasmonate-Responsive Element in the AtJMT Promoter and Its Binding Protein for AtJMT Repression. *PLoS One*. e55482.

157. Shaikhali, J. 2015. GIP1 protein is a novel cofactor that regulates DNA-binding affinity of redox-regulated members of bZIP transcription factors involved in the early stages of Arabidopsis development. *Protoplasma* 252:867-883.
158. Shimada, A., Ueguchi-Tanaka, M., Nakatsu, T., Nakajima, M., Naoe, Y., Ohmiya, H., Kato, H., Matsuoka, M. 2008. Structural basis for gibberellin recognition by its receptor GID1. *Nature*. 456:520-523.
159. Singh, V., Louis, J., Ayre, B.G., Reese, J.C., Pegadaraju, V., Shah, J. 2011. TREHALOSE PHOSPHATE SYNTHASE11-dependent trehalose metabolism promotes Arabidopsis thaliana defense against the phloem-feeding insect Myzus persicae. *Plant Journal*. 67:94-104.
160. Singh, V., Shah, J. 2012. Tomato responds to green peach aphid infestation with the activation of trehalose metabolism and starch accumulation. *Plant Signalling & Behavior*. 7:605-607.
161. Sohn, K.H., Segonzac, C., Rallapalli, G., Sarris, P.F., Woo, J.Y., Williams, S.J., Newman, T.E., Paek, K.H., Kobe, B., Jones, J.D. 2014. The nuclear immune receptor RPS4 is required for RRS1SLH1-dependent constitutive defense activation in Arabidopsis thaliana. *PLOS Genetics*. 10:e1004655.
162. Stadler, R., Sauer, N. 1996. The Arabidopsis thaliana AtSUC2 gene is specifically expressed in companion cells. *Botanica Acta*. 109:299-306.
163. Stankovic, N., Schloesser, M., Joris, M., Sauvage, E., Hanikenne, M., Motte, P. 2015. Dynamic Distribution and Interaction of the Arabidopsis SRSF1 Subfamily Splicing Factors. *Plant Physiology*. 170:1000-1013.
164. Stuttman, J., Peine, N., Garcia, A.V., Wagner, C., Choudhury, S.R., Wang, Y., James, G.V., Griebel, T., Alcázar, R., Tsuda, K., Schneeberger, K., Parker, J.E. 2016. Arabidopsis thaliana DM2h (R8) within the Landsberg RPP1-like Resistance Locus Underlies Three Different Cases of EDS1-Conditioned Autoimmunity. *PLoS Genetics* 12:e1005990.
165. Stuttman, J., Hubberten, H.M., Rietz, S., Kaur, J., Muskett, P., Guerois, R., Bednarek, P., Hoefgen, R., Parker, J.E. 2011. Perturbation of Arabidopsis amino acid metabolism causes incompatibility with the adapted biotrophic pathogen Hyaloperonospora arabidopsidis. *The Plant Cell*. 23:2788-803.
166. Szymanski, D.B., Jilk, R.A., Pollock, S.M., Marks, M.D. 1998. Control of GL2 expression in Arabidopsis leaves and trichomes. *Development*. 125:1161-1171.
167. Thatcher, L.F., Foley, R., Casarotto, H.J., Gao, L.L., Kamphuis, L.G., Melser, S., Singh, K.B. 2018. The Arabidopsis RNA Polymerase II Carboxyl Terminal Domain (CTD) Phosphatase-Like1 (CPL1) is a biotic stress susceptibility gene. *Scientific reports*. 8:13454.
168. Tissier, A.F., Marillonnet, S., Klimyuk, V., Patel, K., Torres, M.A., Murphy, G., Jones, J.D. 1999. Multiple independent defective suppressor-mutator transposon insertions in Arabidopsis: a tool for functional genomics. *The Plant Cell* 11:1841-1852.
169. Tor, M., Gordon, P., Cuzick, A., Eulgem, T., Sinapidou, E., Mert-Turk, F., Can, C., Dangl, J.L., Holub, E.B. 2002. Arabidopsis SGT1b is required for defense signalling conferred by several downy mildew resistance genes. *The Plant Cell*. 14:993-1003.
170. Torrens-Spence, M.P., Bobokalonova, A., Carballo, V., Glinkerman, C.M., Pluskal, T., Shen, A., Weng, J.K. 2019. PBS3 and EPS1 Complete Salicylic Acid Biosynthesis from Isochorismate in Arabidopsis. *Molecular Plant*. 12:1577-1586.

171. Tsuda, K., Sato, M., Stoddard, T., Glazebrook, J., Katagiri, F. 2009. Network properties of robust immunity in plants. *PLoS. Genet.* 5:e1000772.
172. Tyanova, S., Temu, T., Cox, J. 2016. The MaxQuant computational platform for mass spectrometry-based shotgun proteomics. *Nature Protocols.* 11:2301-2319.
173. Van der Biezen, E.A., Freddie, C.T., Kahn, K., Parker, J.E., Jones, J.D. 2002. Arabidopsis RPP4 is a member of the RPP5 multigene family of TIR-NB-LRR genes and confers downy mildew resistance through multiple signalling components. *Plant Journal.* 29:439-451.
174. Van Leene J., Eeckhout D., Cannoot B., De Winne N., Persiau G., Van De Slijke E., Vercruysse L., Dedecker M., Verkest A., Vandepoele K., Martens L., Witters E., Gevaert K., De Jaeger G. 2015. An improved toolbox to unravel the plant cellular machinery by tandem affinity purification of Arabidopsis protein complexes. *Nature Protocols.* 10:169-187.
175. Van Leeuwen, H., Kliebenstein, D.J., West, M.A., Kim, K., van Poecke, R., Katagiri, F., Michelmore, R.W., Doerge, R.W., St Clair, D.A. 2007. Natural variation among Arabidopsis thaliana accessions for transcriptome response to exogenous salicylic acid. *The Plant Cell.* 19:2099-2110.
176. Venugopal, S.C., Jeong, R.D., Mandal, M.K., Zhu, S., Chandra-Shekara, A.C., Xia, Y., Hersh, M., Stromberg, A.J., Navarre, D., Kachroo, A., Kachroo, P. 2009. Enhanced disease susceptibility 1 and salicylic acid act redundantly to regulate resistance gene-mediated signaling. *PLoS genetics*, 5:e1000545.
177. Vicente, J., Cascón, T., Vicedo, B., García-Agustín, P., Hamberg, M., Castresana, C. 2012. Role of 9-lipoxygenase and α -dioxygenase oxylipin pathways as modulators of local and systemic defense. *Molecular Plant.* 5:914-28.
178. Villada, E.S., González, E.G., López-Sesé, A.I., Castiel, A.F., Gómez-Guillamón, M.L. 2009. Hypersensitive response to *Aphis gossypii* Glover in melon genotypes carrying the Vat gene. *Journal of Experimental Botany.* 60:3269-3277.
179. Vlot, A.C., Liu, P.P., Cameron, R.K., Park, S.W., Yang, Y., Kumar, D., Zhou, F., Padukkavidana, T., Gustafsson, C., Pichersky, E., Klessig, D.F. 2008. Identification of likely orthologs of tobacco salicylic acid-binding protein 2 and their role in systemic acquired resistance in Arabidopsis thaliana. *The Plant Journal.* 56:445-456.
180. Voss, M., Toelzer, C., Bhandari, D.D., Parker, J.E., Niefind, K. 2019. Arabidopsis immunity regulator EDS1 in a PAD4/SAG101-unbound form is a monomer with an inherently inactive conformation. *Journal of Structural Biology.* 208:107390.
181. Wagner, S., Stuttmann, J., Rietz, S., Guerois, R., Brunstein, E., Bautor, J., Niefind, K., Parker, J.E. 2013. Structural basis for signalling by exclusive EDS1 heteromeric complexes with SAG101 or PAD4 in plant innate immunity. *Cell Host Microbe.* 14:619-630.
182. Wan, L., Essuman, K., Anderson, R.G., Sasaki, Y., Monteiro, F., Chung, E.H., Osborne Nishimura, E., DiAntonio, A., Milbrandt, J., Dangl, J.L., Nishimura, M.T. 2019. TIR domains of plant immune receptors are NAD⁺-cleaving enzymes that promote cell death. *Science.* 365:799-803.
183. Wang, L., Mitra, R.M., Hasselmann, K.D., Sato, M., Lenarz-Wyatt, L., Cohen, J.D., Katagiri, F., Glazebrook, J. 2008. The genetic network controlling the Arabidopsis transcriptional response to *Pseudomonas syringae* pv. *maculicola*: roles of major regulators and the phytotoxin coronatine. *Molecular Plant Microbe Interactions.* 21:1408-1420.

184. Wang, L., Tsuda, K., Sato, M., Cohen, J.D., Katagiri, F., Glazebrook, J. 2009. Arabidopsis CaM binding protein CBP60g contributes to MAMP-induced SA accumulation and is involved in disease resistance against *Pseudomonas syringae*. *PLoS Pathog.* 5:e1000301.
185. Wang, L., Tsuda, K., Truman, W., Sato, M., Nguyen Le, V., Katagiri, F., Glazebrook J. 2011. CBP60g and SARD1 play partially redundant critical roles in salicylic acid signalling. *Plant Journal.* 67:1029-1041.
186. Wang, Y., Zhang, Y., Wang, Z., Zhang, X., Yang, S. 2013. A missense mutation in CHS1, a TIR-NB protein, induces chilling sensitivity in Arabidopsis. *Plant Journal.* 75:553-565.
187. Wang, D., Zhang, L., Hu, J., Gao, D., Liu, X., Sha, Y. 2018. Comparative genomic analysis of the Lipase3 gene family in five plant species reveals distinct evolutionary origins. *Genetica.* 146:179-185.
188. Wang, J., Hu, M., Wang, J., Qi, J., Han, Z., Wang, G., Qi, Y., Wang, H. W., Zhou, J. M., Chai, J. 2019a. Reconstitution and structure of a plant NLR resistosome conferring immunity. *Science.* 364:eaav5870.
189. Wang, J., Wang, J., Hu, M., Wu, S., Qi, J., Wang, G., Han, Z., Qi, Y., Gao, N., Wang, H. W., Zhou, J. M., Chai, J. 2019b. Ligand-triggered allosteric ADP release primes a plant NLR complex. *Science.* 364:eaav5868.
190. Wasternack C., Song S. Jasmonates: Biosynthesis, metabolism, and signalling by proteins activating and repressing transcription. *J. Exp. Bot.* 2016. 68:1303-1321.
191. Weber, B., Zicola, J., Oka, R., Stam, M. 2016. Plant Enhancers: A Call for Discovery. *Trends in Plant Science.* 21:974-987.
192. Wiermer, M., Feys, B.J., Parker, J.E. 2005. Plant immunity: the EDS1 regulatory node. *Current opinion in plant biology.* 8:383-389.
193. Wildermuth, M.C., Dewdney J., Wu G., Ausubel F.M. 2001. Isochorismate synthase is required to synthesize salicylic acid for plant defence. *Nature.* 414:562-565.
194. Williams, S.J., Sohn, K.H., Wan, L., Bernoux, M., Sarris, P.F., Segonzac, C., Ve, T., Ma, Y., Saucet, S.B., Ericsson, D.J., Casey, L.W., Lonhienne, T., Winzor, D.J., Zhang, X., Coerdts, A., Parker, J.E., Dodds, P.N., Kobe, B., Jones, J.D. 2014. Structural basis for assembly and function of a heterodimeric plant immune receptor. *Science.* 344:299-303.
195. Wirthmueller, L., Zhang, Y., Jones, J.D., Parker, J.E. 2007. Nuclear accumulation of the Arabidopsis immune receptor RPS4 is necessary for triggering EDS1-dependent defense. *Current Biology.* 17:2023-29.
196. Witte, C.P., Noël, L., Gielbert, J., Parker, J., Romeis, T. 2004. Rapid one-step protein purification from plant material using the eight-amino acid StrepII epitope. *Plant Molecular Biology.* 55:135-147.
197. Wroblewski, T., Piskurewicz, U., Tomczak, A., Ochoa, O., Michelmore, R.W. 2007. Silencing of the major family of NBS-LRR encoding genes in lettuce results in the loss of multiple resistance specificities. *Plant Journal.* 51:803-81.
198. Wu, Z., Li, M., Dong, O.X., Xia, S., Liang, W., Bao, Y., Wasteneys, G., Li, X. 2019. Differential regulation of TNL-mediated immune signalling by redundant helper CNLs. *New Phytol.* 222:938-953.
199. Xiao, S., Ellwood, S., Calis, O., Patrick, E., Li, T., Coleman, M., Turner, J.G. 2001. Broad-spectrum mildew resistance in Arabidopsis thaliana mediated by RPW8. *Science.* 291:118-120.

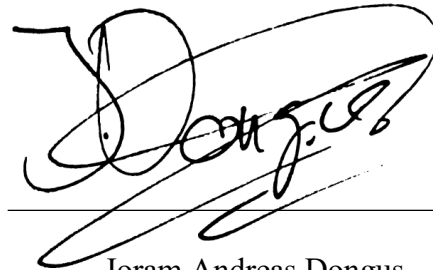
200. Xiong, F., Duan, C.Y., Liu, H.H., Wu, J. H., Zhang, Z.H., Li, S., Zhang, Y. 2020. Arabidopsis KETCH1 Is Critical for the Nuclear Accumulation of Ribosomal Proteins and Gametogenesis. *The Plant Cell*. pii:tpc.00791.2019.
201. Xu, F., Zhu, C., Cevik, V., Johnson, K., Liu, Y., Sohn, K., Jones, J.D., Holub, E.B., Li, X. 2015. Autoimmunity conferred by chs3-2D relies on CSA1, its adjacent TNL-encoding neighbour. *Scientific Reports*. 5:8792.
202. Yan, J., Li, H., Li, S., Yao, R., Deng, H., Xie, Q., Xie, D. 2013. The Arabidopsis F-box protein CORONATINE INSENSITIVE1 is stabilized by SCF^{COI1} and degraded via the 26S proteasome pathway. *The Plant Cell*. 25:486-498.
203. Yang, Y., Xu, R., Ma, C.J., Vlot, A.C., Klessig, D.F., Pichersky, E. 2008. Inactive methyl indole-3-acetic acid ester can be hydrolyzed and activated by several esterases belonging to the AtMES esterase family of Arabidopsis thaliana. *Plant Physiol*. 147, 1034-1045.
204. Yang, H., Shi, Y., Liu, J., Guo, L., Zhang, X., Yang, S. 2010. A mutant CHS3 protein with TIR-NB-LRR-LIM domains modulates growth, cell death and freezing tolerance in a temperature-dependent manner in Arabidopsis. *Plant Journal*. 63:283-296.
205. Yao, N., Greenberg, J.T. 2006. Arabidopsis ACCELERATED CELL DEATH2 Modulates Programmed Cell Death. *The Plant Cell*. 18:397-411.
206. Yelagandula R., Stroud H., Holec S., Zhou K., Feng S., Zhong X., Muthurajan, U.M., Nie, X., Kawashima, T., Groth, M., Luger, K., Jacobsen, S.E., Berger, F. 2014. The histone variant H2A.W defines heterochromatin and promotes chromatin condensation in Arabidopsis. *Cell* 158, 98-109.
207. You, M.K., Shin, H.Y., Kim, Y.J., Ok, S.H., Cho, S.K., Jeung, J.U., Yoo, S.D., Kim, J.K., Shin, J.S. 2010. Novel bifunctional nucleases, OmBBD and AtBBD1, are involved in abscisic acid-mediated callose deposition in Arabidopsis. *Plant Physiology*. 152:1015-1029.
208. Yuan, M., Jiang, Z., Bi, G., Nomura, K., Liu, M., He, S.Y., Zhou, J., Xin, F. 2020 Pattern-recognition receptors are required for NLR-mediated plant immunity. *BioRxiv*. 04.10.031294. doi: <https://doi.org/10.1101/2020.04.10.03129>
209. Zhang, Y., Xu S., Ding P., Wang D., Cheng Y.T., He J., Gao M., Xu F., Li Y., Zhu Z., Li X., Zhang Y. 2010. Control of salicylic acid synthesis and systemic acquired resistance by two members of a plant-specific family of transcription factors. 107:18220-18225.
210. Zhang, X.C., Millet, Y.A., Cheng, Z., Bush, J., Ausubel, F.M. 2015. Jasmonate signalling in Arabidopsis involves SGT1b-HSP70-HSP90 chaperone complexes. *Nature Plants*. 1. pii:15049.
211. Zhang, T., Marand, A.P., Jiang, J. 2016. PlantDHS: a database for DNase I hypersensitive sites in plants. *Nucleic Acids Research*. 44:1148-1153.
212. Zhang, Z., Guo, X., Ge, C., Ma, Z., Jiang, M., Li, T., Koiwa, H., Yang, S.W., Zhang, X. 2017a. KETCH1 imports HYL1 to nucleus for miRNA biogenesis in Arabidopsis. *PNAS USA*. 114:4011-4016.
213. Zhang, Y., Wang, Y., Liu, J., Ding, Y., Wang, S., Zhang, X., Liu, Y., Yang, S. 2017b. Temperature-dependent autoimmunity mediated by chs1 requires its neighboring TNL gene SOC3. *New Phytologist*. 213:1330-1345.
214. Zhang, Y., Song, G., Lal, N. K., Nagalakshmi, U., Li, Y., Zheng, W., Huang, P. J., Branon, T. C., Ting, A. Y., Walley, J. W., Dinesh-Kumar, S. P. 2019. TurboID-based proximity

- labeling reveals that UBR7 is a regulator of N NLR immune receptor-mediated immunity. *Nature Communications*. 10:3252.
215. Zheng, X.Y., Spivey, N.W., Zeng, W., Liu, P.P., Fu, Z. Q., Klessig, D. F., Dong, X. 2012. Coronatine promotes *Pseudomonas syringae* virulence in plants by activating a signalling cascade that inhibits salicylic acid accumulation. *Cell Host Microbe*. 11, 587-96.
216. Zhu, Z., Xu F, Zhang, Y., Cheng, Y.T., Wiermer, M., Li, X., Zhang, Y. 2010. Arabidopsis resistance protein SNC1 activates immune responses through association with a transcriptional corepressor. *PNAS USA*. 107:13960-13965.
217. Zhou, N., Tootle, T.L., Tsui, F., Klessig, D.F., Glazebrook J. 1998. PAD4 functions upstream from salicylic acid to control defense responses in Arabidopsis. *The Plant Cell*. 10:1021-1030.
218. Zicola, J., Liu, L., Tänzler, P., Turck, F. 2019. Targeted DNA methylation represses two enhancers of FLOWERING LOCUS T in Arabidopsis thaliana. *Nature Plants* 5:300-307.

Erklärung

Ich versichere, dass ich die von mir vorgelegte Dissertation selbständig angefertigt, die benutzten Quellen und Hilfsmittel vollständig angegeben und die Stellen der Arbeit – einschließlich Tabellen, Karten und Abbildungen –, die anderen Werken im Wortlaut oder dem Sinn nach entnommen sind, in jedem Einzelfall als Entlehnung kenntlich gemacht habe; dass diese Dissertation noch keiner anderen Fakultät oder Universität zur Prüfung vorgelegen hat; dass sie noch nicht veröffentlicht worden ist, sowie, dass ich eine solche Veröffentlichung vor Abschluss des Promotionsverfahrens nicht vornehmen werde. Die Bestimmungen der Promotionsordnung sind mir bekannt. Die von mir vorgelegte Dissertation ist von Prof. Dr. Jane Parker betreut worden.

Köln, 27. April 2020



Joram Andreas Dongus